Functional analysis of domain I of the hepatitis C virus non-structural NS5A protein

Chunhong Yin

Submitted in accordance with the requirements for the degree of

Doctor of Philosophy

The University of Leeds

Faculty of Biological Sciences

School of Molecular and Cellular Biology

February 2018

The candidate confirms that the work submitted is her own, except where work which has formed part of jointly-authored publications has been included. The contribution of the candidate and the other authors to this work has been explicitly indicated below. The candidate confirms that appropriate credit has been given within the thesis where reference has been made to the work of others.

Chapter 3 to 5 within this thesis has been based on work from a jointly-authored publication:

Yin C, Goonawardane N, Stewart H, Harris M. A role for domain I of the hepatitis C virus NS5A protein in virus assembly. PLoS pathogens. 2018;14(1):e1006834. doi: 10.1371/journal.ppat.1006834.

- C. Yin performed experiments for figures 1, 2, 3, 9, 10, 11 and supporting figures 1, 2, 3, 4, 5, 7, 8, 9 and 10 and co-authored the paper.

- Dr N. Goonawardane performed experiments for figures 4, 5, 6, 7, 8 and supporting figure 6 and co-authored the paper.

- Dr H. Stewart provided supervision and co-authored the paper.

- Prof. M Harris provided supervision and co-authored the paper.

Acknowledgements

I would like to thank my supervisor Prof. Mark Harris for his invaluable supervision of this project. Thanks for his tolerance and patience to witness my English better and better. Without his advice and encouragement over the past three years this project would have never have even got off the ground.

More appreciations should go to Niluka Goonawardane for her scientific input throughout this project. A special thanks to Hazel Stewart for teaching me the ropes and keeping my science on track. Further thanks to past and present members in Lab Garstang 8.61 and other colleagues from Virology group.

A big thank you to my family and to my friends for their never-ending support through some of the less enjoyable times. Thanks in particular to Ruiying Liang for encouragement and ability to cheer me up during my frustrating times. It is only now with hind sight that I really see how important they have been and how lucky I am. I am eternally grateful, and I am sure they are as relieved as I am that I can end my homesickness and get together with them.

I finally would like to acknowledge the China Scholarship Council and University of Leeds Scholarship for funding this project and funding from FBS. I would also like to thank the Microbiology Society and HCV relative Conferences for providing opportunities to present my work to the wider scientific community.

Abstract

The research on hepatitis C virus protein NS5A has developed rapidly over the decades, primarily with the advent of the JFH1 cell culture infectious clone which allowed the study of all aspects of the virus lifecycle from entry to exit. As the important target of DAAs, the NS5A protein of hepatitis C virus (HCV) plays roles in both virus genome replication and assembly. NS5A comprises three domains, of these domain I is believed to be involved exclusively in genome replication. In contrast, domains II and III are required for the production of infectious virus particles and are largely dispensable for genome replication. Domain I is highly conserved between HCV and related hepaciviruses, and is highly structured, exhibiting different dimeric conformations.

To investigate the functions of domain I in more detail, a mutagenic study of 12 absolutely conserved and surface-exposed residues were conducted within the context of a JFH1-derived sub-genomic replicon and infectious virus. Whilst most of these abrogated genome replication, three mutants (P35A, V67A and P145A) retained the ability to replicate but showed defects in virus assembly. Whilst P35A exhibited a modest reduction in infectivity, V67A and P145A produced no infectious virus.

Using a combination of density gradient fractionation, biochemical analysis and high-resolution confocal microscopy, it was demonstrated that V67A and P145A disrupted the recruitment of NS5A to lipid droplets. In addition, the localisation and size of lipid droplets in cells infected with these two mutants were perturbed. Biophysical analysis revealed that V67A and P145A abrogated the ability of purified domain I to dimerize and resulted in an increased affinity of binding to HCV 3'UTR RNA. Taken collectively, we propose that domain I of NS5A plays multiple roles in assembly, binding nascent genomic RNA and transporting it to lipid droplets where it is transferred to Core. In parallel, this study also set out to investigate the interactions of NS5A domain I with cellular proteins by the approach of quantitative proteomic analysis.

This study reveals novel functions of NS5A domain I in assembly of infectious HCV and provides new perspectives on the virus lifecycle.

Table of Contents

Table of Figures

Table of Tables

Abbreviations

A	Ala, alanine
aa	Amino Acid
ACAT	Acyl-CoA: cholesterol acyltransferase
ADRP	Adipose differentiation-related protein
AH	Amphipathic helix
ALT	Alanine aminotransferase
Amph II	Amphiphysin II
ANXA2	Annexin A2
AP2M1	Adapter protein-2 M1
Apo	Apolipoprotein
ARFP	Alternative reading frame protein
ATP	Adenosine triphosphate
BCA	Bicinchoninic acid
BDV	Border disease virus
BMS	Bristol Myers-Squibb
BODIPY	Boron-dipyrromethene
bp	Base Pairs
BPgV	Bat Pegivirus
BSA	Bovine serum albumin
BSL3	Biosafety laboratory level 3
BVDV	Bovine virus diarrhoea virus
C	core protein
C	Cys, cysteine
CAM	Culture adaptive mutations
cAMP	Cyclic adenosine monophosphate
CD81	Cluster of differentiation 81
CE	Cholesterol ester
CH25H	Cholesterol 25-hydroxylase
CHC	Chronic hepatitis C
CHV	Canine hepacivirus
CKI, CKII	Casein kinase I, II
CLDN1	Claudin 1
cLD	Cytosolic lipid droplets
CMV	Cytomegalovirus
cPLA2	Cytosolic phospholipase A2
CTD	C-terminal Domain
CV	Column Volume
Cyp	Cyclophilin
Cys	Cysteine
D	Asp, aspartic acid
Da	Dalton
DAA	Direct Acting Antivirals
DAG	Diacylglyceride

DAGT1	Diglyceride acyltransferase 1
DAPI	4',6-diamidino-2-phenylindole
DENV	Dengue Fever Virus
DEPC	Diethyl pyrocarbonate
DMEM	Dulbecco's modified eagles medium
DMSO	Dimethyl sulfoxide
DMV	Double membrane vesicle
DNA	Deoxyribonucleic acid
dNTP	Deoxynucleotide
E	Glu, glutamic acid
E1	Envelope 1 protein
E2	Envelope 2 protein
EC_{50}	Effective concentration, 50%
EDTA	Ethylenediamine tetraacetic acid
EGFR	Epidermal growth factor receptor
eIF	eukaryotic initiation factors
EM	Electron Microscopy
EMCV	Encephalomyocarditis virus
ER	Endoplasmic Reticulum
ESCRT	Endosomal sorting complex required for transport
F	Phe, phenylalanine
FAS	Fatty acid synthase
FBP	Far upstream element of the c-myc proto- oncogene (FUSE) binding protein
FBS	foetal bovine serum
FDA	Food and Drug Administration
FKBP8	FK506-binding protein 8
g	Gravitational force
G	Gly, glycine
GAGs	Glycosaminoglycans
GAPDH	Glyceraldehyde-3-phosphate dehydrogenase
GBV-B	GB virus -B
GFP	Green fluorescence protein
GLB	Glasgow lysis buffer
GPS2	G protein pathway suppressor 2
GST	Glutathione S-transferases
gt	Genotype
H	His, histidine
HAV	Hepatitis A Virus
Hb-ind1	Human butyrate-induced transcript 1
HBV	Hepatitis B Virus
HCC	Hepatocellular Carcinoma
HCV	Hepatitis C Virus
HCVcc	Hepatitis C virus derived from cell culture
HDL	High density lipoprotein
HEPES	4-(2-hydroxyethyl)-1-piperazineethanesulfonate

HEV	Hepatitis E Virus
HIV	Human immunodeficiency virus
hpe	Hours post-electroporation
HPgV	human Pegivirus
hpi	Hours Post Infection
hpt	Hours Post Transfection
hrs	Hour
HSP72	Heat shock protein 72
HSPGs	Heparan sulphate proteoglycans
Huh7	Human hepatocellular carcinoma cell line-7
Huh7.5	Human hepatocellular carcinoma cell line-7.5
I	Ile, isoleucine
ICAT	isotope-coded affinity tag
IDU	Intravenous drug use
IF	immunofluorescence
IFNα	Interferon-α
IL28B	Interleukin 28-B
IRES	Internal Ribosome Entry Site
IRF	Interferon Regulatory Factor
ISG	Interferon-stimulated gene
IU	Infectious Unit
Jc1	J6/JFH1 chimeric virus
JEV	Japanese encephalitis virus
JFH1	Japanese fulminant HCV isolate 1, genotype 2a
K	Lys, lysine
kb	kilobase
kDa	Kilodalton
L	Leu, leucine
LarI	Luciferase reagent I
LB	Luria-Bertani
LC-MS	Liquid chromatography-mass spectrometry
LCS	Low complexity sequence
LD	Lipid Droplet
LDL	Low Density Lipoprotein
LDLR	Low density lipoproteinreceptor
LVP	Lipoviral particles
M	Met, methionine
MAPK	Mitogen-activated protein kinase
MAVS	Mitochondrial antiviral signalling protein
MW	Membranous web
M.Wt	Molecular weight
m/z	mass to charge
MCS	Multiple Cloning Site
MeOH	Methanol
min	Minutes
MMV	Multi-Membrane Vesicle

MS	Mass Spectrometry
MTP	Microsomal transfer protein
MTTP	Microsomal triglyceride transfer protein
N	Asn, asparagine
NANBH	non-A non-B hepatitis
NAP1L	Nucleosome assembly protein 1-like protein
NF	Nuclear factor
NMR	Nuclear magnetic resonance
NPC1L1	Niemann-Pick C1-like 1
NPHV	non-primate Hepacivirus
NPT	Neomycin phosphotransferase
NS	Non-structural
NS2	Non-structural 2
NS3	Non-structural 3
NS4A	Non-structural 4A
NS4B	Non-structural 4B
NS5A	Non-structural 5A
NS5B	Non-structural 5B
nt	nucleotide
o/n	Overnight
OCLN	occluding
ORF	Open Reading Frame
OSBP	Oxysterol binding protein
OST	One strep tag
P	Pro, proline
PAGE	Polyacrylamide gel electrophoresis
PAMP	Pathogen associated molecular patterns
PBS	Phosphate buffered saline
PCR	Polymerase chain reaction
PDB	Protein database
PEG	Pegylated
PFA	Paraformaldehyde
PI4KIIIα	Phosphatidylinositol-4-kinase-α, type III
PI4P	Phosphatidylinositol-4-phosphate
Pin	Peptidyl-prolyl cis-trans isomerase NIMA- interacting 1
PKA α	cAMP-dependent protein kinase A-α subunit
PKR	Protein Kinase R
PLA	Proximity ligation assay
PLA1A	Phosphatidylserine-specific phospholipase A1
PLB	Passive lysis buffer
PlkI	Polo-Like Kinase 1
PP2.1	Polyproline 2.1
PP2.2	Polyproline 2.2
PPIase	Peptidyl prolyl isomerase
PVDF	Polyvinylidene fluoride
Q	Gln, glutamine

qRT-PCR	Quantative, Real Time PCR
R	Arg, arginine
RAVs	Resistance-associated variants
RBV	Ribavirin
RCA	Rolling circle amplification
RdRp	RNA-dependent RNA-polymerase
RNA	Ribonucleic acid
rpm	Revolutions Per Minute
RT	Room Temperature
S	Ser, serine
SDS	Sodium dodecyl sulphate
SE	Standard Error
sec	Seconds
SEC	Size Exclusion Chromatography
SEC-MALLS	Size Exclusion Chromatography - Multi-Angle Laser Light Scattering
SEM	Standard error of the mean
SGR	Sub-Genomic Replicon
siRNA	Small interfering RNA
SP	Signal peptidase
SPP	Signal peptide peptidase
SOAT1	Sterol O-acyltransferase 1
SOC	Standard of care
SPgV	simian Pegivirus
SRBI	scavenger receptor b1
SREBP	Sterol regulatory element–binding protein
SUMO	Small Ubiquitin-like Modifier
SVR	sustained virological response
T	Thr, threonine
TAE	Tris-Acetate-EDTA buffer
TAG	Triglyceride
TC	Tissue culture
TFR1	Transferrin receptor 1
TGN	Trans-Golgi network
TIP47	Tail-interacting protein of 47 kDa
TJ	Tight junction
TLR	Toll-like receptors
TMD	Transmembrane domain
TMR	Tetramethylrhodamine
TMT	Tandem Mass Tagging
TRAM	Translocation associated membrane protein
TRAPD	Translocon-associated protein subunit delta
TRIF	TIR-domain-containing adapter-inducing interferon-β
U	Uracil
UTR	Untranslated Region
V	Val, valine

v/v	Volume by Volume
VAMP	Vesicle-associated membrane protein
VAP	VAMP-associated protein
VLDL	Very-Low Density Lipoprotein
VLDL	Very-Low Density Lipoprotein
W	Trp, tryptophan
w/v	weight by volume
WHO	World Health Organisation
WT	Wildtype
Y	Tyr, tyrosine
YFV	Yellow Fever Virus

Chapter 1: Introduction

1.1 Hepatitis C Virus

1.1.1 Identification of Hepatitis C virus (HCV)

Hepatitis refers to the inflammation of the liver and is most commonly attributed to viral hepatitis. Infectious viral hepatitis is an important challenge to health worldwide (Stanaway et al., 2016). The causative agents are mainly hepatitis A-E viruses. Hepatitis A virus (HAV) and hepatitis E virus (HEV) are endemic in many low-income countries (Rein et al., 2012, Jacobsen and Wiersma, 2010). Hepatitis B virus (HBV) and hepatitis C virus (HCV) can also cause acute illness but more commonly lead to progressive liver fibrosis, cirrhosis, and an increased risk of liver cancer (specifically hepatocellular carcinoma)(Ott et al., 2012, Mohd Hanafiah et al., 2013).

The hepatitis C virus (HCV) was first identified in 1989 as the causative agent of non-A non-B hepatitis (NANBH) (Bradley et al., 1983, van der Poel et al., 1989, Bradley et al., 1985). It is a blood-borne pathogen and is typically transmitted from exposure to blood products of an infected individual (Chen and Morgan, 2006). Prior to the identification of HCV, the major route of infection was through medical transfusion of unscreened infected blood products. After the implementation of screening the incidence of transfusion acquired HCV dramatically reduced to around 1:2,000,000 (Schreiber et al., 1996). As a result in the US there was a decline in new cases of HCV from an estimated 180,000 in 1988 to around 30,000 by 1995 (Alter et al., 1999). However, increased awareness of disease transmission on the back the HIV epidemic is likely also a factor in this reduction. Despite these dramatic reductions in transmission, due to the asymptomatic nature and long duration until clinical presentation of symptoms, it is difficult to identify acute HCV infection (Patel et al., 2016). Major routes of transmission are now mostly confined to intravenous drug use (IDU), sexual contact and parenteral transmission (Chan et al., 2016).

1.1.2 Pathology of HCV

HCV infection is a main cause of chronic liver diseases worldwide (Calvaruso et al., 2018). After infection with hepatitis C virus, most of acute infection are asymptomatic and undiagnosed, but where symptoms are observed they tend to present after 3-12 weeks, shortly after the typical peak in HCV RNA detected in the serum. More specific symptoms of viral hepatitis can be encountered in a minority of individuals including malaise, loss of appetite, nausea, vomiting, abdominal pain, joint pain and jaundice (Westbrook and Dusheiko, 2014). The level of aminotransferase and HCV RNA in serum is the routine screening indicator for HCV infection.

Following the peak of RNA (10^5-10^7 IU/ml) in serum, only 15%-25% of patients could clear the virus as the RNA becomes undetectable (Chen and Morgan, 2006). Rare percentage of acute infection will process into fulminant hepatic failure (Younis et al., 2015, Chen and Morgan, 2006).

If HCV RNA could be detected beyond 6-month infection, these patients are considered to be chronically infected. Approximately 80% of infected individuals will progress into this stage (Chen and Morgan, 2006). Chronic HCV infection induces end-stage liver diseases such as liver cirrhosis and hepatocellular carcinoma, presenting a public health problem of high socioeconomic impact with 71 million people persistently infected and more than 400 000 deaths per year (Calvaruso et al., 2018). 1–4% per year of infected individuals will develop hepatocellular carcinoma (HCC). The risk factors associated with disease progression are varied, including age at time of infection, gender, coinfection with HIV or HBV, and excessive consumption of alcohol (Chen and Morgan, 2006). In addition, progression of disease is different between genotypes. Genotype 3 infections are often self-cleared during acute infection but have a faster progression to liver fibrosis and steatosis in chronic infections, whereas individuals infected with genotype 4 are more likely to develop chronic infection (Lehmann et al., 2004, Nunez and Soriano, 2005). Liver failure and HCC caused by HCV infection is a leading cause of liver transplantation in many countries, with the added complication of graft re-infection in most cases (Rubín et al., 2011).

There is no protective vaccine against HCV yet. However, the development of direct-acting antivirals targeting different proteins and functions in HCV life cycle has dramatically changed the treatment options for chronic hepatitis C, leading to new hopes to cure HCV (Boson et al., 2017).

1.1.3 Classification of HCV and Epidemiology

HCV belongs to the *Hepacivirus* genus in the *Flaviviridae* family, which also comprises the genera *Flavivirus, Pestivirus* and *Pegivirus* (Figure 1.1A) (Simmonds et al., 2017). Members of the *Hepacivirus* genus are distinct genetically but somewhat similar in genome organisation to members of the *Flavivirus* genus and the recently assigned *Pegivirus* genus (Stapleton et al., 2011). Within *Hepacivirus* genus, HCV is currently the sole human pathogen. GB virus -B (GBV-B) and non-primate hepacivirus (NPHV) are non-human viruses, also in *Hepacivirus* genus, identified in tamarin monkeys, dogs, rodents and horses (Stapleton et al., 2011, Kapoor et al., 2013, Kapoor et al., 2011, Burbelo et al., 2012), which are more closely related to HCV.

Flaviviridae family contains many well-known pathogens, the *Flavivirus* genus is the host to yellow fever virus (YFV), dengue virus (DENV) and Japanese encephalitis virus (JEV); border disease virus (BDV) and bovine viral diarrhea virus (BVDV) belong to the *Pestivirus* genus; simian *Pegivirus* (SPgV/ GBV-A), human *Pegivirus* (HPgV/GBV-C) and bat *Pegivirus* (BPgV /GBV-D) were classified into the *Pegivirus* genus (Stapleton et al., 2011, Simmonds et al., 2017).

The classification of HCV genotypes and subtypes is mainly based on differences of nucleotide and amino acid sequence (Simmonds, 2012, Simmonds et al., 2005). Using consensus criteria, HCV isolates can be classified into 7 genotypes (1-7) and 67 subtypes (a-z) (Smith et al., 2014) (Figure 1.1B). Between genotypes, the genetic variability is approximately 30-35 %, whereas genome sequence between subtypes differs by 20-25% on the average of complete genome, in which regions in E1 and E2 glycoproteins are more variable while nucleotide sequences in core and non-structural proteins are more conserved. 5' UTR shared the highest conservation as its specific sequences and RNA secondary structures are indispensable for genome replication and translation (Simmonds, 2004).

The distribution of HCV genotypes throughout the world varies globally, showing specific geographical ranges in the human population and associations with particular risk groups for infection (Messina et al., 2015). Genotype 1 infections are mostly attributed to subtypes 1a and 1b and widely distributed globally, whereas genotype 3 is prevalent in South Asia (Figure 1.1C). Genotype 1 and 3 infections are more prevalent than all other genotypes globally (Figure 1.1C), accounting for around 83.4 million and 54.3 million infected cases, respectively. The other genotypes 2, 4-7 are responsible for the remaining cases (~25%) of HCV worldwide (Figure 1.1C). Of these, genotype 2 dominates in West Africa, genotype 4 in Central and North Africa, genotype 5 in South Africa, and genotype 6 in South East Asia, with only one genotype 7 isolate in Canada from a Central African immigrant (Figure 1.1C) (Messina et al., 2015).

A

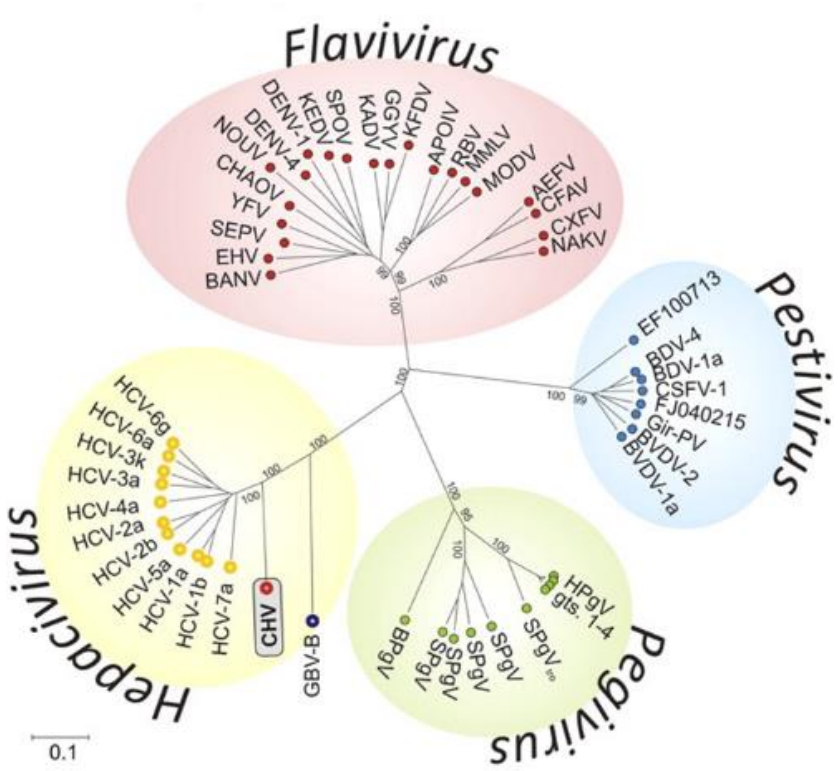
Flavivirus
DENV-1
KEDV
SPOV
KADV
GGYV
KFDV
DENV-4
NOUV
APOIV
RBV
MMLV
MODV
CHAOV
AEFV
CFAV
YFV
CXFV
SEPV
NAKV
EHV
BANV
Pestivirus
EF100713
BDV-4
BDV-1a
CSFV-1
FJ040215
Gir-PV
BVDV-2
BVDV-1a
Hepacivirus
HCV-6g
HCV-6a
HCV-3k
HCV-3a
HCV-4a
HCV-2a
HCV-2b
HCV-5a
HCV-1a
HCV-1b
HCV-7a
CHV
GBV-B
Pegivirus
HPgV
gts. 1-4
BPgV
SPgV
SPgV
SPgV
SPgV
0.1

B

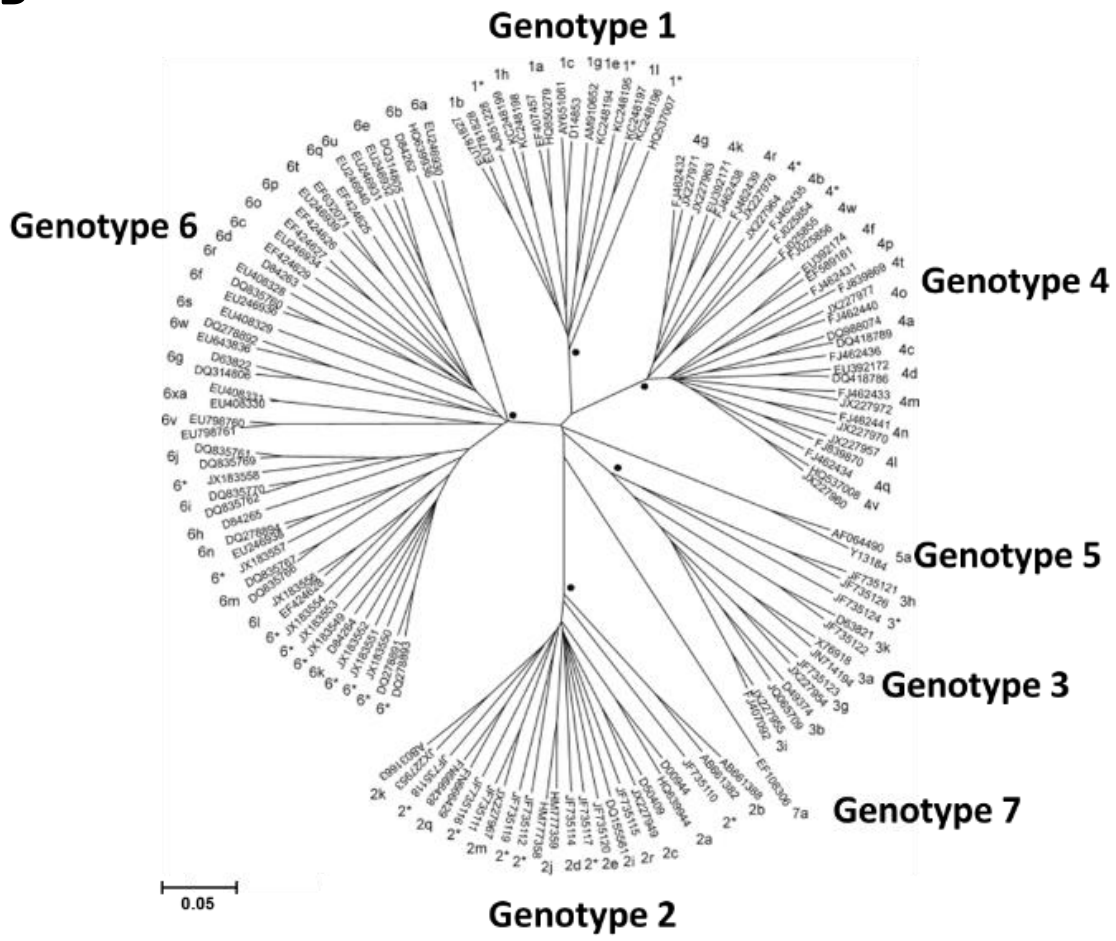
Genotype 1
Genotype 6
Genotype 4
Genotype 5
Genotype 3
Genotype 7
Genotype 2
0.05

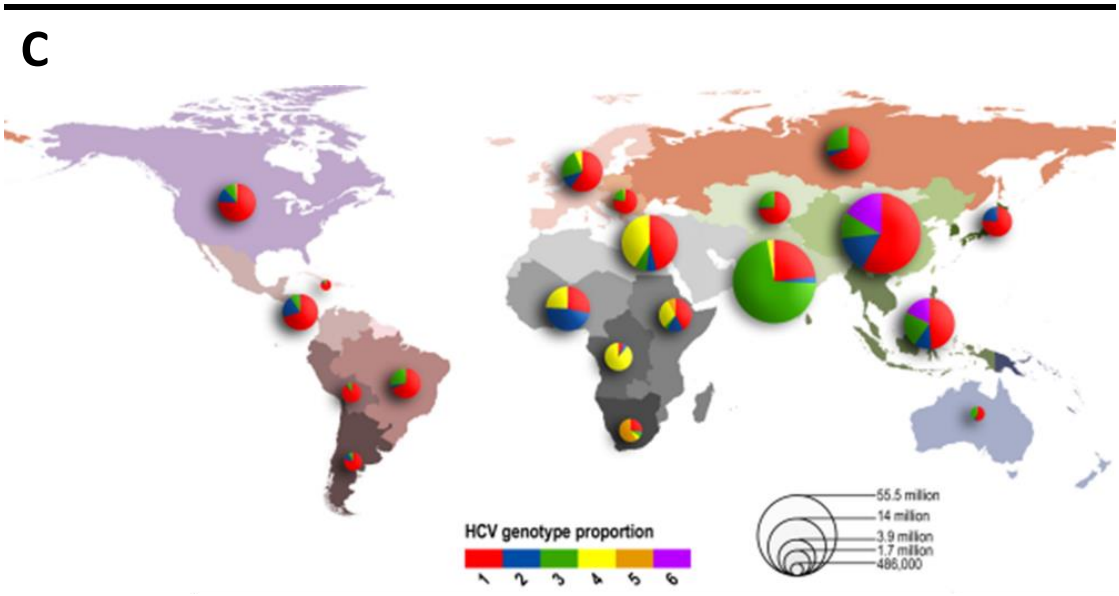

Figure 1.1 Phylogenetic analysis of the *Flaviviridae* family and HCV genotypes and the worldwide distribution.

A. Phylogenetic tree of members of the family *Flaviviridae* showing its primary division into four genera. The tree was based on comparison of conserved regions of the RNA polymerase sequences, adapted from (Kapoor et al., 2011). **B.** Evolutionary tree of 7 genotypes of HCV from 129 representative complete HCV coding sequences, adapted from (Smith et al., 2014). **C.** Global distribution of HCV by genotype and prevalence, size of pie charts is proportional to the number of seroprevalent cases, adapted from (Messina et al., 2015).

HCV is a blood borne pathogen. Acute and chronic HCV patients and chronic HCV carriers are the main source of infection. Transmission of HCV requires contact with contaminated blood products. Medical blood transfusion was the leading cause of HCV transmission (Lauer and Walker, 2001). Incidence rate caused by blood transfusion was dramatically reduced by introduction of routine screening for liver disease, increased serum alanine aminotransferase (ALT) levels and HCV antibodies (Donahue et al., 1992, Schreiber et al., 1996). Currently the majority of the new infections are through intravenous drug-use, which is estimated to account for around 80% of infections in the developed world (Sy and Jamal, 2006). In some developing countries, blood transfusion is still a route of transmission because of continued use of unsafe healthcare related practises. Other routes of transmission are much less common, such as the health care workers, from religious or cultural practices including tattooing, body piercing and acupuncture, sexual contact and perinatal transmission (Alter, 2007).

1.1.4 Therapies for HCV

With approximately 80% of acute infections processing into chronic infections, following that 10-50% of patients will progress to cirrhosis in next 20 years and develop hepatocellular

carcinoma (HCC). HCV plays an important role throughout the evolution of this progress. Hence, in order to prevent or delay the progression of hepatitis, effective antiviral therapy is of paramount importance. The aim of antiviral therapy is to maximize the inhibition of virus replication or even clear the virus, reduce liver necrosis and fibrosis to prevent the progress of cirrhosis, thereby improving the quality of lives of patients and reducing the occurrence of hepatocellular carcinoma.

Prior to the advent of direct acting antivirals (DAAs), the standard of care (SOC) for HCV infection was pegylated interferon-alpha (PEG-IFNα) and ribavirin (RBV). The efficiency of treatment for HCV was classified by a sustained virological response (SVR), defined as undetectable RNA 12-24 weeks after completing treatment. Combination of PEG-IFNα and RBV has been reported to achieve SVR in 54-63% of cases depending on the genotype treated, genotype 2 and 3 respond well to this therapy while genotype 1 is harder to treat. Typically treatment of PEG-IFNα and RBV lasts 24 weeks, which can be reduced to 12 weeks for infection of genotype 2 and 3, but extended to 48 weeks or longer for infection of genotype 1 (Hadziyannis et al., 2004, Manns et al., 2001). However, the major problem for this treatment is that patients frequently discontinue this therapy before SVR is achieved because of the side effects which include headaches, fever, arthralgia, myalgia, haemolytic anaemia, fatigue, dermatitis and depression or weight loss (Manns et al., 2001).

Patients requiring antiviral treatment are heterogeneous and include inexperienced as well as experienced patients such as relapsers, partial-responders or non-responders to combination therapy with PEG-IFNα and RBV. Relapsers initially achieve an undetectable level of HCV RNA by the end of treatment but serum HCV RNA levels become detectable sometime thereafter (Pearlman and Sjogren, 2010). A large number of patients are non-responders who do not achieve viral clearance at the end of therapy (Pearlman and Traub, 2011). There are patients who can respond and achieve a decline of HCV RNA by more than $2\log_{10}$ but still detectable at week 12 and 24, they are partial responders (Rau et al., 2012). Patients who present with acute HCV infections have 90% chance of preventing the development of chronic infection treated with PEG-IFNα alone for 24 weeks (Wiegand et al., 2006).

Treatment related side effects remains a challenge to take treatment decisions in a clinical setting with cost restrictions. Therefore predicting the patient response to therapy is a major consideration. Thus, an individualized therapy concept in clinical practice is mandatory. Together with HCV genotypes, different genetic variants have been identified with a strong association with therapy response, fibrosis and treatment-related side effects. Polymorphisms

of the interleukin 28B (IL28B) gene were identified as a baseline predictors for fibrosis progression and therapy response (Fischer et al., 2012, Rau et al., 2012, Thompson et al., 2010).

With a number of direct acting antivirals (DAA) being approved for use by the Food and Drug Administration (FDA), the treatment of HCV has been dramatically improved for HCV infected patients. The DAAs to date are mainly targeted towards the HCV non-structural proteins NS3/4A protease, NS5A or NS5B polymerase.

The first two DAAs licenced by the FDA were NS3/4A protease inhibitors boceprevir (Merk) and telaprevir (Janssen-Vertex). Both of these drugs are linear peptidomimetic structures that can reversibly form a covalent bond with the catalytic serine of NS3/4A to directly block the viral life cycle (Salam and Akimitsu, 2013, Hazuda et al., 2013, Kwong et al., 2011). To date, the single DAA in combination with RBV and PEG-IFNα are only licenced for the treatment of genotype 1 infection, which improved SVR rates from 45% to 75% (Manns and von Hahn, 2013). Despite the increased SVR rate, both boceprevir and telaprevir have a number of drawbacks such as a narrow genotype specificity and emergence of resistance-associated variants (RAVs) (for example R155K) (Sarrazin and Zeuzem, 2010, McCown et al., 2009), which calls for generation of more efficient drugs. Still targeting NS3/NS4 protease, the second generation of DAA-grazoprevir retains NS3/4A binding properties even in absence of R155K and was recently licensed in a combination therapy with the NS5A inhibitor elbasvir and RBV (Keating, 2016, Lahser et al., 2016).

The RNA-dependent RNA polymerase (NS5B) from hepatitis C virus (HCV) is a key enzyme in HCV replication. Thus, NS5B is a major target for the development of antiviral compounds directed against HCV. Hence, the second group of DAAs are targeting the viral polymerase NS5B with drugs classified into nucleotide or non-nucleotide inhibitors (Sofia et al., 2012). The non-nucleotide inhibitors inhibit the NS5B polymerase through an allosteric mechanism via binding to thumb domain site I and II or palm sites of NS5B (Kukolj et al., 2005). The representative of non-nucleotide inhibitors are beclabuvir (BMS-791325) (Rigat et al., 2014) and dasabuvir (Gentile et al., 2014). Currently, dasabuvir (Viekira Pak) was licenced in the multi DAA therapy (Mantry and Pathak, 2016). Nucleoside-based DAAs became the backbone of HCV therapeutic regimens as they show pan-genotype activity and a high barrier to resistance (Feld, 2014). Sofosbuvir, a nucleoside analogue inhibitor, is the first approved DAA with potent activity and high genetic barrier against all HCV genotypes (Marino et al., 2014).

Another effective HCV inhibitor is Daclatasvir (Bristol-Myers Squibb), targeting the NS5A protein and active at pM concentrations (Belema and Meanwell, 2014). Clinical trials to date showed that combination of Daclatasvir and Sofosbuvir with or without RBV once daily for 12 or 24 weeks achieved SVR rates >90% for genotype 1 including difficult -to -treat patients (Pol et al., 2016). Ledipasvir, velpatasvir, pibrentasvir, ombitasvir and elbasvir are all currently licenced in combination with either NS5B, NS3/NS4 protease or Cytochrome P450-3A4 inhibitors and achieved high SVR rates (Afdhal et al., 2014, Hezode et al., 2017, Poordad et al., 2017, Lawitz et al., 2015, Sulkowski et al., 2015, Kwo et al., 2017). The effectiveness of NS5A inhibitors in combination with the nucleotide inhibitor sofosbuvir indicate that this combination will become common components of many if not all therapies in the future.

Even the development of DAAs has resulted in dramatic improvement in the tolerability and efficacy of treatment of HCV, with profound potential to prevent liver disease, high price of DAAs remains the major obstacle to popularize use of DAAs. Therefore, it is necessary to find a balanced way for both patients and pharmaceutical companies to increase access to hepatitis C virus treatment (Rosenthal and Graham, 2016).

Manufacturer (Brand)	DAA (Target)	Combination therapy	Genotype
Bristol-Myers Squibb Company (Daklinza)	daclatasvir(NS5A) sofosbuvir (NS5B polymerase)	N/A	1 or 3
Gilead Sciences (Epclusa)	sofosbuvir(NS5B polymerase) velpatasvir(NS5A)	N/A[a]	1, 2, 3, 4, 5, or 6
Gilead Sciences (Harvoni)	ledipasvir (NS5A) sofosbuvir(NS5B polymerase)	b	1, 4, 5or 6
Vertex Pharmaceuticals (Incivek)	telaprevir (NS3/4A protease)	RBV / Peg-IFNα	1
AbbieVie (Mavyret)	glecaprevir (NS3/4A protease) pibrentasvir (NS5A)	N/A [c]	1, 2, 3, 4, 5 or 6
Janssen Pharma (Olysio)	simeprevir (NS3/4A protease))	RBV / PEG-IFNα[c]	1
Gilead Sciences (Sovaldi)	sofosbuvir (NS5B polymerase)	RBV / PEG-IFNα RBV	1 or 4 2 or 3
AbbVie Inc. (Technivie)	ombitasvir (NS5A) paritaprevir(NS3/4A protease) ritonavir(Cytochrome P450-3A4)	RBV	4
Merck & Co. (Victrelis)	boceprevir (NS3)	RBV / PEG-IFNα	1
AbbVie Inc. (Viekira Pak)	ombitasvir (NS5A) paritaprevir(NS3/4A protease) ritonavir(Cytochrome P450-3A4) dasabuvir (NS5B polymerase)	RBV[c]	1
Merck Sharp Dohme (Zepatier)	elbasvir (NS5A) grazoprevir (NS3/4A protease)	RBV	1 or 4

Table 1.1: Current FDA approved therapies for HCV.

a-with compensated cirrhosis or with decompensated cirrhosis for use in combination with ribavirin; b-In those with genotype 1 and advanced cirrhosis (decompensated) or with genotype 1 or 4 with or without cirrhosis (compensated) who have had a liver transplant, Harvoni is used with ribavirin; c-without cirrhosis or with compensated cirrhosis.

1.2 Molecular virology of HCV

1.2.1 Genomic organisation

HCV is a positive-sense single-strand RNA virus, prototype member of the *Hepacivirus* genus of the family *Flaviviridae* (Simmonds, 2013). The HCV genome consists of a single- stranded RNA of about 9,600 nucleotides comprising a single large open reading frame (ORF) and flanked by 5' and 3' untranslated regions (UTRs) (Figure 1.2). The 5' UTR is highly structured and consists of the internal ribosome entry site (IRES), which is important for the initiation of cap-independent translation of the polyprotein (Hashem et al., 2013). The 3'UTR consists of a short genotype-specific variable region, a tract of variable length comprising solely pyrimidine residues (predominantly U), and a conserved 98-nucleotide sequence, known as the X region, containing three stem-loops (Blight and Rice, 1997, Kolykhalov et al., 1996). The 3' UTR is the initiation site for the synthesis of the negative-strand RNA during viral replication and is involved in translational regulation (Song et al., 2006). The ORF encodes a polypeptide precursor of about 3,000 amino acids, which is cleaved co- or post translationally by cellular and viral proteases into ten mature products (Figure 1.2). The first three proteins cleaved from amino-terminal region of the polyprotein are structural proteins core (C), envelope proteins E1 and E2, which are the components of virus particles. Following them, p7 and NS2 support particle assembly while not being incorporated into the particles, denoted as non-structural (NS) proteins (Bartenschlager et al., 2011); the remaining polyprotein cleavage products are NS3, NS4A, NS4B, NS5A and NS5B, which are required for membrane-associated RNA replication (Lohmann et al., 1999a) (Figure 1.2). There is the other small ORF overlapping with the core protein ORF, encoding a single protein, alternative reading frame protein (ARFP) or frame protein (F) (Walewski et al., 2001, Varaklioti et al., 2002).

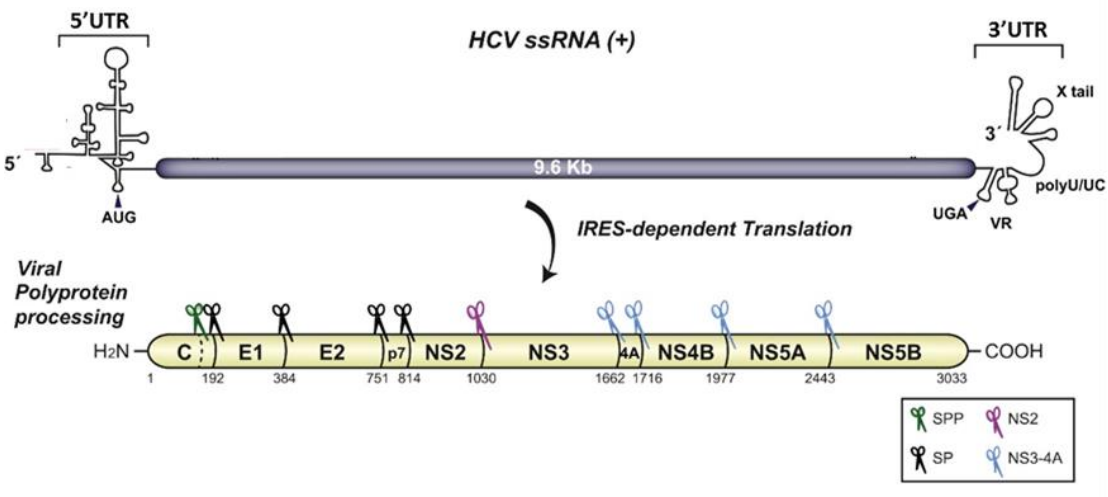

Figure 1.2 Organization of the HCV genome.

The genome of HCV consists of a single open reading frame encoding a polyprotein of approximately 3000 aa, flanked by UTRs (5'UTR and 3'UTR). Post translation, the polyprotein is cleaved by signal peptide peptidase (SPP), signal peptidase (SP), NS2- NS3 protease (NS2), and NS3 protease and NS4A complex (NS3-4A), leading to the production of functional HCV protein. Numbers refer to position of amino acids of genotype 2a JFH1 isolate (Genbank accession: AB047639). Picture is adapted from (Paul et al., 2014).

1.2.2 Structural proteins

1.2.2.1 Core protein - nucleocapsid protein

Core protein of HCV is a dimeric protein with multiple functions. The main function is to form the viral capsid to surround and protect the genomic RNA, while the virus passes from a cell to another (Polyak et al., 2006). The monomeric core containing 191 aa can be separated into two domains by different amino acid compositions and hydrophobicity profiles. Domain I, N-terminal domain, is hydrophilic and rich in basic amino acid residues, which are highly conserved. Domain I plays important roles in RNA binding and oligomerization during nucleocapsid formation, 1-82 amino acids as the intrinsically disordered region are sufficient to package genomic RNA into the virus particle (Ivanyi-Nagy et al., 2006, Fromentin et al., 2007). By contrast, domain II is hydrophobic and is responsible for coordinating core localisation to the ER and lipid droplet (LD) membranes, and is considered as the LDs binding domain (Boulant et al., 2006). Domain II contains two amphipathic helices separated by a short hydrophobic loop and interacts in-plane with the phospholipid monolayer of lipid droplets (cLDs) (McLauchlan et al., 2002). The association of core with LD is critical for assembly of viral particles (Shavinskaya et al., 2007). Apart from a function in virus assembly, core has been

shown to be involved in a number of host processes including cell apoptosis, gene transcription, cell signalling and immune regulation (McLauchlan, 2000).

1.2.2.2 E1 and E2- envelope glycoproteins

HCV E1 and E2 envelope glycoproteins are the major viral structural proteins expressed on the surface of virus particles, which are essential for viral entry and release via mediating receptor binding at the cell surface. E1 and E2 are type 1 transmembrane glycoproteins, which are translocated into the endoplasmic reticulum (ER), where they interact to form noncovalent heterodimers between their transmembrane domains and ectodomains (Duvet et al., 1998, Dubuisson et al., 2002). In the mature virions, they can form large complexes stabilised by disulphide bridges (Vieyres et al., 2010). E1 and E2 show in complicated folding patterns mediated by a range of host chaperons and are post-translationally modified by N-glycosylation in different sites (Goffard et al., 2005, Vieyres et al., 2014). X-ray crystallography revealed the structures of N-terminal domain E1 and core ectodomain of E2 (El Omari et al., 2014, Khan et al., 2014a). The E2 ectodomain consists of a compact, globular domain structure, consisting mostly of β-strands and random coil with two small α-helices. The β-strands mainly are formed by an immunoglobulin-like fold and an additional novel domain (Khan et al., 2014a). E1 N-terminal domain exhibits in homodimers and is also rich in β-sheets like E2 but with a single long α-helix sandwiched between antiparallel β strands (El Omari et al., 2014). Structural data also showed that E1 of HCV does not resemble the class II fusion protein fold, whereas other members of family *Flaviviridae* encode class II fusion proteins which mediate virion envelope fusion with the host cell membrane (Kielian, 2006). Therefore, it indicates that HCV membrane fusion mediated by E1 and E2 might proceed by another mechanism that is still unclear (Khan et al., 2015, Li and Modis, 2014).

1.2.3 Non-structural proteins

1.2.3.1 p7

Following the structural proteins is p7, a viroporin of only 63 amino acids, which is essential for virus assembly, maturation and release (Jones et al., 2007a, Steinmann et al., 2007, Wozniak et al., 2010). First, p7 is required for an early stage of virus assembly through interaction with NS2 recruiting core from LD to the proposed site of virus assembly on ER-derived membraned (Boson et al., 2011, Tedbury et al., 2011). The second major role of p7 is that it oligomerizes to form hexameric and heptameric cation-specific ion channels (Griffin et al., 2003, Premkumar et al., 2004, Montserret et al., 2010). The formation of oligomeric p7 ion

channels equilibrates pH gradients within the secretory and endolysosomal vesicles in the egress and release pathways that would otherwise increase acidic conditions and damage maturation of virions (Wozniak et al., 2010, Gentzsch et al., 2013). p7 protein is considered to be a nonstructural (NS) protein as it is not incorporated into HCV virions (Vieyres et al., 2013).

1.2.3.2 NS2

Non-structural protein 2 (NS2) is a membrane protein of 23 kDa containing three N-terminal transmembrane domains and a C-terminal cysteine protease domain. The N-terminal domain is composed of three transmembrane α-helices, which are important for anchoring NS2 to ER membranes (Jirasko et al., 2010, Jirasko et al., 2008). The C-terminal domain I is a catalytic cysteine protease which is responsible for the cleavage on the NS2-3 boundary of the HCV polyprotein by autoprotease activity (Grakoui et al., 1993). However, optimisation of HCV sub-genomic replicons demonstrated that NS2 is not required for genome replication (Lohmann et al., 1999a), NS2 protease activity is required for polyprotein processing and RNA replication of full-length HCV genomes (Kolykhalov et al., 2000, Welbourn et al., 2005). Whereas, NS2 is involved in early stage of virus assembly, bringing together E1-E2 glycoprotein complex, p7, and the NS3-4A enzyme complex within the plane of the ER membrane via N-terminal TM domains of NS2 (Phan et al., 2009, Jirasko et al., 2010, Boson et al., 2011, Ma et al., 2011, Popescu et al., 2011, Stapleford and Lindenbach, 2011). These protein-protein interactions are required to recruit core protein from LDs into sites of virus assembly (Counihan et al., 2011).

1.2.3.3 NS3/4A complex

The NS3-4A enzyme complex is essential for HCV polyprotein processing and genome replication. NS3 of 70 kDa is a multifunctional protein divided into two domains that encodes two enzymatic activities. The first N-terminal 180 residues of NS3 forms a serine protease while 181-631aa of the C-terminal domain function as NTPase/RNA helicase (Morikawa et al., 2011). The small NS4A protein (6 kDa) works as a cofactor for both NS3 serine protease and RNA helicase activities (Bartenschlager et al., 1995). NS4A contains an N-terminal TM domain, a central peptide assisting the NS3 serine protease domain, and a C-terminal acidic peptide involved in RNA replication and virus assembly, perhaps through its ability to modulate NS3 RNA helicase activity (Beran et al., 2009, Phan et al., 2011).

The N-terminal serine protease of NS3 is responsible for cleavage of both itself and the remaining of polyprotein. Post NS3 cleavage, N -terminal transmembrane domain of NS3A will anchor into ER membranes. Efficient protease processing of NS3 requires the NS4A cofactor

which both contributes to the protease fold of NS3 and anchors the NS3/4A protein to membranes. For the processing of remaining polyprotein (NS4A-NS5B), NS3/4A protease first cleaves the NS5A-NS5B boundary to release mature NS5B. The resulting NS4A-NS5A is next processed between NS4A and NS4B followed by the final cleavage at the junction of NS4B and NS5A to achieve every separate NS proteins (Morikawa et al., 2011).

The C-terminal helicase domain of NS3 is a DExH/D-box protein belonging to the RNA helicases superfamily 2 (Huang et al., 2010). The helicase activity of NS3/NS4A is shown to unwind dsRNA and highly structured RNA in a 3'–5' direction (Tai et al., 1996). High-resolution crystal structures of three conformations allowed us to unambiguously track the positional changes of RNA bound to full-length HCV NS3 during helicase activity (Appleby et al., 2011, Gu and Rice, 2010). A "ratchet" mechanism of NS3 helicase is identified in the unidirectional translocation along RNA with a step size of one base per nucleotide hydrolysis cycle, which provides the opportunities to develop specific inhibitors to block this action (Gu and Rice, 2010).

Post polyprotein processing, NS3-4A is involved in other stages of the virus lifecycle including virus assembly (de Chassey et al., 2008, Ma et al., 2008). Interestingly, mutations in NS3 that enhance RNA replication cause defects in virus assembly, suggesting that NS3 may contribute to the switch between RNA replication and virus assembly (Pietschmann et al., 2009). Furthermore, the interaction between NS2 and NS3-4A is involved in recruiting LD-associated core protein into virus assembly (Counihan et al., 2011). Moreover, HCV NS3/NS4A protease works to evade the innate immune response as MAVS, TRIF, and Riplet are the targets of NS3/NS4A protease and the cleavage by NS3/4A will inactivate both RIG-I/MDA5 and TLR3-independent antiviral innate immunity pathways (Morikawa et al., 2011, Schoggins and Rice, 2013, Li et al., 2005, Gokhale et al., 2014).

1.2.3.4 NS4B

NS4B is a highly hydrophobic protein (27 kDa), which is membrane protein that plays an essential role in the formation of HCV RNA replication complexes. It consists of two α-helices at its N-terminus, four central transmembrane domains and a C-terminal helices (Gouttenoire et al., 2010a). The second N-terminal α-helix functions as a transmembrane helix identified as a major determinant for the oligomerization of NS4B formation of the membranous web, representing sites of HCV RNA replication (Lundin et al., 2006, Gouttenoire et al., 2010b, Egger et al., 2002, Paul et al., 2011). Therefore, NS4B is important for RNA replication through

involvement in multiple interactions with other viral proteins (Jones et al., 2009, Paredes and Blight, 2008, David et al., 2015), and production of infectious HCV particles (Han et al., 2013).

1.2.3.5 NS5A

NS5A is a highly phosphorylated and multifunctional protein that play essential roles throughout HCV life cycles from genome replication to production of virus. RNA of NS5A encodes approximately 448 amino acids of 49 kDa theoretically, but actually presents in 56kDa and 58kDa forms, termed basal- and hyper-phosphorylated NS5A respectively, resolvable by SDS-PAGE analysis (Kaneko et al., 1994). It consists of three domains linked by low complexity sequences (LCS) and an N-terminal α-helix associated with phospholipid membranes (Figure 1.3A) (Tellinghuisen et al., 2004). A detailed consideration of NS5A protein will be presented in Section 1.3.

1.2.3.6 NS5B

NS5B (62 kDa) is the RNA-dependent RNA polymerase (RdRp) that replicates the viral genome by synthesis of both intermediary negative sense and positive sense RNA. It is composed of an N-terminal catalytic domain, a linker, and a hydrophobic transmembrane domain (TMD) comprising the C-terminal 21aa, anchoring the protein to intracellular membranes. Three dimensional crystal structures of HCV NS5B showed in a typical right-hand shape with fingers, thumb, and palm subdomains, which is shared by most other polymerases (Ago et al., 1999, Bressanelli et al., 1999, Lesburg et al., 1999). Fingers and thumb subdomains provide important contacts for the nucleic acid substrate, while the palm contains the catalytic active site. These subdomains form the so-called ‘‘closed’’ conformation of the polymerase for initiation of RNA synthesis. De novo priming by NS5B at the 3’ UTR requires two nucleotide binding sites in the catalytic pocket to synthesize a dinucleotide stimulated by high concentrations of GTP (Ferrari et al., 2008, Lohmann et al., 1999b). Binding of GTP to NS5B is likely to trigger the conformational changes of NS5B from closed formation to RNA elongation state which open the catalytic pocket to accommodate dsRNA (Harrus et al., 2010, Ranjith-Kumar et al., 2003, Mosley et al., 2012, Scrima et al., 2012). Compared with genotype 1, JFH1 from genotype 2a exhibited a much-closed conformation of NS5B that is more suited to hold a single-stranded template required for *de novo* initiation of RNA synthesis. This structural property of JFH1 contributes to the higher replication efficiency than genotype 1 isolates (Simister et al., 2009).

The catalytic palm pocket contains a GDD motif of NS5B polymerase active site responsible for coordinating two magnesium ions (Jablonski and Morrow, 1995). GDD motif is typically

mutated into GND to inactivate NS5B polymerase by disrupting its coordination, and this mutation (GND) is usually used as a non-replicating (polymerase-defective) negative control in our research.

1.3 NS5A

1.3.1 Structure of NS5A

The Non-Structural 5A protein (NS5A) is a 49 kDa protein, however 56 and 58 kDa forms, termed basal- and hyper-phosphorylated respectively, are resolvable by SDS-PAGE (Neddermann et al., 1999), which has an essential role throughout the virus life cycle (Ross-Thriepland and Harris, 2014b, Ross-Thriepland and Harris, 2015). It is comprised composed of three major domains (I, II and III) linked by low complexity sequences (Tellinghuisen et al., 2004) (Figure 1.3A). The protein is anchored to phospholipid membranes by an N-terminal amphipathic helix (residues 1-33) in a manner essential for replication (Brass et al., 2002, Penin et al., 2004).

NS5A N-terminal membrane anchor domain (1-33aa) is highly conserved (Brass et al., 2007) and its helical structure is the determinant for ER membrane targeting and binding, which provides a platform for the stabilization of NS5A in the HCV replication complex (Penin et al., 2004, Brass et al., 2002, Sapay et al., 2006). N-terminal amphipathic helix domain is embedded in-plane in the cytosolic leaflet of the ER membrane, with a hydrophobic side buried in the membrane and a polar/charged side accessible from the cytosol. The Trp rich, N-terminal amino acids 5 to 12 of the helix, seem to be located more closely to the membrane interface, whereas the Lys-rich, C-terminal amino acids 19 to 26 appears to be buried slightly more deeply into the hydrophobic core of the membrane (Penin et al., 2004, Brass et al., 2002). N-terminal membrane anchor is functionally conserved among HCV and related viruses, which is essential for the assembly of a functional viral replication complex (Brass et al., 2002, Penin et al., 2004, Sapay et al., 2006, Brass et al., 2007).

Following the α-helix, is a both conserved and highly structured domain I which folds into an unusual structure and mediates homodimerization. Domain I is the only domain of NS5A with a crystal structure (Lambert et al., 2014, Love et al., 2009, Tellinghuisen et al., 2005). The structures revealed that domain I coordinates a zinc atom within a tetracysteine motif, has a disulphide bond at the C terminus, and the presence of a basic RNA-binding groove between the NS5A dimer interfaces (Figure 1.3B). Both structure and function of domain I are introduced in detail in section 5.1.

Although dimeric in the crystal structure, limited evidence exists to support a dimeric structure in vivo (Lim et al., 2012). Models for NS5A dimers associated with the membrane have been proposed, however these lack experimental evidence (Ross-Thriepland and Harris, 2015). Both the tetracysteine motif and disulphide bond are required for maintaining the structure of domain I (Tellinghuisen et al., 2005).

A number of HCV related hepaciviruses have been identified which share a high degree of sequence homology with domain I but not domains II and III (Burbelo et al., 2012, Kapoor et al., 2011, Kapoor et al., 2013). Secondary structure prediction programs indicate that the organisation of NS5A into three domains separated by LCS are shared among the hepaciviruses (Lauck et al., 2013).

Unlike domain I, domain II and domain III are natively unfolded (Liang et al., 2007, Hanoulle et al., 2009b, Verdegem et al., 2011). Structural analysis of domain II by nuclear magnetic resonance(NMR) identified α-helical structures within domain II containing a classical poly-proline Src homology 3 (SH3) binding motif (Feuerstein et al., 2012). Domain III of NS5A is less conserved and apparently possesses a great deal of inherent flexibility (Remenyi et al., 2014, Tellinghuisen et al., 2008b, Arumugaswami et al., 2008), as it tolerates large heterologous insertions, such as green fluorescent protein (GFP), and still retains its activity during RNA replication (McCormick et al., 2006, Moradpour et al., 2004).

The first low complexity sequence (LCS I), a region rich in serine, is composed of 36 amino acids and links domain I and domain II. LCS I is absolutely conserved across all genotypes of HCV, implying an essential role in the virus life cycle. It is documented that LCS I is the predominant location for phosphorylation of NS5A (Ross-Thriepland and Harris, 2014b, Katze et al., 2000, Lemay et al., 2013, Appel et al., 2005b, Hsu et al., 2017). More recent research point out that phosphorylation of NS5A is by regulatory mechanisms via sequential phosphorylation cascade such that phosphorylation of S235 is a prerequisite to S238 phosphorylation (Hsu et al., 2017). However, the exact mechanism remains to be further elucidated.

The low complexity sequence II (LCSII) is a short (13aa), proline rich region of NS5A linking domain II and III. Within this region, there are two closely spaced polyproline motifs that are able to bind to the SH3 domains of Src-family tyrosine kinases, which are involved in RNA replication and viral assembly (Macdonald et al., 2004, Ross-Thriepland and Harris, 2014a).

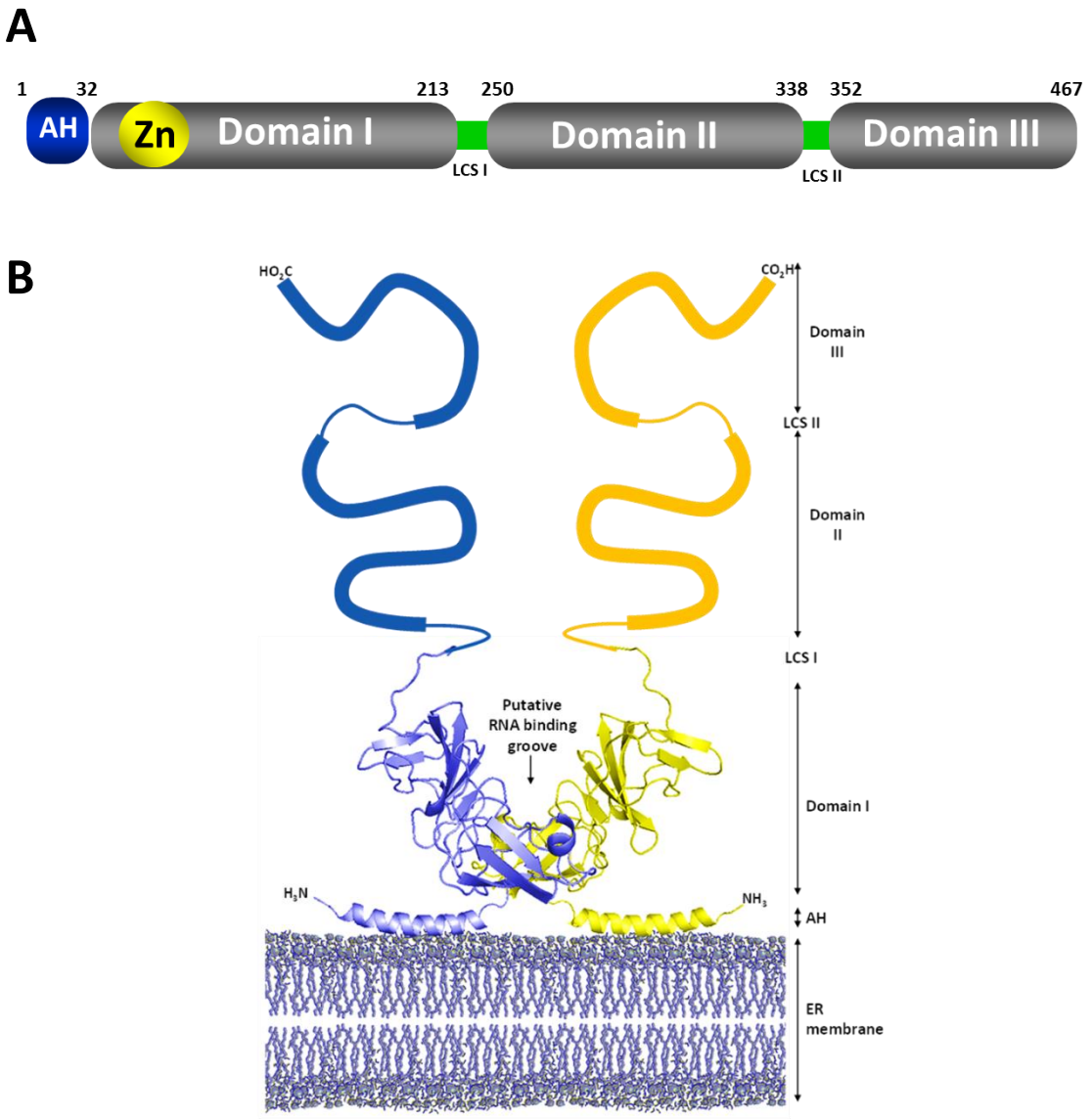

Figure 1.3 Schematic representation of NS5A protein.

A. NS5A is composed of three domains divided by two low complexity sequences (LCS I and LCS II) and is linked with an N-terminal (1-33aa) amphipathic helix (AH). Domain I coordinates a zinc ion in a highly ordered manner. Number of positions is based on genotype 2a JFH1 isolate. **B.** Model of structure of N5SA. AH anchors to the membrane and two domain I monomers form into the dimeric conformation revealed by (Tellinghuisen et al., 2005). The unstructured domain II and III are illustrated.

1.3.2 Functions of NS5A in HCV lifecycle

NS5A plays multifunctional roles in different stages of the virus lifecycle from genome replication to virus assembly, the separation of which is regulated by different domains of NS5A. As a membrane-bound protein, the N-terminal α-helix plays a critical role in membrane association (Palomares-Jerez et al., 2010, Brass et al., 2002) and also is required for RNA replication (Elazar et al., 2003). Domains I and II are mostly required for genome replication (Tellinghuisen et al., 2005, Ross-Thriepland et al., 2013). In comparison, although domain III contributes to genome replication it is dispensable and is instead required for HCV assembly (Tellinghuisen et al., 2008b, Tellinghuisen et al., 2008a, Hughes, 2010, Hughes et al., 2009b, Hughes et al., 2009a, Appel et al., 2008, Zayas et al., 2016).

Within the membrane anchoring N-terminal fragment of NS5A, introduction of three helix-disrupting mutations completely abrogated the ability of the replicon to establish G418-resistant colonies, implying that NS5A membrane association is an indispensable event during HCV RNA replication (Elazar et al., 2003, Penin et al., 2004).

The detailed functions of domain I throughout the HCV life cycle will be described in Section 5.1.

The serine-rich cluster LCS I linking domain I and domain II is highly phosphorylated, and is involved in genome replication and virus assembly. It was proposed that hyperphosphorylation inhibits genome replication as it was identified that mutations that significantly reduce hyperphosphorylation yet have no effect on either genome replication or virus assembly and release (e.g., S146D and S225D) (Ross-Thriepland and Harris, 2014b).

In contrast to domain I, domain II has been more extensively studied and is well known to be involved in replication and virus assembly via interactions with viral and host proteins. Apart from the N-terminal 30 residues of this domain, residues spanning the remainder were shown to be essential for genome replication with different genotypes (Tellinghuisen et al., 2008b, Appel et al., 2008, Ross-Thriepland et al., 2013). Intriguingly, there were a number of residues towards the C terminus of domain II that were conserved between the two genotypes (1b and 2a) yet when mutated exhibited different phenotypes, for example Y317A in JFH1 had a null phenotype (Ross-Thriepland et al., 2013) but was lethal in the corresponding residue in Con1 (Y321A) (Tellinghuisen et al., 2008b) and mutations of residues W312, A313, Y330 and V336 in JFH1 were lethal, but in Con1 the corresponding mutations have either a null or partial

phenotype. This observation suggests that it is not possible to extrapolate between the different genotypes and may perhaps reflect differences in protein - protein interactions.

Between domain II and III, there are two closely spaced polyproline motifs (termed PP2.1 and PP2.2), with the consensus sequence Pro-X-X-Pro-X-Lys/Arg in LCS II shared by both genotypes 1b and 2a, which have been characterized to mediate interactions with cellular SH3 domains. Mutagenesis analysis proved that LCS II is required for both RNA replication and virus assembly (Hughes et al., 2009a). PP2.1 has been shown to be only required for genotype 1b RNA replication. It's worth mentioning that P346A within PP2.1 dramatically attenuated genotype 1b replication, but corresponding P342A in genotype 2a showed a reduction in virus production without any effect on RNA replication (Hughes et al., 2009a). PP2.2 is not required for RNA replication of all subgenomic replicons, while it may play roles in virus persistence through ion channel modulation and inhibition of apoptosis (Mankouri et al., 2009, Amako et al., 2013).

NS5A domain III is mostly involved in virus assembly. In particular, the C-terminal 38 amino acids are required for virus assembly. Deletions in domain III perturb co-localisation between NS5A with core on LDs, suggesting that it might be linked with production of infectious virus. Based on this evidence, a model is put forward in which core recruits either NS5A or the NS5A-containing replication complex (RC) via direct interaction with domain III to the assembly site (Appel et al., 2008). Additionally , a 19-residue insertion near the C terminus of domain III found exclusively in genotype 2 HCV isolates is dispensable for assembly, with deletion only modestly effecting genome replication (Hughes et al., 2009b). A C-terminal serine cluster in domain III, a determinant of the NS5A-core interaction via phosphorylation, is important for virion production (Masaki et al., 2008). Mutations of serine 452,454 and 457 disrupt the interaction with core and reduce the amount of RNA co-immunoprecipitated with core. Of note, these mutations shift the localisation of NS5A from fractions enriched in LD proteins towards ER fractions, indicating that domain III is important to regulate RNA replication and HCV particle formation. Additional evidence shows that mutations in NS5A that enhance RNA replication cause decreases in virus assembly, suggesting that NS5A may contribute to the switch between replication and assembly (Pietschmann et al., 2009).

1.3.3 NS5A-interacting partners

1.3.3.1 RNA

As one important component of the replication complex essential for RNA replication, NS5A has been shown to bind RNA in vitro (Foster et al., 2010, Huang et al., 2005). It is also demonstrated that each of the three domains possess the ability to bind the HCV 3'UTR. For the binding determinant in 3'UTR, full-length NS5A lacking the N-terminal amphipathic helix exhibited a higher affinity for the poly(U/UC) region than for the X-region (Foster et al., 2010). Peptidyl-prolyl isomerase cyclophilin A (CypA) can bind to domain II and stimulate the RNA-binding activity of domain II but not of domains I and III (Foster et al., 2011). Detailed biochemical characterization of NS5A-RNA binding revealed that it was inhibited by a high concentration of EDTA, implying a requirement for Zn^{2+} or other divalent cations. Cysteines (Cys-39, Cys-57, Cys-59, and Cys-80) of NS5A domain I critical for dimerization are also important for RNA-binding and replication (Lim et al., 2012). It is proposed that dimerization of domain I is correlational with RNA binding activity of NS5A domain I. Based on the nature of revealed structures of domain I, there is a large groove in dimers providing an attractive RNA-binding pocket (Tellinghuisen et al., 2005). However, the mechanism of how NS5A is involved during RNA synthesis remains to be determined. These experiments might ultimately provide clues as to how the replicase machinery works to replicate HCV RNA.

RNA binding of NS5A plays an essential role in the switch from RNA replication to virus assembly. It was reported that mutation blocks the NS5A-core protein interaction, resulting in perturbation of association between the core protein and HCV RNA. It is thus tempting to consider that NS5A can transport the viral genome RNA synthesized by the replication complex to the surface of LDs or LD-associated membranes, where the core protein localizes, leading to facilitation of nucleocapsid formation (Masaki et al., 2008).

1.3.3.2 Viral proteins

Apart from RNA binding activity, when NS5A is involved in the replication complex it can interact with various cellular factors and viral proteins, which are required for HCV replication (Paul et al., 2014). In the replication complex, the phosphorylation of NS5B RdRp was activated by NS5A, at least in vitro. This activation might be mediated by the RNA-binding ability of NS5A or by direct interaction with NS5B (Shirota et al., 2002, Quezada and Kane, 2013). It was also shown that deletions within NS5A that abrogated the interaction with NS5B also rendered the

subgenomic replicon non-functional, whereas a deletion that had no effect on NS5B binding was replication-competent (Shimakami et al., 2004).

Interestingly, NS4B, together with NS3 and NS4A, seem to be directly involved in modulation of NS5A hyperphosphorylation (Koch and Bartenschlager, 1999, Neddermann et al., 1999). NS4B direct association with NS5A might thus play a role in the regulation of NS5A hyperphosphorylation. Recent research demonstrated that domain I of NS5A was sufficient to mediate its interaction with NS4B, and then affect viral genome replication (David et al., 2015).

A combination of standard biochemical and genetic protein-protein interaction assays, demonstrated that NS5A was able to interact independently with all the non-structural proteins, including itself (Dimitrova et al., 2003). Taken together with these observations, it is clear that NS5A does indeed participate in a multi-protein replication complex. However, the molecular details of the structure and function of this complex remain major challenges.

NS5A participation in virus production has been demonstrated to result from its interaction with core protein. Alanine substitutions for the C-terminal serine cluster in domain III of NS5A impaired NS5A basal phosphorylation, leading to a marked decrease in NS5A-core interaction, disturbance of the subcellular localization of NS5A, and disruption of virion production (Masaki et al., 2008).

1.3.3.3 Host factors

Due to the tight interplay between the HCV non-structural proteins during viral replication and assembly, proteomics approaches have been used to characterize these interactions (Douam and Ploss, 2015), which could also be targeted by antiviral therapies. Targeting NS5A, over 130 cellular interaction partners have been identified by proteomic approaches (Tripathi et al., 2013), of which approximately 60 proteins have been proved to function with NS5A during HCV life cycle. The explanation that NS5A can interact with a large number of partners is likely the intrinsically disordered domains II and III, which might adopt different conformations (Feuerstein et al., 2012).

1.3.3.3.1 **Host factors required for RNA replication**

A great number of host proteins have been shown to interact with NS5A in a manner critical for the replication of HCV. Firstly, HCV replication is intrinsically linked to lipid metabolism in hepatocytes (Kapadia and Chisari, 2005). Recruitment and activation of the lipid kinases by HCV is essential for integrity of the membranous web and RNA replication. Of them, NS5A

directly interacts and activates the phosphatidylinositol 4-kinase (PI4K) IIIα which increases the quantity of Phosphatidylinositol 4-phosphate (PI4P), which is required to maintain the membranous web (Reiss et al., 2011). Four conserved amino acids (PFIS) at the C-terminus of domain I of NS5A are responsible for this interaction resulting in the activation of kinase, but negatively regulating of NS5A hyperphosphorylation (Reiss et al., 2013).

Cyclophilins, a family of peptidylprolyl isomerase (PPIase), exhibit as critical host factors for a variety of viruses (Kapadia and Chisari, 2005). Two isoforms CypA and CypB have been shown to be important for RNA replication through interaction with NS5A (Verdegem et al., 2011, Coelmont et al., 2010, Foster et al., 2011, Chatterji et al., 2009, Hanoulle et al., 2009a). With the development of several CypA inhibitors in clinical trials, the majority of research is to understand the molecular mechanism of NS5A-CypA interactions (Paeshuyse et al., 2006). Structural analysis suggests that the active site of CypA interacts with C-terminus of domain II to further catalyse the cis-trans isomerisation of the peptide bond within this region (Coelmont et al., 2010, Grise et al., 2012). Moreover, it has been shown that CypA stimulates RNA binding of NS5A domain II in an isomerase dependent manner. Hence, the role of CypA in the enhancement of HCV RNA replication may be dependent, to some extent, on its stimulation of the RNA binding ability of NS5A (Foster et al., 2011).

As has been mentioned in the section of structure of NS5A, LCSII of NS5A contains two polyproline motifs, providing SH3 domains binding regions. A number of cellular proteins contain Src homology 3 (SH3) domains which mediate protein-protein interactions with NS5A. Such interactions cause the regulation of apoptosis through the SH3-domain-containing kinase mixed lineage kinase 3 (Amako et al., 2013) and amphiphysin II (Zech et al., 2003), and trafficking of epidermal growth factor receptor (Mankouri et al., 2008) through the Cas ligand with multiple SH3 domains (Mankouri et al., 2008, Igloi et al., 2015).

Comparison of messenger RNA (mRNA) expression levels in chronic hepatitis C (CHC) liver biopsies identifies that cholesterol25-hydroxylase (CH25H) mRNA is up-regulated. Moreover, a product produced by CH25H, 25-hydroxycholesterol (25HC), profoundly blocks HCV RNA replication by preventing formation of the viral replication factory via directly interacting with and inhibiting NS5A dimerization (Anggakusuma et al., 2015, Chen et al., 2014). Kinase Raf-1 is another cellular binding partner of NS5A, binding to the C-terminal domain of NS5A, which has been identified to be crucial for HCV replication (Burckstummer et al., 2006). It is worthy to note that TBC1D20 and its cognate GTPase Rab1 play important roles in virus replication via

interaction with NS5A around LD, which might be involved in the recruitment of other host mediators to promote the viral life cycle (Nevo-Yassaf et al., 2012).

Mass spectrometry studies on NS5A have identified multiple phosphorylation sites within the NS5A LCSI and indicate a complex regulation of NS5A functions (Lemay et al., 2013, Masaki et al., 2014, Ross-Thriepland and Harris, 2014b). A number of host kinases have been reported to phosphorylate NS5A (Table 1.2). Serine 457 of NS5A domain III is likely a target for casein kinase II (CKII) phosphorylation and phosphorylation of this residue appears to be an important regulatory step in infectious virus production (Kim et al., 1999, Tellinghuisen et al., 2008a). CKI-α has been shown to phosphorylate S232 dependent on S229 phosphorylation (Quintavalle et al., 2007). Inhibition and siRNA silencing studies have confirmed the activity of CKI-α on NS5A in vivo indicating that S225 and S232 may be key residues for CKI-α-mediated NS5A hyperphosphorylation and regulation of virion assembly (Masaki et al., 2014). Alanine substitution of serine 225 (S225A) in LCSI resulted in the reduction in both NS5A hyperphosphorylation and genome replication. Quantitative proteomic analysis of NS5A-interacting proteins between WT and S225A revealed that nucleosome assembly protein 1-like 1 (NAP1L1) interacting with NS5A contributes to genome replication and the distribution of replication complexes throughout the cytoplasm (Goonawardane et al., 2017). In reverse, NS5A targets NAP1L1 to modulate the innate cellular response via activating RIG-I and Toll-like receptor 3 (TLR3) antiviral responses (Cevik et al., 2017). Threonine 356 in domain III can be phosphorylated by PKA (Cordek et al., 2014). Inhibition of PKA reduces the infectivity of secreted virus particles with no effect on replication or the formation of intracellular infectious particles (Farquhar et al., 2008). PLK phosphorylates NS5A in vitro to both the 56 and 58 kDa forms, PLKI inhibitors reduce HCV NS5A S235 phosphorylation and further impair HCV replication (Lee et al., 2016, Chen et al., 2010a). The vesicle-associated membrane protein (VAMP)-associated protein A and B (VAP-A /B) have been identified be to also involved in phosphorylation of NS5A (Evans et al., 2004, Goonawardane et al., 2017, Gao et al., 2004, Hamamoto et al., 2005) . VAP-A interacts with both NS5A and NS5B and knockdown of VAP-A results in relocalisation of NS5B and a small reduction in RNA replication (Gao et al., 2004). There is an inverse correlation between NS5A phosphorylation and VAP-A binding, which suggests a possibility that hyperphosphorylation of NS5A disrupts interaction with VAP-A and negatively regulates viral RNA replication (Evans et al., 2004).

Host Protein	Functions	Determinant in NS5A	Reference
AmphII	Inhibits phosphorylation of NS5A	Unknown	(Masumi et al., 2005)
CH25H	Inhibits RNA replication	Domain I	(Chen et al., 2014, Anggakusuma et al., 2015)
CKII	Phosphorylation of NS5A	Serine in domain III	(Tellinghuisen et al., 2008a)
CKIα	Hyperphosphorylation of NS5A	LCSI serine residues	(Masaki et al., 2014, Quintavalle et al., 2007)
Cyp A	RNA replication	C-terminus of Domain II and Domain III	(Foster et al., 2011, Chatterji et al., 2009, Hanoulle et al., 2009a)
FBP	RNA replication	Unknown	(Zhang et al., 2008)
FKBP8	RNA replication	Unknown	(Okamoto et al., 2006)
GPS2	RNA replication	Domain I	(Xu et al., 2013)
hB-ind1	RNA replication	Unknown	(Taguwa et al., 2008)
HSP72	RNA replication	Domain I	(Chen et al., 2010b)
NAP1L1	Phosphorylation of NS5A	Serine 225 in LCSI	(Goonawardane et al., 2017)
PI4KIIIα	Phosphorylation of NS5A, membranous web formation and RNA replication	C-terminus of domain I	(Reiss et al., 2011, Reiss et al., 2013)
Pin1	RNA replication		(Lim et al., 2011)
PKAα	Phosphorylation of NS5A	Threonine in domain III	(Cordek et al., 2014)
PLKI	Hyperphosphorylation of NS5A	Serine in LCS I	(Lee et al., 2016, Chen et al., 2010a)
Rab1	Replication	Unknown	(Nevo-Yassaf et al., 2012)
Rab18	Replication and virus release	Unknown	(Salloum et al., 2013)
Raf-1	RNA replication	C-terminus of NS5A	(Burckstummer et al., 2006)
TBC1D20	RNA replication	N -terminus of NS5A	(Sklan et al., 2007b, Nevo-Yassaf et al., 2012)
VAP-A	Hyperphosphorylation of NS5A and RNA replication	Serine in LCS I	(Evans et al., 2004, Goonawardane et al., 2017, Gao et al., 2004)
VAP-B	Hyperphosphorylation of NS5A and RNA replication	N-terminus and C-terminal polyproline cluster	(Hamamoto et al., 2005, Goonawardane et al., 2017)

Table 1.2 NS5A interacting proteins required for RNA replication and NS5A phosphorylation.

AmphII: Amphiphysin II; CH25H: Cholesterol 25-hydroxylase; CKII: Casein Kinase II; CKIα: Casein Kinase I-alpha; FBP: Far upstream element of the c-myc proto- oncogene (FUSE) binding protein; FKBP8: FK506-binding protein; GPS2: G protein pathway suppressor 2; hB-ind1: Human butyrate-induced transcript 1; HSP72: Heat shock protein 72; nucleosome assembly protein 1-like 1 (NAP1L1); PI4KIIIα: Phosphatidylinositol-4 kinase III alpha; Pin1: peptidyl-prolyl cis-trans isomerase NIMA- interacting 1; PKAα: cAMP-dependent protein kinase A-α subunit PKA ; PLKI: Polo-like Kinase I; Rab1/18: Ras-related protein 1 AND 18; TBC1D20:(Tre-2, Bub2, and Cdc16)-1 domain family, member 20; VAP-A/B: Vesicle-associated membrane protein (VAMP)-associated protein A/B.

1.3.3.3.2 **Host factors required for virus assembly**

It is widely accepted that domain III of NS5A is mostly involved in virus production so that the protein-protein interaction of NS5A participating in virus assembly are attributed to domain III (Table 1.3).

Proteomic analysis of HCV replication complexes has shown that the NS5A protein interacts with Annexin A2 mediated by domain III. Intriguingly, knockdown of annexin A2 does not impair viral RNA replication but significantly reduces infectious HCV titers with decreased secretion of viral core protein. Therefore, ANXA2 might play a role in assembly rather than the release of infectious HCV virions but remains to be investigated (Backes et al., 2010).

The interaction of NS5A with apolipoproteins is important for the formation of lipoparticles and virus assembly and maturation (Section 1.4.1). Both yeast two-hybrid system and biochemical analysis demonstrate that ApoE can directly interact with NS5A and furthermore knockdown of ApoE has shown to impair the production of virus. The interaction between NS5A and ApoE can be disrupted by the deletion of domain III. Moreover, mutations at the positions 99 to 101 or 102 to 104 of NS5A domain I (JFH1AAA^{99} and JFH1AAA^{102}) were also identified to abrogate the interaction with ApoE, which can explain why these mutants of domain I failed to the produce infectious viruses (Miyanari et al., 2007, Benga et al., 2010). This is the only case that is related to domain I that is involved in virus assembly. Apolipoprotein J, a glucose-upregulated VLDL-associated molecular chaperone, can interact with HCV core and NS5A and stabilize the dual protein complex (Lin et al., 2014).

Diacylglycerol acyltransferase 1 (DGAT1) was initially found to interact with HCV core protein and catalyse core trafficking to LD for virus assembly (Herker et al., 2010). Subsequently it was shown that DGAT1 could also bind NS5A, enhance interactions of NS5A with the viral capsid core, and enable lipid droplet localization of NS5A (Camus et al., 2013). Hence, DGAT1, core and NS5A interact in one complex, DGAT1 serves as a cellular hub guiding both core and NS5A onto the surface of LDs. A catalytically inactive mutant of DGAT1 (H426A) blocks the localization of NS5A, but not core, which suggests that catalytical determinants in DGAT1 are different for NS5A and core (Camus et al., 2013).

Proteomics analysis with NS5A tagged with Strep-tag protein revealed that oxysterol binding protein (OSBP) is an NS5A interacting partner with domain I as the approximate binding site for OSBP. OSBP deletion mutation failed to localize NS5A to the Golgi compartment, which

provides a possibility that interaction of OSBP and NS5A play roles in the viral assembly and or secretion processes (Amako et al., 2009).

Phosphatidylserine-specific phospholipase A1 (PLA1A) is another important host factor that is involved in the initiation of the viral assembly in close proximity to core-decorated LDs interaction with E2- NS2 complex, and NS5A-associated replication complex (Guo et al., 2015). Similarly, Rab18, a member of the Rab family of small GTPases, also promotes interaction between NS5A and LDs and may also enhance virion assembly by bringing sites of replication in close physical proximity to sites of virion assembly. In addition, the recruitment of NS5A to LDs could be inhibited by shRab18 RNA, but HCV core protein can localize with LDs, suggesting that the interaction between core protein and LDs is Rab18-independent (Salloum et al., 2013).

Tail-Interacting Protein 47 (TIP47), as a lipid droplet-binding protein, plays multi-roles throughout HCV life cycle. It is documented that overexpression of TIP47 increases the amount of released viruses, while silencing of TIP47 abolishes virus replication (Ploen et al., 2013). More evidence points out that it is TIP47 recruiting LD containing membranes to membranous web that facilitates RNA replication via interaction with NS5A (Vogt et al., 2013).

Host protein	Function	Determinant in NS5A	Reference
Annexin A2 (ANXA2)	Virus assembly	Domain III	(Backes et al., 2010)
Apolipoprotein E (ApoE)	Virus assembly	Domain I and III	(Benga et al., 2010)
Apolipoprotein J (ApoJ)	Virus assembly	Unknown	(Lin et al., 2014)
Diacylglycerol acyltransferase 1 (DGAT1)	Virus assembly	Unknown	(Camus et al., 2013)
Oxysterol binding protein (OSBP)	Virus assembly	Domain I	(Amako et al., 2009)
Phosphatidylserine-specific phospholipase A1(PLA1A)	Virus assembly	Unknown	(Guo et al., 2015)
Rab18	Virus assembly	Unknown	(Salloum et al., 2013)
Tail-Interacting Protein (TIP47)	Virus production	Unknown	(Ploen et al., 2013, Vogt et al., 2013)

Table 1.3 NS5A interacting proteins required for virus assembly.

1.4 Lifecycle of HCV

1.4.1 HCV virus particle composition

HCV particles are enveloped and contain the viral core protein, which likely combines with the viral genome to form a nucleocapsid, and two surface glycoproteins, E1 and E2 (Figure 1.4A). Filtration and electron microscopy (EM) studies have identified predominately spherical particles with a heterogeneous diameter of 40-80 nm, which are more irregular in structure in comparison with other members of the Flaviviridae family (Bradley et al., 1985, Gastaminza et al., 2010, He et al., 1987, Merz et al., 2011, Catanese et al., 2013). However, despite many efforts, the clear architecture and composition of the HCV particle has remained enigmatic.

The HCV life cycle is closely linked to the hepatic lipoprotein metabolism as viral particles associate with lipoproteins and lipids during maturation to form lipoviroparticles (LVPs) (Andre et al., 2002). The most striking feature of infectious HCV particles is its buoyant density, which is unusually low and heterogeneous for an enveloped RNA virus. Both serum-derived HCV and HCV derived from cell culture (HCVcc) particles with high specific infectivity have buoyant densities ranging between <1.06 g/ml in the case of serum-derived particles (Andre et al., 2002) and ~1.1g/ml for HCVcc's (Lindenbach et al., 2005, Hijikata et al., 1993, Lindenbach et al., 2006), which is significantly lower than those of other enveloped RNA viruses. Moreover, HCVcc particles produced in Huh7-derived cells show a higher buoyant density compared to *in vivo*- or primary hepatocyte-derived samples, correlating with a lower specific infectivity (Podevin et al., 2010, Lindenbach et al., 2006). As Huh7 cells are deficient in lipoprotein metabolism, they do not produce very low-density lipoproteins (VLDLs), and produce instead apolipoprotein B (ApoB)-containing particles that resemble low-density lipoproteins (LDLs) (Podevin et al., 2010, Meex et al., 2011).

The low density of the HCV virion is tightly associated with lipoprotein components such as apolipoprotein A-I (apoA-I), apoB-48, apoB-100, apoC-I and apoE in low-density lipoprotein (LDL) or very low-density lipoproteins (VLDL) particles (Figure 1.4B) (Catanese et al., 2013, Thomssen et al., 1992, Kono et al., 2003, Felmlee et al., 2010, Diaz et al., 2006), and their lipid composition is similar to serum lipoproteins by lipid profiling of highly purified HCVcc particles (Merz et al., 2011). Therefore, it is proposed that HCV particles form hybrid lipoviral particles (LVP), either through transient interactions with serum lipoproteins in the two-particle model (Figure 1.4C), or by directly sharing an envelope with a low-density lipoprotein (LDL) in the single particle model (Figure 1.4D). The two-particle model (Figure 1.4C) is much more favourable as HCVcc particles chemically stripped of cholesterol lose their infectivity, which can

be restored by adding back exogenous cholesterol (Aizaki et al., 2008). Moreover, the buoyant density of HCV particles in serum rapidly shifts in relation to dietary triglycerides, suggesting that the interaction of HCV particles with serum lipoproteins is transient and exchangeable (Felmlee et al., 2010).

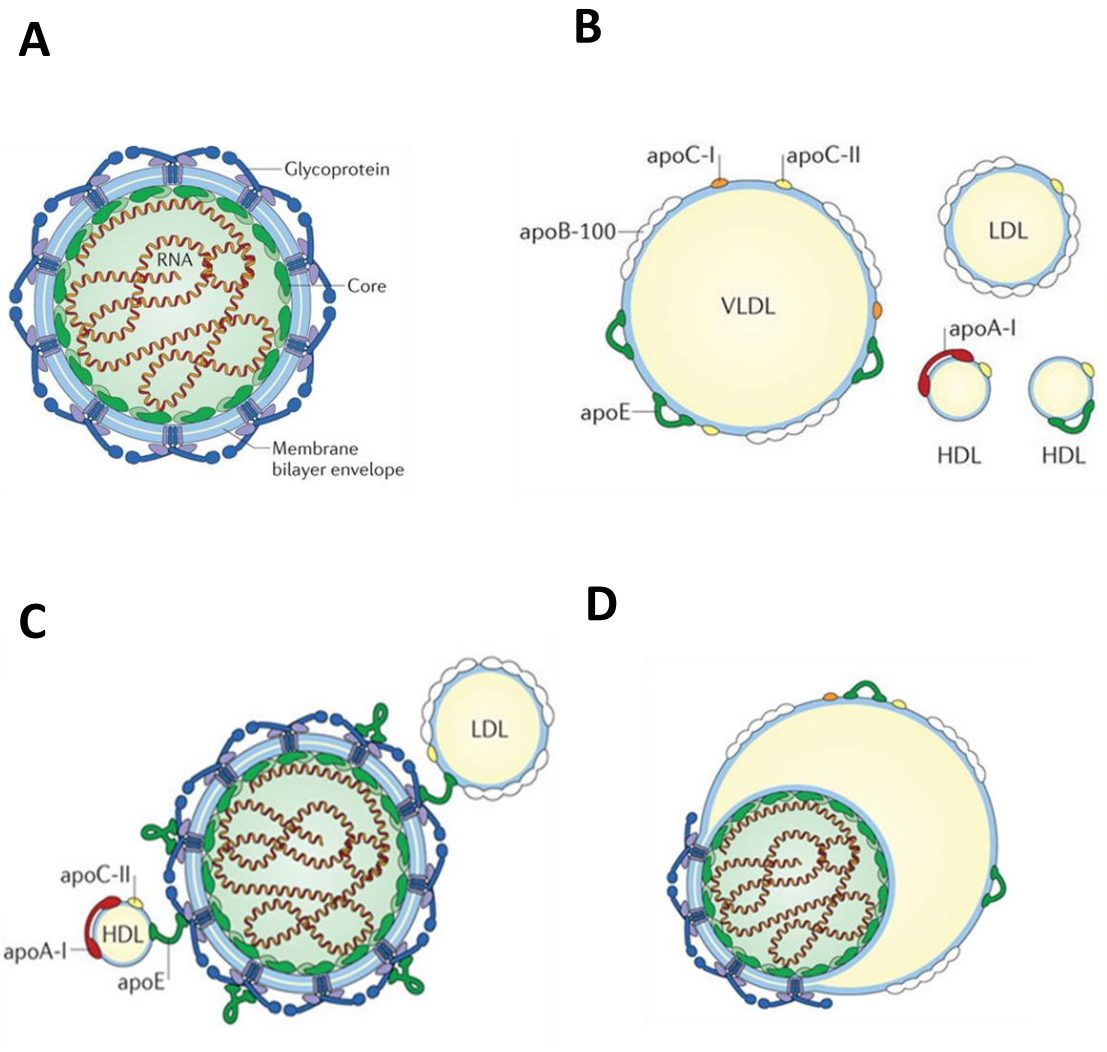

Figure 1.4 Schematic representation of HCV virion architecture.

A. Viral particles are composed of nucleocapsid (core) containing the viral RNA surrounded by a host cell-derived lipid envelope in which the E1 and E2 envelope glycoproteins are embedded. **B.** Representation of different types of serum lipoprotein particles. Both Very low-density lipoprotein (VLDL) and low-density lipoprotein (LDL) display the large apolipoprotein B-100 (apoB-100) and the small apoC II) and (I and apoE on their surface, which consists of a phospholipid monolayer surrounding a hydrophobic core of triglycerides, cholesterol and cholesterol esters. High-density lipoprotein (HDL) particle mainly displays apoA-I, apoC-II and/or apoE. **C.** Two-particle model of HCV virion with transient interaction between serum lipoproteins and HCV particles. **D.** Single particle model with membrane sharing between HCV and low-density lipoprotein. Pictures are adapted from (Lindenbach and Rice, 2013).

1.4.2 Binding and entry of HCV

Hepatocytes are the cellular target of HCV and the entry of HCV is a complicated multistage process. After infection, HCV circulates in the blood and thus has direct contact with the basolateral surface of hepatocytes, allowing virus to bind a number of receptors on cell surface (Figure 1.5). The binding to receptors will initiate clathrin-dependent endocytosis.

The binding of HCV with low-affinity interaction such as low-density-lipoprotein receptor (LDLR) and glycosaminoglycans (GAGs) present on heparan sulphate proteoglycans (HSPGs) is the initial step of entry via the interaction with virion-associated apoE (Agnello et al., 1999, Germi et al., 2002, Monazahian et al., 1999). Scavenger receptor class B member 1 (SRB1) is a co-receptor, which interacts with virus-associated lipoproteins to dissociate virus particles from lipoproteins for productive virus entry (Dao Thi et al., 2012, Zahid et al., 2013). Additionally, the interaction with SRB1 can expose the CD81-binding derminant on HCV E2 glycoprotein (Scarselli et al., 2002, Dao Thi et al., 2012, Bankwitz et al., 2010).

CD81 is a ubiquitously expressed cell surface tetraspanin that directly binds HCV E2, which mediates the low-pH fusion post attachment (Bertaux and Dragic, 2006, Sharma et al., 2011). In addition, interaction of CD81 with tight junction protein claudin 1 (CLDN1) is required for this function of CD81 in HCV entry (Harris et al., 2010). The tight junction is a critical cellular component for maintenance of tissue integrity, cellular interactions and cell-cell communications, and it also works as a gate for the entry of viruses (Lee and Luk, 2010). CLDN1 is one of the membrane proteins located on tight junctions that induce HCV internalisation via the interaction with CD81 (Evans et al., 2007). Like CLDN1, occluding (OCLN) is another tight junction protein also involved a post-attachment step during HCV entry, although the precise role is still unclear (Sourisseau et al., 2013). Another receptor transferrin receptor 1 (TFR1) and Niemann-Pick C1-like one (NPC1L1) are also demonstrated to be important for a post-CD81-binding event as the inhibitions on TFR1 will impair HCV infection (Martin and Uprichard, 2013, Sainz et al., 2012, Jia et al., 2011).

The interaction between CD81 and CLDN-1 is modulated by several signal transduction pathways including epidermal growth factor receptor (EGFR) and downstream RAS GTPase signalling, as well as RHO GTPases (Lupberger et al., 2011, Diao et al., 2012, Brazzoli et al., 2008). These signalling pathways will facilitate complex HCV-CD81 and CLDN1 to induce clathrin- mediated endocytosis (Farquhar et al., 2012).

Following clathrin-mediated endocytosis, both HCV and receptors are trafficked to Rab5a expressing endosomal compartments (Coller et al., 2009, Farquhar et al., 2012). Subsequently low pH of the endosomes induces envelope directed membrane fusion and release of genomic RNA into the cytosol for further viral translation and replication (Sharma et al., 2011).

Antibody treatment is an attractive therapeutic direction by targeting factors involved in HCV entry. A number of monoclonal antibodies directed to viral and host factors are under development (Zeisel et al., 2013), but are still clinically unavailable (Fukasawa et al., 2015).

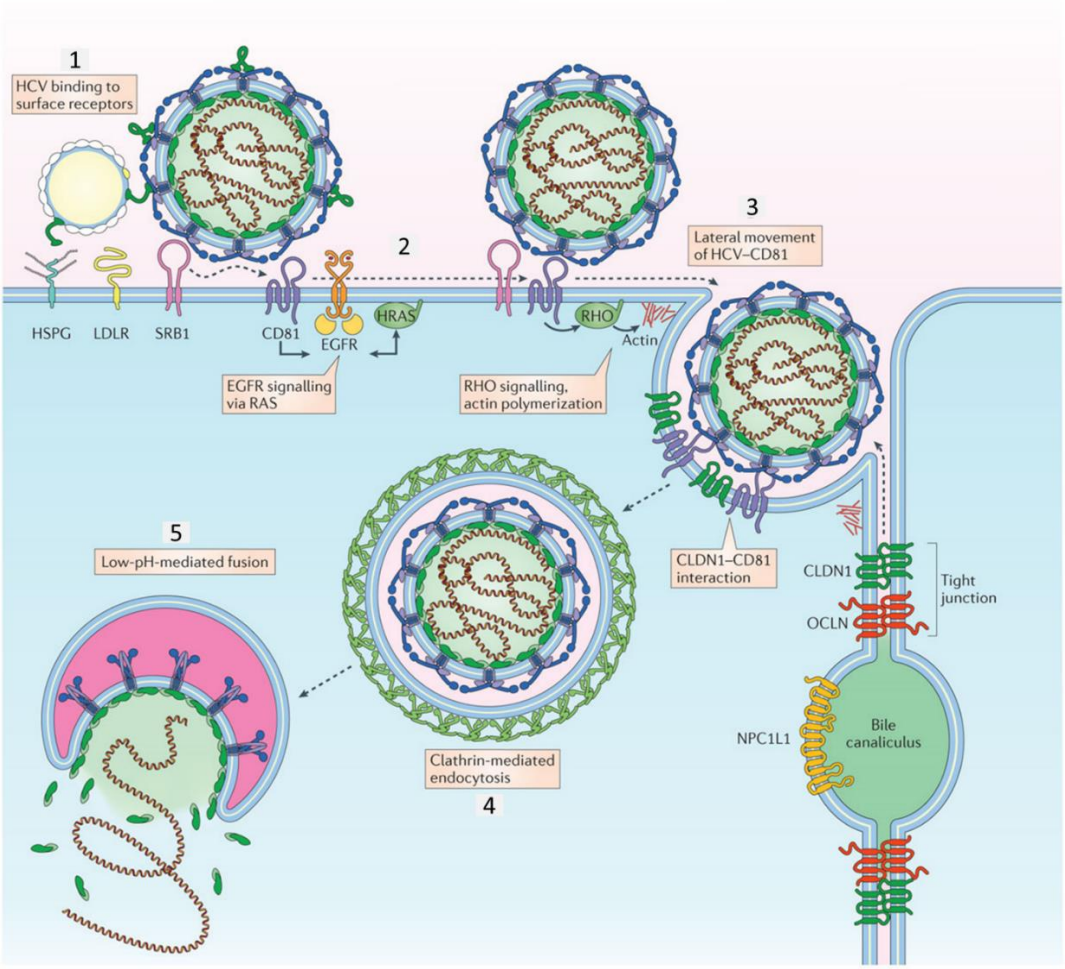

Figure 1.5 Binding and entry of HCV to host cell.

1. HCV lipoviral particles interact with cell receptors including heparin sulphate proteoglycans (HSPGs), low-density-lipoprotein receptor (LDLR) and scavenger receptor class B member 1 (SRB1), inducing the exposure of the CD81-binding site in E2 ; 2. Signal transduction mediated by interaction of E2 with CD81 through epidermal growth factor receptor (EGFR), HRAS and RHO GTPases; 3. Lateral movement of HCV to sites of cell-to-cell contact; 4. HCV internalisation by clathrin-mediated endocytosis though interaction of CD81 with CLDN1; 5. HCV fusion and release of RNA in the endosome of low pH. NPC1L1: Niemann-Pick C1-like 1, OCLN: occludin. Picture was adapted from (Lindenbach and Rice, 2013).

1.4.3 Polyprotein processing

Post release of genomic RNA into the cytosol, the positive sense RNA acts directly as mRNA to direct translation of polyprotein at the rough endoplasmic reticulum (ER). As HCV RNA lacks a 5'-terminal cap and 3'-terminal poly(A) tract but contains highly structured 5'UTR and 3'UTR (details in Section 1.2.1), translation of HCV is in a cap-independent manner through recruitment of the 40S ribosome subunit directly via interactions with the IRES in the 5' UTR and associated eukaryotic initiation factors (eIF) (Jaafar et al., 2016). Binding of the HCV IRES to the 40S ribosomal subunit induces rotation of the head domain and opening of the mRNA binding channel (Spahn et al., 2001). Subsequent recruitment of the 60S ribosomal subunit forms an active 80S ribosome positioned directly on the HCV initiation AUG codon (Reynolds et al., 1996, Reynolds et al., 1995). Correct positioning of the ribosome on the start codon requires both sequence and structural stability of domain IV. Translation of the primary ORF result in a large polyprotein until an initiation AUG codon is encountered, and polyprotein is later cleaved into the individual proteins.

The signal peptidase cleavage of core-E1, E1-E2, E2-p7 and p7-NS2 takes place co-or post translationally to leave mature core, membrane embedded E1 and E2 and transmembrane p7. An autoprotease activity that maps to both NS2 and NS3 cleaves at the NS2-3 boundary to free NS2 from the polyprotein (Figure 1.2) (Grakoui et al., 1993). The remaining NS polyprotein is cleaved by NS3 with its cofactor NS4A (Bartenschlager et al., 1994, Bartenschlager et al., 1995). Production of mature viral proteins proceed to function in genome replication, assembly and ultimately release of infectious virions.

1.4.4 RNA replication

After translation and proteolytic processing of polyprotein, the viral replicase complex (RC) is constituted. This translation take places rapidly followed by RNA replication and translation of RNA within 8 hours. From that point the intracellular levels of both viral protein and genomes increase exponentially until a steady state is reached at around 24 hours (Binder et al., 2013).

Positive-strand RNA viruses, including members of the Flaviviridae family, replicate their genomes in association with remodelled cytoplasmic membranes (Paul and Bartenschlager, 2015). Replication of HCV requires non-structural proteins NS3 to NS5B, and these proteins are tightly associated to endoplasmic reticulum (ER) membranes and together with cellular factors induce, in a concerted fashion, membrane rearrangements that lead to the formation of viral

replication organelles termed membranous web (MW) (Miller and Krijnse-Locker, 2008, Paul and Bartenschlager, 2015).

Electron microscopy (EM) and soft X-ray microscopy revealed that HCV infection contributes to the accumulation of membrane vesicles, mostly double membrane vesicles (DMV), embedded in a compact membrane network (Egger et al., 2002, Gosert et al., 2003, Romero-Brey et al., 2012, Perez-Berna et al., 2016). Purified DMV contain active polymerase and the presence of both NS5A and double stranded RNA and the expression of NS3-5B alone is sufficient to induce DMV structure (Romero-Brey et al., 2012, Ferraris et al., 2010). Of them, NS4B is the major viral protein and primary inducer required for the formation of DMV, but the individual expression of NS4B is insufficient to induce DMVs (Egger et al., 2002, Romero-Brey et al., 2012). Interaction of NS5A and host factor phosphatidylinositol-4 kinase-III α /β (PI4KIII α /β) is critical for the formation of membranous web (Reiss et al., 2011). Expression of NS3/4A or NS5B alone resulted in altered vesicle architectures, suggesting a less critical role in DMV formation (Romero-Brey et al., 2012). Apart from NS proteins of HCV, a large number of host factors are involved in the membranous web formation and virus replication.

Post the formation of DMV, additional modifications to the DMV scaffold such as net increase of intracellular membrane surface and recruit additional accessory factors, are required for the functional replication factories (Paul and Bartenschlager, 2015). The increased positive membrane curvature requires the *de novo* synthesis of membrane lipids. High-throughput lipidomic profiling of HCV infected cells has revealed significant alterations to lipid compositions (Diamond et al., 2010). HCV relies on sterol regulatory element-binding protein (SREBP)-mediated transcriptional activation of lipogenic biosynthetic enzymes, leading to elevated levels of lipogenic transcripts, such as FAS (fatty acid synthase) and HMG-CoA (3-hydroxy-3-methylglutaryl coenzyme-A) reductase (Waris et al., 2007). The phosphatidylinositol 4-kinase IIIα (PI4KIIIα) and its product phosphatidylinositol 4-phosphate (PI4P) are other important components for lipid composition and integrity of HCV membrane structures (Trotard et al., 2009, Reiss et al., 2011, Berger et al., 2009). Upon HCV infection, subcellular localization of PI4KIIIα is altered presumably via interactions with NS5A and NS5B, concomitant with an increase in intracellular PI4P levels and a decrease of the PI4P plasma membrane pool, which is dispensable for DMV functionality (Figure 1.6) (Bianco et al., 2012, Reiss et al., 2011, Altan-Bonnet and Balla, 2012).

HCV replication factories are significantly enriched in cholesterol over ER membranes and its removal from DMV reduces their size and HCV genome stability (Paul et al., 2013). Addition of

PI4P to membranes also functions to recruit lipid transfer proteins for the storage of lipids. Oxysterol-binding protein (OSBP) and glycosphingolipid transporter four-phosphate adaptor protein 2 both linked with PI4P involved in nonvesicular cholesterol transport is required for HCV replication (Wang et al., 2014, Khan et al., 2014b). This pathway is further stimulated by VAP-A and VAP-B, which are recruited by NS5A (Figure 1.6) (Wang et al., 2014, Evans et al., 2004, Gao et al., 2004, Khan et al., 2014b). OSBP interacts with VAPs via its FFAT motif, which is essential to promote cholesterol transport to HCV-remodelled membranes and hence viral replication (Mesmin et al., 2013).

Within the well-formed replication factories, the process of genome replication is performed by NS5B RNA-dependent RNA polymerase (RdRp) to direct the synthesis of the negative-strand intermediate that serves as a template for the production of excessive amounts of new positive-strand RNA molecules. These RNAs can be used for polyprotein synthesis or as templates for new negative-strand RNAs or can be incorporated into viral particles (Appleby et al., 2015).

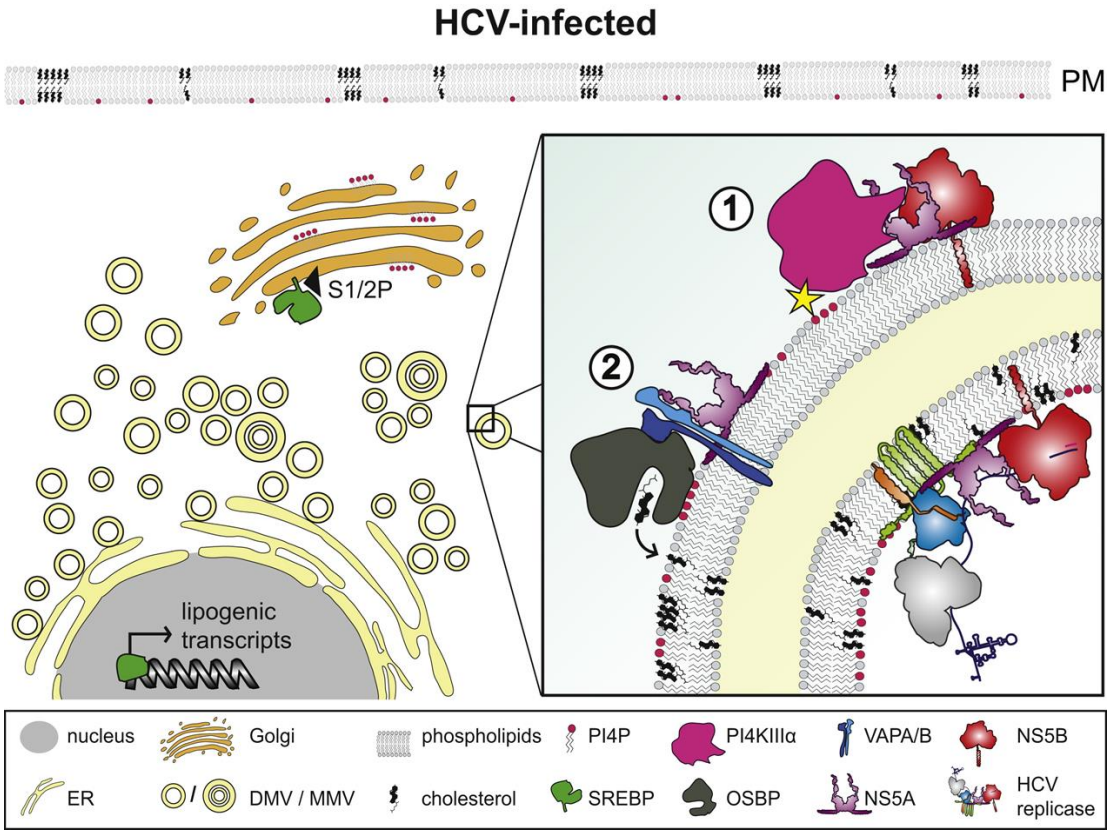

Figure 1.6 Model of HCV induced replication factory.

HCV infection induces extensive remodelling of intracellular membranes, most notably double-membrane vesicles (DMVs) and less frequently multimembrane vesicles (MMVs) involving a large range of host cell proteins and lipids implicated in MW biogenesis. 1. PI4KIIIα interacts with NS5A and NS5B to induce elevated levels of PI4P. 2. Subsequently, oxysterol-binding protein (OSBP) delivers cholesterol to HCV-remodelled membranes. Locally elevated PI4P levels as well as interactions with VAPs and NS5A facilitate OSBP recruitment. Picture is adapted from (Paul et al., 2014).

1.4.5 Assembly and release

The lipid droplets (LDs) are organelles that are used for the storage of neutral lipids. Those are mainly cytosolic (cLD) along with a small nuclear population (nLD), hence LDs thoughtout indicate cLD in most cases. The assembly and release of HCV particles crucially depends on an association of core protein with cytosolic lipid droplets (cLDs) following synthesis and maturation on the ER. This process must bring together the viral core protein, E1, E2 and the viral genome to be packaged in a temporally and spatially organized manner. Nascent virus particles undergo maturation into low-buoyant-density particles and release from cells by transiting through the secretory pathway or a newly reported trans-Golgi network-to-endosome pathway independent of VLDL secretion (Gastaminza et al., 2008, Gastaminza et al., 2006, Mankouri et al., 2016).

1.4.5.1 Virus assembly

The process of HCV assembly can be divided into two events: the formation of RNA-core nucleocapsid in the early stage and then this nucleocapsid is enveloped at a late stage. Although the early process whereby genome RNA associated with mature, lipid droplets (LDs) localised core to form a nucleocapsid is still poorly defined, it is well validated that the association of core with LDs is critical for the production of infectious particles (Miyanari et al., 2007, Targett-Adams et al., 2008, Boulant et al., 2008, Bartenschlager et al., 2011).

Cytosolic lipid droplets (cLD) are cellular lipid storage organelles containing a hydrophobic core with a phospholipid monolayer that is derived from the outer leaflet of the ER membrane (Gross and Silver, 2014). Following synthesis on the ER, the mature core protein migrates to the surface of LDs. Trafficking of core protein to LDs requires the MAPK-regulated cytosolic phospholipase A2 (cPLA2) as the signalling pathway downstream of cPLA2 (Menzel et al. 2012). This targeting of core to LDs also can be enhanced by diacylglycerol acetyltransferase 1, DGAT1, which is thought to fuel LD formation at ER membranes as triglyceride-synthesizing enzymes (Herker et al., 2010, Yen et al., 2008).

Multiple interactions between the HCV proteins facilitate this pathway. One of the first key steps in HCV assembly is the interaction of NS5A with the LD-bound core protein, by which viral RNA is delivered to the LDs allowing regulation between replication and assembly (Miyanari et al., 2007, Appel et al., 2008, Masaki et al., 2008). Essential roles of NS5A in virus particle assembly largely depend on the determinants in domain III (Appel et al., 2008, Tellinghuisen et al., 2008a, Kim et al., 2011). Two distinct regions in domain III, comprising a

cluster of basic amino acids and a separate cluster of serines, are involved in recruitment of replication complexes to core, and transfer of HCV RNA to core respectively (Zayas et al., 2016). Apart from the interaction with core protein, NS5A can also interact with host factors including the just mentioned core-partners DGAT1, apolipoprotein E (ApoE), annexin A2 and Rab18 (Camus et al., 2013, Benga et al., 2010, Cun et al., 2010, Backes et al., 2010, Salloum et al., 2013), which all enhance assembly.

In the late events of virus particle assembly, the core protein must be retrieved from the surface of cLDs to the site of viral budding at the ER where the E1-E2 glycoprotein complex are brought together with nucleocapsid. Post translocation of RNA from replication sites to core, NS2 is another important non-structural protein required for organizing the virus assembly complex, which is achieved via recruitment of E1-E2, other non-structural proteins and core-RNA-containing cLDs (Jirasko et al., 2010, Popescu et al., 2011, Phan et al., 2009, Boson et al., 2011, Ma et al., 2011, Stapleford and Lindenbach, 2011). NS2 interacts with the small, membrane-bound NS protein p7, facilitating the localisation of core-containing cLDs to site of viral budding at the ER (Jirasko et al., 2010, Popescu et al., 2011). p7-NS2 complex interacts with the NS3‑4A enzyme, and this is a key step in the retrieval of the viral core protein from cLDs and into nascent virus particles (Jirasko et al., 2010, Ma et al., 2008, Jones et al., 2011) (Phan et al., 2009)(Figure 1.7). A host protein AP2M1 (clathrin assembly protein complex 2 medium chain is shown to be essential for retrieval of core protein from cLDs and for virus assembly (Neveu et al., 2012). While for the RNA that core bound, helicase activity of NS3‑4A was proposed to serve to package viral RNA during nucleocapsid formation. It remains to be determined whether NS4B and NS5B play any role in virus assembly.

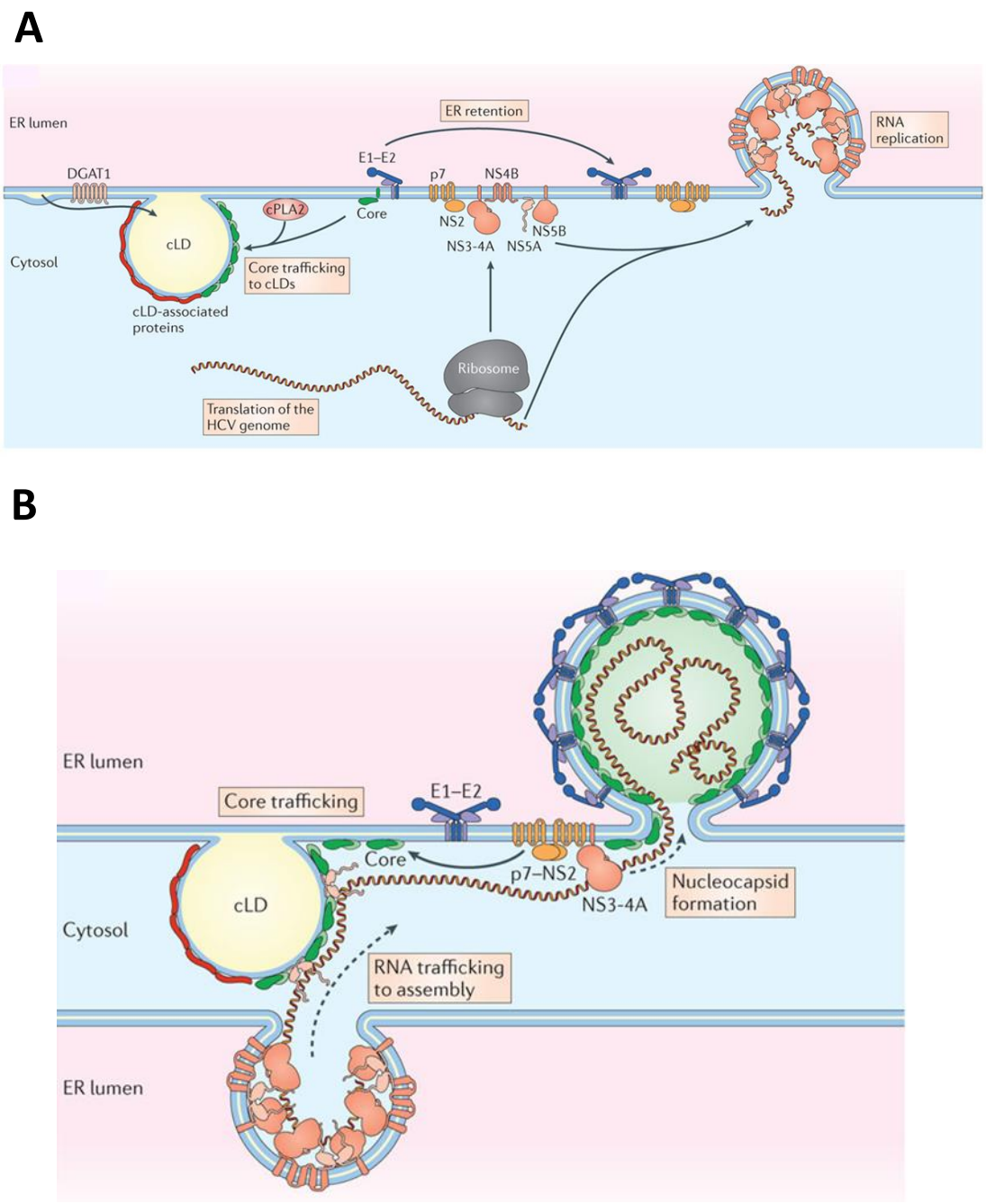

Figure 1.7 Model of HCV assembly.

A. Post translation of viral protein, RNA replication in replication complex, retention of the E1–E2 and p7–NS2 complexes on ER, core trafficking to cytosolic lipid droplets (cLDs) is mediated by cPLA2 and DGAT1. **B**. After association of core to cLDs, viral RNA is shifted out of replication and translation and towards virus assembly by NS5A. The interaction of p7–NS2 with NS3-4A recruits viral core protein from cLDs to the late site of virus assembly. Virus particles assemble by recruitment of E1-E2 complexes and budding into the ER. cPLA2: cytosolic phospholipase A2; DGAT1: diacylglycerol O-acetyltransferase 1. Picture is adapted from (Lindenbach and Rice, 2013).

1.4.5.2 Viral budding, maturation and release

Budding of HCV progeny virions is believed to utilize the ESCRT (endosomal sorting complex required for transport) pathway which involves ubiquitination of NS2 to facilitate direct interactions with the ESCRT machinery (Ariumi et al., 2011, Barouch-Bentov et al., 2016, Corless et al., 2010, Lai et al., 2010, Tamai et al., 2012).

E1-E2 present on extracellular virus particles contain some complex modifications (Vieyres et al., 2010). Hence post assembly, virions transit through the trans-Golgi network (TGN) and endosome pathways in a process of maturation where the E1/E2 envelope proteins are glycosylated (Gastaminza et al., 2008). After glycosylation, HCV virions were released at the plasma membrane in a VAMP1-dependent manner (Coller et al., 2012).

In addition to glycoprotein modifications, HCV particles may undergo post-synthetic lipidation, similar to the VLDL assembly pathway. There is evidence exhibiting that HCVcc in an intermediate buoyant density much like VLDL particles (Gastaminza et al., 2008), and the inhibition of microsomal triglyceride transfer protein (MTP) disrupt the production of HCV particles (Huang et al., 2007a). Both HCV and triglyceride-rich VLDLs secreted in a complex in different cell lines is further verified that the production of the infectious HCVcc particles in Huh7 cells is in an ApoE-dependent and ApoB-independent manner (Jiang and Luo, 2009, Jammart et al., 2013). However, a more recent research points out that the release of HCV particles is via a trans-Golgi network-to-endosome pathway, which is independent of VLDL secretion (Mankouri et al., 2016).

1.5 Systems for the study of HCV

1.5.1 Cell culture systems

Cell culture systems for efficient viral propagation are crucial to obtain a detailed understanding of intracellular life cycle and the virus host cell interaction. Originally cloned in 1989 (Choo et al., 1989), the viral genome of HCV is now well characterized. Despite the availability of cloned infectious genomes, molecular studies of HCV replication and the development of antiviral drugs have been hampered by the low efficiencies of currently available cell culture systems and by the fact that the only animal model is the chimpanzee. For HCV, the development of permissive and authentic culture models has been and continues to be a challenging task. Here it is time to discuss the different types of systems available for investigating HCV.

The ability to study HCV life cycle was realized since the development of the first sub-genomic replicon (SGR) system capable of reproducing the HCV replication cycle (Lohmann et al., 1999a). It was a bicistronic system wherein the first ORF, driven by the HCV IRES from the 5'UTR, encoded for a reporter gene followed by the EMCV IRES driving the expression of the non-structural genes either NS2-5B or NS3-5B in addition to the non-coding 3'UTR (Figure 1.8). A neomycin phosphotransferase (NTP) reporter gene was initially used as it allowed for positive selection of replication. The use of NPT reporter for the resistance to the G418 drove the selection for culture adaptive mutations (CAMs) which were important for achieving the detectable levels of replication (Lohmann and Bartenschlager, 2014). The minimal requirement of polyprotein for HCV RNA replication is NS3-NS5B as there is a detrimental effect on the replication ability when NS2 was incorporated into SGR (Lohmann et al., 1999a, Bartenschlager and Sparacio, 2007).

A genotype 2a strain of HCV from a patient with fulminant hepatitis, termed JFH1 was identified in 2003, which significantly improved replication level in the absence of adaptive mutations (Kato et al., 2003). The incorporation of a firefly luciferase (luc) instead of npt gene allows for the easy and accurate quantification of replication kinetics and facilitates the high throughput screening of anti-HCV compounds for the first time (Targett-Adams and McLauchlan, 2005). Since then, the majority of antivirals against HCV replication have used JFH1 or culture-adapted genotype 1 SGR spanning NS3-NS5B (Kwong, 2014).

To investigate entire HCV lifecycle, full JFH1 virus construct was successfully developed, thus allowing studies on the entire lifecycle from virus entry to release in the hepatocellular carcinoma cell line Huh7 (Zhong et al., 2005, Wakita et al., 2005). Jc1, a chimeric virus, composed of structural genes (5'UTR to p7) from the genotype 2a J6CF and non-structural proteins (NS2-3'UTR) showed a significant increase in virus release over JFH1 (Figure 1.8) (Pietschmann et al., 2006). To take advantage of this chimeric approach, a series of chimeric viruses all based on JFH1 non-structural elements were constructed with different levels of virus release for all major genotypes (Vieyres and Pietschmann, 2013, Bartenschlager and Sparacio, 2007).

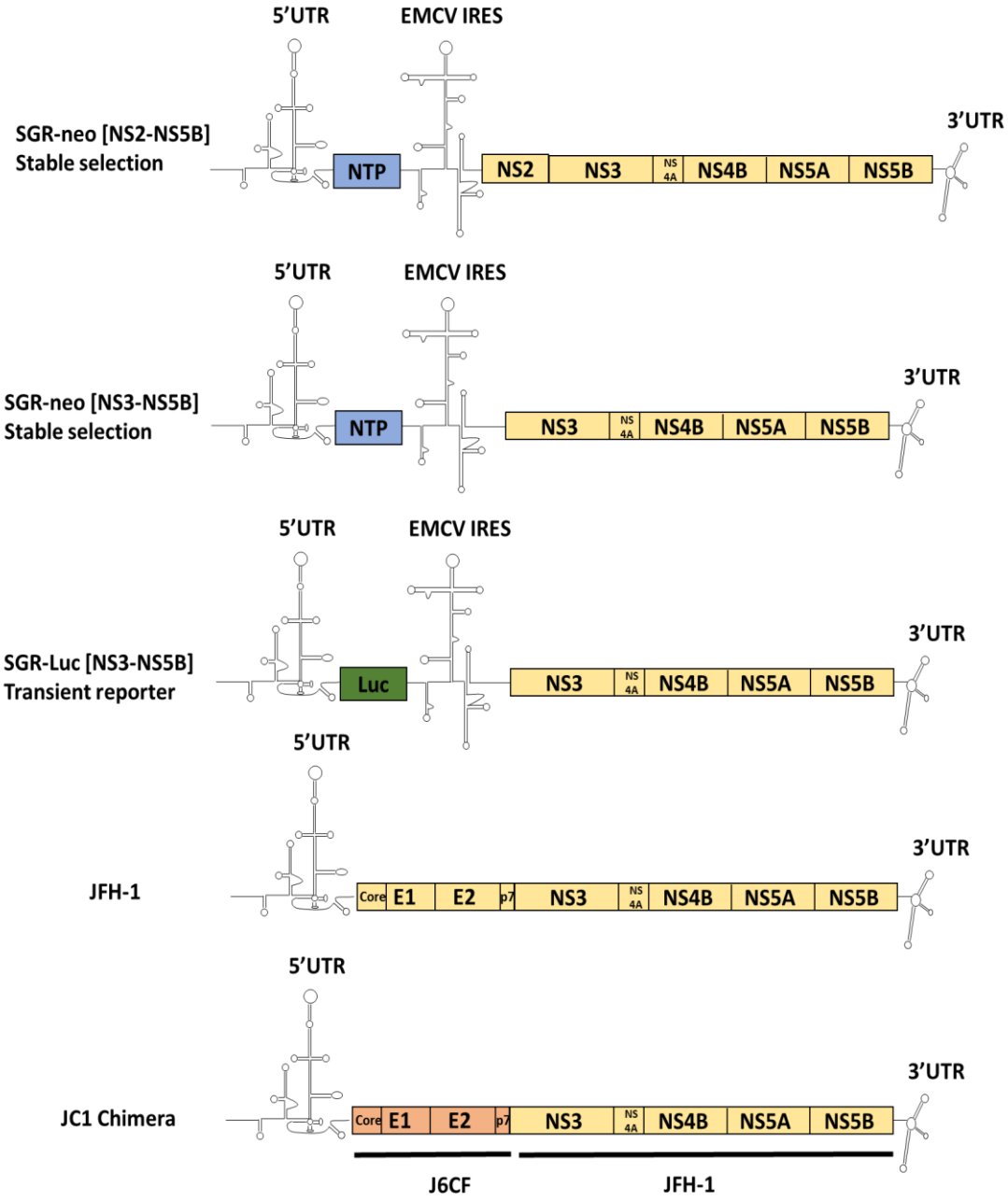

Figure 1.8 Structure of current SGR and virus constructs.

Both SGR-neo and SGR-Luc are two common subgenomic replicon system. SGRs incorporated with neomycin phosphotransferase (NTP) are used for the selection of stable cell lines using G418. SGR-neo has the constructs spanning either NS2-5B or NS3-NS5B. SGR with firefly luciferase (Luc) gives an easy and sensitive reporter but requires transient electroporation into cells. The genotype 2a JFH1 isolate and chimeric JC1 are common virus constructs.

HCV replicates primarily in human hepatocytes, but multiple reports suggest that also extrahepatic reservoirs exist which may include the lymphatic system, gut and the brain (Blackard et al., 2006). The most permissive cell line for efficient RNA replication in vitro is the human hepatoma cell line Huh7 and its clonal descendants (Nakabayashi et al., 1982, Steinmann and Pietschmann, 2013). To some extent, HCV replication appears to be restricted in Huh7 cell line although adaptive mutations in the HCV nonstructural proteins typically enhance the replicative capacity. In order to obtain cell lines more permissive for HCV replication in the absence of G418 selection or adaptive mutations, clearing selectable SGR from Huh7 cell line with prolonged treatment of IFN-α therefore yields a population of cells, more permissive to the HCV lifecycle, termed Huh7.5, which allows us to examine replication of subgenomic replicons lacking neo as well as full-length HCV after transfection (Blight et al., 2002). The enhanced replication capacity in Huh7.5 can be partially attributed to the defective RIG-I so that IFN-α/ β and ISGs pathway cannot be activated by RIG-I as a signal transducer and HCV RNA PAMP receptor (Sumpter et al., 2005). It was documented that secondary or tertiary RNA structures of HCV viral RNA acting as the pathogen-associated molecular pattern (PAMP) could be recognized by RIG-I . The binding of RIG-I to viral RNA activates the IRF3 via RIG-I CARD-homology domain, followed by the activation of innate antiviral defence pathways IFN-α/ β and ISGs via phosphorylation of IRF3 (McWhirter et al., 2004, Foy et al., 2003, Sumpter et al., 2005).

1.5.2 Animal models

Besides humans, chimpanzees were the only other species to be susceptible to HCV infection (Bassett et al., 1998). That is why the development and evaluation of effective therapies and vaccines for HCV and the study of its interactions with the mammalian host have been hindered for a long time (Bukh, 2004). It was found that genomes that acquired cell culture adaptive mutations were highly attenuated in chimpanzees, or even reverted to the wildtype when injected in chimeric mice with humanized liver. This underscores the discrepancies of infections between tissue culture and animal models and the limitations of the biological relevance of in vitro systems (Bukh et al., 2002, Kaul et al., 2007). Additionally, chimpanzees inoculated with JFH1 only caused limited viremia and was cleared in 3 days, that is why few chimpanzees can evolve to the chronic infection in the clinical course (Boonstra et al., 2009).

Apart from chimpanzees, a lot of work has tried to establish mice model for the research of HCV lifecycle. To adapt HCV to the mouse environment, genetic manipulation of the host can be used to knock down murine factors that hamper productive HCV infection or to

complement the mouse with human factors that are essential for this process. Hence, by transient expression of the human restriction factors CD81 and OCLN into mice, lifecycle of HCV has been recapitulated (Dorner et al., 2011). Liver chimeric mice in which human hepatocytes are xenografted is another important innovation for the study of HCV (Mercer et al., 2001, Bissig et al., 2010). However, Human-liver chimeric mice in their current state completely lack or contain only very limited cellular immunity, and therefore are not yet useful for vaccine studies. Therefore, more efforts need to be exerted to improve HCV animal models until HCV has been eradicated worldwide.

1.6 Aims and objectives

HCV infects more than 70 million people worldwide, causing long-term liver disease (Polaris Observatory, 2017). Recently new therapies comprising direct-acting antivirals (DAAs), small molecule inhibitors of virus proteins, have revolutionised treatment for infected patients. Despite this, we have a limited understanding of how the virus replicates in infected liver cells. NS5A protein is critical during the virus lifecycle with a number of unknown functions, one of which is the hypothesised link between HCV replication and assembly. This study aimed to address the current lack of knowledge in these areas. NS5A is comprised of three domains. Previously it was thought that domain I was only involved in replicating the virus genome, and functions of virus assembly were mainly mapped to domain II and III. However, based on both structural and sequence analysis, domain I is the most highly conserved and structured region in NS5A compared with domain II and III. Domain I is also the site for mutations that confer resistance to DAAs. Hence, I suspected that domain I might be involved in more important functions during HCV lifecycle, which are common in HCV genotypes and in related *Hepaciviruses*. Hence, my project aimed to address this deficiency by conducting a rational mutagenic analysis of domain I.

In this study, a mutagenic study was performed within the context of a JFH1-derived sub-genomic replicon and infectious virus based on analyses of sequence alignment and three-dimensional structures. Phenotypes of domain I mutants were further investigated taking advantages of high-resolution confocal microscopy and a series of biochemical analyses. Finally, comparative proteomic approach was utilised to identify the protein-protein interaction pathways involved by NS5A domain I. As domain I is the putative target for one class of DAAs, our observations may have implications for the yet undefined mode of action of these compounds.

Chapter 2: Materials and Methods

2.1 General materials

2.1.1 Bacterial strains

Escherichia coli (E. coli) DH5α: Genotype F- Φ80lacZΔM15 Δ (lacZYA-argF) U169 recA1 endA1 hsdR17 (rk-, mk-) phoA supE44 λ- thi-1 gyrA96 relA1 were used for molecular cloning.

BL21 (DE3) pLysS: Genotype F- ompT gal dcm lon hsdSB (rB- mB-) λ (DE3) pLysS (cmR) were used for protein expression.

2.1.2 Mammalian cell lines

Huh7 (human hepatocellular carcinoma) (Nakabayashi et al., 1982) cells and Huh7.5 (a HCV cured cell line) (Blight et al., 2002) were used for electroporation and infection assays throughout, respectively. A polyclonal population of cells stably expressing SGR-Neo-JFH1 or SGR-Neo-JFH1 (NS5A-OST) were produced in Huh7.5 cells by Douglas Ross-Thriepland at the University of Leeds.

2.1.3 Plasmid and virus constructs

All the DNA constructs and HCV isolates are listed in Appendix Tables 9.1 and 9.2. DNA constructs of either sub-genomic replicon with luciferase reporter (mSGR-luc-JFH1) (Hughes et al., 2009b) or full-length virus mJFH1 (Wakita *et al*., 2005) were used. *pcDNA3.1 (+)* was used as the vector to subclone the *BamH*I*/Hind*III JFH1 NS5A fragment for site-directed mutagenesis. The *pCMV10-NS3-5B (JFH1)* was constructed by a previous colleague (Ross-Thriepland et al., 2013). mJFH1 digested with both *Nsi*I and *BsrG*I were inserted with NS5A containing One-Strep-tag fragments with corresponding mutations digested from SGR-Neo-JFH1(NS5A-OST)(Amako et al., 2009).

pET28a-SUMO plasmid, a kind gift from John Barr, and pGEX6P-2 were used as the vectors for the construction of NS5A domain I expression plasmids. DNA fragments flanked with *BamH*I and *Xho*I restriction sites encompassing NS5A domain I amino acids 35 to 215 and 35 to 249 were amplified by PCR using wildtype or mutant JFH1 SGRs as templates. PCR products were cleaved with *BamH*I and *Xho*I and cloned into either pET28a-SUMO or pGEX6P-2 vectors to allow expression of domain I N-terminally fused to either a His-SUMO or GST affinity tag.

2.1.4 Oligonucleotide primers

DNA oligonucleotides were ordered from Integrated DNA Technologies and resuspended in deionised water to 100 µM and stored at -20°C. All primers used are listed in Appendix Tables 9.3-9.5.

2.1.5 Antibodies

The following primary antibodies were used: sheep anti-NS5A (in-house polyclonal antiserum), mouse anti-NS5A (9E10) (kind gift from Tim Tellinghuisen, Scripps Florida), rabbit anti-core (polyclonal serum R4210) and sheep anti-ADRP (kind gifts from John McLauchlan, Centre for Virus Research, Glasgow), sheep anti-GST (in-house), mouse anti-DGAT1 (Santa Cruz), mouse anti-Rab18, anti-ApoE (Santa Cruz) anti-β-Actin and anti-His (Sigma Aldrich).

Secondary antibodies were also as listed below: donkey anti-sheep (800nm) (Li-Cor), donkey anti-mouse (700nm) (Li-Cor), donkey anti-rabbit (800nm) (Li-Cor) were used in western blot; Alexa Fluor labelled donkey anti-sheep (488, 594 or 647nm), donkey anti- mouse (488 or 594nm) and donkey anti-rabbit (488nm or 594nm) (life technologies) at dilution 1:750.

2.1.6 Chromatography columns and resins

Glutathione Sepharose 4B and HisTrap™ HP 1ml columns were purchased from GE Healthcare, Strep-Tactin® Sepharose® and GFP-Trap® were from IBA and ChromoTek, respectively.

2.2 Basic techniques of molecular biology

2.2.1 Manipulation of nucleic acid

2.2.1.1 Preparation of plasmid DNA from bacteria

100µl chemically competent bacteria DH5α were mixed with plasmid DNA or ligation products at a volume ratio of 100:1 (plasmid DNA, 1µg) or 100:20 (ligation products, 20µl) respectively, and kept on ice for 30 min followed by the incubation for 60 min at 37 °C by adding 900µl Luria broth (LB) medium (Inoue et al., 1990). Transformed bacteria post incubation were coated on the agar plates supplemented with the appropriate antibiotics and incubated at 30 or 37°C overnight. Subsequently, single colonies were picked from these agar plates into LB medium with the same antibiotic, cultures were grown at 30 or 37°C with 180 rpm agitation overnight. Transformation of DNA containing HCV NS5A fragment were grown and cultured at 30 °C and all other transformations were grown at 37°C. Bacterial cultures were pelleted at 4000 g (RCF) for 30 min at 4 °C, and supernatants were discarded. Bacteria cell pellets were processed for purification of DNA plasmid using commercial Miniprep or Midiprep Kit following manufacturer's instructions (Qiagen). Long-term storage of DNA was as glycerol preparations of bacterial cultures by taking 700 µl bacterial culture with 300 µl glycerol and then freezing to -80°C.

2.2.1.2 Polymerase chain reaction (PCR)

The polymerase chain reaction was used to amplify DNA from plasmid DNA or reverse transcribed RNA in site-directed mutagenesis (Section 2.2.1.3) or PCR cloning. PCR reaction mixtures (50 µl) comprised of 100 ng template DNA, 10 µM forward and reverse primers, 1 mM dNTP and 1 U vent ® DNA polymerase with 5µl Thermopol ® reaction buffer (NEB). Reactions were initially denatured at 94°C for 1min followed by 40 cycles of a second denaturation at 94 °C for 30 sec, annealing step at 55 °C for 60 sec and extension step at 72°C for 1 min/Kb. Finally, last extension step were performed at 72 °C 10 min.

2.2.1.3 Site directed mutagenesis reactions

In order to introduce single amino acid mutations into HCV NS5A protein, primers used for Quickchange site-directed mutagenesis were complementary based on the HCV NS5A sequence, 30-45 nucleotides in length with required mutations centrally. Mutagenesis PCR were performed with an initial denaturation at 95 °C for 30 sec, then 5 cycles of denaturation at 95 °C for 30 sec, annealing at 52 °C for 60 sec and extension at 68 °C for 25 min followed by a further 13 cycles with an elevated annealing temperature at 55 °C following the manufacturer instruction of pfuTurbo Polymerase (Agilent). Reaction mixtures were supplemented with *Dpn*I at 37°C for 1h to remove Parental DNA and then transformed into component DH5α described in section 2.2.1.1.

2.2.1.4 DNA agarose gel electrophoresis

DNA agarose gels were prepared by adding 1% (w/v) agarose into 1x TAE buffer (40 mM Tris, 20 mM Acetate and 1 mM EDTA) heated until the agarose melted and supplemented with SYBR® safe DNA gel Stain (Invitrogen) 1:10,000. After loading with DNA samples containing gel loading buffer together with Hyper ladder I marker (Bioline), gels were run in 1x TAE buffer at a constant voltage of 100 V for 50 min. DNA was visualised by ultraviolet illumination using a Gene Genius bio-imaging system (Syngene).

2.2.1.5 DNA sequencing and sequence analysis

All DNA constructs were sequenced by Beckman Coulter Genomics Sequence Company using Sanger sequencing with custom primers directed to relevant sequences. DNA sequences were aligned and analysed in DNA Dynamo Sequence Analysis Software.

2.2.1.6 DNA purification from DNA agarose gel

After running agarose gels, DNA bands were visualised in a darkroom by UV excitation. These bands were cut out with minimal agarose and placed into 1.5ml microtube. DNA purification was performed using QIAquick Gel Extraction Kit (QIAGEN) following manufacturer's instructions.

2.2.1.7 Endonuclease digestion of DNA

Restriction Endonucleases throughout were purchased from New England Biolab (NEB). Typically, digestion reactions containing 3-10 µg DNA were carried out in 50 µl volume using relevant commercial buffers and enzymes at 37°C for at least 1 hr. Digested DNA fragments were separated by DNA agarose gel electrophoresis and extracted as described in section 2.2.1.4.

2.2.1.8 Ligation of DNA

After digestion with restriction enzymes, vector and DNA inserts with same cohesive ends were ligated at 1:3 molar ratio by T4 DNA ligase in 20 µl reaction and incubated at 25°C or 16°C for 1-16 hrs. Subsequently, the ligation reaction mixture was subjected to transformation into competent DH5α.

2.2.1.9 Phenol: Chloroform purification of DNA

DNA used for in vitro transcription were purified from solutions contaminated with proteins by addition of an equal volume of phenol: chloroform: isoamyl alcohol (25:24:1), vortexed thoroughly and centrifuged at 13,000 rpm for 5 min at 4 °C. Upper Aqueous phase layer was carefully removed and transferred to a fresh tube. An equal volume of chloroform was then added and vortexed for centrifugation at 13,000 rpm at 4°C. DNA in second aqueous phase was precipitated with 2 volumes of 100% ethanol and 0.1 volume 3M ammonium acetate (pH5.2) followed by incubation at -20 °C for 20 min and pelleted at 13,000 rpm for 20 min. Recovered DNA pellet was washed in 70% ethanol and then resuspended in 20 µl deionised water after centrifugation and air dry.

2.2.1.10 DNA quantification

Concentration and purity of nucleic acid were quantified by measuring absorbance at 260 and 280nm using Nanodrop spectrophotometer (Thermo Scientific). Ratio of absorbance at 260 nm to 280 nm (260/280) was used for checking purity of DNA.

2.2.1.11 In vitro transcription of RNA

Before in vitro transcription of RNA, DNA template constructs (e.g. mSGR-Luc JFH1 or mJFH1) were firstly linearized in a 50 µl reaction with *Xba*I at 37°C overnight. To get rid of overhanging ends from linearized DNA, reactions were treated with Mung Bean Nuclease (NEB) at 30°C for an extra 30 min. Linearized DNA was then phenol/chloroform extracted and used as the template for transcription of RNA.

In vitro transcription was performed using 1 µg of linear DNA as template following the manufacturer's instructions of T7 RiboMax Express kit (Promega). Post treatment with DNase for 30 min, RNA transcripts were purified using phenol/chloroform (pH 5.2) extraction. After centrifugation, aqueous phase was mixed and vortexed together with 1 volume of phenol/chloroform again. Then aqueous phase was extracted, precipitated with 0.1 volume 3M sodium acetate (pH5.2) and 1 volume isopropanol and placed on ice for 2-5 min before centrifugation at 13,000 rpm for 10min. RNA pellets were washed in 1ml 70% ethanol and resuspended in 20 µl Diethyl pyrocarbonate (DEPC)-treated water. Concentration of RNA can was quantified by absorbance at 260 nm using a Nanodrop spectrophotometer (Thermo Scientific). RNA purity was also analysed by RNA agarose gel electrophoresis.

2.2.1.12 RNA agarose gel electrophoresis

RNA agarose gels were prepared by adding 1% (w/v) agarose into 30 ml MOPS (3-(N-morpholino) propanesulphonic acid) buffer (40 mM MOPS, 10 mM sodium acetate, 1 mM EDTA) and microwaved at 340 W for 2 min until it dissolved. 6.5% (v/v) of formaldehyde and SYBR® safe DNA gel Stain (Invitrogen) (1:10,000) were added and poured into the gel cast. 1 µg of RNA samples in RNA loading buffer (47.5% Formamide, 9 mM EDTA, and 0.0125% SDS, Xylene Cyanol, and Bromophenol Blue (w/v)) were heated at 65°C for 10 min before loading into gels with 1 µg ssRNA ladder (NEB) alongside. Gel was electrophoresed at 70 V for 1 hr.

2.2.2 Protein technology

2.2.2.1 Quantification of protein

Protein samples from cell lysates were quantified using the Pierce BCA protein assay kit (Thermo Scientific) taking advantage of the bovine serum albumin (BSA) standard curve. Firstly, protein samples were diluted (1:10) in dH_2O to 50 µl in 96-well plates For the preparation of BSA standard samples, BSA was prepared to 1 mg/ml in dH_2O and diluted serially by 2-fold for 8 concentrations. Both protein samples and BSA standard were added with 50 µl BCA solution

following the manufacturer's instructions. 96-well plates were incubated at 37°C for 30 min before measuring absorbance at 570 nm using the Infinite F50 plate reader and Magellan for F50 software (Tecan). Protein concentrations could be calculated manually using a linear regression equation.

For the purified protein samples, their concentration was measured by absorbance at 280 nm using Nanodrop spectrophotometer (Thermo Scientific) taking Molecular Weight (MW) and Extinction Coefficients into account.

2.2.2.2 Preparation of SDS-PAGE

Separation gel (7.5% -15%, percentage depending on experiment) was firstly made by adding 7.5% -15% (v/v) acrylamide, 376 mM Tris-HCl (pH 8.8), 0.1%(w/v) ammonium persulphate (APS), 0.1%(w/v) SDS and 0.01% (v/v) Tetramethylethylenediamine (TEMED). After solidification, stacking gel (6% acrylamide, 376 mM Tris-HCl (pH 6.8), 0.1% APS, 0.1% SDS, 0.01% TEMED) was poured on top of the separating gel and a gel comb inserted in the stacking gel. Protein samples were mixed with SDS gel-loading buffer (62.5 mM Tris-HCl, pH 6.8, 10% (v/v) Glycerol, 2% (w/v) SDS, 0.01 % (w/v) Bromophenol blue, 5% (v/v) ß-mercaptoethanol) and boiled at 95 °C for 10 min before loading. Gels were run in 1x SDS-PAGE running buffer (25 mM Tris, 192 mM Glycine, 0.01(w/v) SDS) at 180 V for 1 hr. Color Prestained Protein Standard, Broad Range (11–245 kDa) was loaded alongside for comparison of protein size.

2.2.2.3 Coomassie blue staining

Gels were stained with 0.25% Coomassie Blue R250 in 10% (v/v) acetic acid, 50% (v/v) methanol, and 40% H_2O for the minimum time (typically less than one hour) necessary to visualize the bands of interest. Destaining of the gels were performed by soaking them in 10% acetic acid, 50% methanol, and 40% H_2O for at least 2 hrs with changes of this solvent until the background was nearly clear.

2.2.2.4 Western blot

After gel electrophoresis, proteins were transferred to a polyvinylidene fluoride (PVDF), Immobilon-FL Transfer Membrane pre-soaked in transfer buffer (25 mM Tris, 192 mM Glycine, 20% (v/v) methanol). After then, membranes were blocked in 50 % (v/v) Odyssey blocking buffer (Li-Cor) in TBS (25 mM Tris-HCl, pH7.4, 137 mM NaCl) for 1 hr at room temperature (RT). Membranes were incubated with primary antibodies diluted in 25 % (v/v) Odyssey blocking buffer in TBS for at least 1 hr at RT or 4°C overnight and then washed with TBST (TBS

supplemented with 0.1% (v/v)Tween-20) for at least 3 times and 5 min per wash. Membranes were further incubated with the recommended dilution of conjugated secondary antibody in 25% Odyssey blocking buffer at room temperature for at least 1 hr or 4°C overnight. Following removal of unbound antibodies by washing with TBST, membranes were allowed to dry before imaging on a Li-Cor Odyssey Sa Imager (Li-Cor).

2.2.2.5 Concentration of purified protein

Protein samples were concentrated using Amicon® Ultra 15 mL centrifugal filter (Merck) by centrifugation at 4,000 rpm at 4°C until reaching the required concentration.

2.3 Mammalian tissue culture techniques

2.3.1 Passaging of mammalian cells

Huh7 and Huh7.5 cells were cultured in Dulbecco's Modified Eagles Medium (DMEM, Sigma) supplemented with 10 % (v/v) fetal bovine serum (FBS), 100 µg/ml streptomycin, 100 IU penicillin/ml, and 1 % non-essential amino acids (Lonza) (complete medium) typically in T175 flasks incubated in a humidified incubator at 37 °C with 5 % CO_2. When cells reached confluency, media was removed and washed with phosphate buffered saline (PBS). Trypsin-EDTA solution was then used to detach cells by incubating for 5 min at 37 °C before inactivating trypsin through the addition of excess complete media to resuspend and reseed cells for next passage or for certain experiment. Complete medium needs to be supplemented with 25 mM HEPES for virus propagation.

2.3.2 RNA electroporation

Huh7 or Huh7.5 cells were washed twice in DEPC-treated PBS and counted before electroporating $4x10^6$ cells in ice cold DEPC-PBS with 2 µg RNA at 950 µF and 270 V in the chilled 4mm electroporation cuvette (Geneflow). Cells were resuspended in an appropriate volume of complete medium and then seeded into 96-well plates and 6-well plates at required density for luciferase assay and western blot analyses, respectively.

2.3.3 Transfection of DNA

FuGene6 transfection reagent (Promega) was used for transfection of DNA into mammalian cells according to the manufacturer's instructions. In brief, prior to transfection, cells were seeded in 6-well plates at the density of $2x10^5$/well for 24 hrs. On the day of transfection, 1 µg DNA was diluted into 96 µl Opti-MEM (Life Technology) followed by the addition of 3 µl

FuGene6 reagent. Transfection reaction was gently mixed and incubated for 30 min at RT before adding to seeded cells.

2.3.4 Harvest of cell lysate

Post electroporation or transfection at appropriate time points, cells were washed twice in PBS and scraped in PBS by cell scraper followed by centrifugation at 1500 rpm for 5min at 4°C. Cell pellets were lysed by resuspension in Glasgow lysis buffer (GLB, 10 mM PIPES, pH 7.2, 120 mM KCl, 30 mM NaCl, 5 mM $MgCl_2$, 1% Triton X-100, 10% Glycerol) supplemented with protease and phosphatase inhibitors, and then incubated on ice for 30 min. Cell debris was pelleted by centrifugation at 15,000 rpm for 5 min at 4°C. Supernatants were used for western blot analysis or other required experiment.

2.4 Subgenomic replicon assays

2.4.1 Transient replication assay

After 4, 24, 48 and 72 hours post electroporation (hpe), cells were harvested with 30 µl or 200 µl passive lysis buffer (PLB, Promega), for 96-well or 6-well plates and placed on ice for 30 min or stored in -20°C freezer. Luciferase activity was measured using a BMG plate reader by automated addition of 50 µl LARI regent (Promega) and value of light emission was measured.

2.4.2 Drug efficacy assay

Huh7.5 cells were electroporated and seeded as described above to check replication levels in 96-well plates by luciferase activity. Daclatasvir (DCV) to be used was diluted serially 10 fold from 10 µM in DMSO for 12 dilutions in 96- well plates. At 4 hpe, cells were treated with serially diluted DCV and incubated in normal tissue culture conditions. At 72 hpe, medium was removed and washed in PBS 3 times followed by addition of 30 µl PLB. Luciferase activity was determined using BMG plate reader by adding 50 µl LAR-1 reagent and recording light emission over 6 seconds. Data were modelled using the model of log (agonist) vs. response model and EC_{50} were calculated through Graphpad Prism 7.

2.5 JFH1 full-length virus assays

2.5.1 Electroporation of JFH1 constructs into cells

$8x10^6$ of Huh7 and Huh7.5 cells in ice-cold DEPC-PBS were electroporated with 10 µg RNA at 950 µF and 270 V using 4mm electroporation cuvette (Geneflow). After resuspension in complete media supplemented with 25 mM HEPES, cells were seed in both 6-well plates (3 x 10^5) and T75cm^2 Flasks (remaining cells) and incubated for 48 hrs and 72 hrs, respectively. Cells

in 6- well plates at 48 hpe were fixed in 4% (w/v) paraformaldehyde (PFA) used for IncuCyte ZOOM to check virus replication and in T75 cm^2 Flask were subjected to virus harvest for titration. After 72 hpe, supernatant was removed and kept in 4°C fridge as extracellular virus. Cells were washed in 10 ml PBS and then scrapped in 1ml PBS before storing at -80 °C.

2.5.2 Use of the IncuCyte ZOOM

Following immunofluorescence staining for viral antigens, with an Alexa Fluor 594-conjugated ("red") secondary antibody, fixed microtitre plates were imaged with the IncuCyte ZOOM (Essen BioScience) to determine the total number of virus-positive cells/well (Stewart et al., 2015). Viral titres were obtained by multiplying the number of virus-positive cells/well by the reciprocal of the corresponding dilution factor, corrected for input volume. As this method measures the absolute number of infected cells, rather than the number of foci of infected cells, the titre is represented as infectious units per mL (IU/mL).

2.5.3 Titration of virus

Culture supernatants in T75 flasks were harvested at 72 hpe, and extracellular virus titres were determined. Cell lysates harvested in PBS were freeze-thawed for 5 times and centrifuged at 3000 rpm for 5 min and supernatant was harvested as intracellular virus and store at -80 °C. Naïve Huh7 and Huh7.5 cells were seeded into 96 well plates ($8.0x10^3$ cells/well, 100 µL total volume) and allowed to adhere for 6 hrs. Clarified virus was serially diluted two-fold into the existing media (final volume 100 µL per well). Cells were incubated for 48 hrs post infection (hpi) before the detection of viral antigens by indirect immunofluorescence. Virus-positive cells were counted using IncuCyte ZOOM and the titre (IU/mL) was calculated from the wells of multiple virus dilutions.

2.5.4 Purification of HCV particles

Culture medium from JFH1 infected cells was concentrated 100-fold using 10% PEG 8000 (w/v) (Fisher Scientific) and centrifugation at 3000 g for 30 min. The pellet was resuspended in 1ml of PBS and overlaid over a 1 ml cushion (20% sucrose, w/v, in PBS), followed by ultracentrifugation at 150,000 g for 3 hrs at 4°C in an S55S rotor. The resulting pellet was resuspended in 200 µl PBS and then loaded on a 10-40% iodixanol gradient in 2.2 mL tubes followed by centrifugation at 150,000 g for 4 hrs at 4°C. The gradient was fractionated into 12 fractions of 180 µl each. Each fraction was used for virus titration as well as RNA extraction for qRT-PCR analysis, the remainder of each fraction was mixed with ice-cold methanol (1:3) and proteins precipitated at -80°C overnight. Precipitated proteins were recovered by

centrifugation at 13,000 rpm for 30 min at 4°C, and pellets were resuspended in 25 µl SDS-PAGE loading buffer, prior to western blot analysis.

2.5.5 Genome quantification by qRT-PCR

Total cell RNA was extracted using TRIzol following manufacturer's instructions (Invitrogen). In qRT-PCR reactions, 200ng extracted RNA (200 ng) was analysed using a One-step RT qPCR mastermix directed by the manufacturer (Eurogentec). Reaction was performed at 65°C for 30 min for reverse transcription and then 95°C for 10 mins denaturation followed by 40 cycles of amplification at 95°C for 15 sec then 60°C for 30 sec to harvest signal. For the preparation of standard curve, in vitro transcribed mJFH1 RNA was quantified and diluted by 10-fold for 12 dilutions. 2 µL of each dilution was added into this reaction. The primers and probes were designed against the HCV JFH1 5'UTR shown in Appendix Table 9.5.

2.5.6 Immunofluorescence analyses

Virus RNA electroporated cells were seeded onto 19 mm glass coverslips in 12 well plates, at 72 hpe cells were fixed in 4 % PFA and cellular membranes were permeabilised with 0.1 % (v/v) Triton X-100 (Sigma-Aldrich) in PBS for 7 min. Coverslips were washed twice in PBS and the primary antibody applied at the relevant dilution in 10 % (v/v) FBS in PBS and incubated for 2 hrs at RT. To remove any unbound primary antibody, cells were washed three times in PBS before the application of the relevant Alexa Fluor-488, 594 or 647 conjugated secondary antibodies diluted 1:750 in 10 % (v/v) FBS in PBS followed by 2 hrs incubation at RT in the dark. Lipid droplets were stained using BODIPY (558/568)-C12 dye at 1:1000 (Life Technology). The coverslips were washed three times in PBS before the nucleus was stained by the addition of 4', 6'-diamidino-2-phenylindole dihydrochloride (DAPI) diluted 1:10 000 in PBS for 30 min at RT in the dark. Coverslips were washed three times in PBS and mounted on a glass microscope slide in ProLong Gold antifade reagents (Invitrogen, Molecular Probes) and sealed with nail varnish. Slides were stored at 4^{o}C in the dark until required and examined. Confocal microscopy images were acquired on a Zeiss LSM880 microscope with Airyscan, post-acquisition analysis was conducted using Zen software (Zen version 2015 black edition 2.3, Zeiss) or Fiji (v1.49) software.

2.5.7 Co-localisation analysis

For co-localisation analysis, Manders' overlap coefficient was calculated using Fiji ImageJ software with Just Another Co-localisation Plugin (JACoP) (National Institutes of Health). Coefficient M1 reports the fraction of the LD signal that overlaps either the anti-NS5A or anti-

core signal or the fraction of anti-core signal that overlaps the anti-NS5A signal. Coefficient M2 reports the fraction of either the anti-NS5A or anti-core signal that overlaps the LD signal or the fraction of anti-NS5A that overlaps the anti-core signal. Coefficient values range from 0 to 1, corresponding to non-overlapping images and 100% co-localization images, respectively. Co-localisation calculations were performed on >10 cells from at least two independent experiments.

2.5.8 Quantification of LD distribution and size

For the quantification of LD spatial arrangement, images were acquired with the same acquisition parameters, but with variable gain to ensure correct exposure. The two-dimensional coordinates of the centroids of LDs were calculated using the Analyze Particles module of Fiji (ImageJ). The distance of each particle to the edge of the cell's nucleus, visualised using DAPI stain, was looked up using a Euclidean distance map computed with the Distance Transform module of Fiji and exported as a list of distance 2D measurements via the Analyze Particle function. Box and whisker plots of these distance measurements were constructed using GraphPad Prism and compared between samples using a one-way ANOVA and Bonferroni-corrected post-hoc t-tests.

Two-dimensional areas of the LDs were also measured using the Analyze Particles function in Fiji. Lists of the area measurements were used for constructing frequency histograms using a custom-written programme implemented in IDL. The shapes of these histograms were compared using a chi-squared test, implemented in IDL.

2.5.9 Isolation of lipid droplets

Four 10cm^2 dishes of Huh7.5 cells electroporated with mJFH1 virus RNA (80% confluent) were scraped into 10 mL of PBS at 72 hpe. The cells were pelleted by centrifugation at 1,500 rpm for 5 min and then resuspended with 500 µL buffer A (20 mM Tricine, 250 mM sucrose, pH 7.8) supplemented with protease and phosphatase inhibitors and kept on ice for 20 min. The suspension was homogenized with a plastic tissue grinder homogenizer. Samples after homogenization were centrifuged at 3000 g for 10 min at 4°C to remove nuclei and the post nuclear supernatant (PNS) was collected, transferred into 2.2 mL tubes and overlaid with 1 mL of buffer B (20 mM HEPES, 100 mM KCl and 2 mM $MgCl_2$ pH 7.4) plus protease inhibitors. Tubes were centrifuged in a S55S rotor at 100,000 g for 1 hr at 4°C. After centrifugation, the LD fraction on the top of the gradient was recovered in buffer B and washed twice by centrifugation at 20,000 g for 5 min at 4°C to separate the LDs from the buffer. Underlying

solution was removed and discarded. Proteins and lipids in LD samples were separated with 2 volumes of ice-cold acetone and chloroform (1:1) to precipitate proteins. The collected LD fraction was dissolved in 50µL of SDS sample loading buffer for western blot.

2.5.10 Proximity Ligation Assay (PLA)

Cells were washed with PBS before fixation for 15 min at room temperature in 4% (wt/vol) paraformaldehyde (PFA); cells were subsequently permeabilized in 0.1% (vol/vol) Triton X-100 –PBS and blocked with PBS-Tween (PBS-T) and 5% (wt/vol) bovine serum albumin (BSA) before immunostaining for anti-NS5A (Sheep polyclonal, 1:1,000) and anti-ApoE (Mouse monoclonal, 1:100) overnight at 4 °C. Coverslips were washed 3 times for 5 min in PBS-T buffer under gentle shaking and incubated with proximity ligation assay (PLA) probes Duolink In Situ PLA Probe Anti-Mouse PLUS (DUO92001; Sigma-Aldrich) and Duolink In Situ PLA Probe Anti-Sheep MINUS (DUO92005) for 2 hrs at 37°C. For PLA, all incubations were performed in a preheated humidity chamber and according to manufacturer's recommendations using a Duolink In Situ Detection Reagents Red kit (DUO92008). Coverslips were washed 3 times for 5 min in PBS-T buffer under gentle shaking and incubated with a DNA ligase previously diluted in ligation buffer for 30 min at 37°C. Coverslips were washed 3 times for 5 min in PBS-T buffer under gentle shaking and incubated with a DNA polymerase previously diluted in amplification buffer for 90 min at 37°C. Finally, coverslips were washed for 20 min under gentle shaking and then washed for 2 min with PBS and air dried. Coverslips were mounted with Duolink In Situ mounting medium with 4',6'-diamidino-2-phenylindole (DAPI), and fluorescence was visualized with a Zeiss LSM880 upright microscope.

2.5.11 Purification of OST-NS5A

In vitro transcribed JFH1-5A-OST RNAs were electroporated into Huh7.5 cells and seeded in 10cm x10cm dishes. Cells were washed twice in PBS 72 hpe, pelleted at 1500 g for 5 min at RT, before lysis in GLB (1ml per dish). Lysates were clarified by centrifugation at 10,000 g for 5 min at 4°C. Supernatants were applied to 100 µL of Strep-Tactin Sepharose for batch affinity purification of NS5A-OST following the manufacturer's instructions. After incubation overnight at 4 °C, the mixtures were washed with wash buffer (100 mM Tris-HCl, pH 8.0, 150 mM NaCl 1mM EDTA) three times. Bound protein was eluted with 50 µL of SDS sample buffer and heated for 10 min at 95 °C for western blot analysis.

2.6 In vitro protein assays

2.6.1 Purification of NS5A domain I

DNA fragments flanked with *BamH*I and *Xho*I restriction sites encompassing amino acids 35 to 215 and 35 to 249 of NS5A were amplified by PCR using wildtype or mutant JFH1 SGRs as templates (primer sequences are available in Appendix Table 9.4). PCR products were cleaved with *BamH*I and *Xho*I and cloned into pET28a-SUMO vector to allow expression of Domain I N-terminally fused to a His-SUMO affinity tag. The resulting plasmids were transformed into cultures of Escherichia *coli* BL21 (DE3) pLysS, which were grown to OD_{600} 0.6-0.8 at 37 °C and induced with 100 µM isopropyl β-D-1-thiogalactopyranoside (IPTG) at 18°C for 6 hrs. Cells were recovered by centrifugation and resuspended in 20ml His-SUMO-Domain I (His-SUMO-DI) lysis buffer (binding buffer (100 mM Tris pH 8.2, 200 mM NaCl, 20 mM imidazole) supplemented with 40 µl DNase, 40 µl RNaseA, 2 mg/ml Lysozyme and protease inhibitors (Roche)) per 1 L of pelleted culture. Cell suspension were placed on ice for 30 min and lysed by sonication on ice at amplitude of 10 microns for 12 pulses of 20 sec separated by 20 sec. The extract was clarified by centrifugation at 18,000 rpm for 30 min at 4 °C twice and then supernatant was filtered through a 0.45 µm syringe filter. His-SUMO-DI protein samples were applied to wash buffer equilibrated HisTrap column (GE Healthcare). The column was washed 3 times with 5 column volumes binding buffer and eluted using the same buffer with 250 mM imidazole. Elution fractions of His-SUMO-DI proteins were then dialyzed into dialysis buffer (20 mM Tris-HCl, pH 8.2, 150 mM NaCl and 10% (v/v) glycerol) prior to addition of SUMO protease. After SUMO protease cleavage, the His-SUMO tag and SUMO protease were removed from the cleavage sample by passing it through a second HisTrap column. After checking by SDS-PAGE, The flow-through and wash fractions containing domain I were pooled and concentrated using 10 kDa molecular mass centrifugal concentrators (Merck) and stored at -80 °C after flash freezing in liquid nitrogen.

For the expression and purification of Domain I (35-249) with GST tag, DNA fragments flanked with *BamH*I and *Xho*I restriction sites were cloned into either pGEX6P-2 vector to allow expression of Domain I N-terminally fused to either GST. The resulting plasmids were transformed into cultures of E. coli BL21 (DE3) pLysS and induced for expression at 18°C for 6 hrs as described above. Cells were recovered by centrifugation and resuspended in 20 mL GST-Domain I (GST-DI) lysis buffer (50mM Tris-HCl, pH 8.0, 100mM NaCl, 10% glycerol) supplemented with 40 µl DNase, 40 µl RNaseA, 2 mg/ml Lysozyme and protease inhibitors (Roche) per 1L of pelleted culture. Cell suspensions were placed on ice for 30 min and lysed by

sonication followed by centrifugation at 18,000 rpm for 30 min at 4 °C twice and then supernatant was filtered through a 0.45 µm filter. GST-DI protein was applied to glutathione Sepharose 4B resin (GE Healthcare) following the manufacturer's instructions. The resin was eluted with elution buffer (50 mM Tris-HCl, 10 mM reduced glutathione, pH 8.0) and the eluates were dialyzed against dialysis buffer (50 mM Tris-HCl, pH 7.5, 100 mM NaCl, 5 mM MgCl2, 10% glycerol, 0.5% NP-40). The purified proteins were aliquoted and stored at -80 °C.

2.6.2 Size exclusion chromatography

Size-exclusion chromatography (SEC) is a type of liquid chromatography commonly used for analysis of polymeric status of NS5A Domain I. HiLoad Superdex 75 pg column (GE Healthcare) was used and connected to AKTA Prime pump system at 4 °C. Absorbance at 280 nm was measured to monitor protein eltutions. All the buffers containing distilled water, gel filtration running buffer and 70% ethanol were filtered through 0.45 µm membranefilters (Millipore)and degassed. After thorough wash by water, the Superdex 75 pg column was equilibrated with gel filtration running buffer (20 mM Tris-HCl, pH 8.2, 150 mM NaCl and 10% (v/v) glycerol). 5 ml concentrated domain I protein sample was then filtered through a 0.2 µm syringe filter before being injected into the column with 5 mL loop. The column was eluted and fractions (3 ml/ fraction) were collected until a full column of volume of running buffer (320 ml) was loaded. According to the recording of A280, each fraction collected was analysed by SDS-PAGE.

2.6.3 Protein identification by mass spectrometry

2.6.3.1 Gel processing and tryptic digestion

Gel bands were excised and chopped into small pieces (~ 1 mm^3), covered with 30 % ethanol in a 1.5 mL microcentrifuge and heated to 70 °C for 30 min with shaking. The supernatant was removed and replaced with fresh ethanol solution and again heated to 70 °C for 30 min with shaking. This was repeated until all Coomassie stain was removed from the gel. The gel slices were covered with 25 mM ammonium bicarbonate/50% acetonitrile and incubated for 10 min with shaking. The gel slices were then covered with 100% acetonitrile and left for five minutes before the supernatant was discarded and replaced with a fresh aliquot of acetonitrile. 100 µL 20 mM DTT solution was then added and the sample was incubated at 57 °C for 1 hr with shaking. The supernatent was removed and once the gel pieces were at room temperature 100 µL 55 mM iodoacetic acid was added. The samples were then incubated at room temperature in the dark for 30 min with shaking. After removing the supernatant, the gel slices were then covered with 100% acetonitrile and left for 5 min. The acetonitrile was removed and the gel

pieces were left to dry in a laminar flow hood for 60 min. Once dry, the gel slices were cooled on ice then they were covered with ice-cold trypsin solution (20 ng µL-1 in 25 mM ammonium bicarbonate) and left on ice for 10 min to rehydrate. Excess trypsin solution was removed and the gel slices were covered with a minimal amount of 25 mM ammonium bicarbonate. After briefly vortexing and centrifuging, the gel slices were incubated at 37 °C with shaking for 18 hrs. The resulting digest was vortexed and centrifuged. The supernatant was recovered and added to an eppendorf containing 5 µL acetonitrile/ water/ formic acid (60/35/5; v/v). 50 µL acetonitrile/ water/ formic acid (60/35/5; v/v) was added to the gel slices and vortexed for an additional 10 min. The supernatant was pooled with the previous wash and one additional wash of the gel slices was performed. The pool of three washes was dried by vacuum centrifugation. The peptides were reconstituted in 20 µL 0.1% aqueous trifluoroacetic acid.

2.6.3.2 Liquid chromatography-mass spectrometry (LC-MS)

LC separation of the peptide mixtures was performed on an ACQUITY M-Class UPLC (Waters UK, Manchester). 1 µL of each sample was loaded onto a Symmetry C18 trap column (180 µM i.d. * 20 mm) and washed with 1% acetonitrile/0.1% formic acid for 5 min at 5 µL /min. After valve switching, the peptides were then separated on a HSS T3 C18, 75 µm i.d. x 150 mm analytical column (Waters UK, Manchester) by gradient elution of 1-60% solvent B in A over 30 min at 0.3 µL /min. Solvent A was 0.1% formic acid in water, solvent B was 0.1% formic acid in acetonitrile.

The column eluant was directly interfaced to a quadrupole-ion mobility - orthogonal time of flight mass spectrometer (Synapt G2Si, Waters UK, Manchester) via a Z-spray nanoflow electrospray source. The MS was operated in positive TOF mode using a capillary voltage of 3.0 kV, cone voltage of 40 V, source offset of 80 V, backing pressure of 3.58 mbar and a trap bias of 2 V. The source temperature was 80°C. Argon was used as the buffer gas at a pressure of 8.6 × 10-3mbar in the trap and transfer regions. Mass calibration was performed using Glu-fibrinopeptide (GFP) at a concentration of 250 fmol /µL. GFP was also used as a lock mass calibrant with a one second lock spray scan taken every 30 s during acquisition. Ten scans were averaged to determine the lock mass correction factor. Data acquisition was using data dependent analysis with a 0.2 sec scan MS over m/z 350-2000 being followed by five 0.5 sec MS/MS taken of the five most intense ions in the MS spectrum. CE applied was dependent upon charge state and mass of the ion selected. Dynamic exclusion of 60 sec was used. Data processing was performed using the MassLynx v4.1 suite of software supplied with the mass spectrometer. Peptide MS/MS data were processed with PEAKS Studio (Bioinformatic Solutions

Inc, Waterloo, Ontario, Canada) and compared with NS5A domain I sequence. Carbamiodomethylation was selected as a fixed modification, variable modifications were set for oxidation of methionine and deamidation of glutamine and asparagine. MS mass tolerance was 20 ppm, and fragment ion mass tolerance was 0.05 Da. The false discovery rate was set to 1%.

2.6.4 SEC-MALLS

SEC-MALLS was carried out by Maren Thomsen (School of Biomedical Sciences, University of Leeds).

2.6.5 GST-pull down assay

After purification, GST-Domain I (GST-DI) and His-SUMO-Domain I (His-SUMO-DI) were dialyzed against dialysis buffer (50 mM Tris-HCl, pH 7.5, 100 mM NaCl, 5 mM $MgCl_2$, 10% glycerol, 0.5% NP-40). Meanwhile, 10 µg of GST or GST-fusion proteins were mixed with 5 µg of His-SUMO-DI in binding buffer (20mM Tris-HCl, pH 7.2, 0.5 M NaCl, 200 Mm KCl, and 1% NP-40) for 3 hrs at 4 °C on a rotating platform. Then the mixture was added to glutathione beads and incubated overnight at 4°C. After washes using binding buffer, bound material was eluted with 50 µL of SDS sample buffer and heated for 10 min at 95 °C. After centrifugation, these samples were analysed by western blot using anti-GST and anti-His antibodies.

2.6.6 In vitro transcription and labelling of RNA probe

The 3'UTR of HCV genotype 2a (JFH1) (9443-9678), amplified and flanked with *Hind*III and *Xba*I was cloned into pcDNA3.1 vector. As negative control, an aptamer selected against the foot-and-mouth disease virus (FMDV) 3D RNA-dependent RNA polymerase was used (5'-GGGAAAGGAUCCACAUCUACGAAUUCGGCUCAAAAAUAGUCCGCACCAUACAUUCACUGCAGAC UUGACGAAGCUU-3'). Complementary oligonucleotides with BamHI and XbaI were synthesized. Post annealing, the fragment of this aptamer was digested with NheI and XbaI and then inserted into pcDNA3.1 vector with same adhensive ends. pcDNA3.1 -3'UTR and pcDNA3.1 –FMDV 3D aptamer were linearized by *Xba*I as a template for in vitro transcription.

In vitro transcription reactions consisted of 500 µM each of ATP, CTP, and GTP; 20 µM UTP; 50 µCi (α-^{32}P) UTP; 40 U of T7 RNA polymerase; 2µl 10x T7 transcription buffer (Roche); 40 U of RNaseOUT RNase (Invitrogen) and 1µg linearized DNA template). Reactions were incubated for 1.5 hrs at 37°C before addition of 1U RQ1 DNase (Promega) to remove template DNA. RNA transcripts were then purified using NucAway spin columns (Ambion) before extraction with acidified phenol-chloroform and ethanol precipitation described in section 2.2.1.11. Purified

RNA transcripts were analysed on 1 % RNA agarose gels. Concentrations of radioactive RNAs were determined by absorbance at 260 nm.

2.6.7 RNA filter binding assay

His-SUMO-DI proteins were cleaved with SUMO protease to produce native domain I. Following purification in 2.6.1, domain I was incubated with in vitro transcribed (α-^{32}P) radiolabelled RNAs. Then aliquots of each binding reaction were applied to a pre-assembled slot blot apparatus and filtered through firstly a nitrocellulose membrane (Schleicher & Schuell) to capture soluble protein-RNA complexes, and secondly a Hybond-N nylon membrane (Amersham Biosciences) to bind free RNA. After washing and air drying of both membranes, quantification of radioactivity was performed by phosphoimaging using an FLA 5000 Imaging system (Fuji), and ImageJ software. These data were fitted to the hyperbolic equation "R=Rmax×P/(Kd+P)". R is the percentage of bound RNA, Rmax is the maximal percentage of RNA competent for binding, P is the concentration of domain I, and Kd is the dissociation constant.

2.6.8 Tandem Mass Tag (TMT) comparative proteomic analysis

TMT mass spectrometry was carried out by Kate Heesom (University of Bristol Proteomics Facility) and analysed against both positive and negative control samples.

In brief, for multiplexed comparative proteomics 100 µg of each cell lysate was digested with trypsin and labelled with tandem mass tag (TMT) reagents according to the manufacturer's protocol (Thermo Fisher Scientific, Waltham, Massachusetts, USA). The labelled samples were then pooled, evaporated to dryness and resuspended prior to fractionation by high pH reversed-phase chromatography using an Ultimate 3000 liquid chromatography system (Thermo Fisher Scientific). After high pH reversed-phase chromatography, fractions were further subjected to the Nano-LC Mass Spectrometry. The raw data files were processed and quantified using Proteome Discoverer software v1.4 (Thermo Scientific) and searched against the Uniporter Human database (134169 sequences) plus HCV protein sequences using the SEQUEST algorithm. All peptide data was filtered to satisfy false discovery rate (FDR) of 5%.

2.7 Statistical analysis of data

Statistical analysis of data was carried out using a Students t-test assuming a two-tailed distribution with an unequal variance. Error bars presented on all graphs illustrate the Standard Error (SE) of the Mean.

Chapter 3: The role of NS5A domain I in virus replication

3.1 Introduction

Following uncoating and release of the HCV RNA genome into the cytoplasm post infection, the RNA is translated at the rough ER, which contains the cellular proteases that cleave part of the polyprotein. HCV replicase proteins (NS3-NS5B), presumably in concert with host cell factors, induce massive rearrangement of intracellular membranes, including the formation of double-membraned vesicles (Wang and Tai, 2016). These membranous structures exhibit as vesicle clusters that designate the membranous web and constitute the sites of HCV RNA replication (Penin et al., 2004). Replication of all positive strand RNA viruses is associated with cellular membranes, and depending on the virus replication might occur on altered membranes derived from the ER, Golgi apparatus, mitochondria or even lysosomes. In HCV infected cells, NS5A localizes to the endoplasmic reticulum (ER), virus-induced multiple-membrane vesicles (MMV) that host RNA replication complexes (also called the membranous web), and to lipid droplets. The MMV contain the NS proteins NS3-NS5B and virus RNA and represent sites of active genome replication, which are called replication complexes (RCs) (Paul and Bartenschlager, 2013, Egger et al., 2002, Gosert et al., 2003, Paul et al., 2014, Romero-Brey et al., 2012).

Within RC, NS5A is indispensable for RNA replication, which is mediated by binding to viral RNA (Foster et al., 2010, Huang et al., 2005), and interactions with other NS proteins and various cellular factors, including vesicle-associated membrane protein-associated proteins A and B (VAP-A, VAP-B), cyclophilin A (CypA) and phosphatidylinositol-4-kinase IIIα (PI4KIIIα) as described in Section 1.3.2 (Berger et al., 2009, Gao et al., 2004, Hamamoto et al., 2005, Ngure et al., 2016, Goonawardane et al., 2017). Nevertheless, most investigations of the mechanism of RNA replication are focused on domain II and III, so it remains to be determined how domain I functions during RNA replication.

By primary sequence comparison, domain I of NS5A shares a high sequence homology among both primate and non-primate species (Burbelo et al., 2012, Kapoor et al., 2011, Kapoor et al., 2013, Lauck et al., 2013), while domain II and III exhibit a lower level of homology. Secondary structure predictions using PSIPRED indicated a similar topology consisting of two α-helices and three β-strands across domain I, and tertiary modelling supported high structural similarity between zinc-binding motifs with predicted β-strands arranging to form an antiparallel β-sheet in all hepaciviruses including GHV and GBV-B (Arumugaswami et al., 2008). However, domain II and III share a low homology. These observations suggest that domain I has critical and well-conserved functions that are common to all hepaciviruses, whereas the functions of the other

two domains may be specific to individual genotypes. Consistent with this hypothesis, transposon mutagenesis demonstrated that very few insertion sites in domain I were tolerated (in comparison to domains II and III) (Arumugaswami et al., 2008). Later, saturation mutagenesis in combination with next-generation sequencing technology systematically quantified the effect of every possible amino acid substitution in the N-terminus of domain I, the potential drug-targeted region. The relative fitness and drug sensitivity profiles results revealed that very few residues in the N-terminus of domain I (amino acids 18-103) can tolerate substitutions (Qi et al., 2014).

Moreover, domain I is highly structured in comparison with domain II and III. There are four different dimeric forms of NS5A domain I from genotype 1a and 1b by three independent groups. All the structures agreed on the same monomeric unit, but the monomers assembly into dimers with different rotations and interfaces (Lambert et al., 2014, Love et al., 2009, Tellinghuisen et al., 2005). The 'claw-like' dimer of NS5A domain I from genotype 1b revealed by Tellinghuisen (Tellinghuisen et al., 2005), designated as "open" conformation (1ZH1) (Ross-Thriepland and Harris, 2014b), generated a groove facing away from the membrane, where it could accommodate either single- or double-stranded RNA. The deep, highly basic portion of the groove could favour contacts with RNA whereas the 'arms' extending out past this groove are more acidic, and might serve to prevent RNA from exiting the groove (Tellinghuisen et al., 2005). RNA binding properties of NS5A and domain I have been confirmed biochemically in *vitro* (Foster et al., 2010, Huang et al., 2005). However, how domain I is involved in RNA replication is still not well understood yet. The other "closed" conformation exhibited an extensive buried surface area to form the dimer interface by residues 92 to 99, 112 to 116, 139 to 143, 146 to 149, and 160 to 161 from each monomer (Love et al., 2009). It is suspected that these two alternate structural forms of domain I reflect two different functional states of membrane-anchored NS5A and the differential exposure of surface features of both dimers would allow an alternative set of interactions between domain I and other HCV or host proteins. The "open" dimeric state, with its suggestive binding cleft, might promote RNA binding during NS5A's participation in the replication phase, whereas the "closed" dimeric state might be a prerequisite for NS5A roles in lipid droplets (LDs) association and/or particle assembly (Love et al., 2009, Ross-Thriepland and Harris, 2014b). Nevertheless, all the crystal structures of domain I are from HCV genotype 1, and there are no more crystal structures from other genotypes so far. Hence, both the "open "and "closed" dimeric structures were used as the model for analysis in my research.

Based on these observations, it was suggested that domain I has critical and well-conserved functions that are common to all hepaciviruses, whereas the functions of the other two domains may be specific to individual genotypes In this regard, it is generally accepted that the function(s) of domain I are required exclusively for genome replication, and the majority of domain II together with all of domain III are dispensable for replication. In this study, I present evidence that domain I of NS5A plays a key role in genome replication in details by combining analyses of both sequences alignment from 7 HCV genotypes and dimeric structures.

3.2 Results

3.2.1 Generating a panel of alanine mutations in domain I

In comparison with domain II and domain III (domain organization and position in NS5A was presented in Figure 3.1A), domain I of NS5A is highly conserved throughout all HCV isolates, and is also well conserved in related viruses such as GB virus type B (GBV-B) and the novel hepaciviruses that have recently been identified in a variety of species (Figure 3.1B). In addition, the structure of domain I has been determined by three independent studies (Huang et al., 2007b, Ross-Thriepland et al., 2013, Tellinghuisen et al., 2004) - all three studies agree on the monomer structure but show these monomers assembling into dimers with different monomer orientations and dimer interfaces (Figure 3.2). In this study, I initially set out to define residues in domain I that were required for viral genome replication. To this end, amino acid sequences of NS5A domain I were first aligned from 29 isolates representing all 7 HCV genotypes, together with 10 related viruses such as bat hepacivirus (BHV), GB virus-B (GBV-B), guereza hepacivirus (GHV), non-primate hepacivirus (NPHV) and rodent hepacivirus (RHV) (Appendix Table 9.2) . This analysis revealed 24 absolutely conserved residues (Table 3.1). Then these conserved residues were mapped on to the two genotype 1b monomeric structures (PDB 1ZH1 and 3FQM) of domain I to identify surface exposed residues, particularly those that are charged (Figure 3.2). This analysis revealed 11 residues that were then targeted for alanine scanning mutagenesis and subsequent profiling in the context of the JFH1 sub-genomic replicon (SGR). In addition, a conserved surface exposed cluster (residues 153 to 158) was mutated collectively to alanine as these residues were located in close proximity on the tertiary structure (Table 3.1).

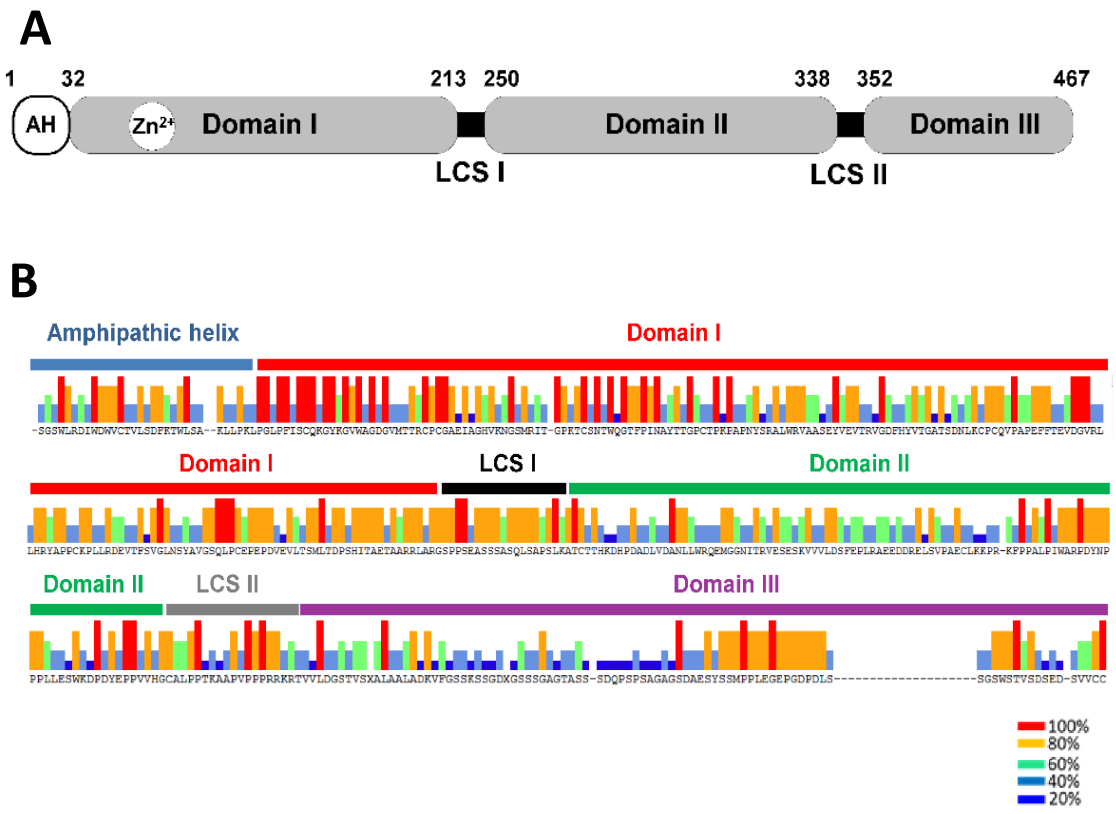

Figure 3.1 Alignment of NS5A sequences from 7 HCV genotypes and related hepaciviruses.

A. Schematic representation of the domain organization of NS5A showing the locations of the three domains (I-III), the linking low complexity sequences (LCSI and II), and the membrane anchoring amphipathic helix (AH). Numbers indicate positions of amino acids in the JFH1 genotype 2a NS5A sequence. **B.** Conservation of three different NS5A domains from 15 HCV isolates representing each genotype and related hepaciviruses. Isolates used for conservation analysis of whole NS5A are listed and underlined in Appendix Table 9.2. Filled bars in different colours indicate the percentage conservation at each residue as indicated in the key below. Gaps refer to locations where there are insertions in the JFH1 sequence, compared to consensus, particularly the 18 amino acid insertion between residues 432-450.

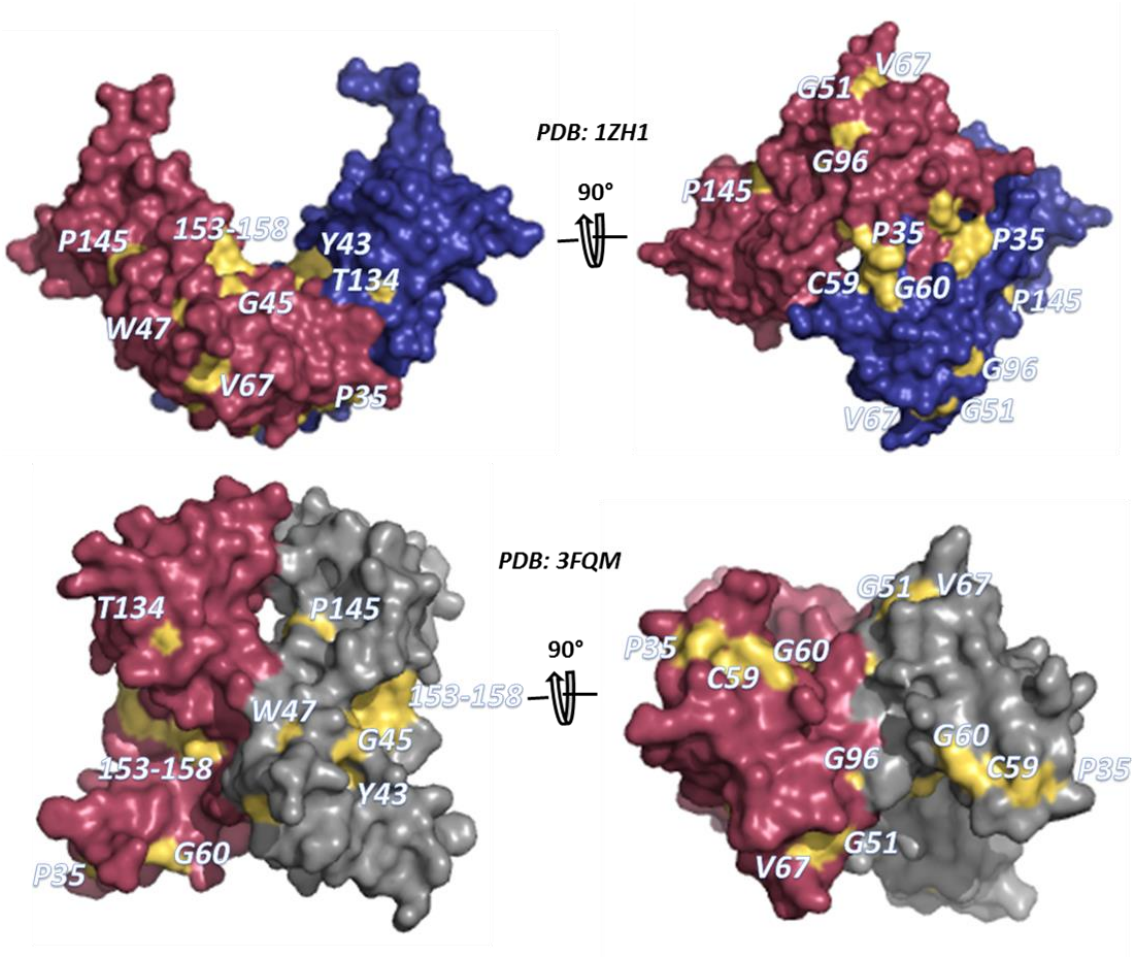

Figure 3.2 Analysis of the three dimensional structures of domain I.

Analysis of the three dimensional structures of domain I (1ZH1 – open conformation - and 3FQM – close conformation) using Pymol. Residues highlighted are the conserved amino acids that are located on the surface of two dimeric conformations at positions indicated in Table 3.1.

Conserved residues	Surface(1ZH1)	Surface(3FQM)	Mutation
P35	+	+	+
C39	++	++	
Y43	+	+	+
G45	+	+	+
W47	+	+	+
G51	+	+	+
C57	++	++	
C59	++	++	+
G60	+	+	+
V67	+	+	+
C80			
P89			
I90			
N91		+	
G96	+	+	+
P100			
G132			
T134	+	+	+
P145	+	+	+
V153	+	+	
D154	+	+	
G155	+	+	+
V156	+	+	
L158	+	+	

Table 3.1 Summary of selection of residues for mutation in NS5A domain I and their phenotypes.

'+' indicates that the residue is located on the surface of domain I.
'++' indicates that the residue is both surface exposed and at the zinc-binding site.

3.2.2 The role of domain I in genome replication

To investigate the role of the selected conserved residues in domain I, the mutants were cloned into a previously described JFH1 derived SGR (mSGR-luc-JFH1) in which the NS5A coding sequence was flanked by unique restriction sites to facilitate sub-cloning. RNAs transcribed from the mutant panel were electroporated into Huh7 cells and luciferase activity was measured at 4, 24, 48 and 72 hpe. The luciferase activity at 4 hpe correlates with translation of input transcripts prior to onset of replication and subsequent time points were normalized to the 4 hpe signal to account for electroporation efficiency. As a negative control an inactive mutant of the NS5B polymerase was used (GND) (Appel et al., 2008, Penin et al., 2004) .

Nine of the mutations (Y43A, G45A, W47A, G51A, C59A, G60A, G96A, T134A and 153-158A) were shown to completely disrupt the ability of the mSGR-luc-JFH1 to replicate in Huh7 cells (Figure 3.3A and B), being indistinguishable from the GND negative control. However, three mutants (P35A, V67A and P145A) were able to replicate, albeit at levels lower than wildtype (WT). P35A exhibited a modest but non-significant defect, in contrast V67A and P145A replicated at significantly lower levels than WT ($p<0.05$) (Figure 3.3A and B). All mutants showed broadly comparable luciferase activity at 4 hpe, demonstrating that the replication phenotypes observed were not due to differences in electroporation efficiency (Figure 3.3A). To further support the luciferase data, total protein at 72 hpe was analysed by SDS-PAGE/western blot for both NS5A and GAPDH (Figure 3.3C). The western blot result showed that NS5A of P35A could be detected at low levels, but only in the basal phosphorylated form. For V67A and P145A, the absence of NS5A was expected, due to the very low levels of replication.

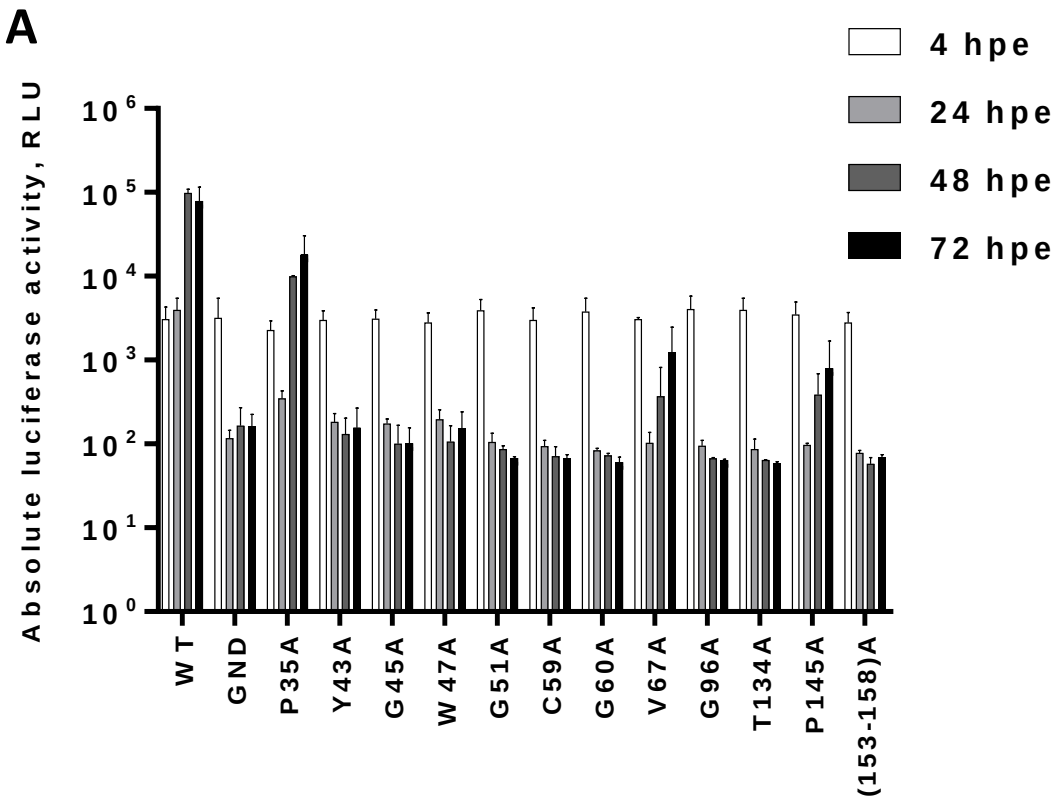
A
Absolute luciferase activity, RLU
10 6
10 5
10 4
10 3
10 2
10 1
10 0
4 hpe
24 hpe
48 hpe
72 hpe
WT
GND
P35A
Y43A
G45A
W47A
G51A
C59A
G60A
V67A
G96A
T134A
P145A
(153-158)A

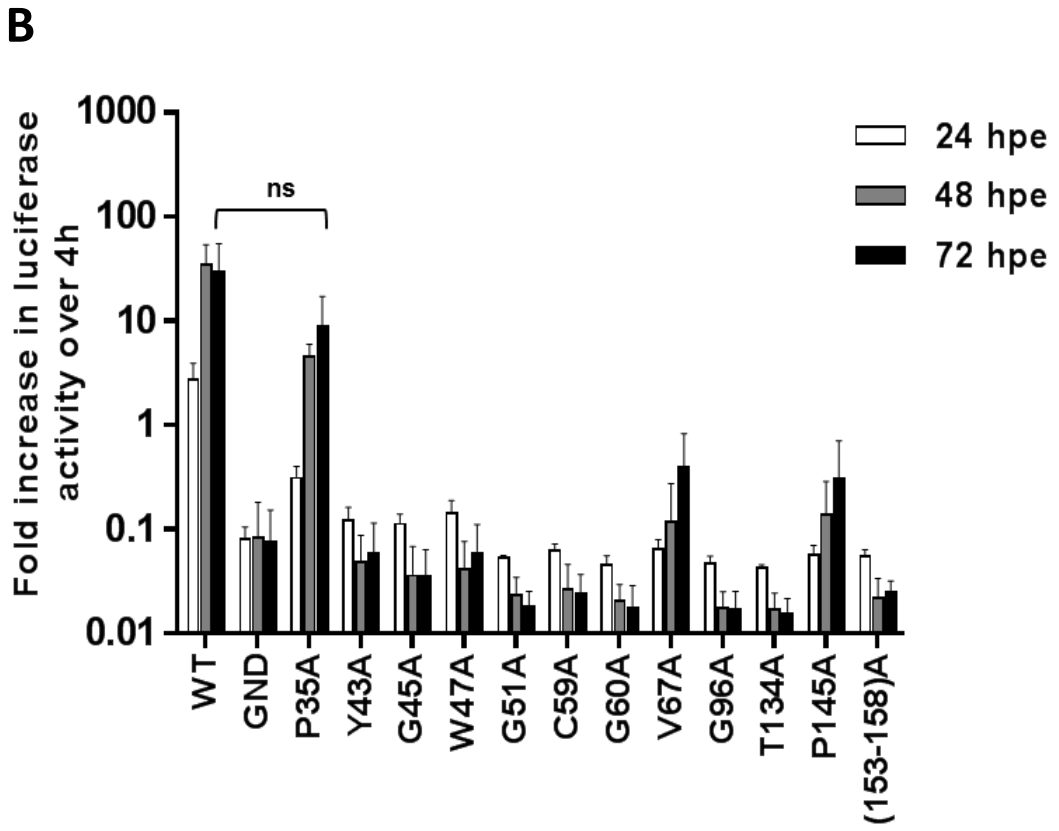
B
Fold increase in luciferase activity over 4h
1000
100
10
1
0.1
0.01
ns
24 hpe
48 hpe
72 hpe
WT
GND
P35A
Y43A
G45A
W47A
G51A
C59A
G60A
V67A
G96A
T134A
P145A
(153-158)A

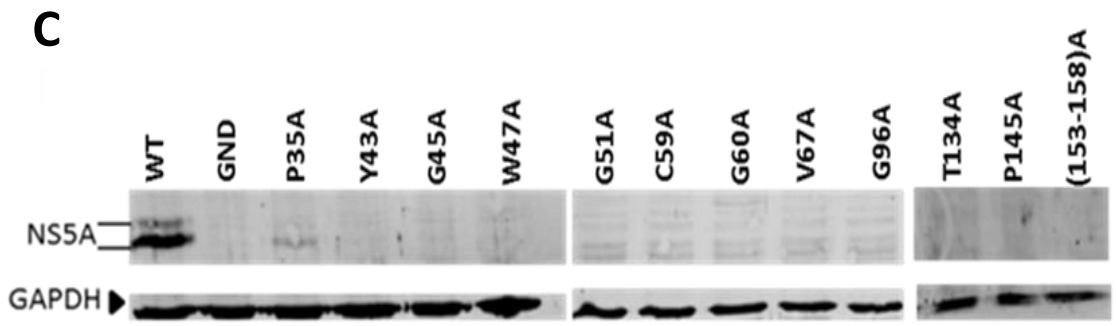

Figure 3.3 Genome replication phenotypes of NS5A domain I mutants in Huh7 cells.

A. In vitro transcripts of mSGR-luc-JFH1 containing the indicated mutations were electroporated into Huh7 cells. Luciferase activity was measured at 4, 24, 48 and 72 hpe and was normalized to 4 hpe (**B**). **C.** Cell lysates at 72 hpe were analysed by SDS-PAGE/western blot with anti-NS5A and anti-GAPDH. For non-replicating mutants, the expression of NS5A cannot be detected. For partially defective mutants, the NS5A (P35A) only can be detected at low levels, and NS5A (V67A and P145A) is not detectable because of the low replication levels. ns indicates not statistically significant. Data from three independent experiments are shown and error bars represent the standard error of the mean.

I then assessed whether the replication defects exhibited by these mutants could be a result of an innate immune response, rather than a lack of replicative capacity. It was reasoned that if mutants had a reduced replication capacity they might be more sensitive to inhibition by cytoplasmic innate immune sensors such as RIG-I, a pathogen receptor that binds HCV RNA and activates the IRF3 signalling pathway. To test this I evaluated the mutation panel in Huh7.5 cells which were derived from Huh7 cells and have an inactivating, dominant negative, mutation in one copy of the RIG-I gene (Tellinghuisen and Foss, 2008, Tellinghuisen et al., 2008b). This renders them highly permissive for HCV genome replication. As shown in Fig 3.4, those mutants that were unable to replicate in Huh7 cells (Y43A, G45A, W47A, G51A, C59A, G60A, G96A, T134A and 153-158A) exhibited the same phenotype in Huh7.5 cells, confirming that these residues are absolutely required for the function of NS5A in genome replication. However, the three mutants that were able to replicate in Huh7 cells, albeit at a lower level than WT, (P35A, V67A and P145A) were able to replicate more efficiently in Huh7.5 cells, reaching levels almost equivalent to the WT with modest but non-significant impairment (Figure 3.4A and B). The western blot result showed that the NS5A expression level of P35A, V67A and P145A had increased significantly. The hyperphosphorylated NS5A can be detected for P35A. For V67A and P145A, the NS5A can now be detected in basal form (Figure 3.4C). It is likely that the RIG-I deletion in Huh7.5 attenuates the innate response to early replication events allowing mutants with a partial defect to replicate with high efficiency.

A

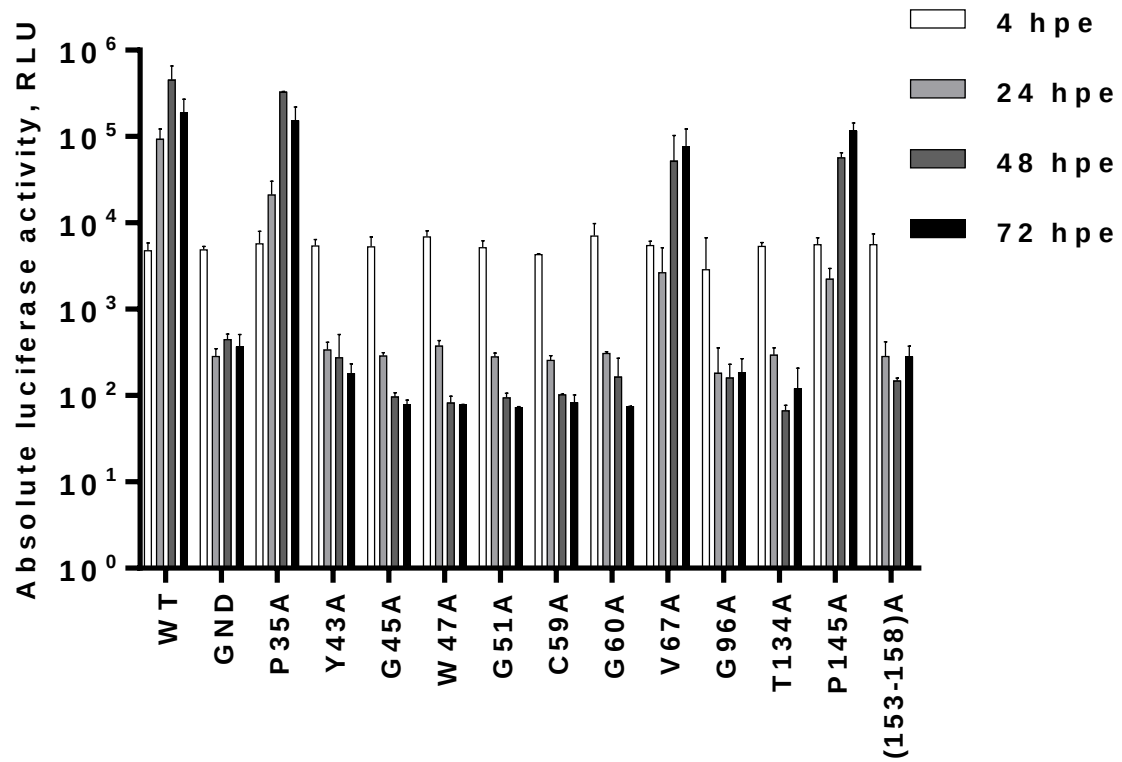
Absolute luciferase activity, RLU
10 6
10 5
10 4
10 3
10 2
10 1
10 0
4 hpe
24 hpe
48 hpe
72 hpe
WT
GND
P35A
Y43A
G45A
W47A
G51A
C59A
G60A
V67A
G96A
T134A
P145A
(153-158)A

B

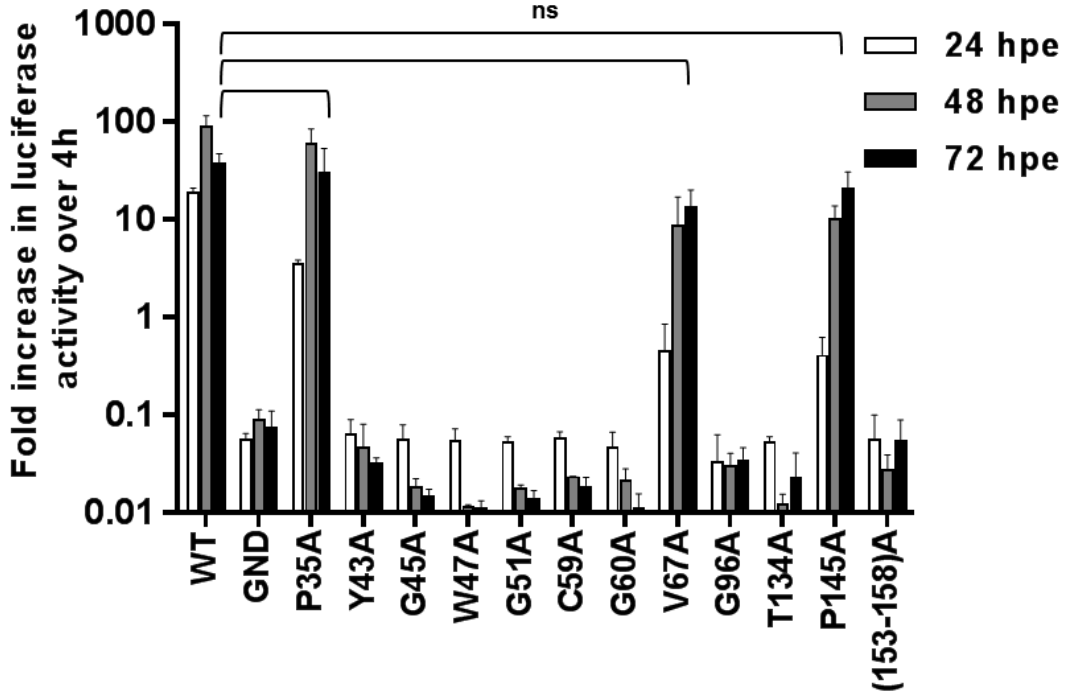
Fold increase in luciferase activity over 4h
1000
100
10
1
0.1
0.01
ns
24 hpe
48 hpe
72 hpe
WT
GND
P35A
Y43A
G45A
W47A
G51A
C59A
G60A
V67A
G96A
T134A
P145A
(153-158)A

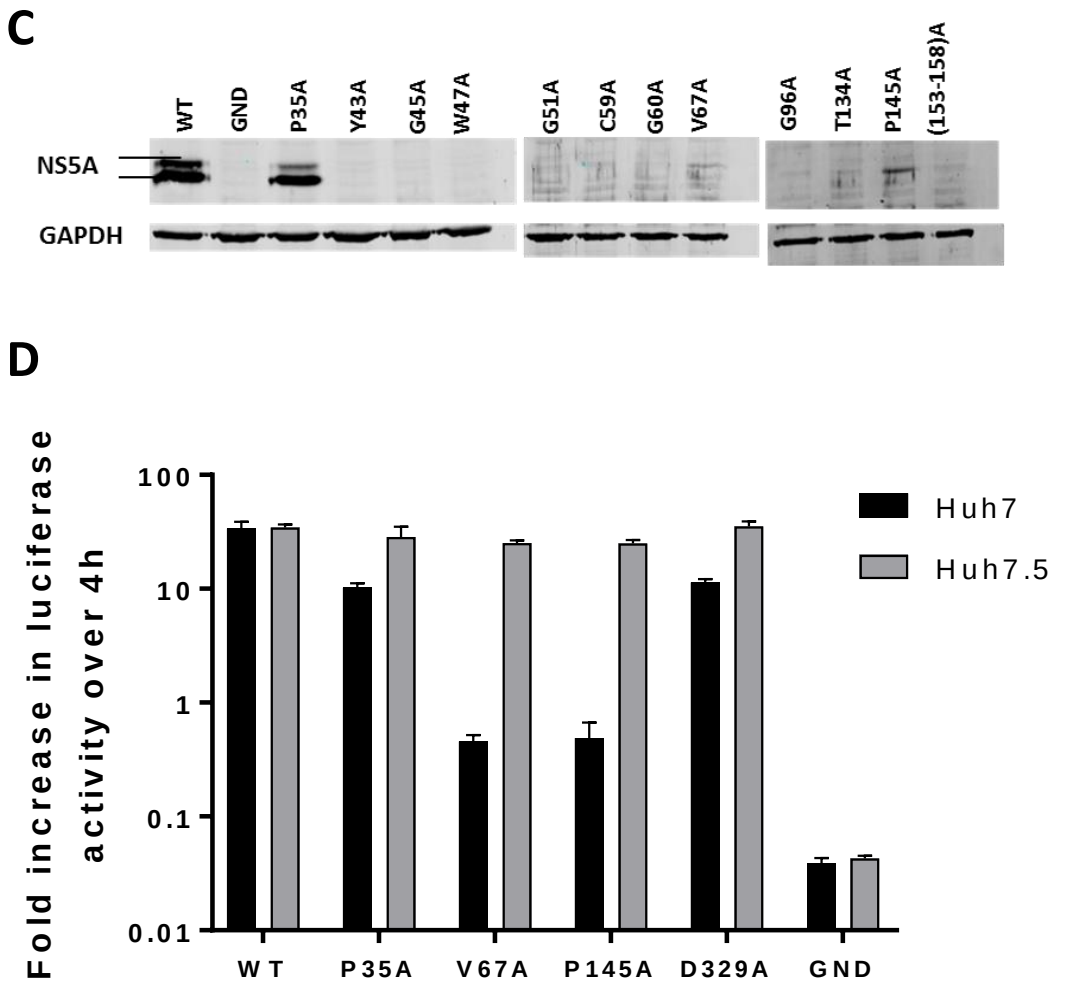

Figure 3.4 Genome replication phenotypes of NS5A domain I mutants in Huh7.5 cells.

A. In vitro transcripts of mSGR-luc-JFH1 containing the indicated mutations were electroporated into Huh7.5 cells. Luciferase activity was measured at 4, 24, 48 and 72 hpe and was normalized to 4 hpe (**B**). **C.** Cell lysates at 72 hpe were analysed by SDS-PAGE/western blot with anti-NS5A and anti-GAPDH. For non-replicating mutants, the expression of NS5A cannot be detected. For partially defective mutants, the NS5A of P35A can be detected in both basal and hyperphosphorylated forms, and NS5A (V67A and P145A) can only be detectable in basal form because of the low replication levels. **D.** A Comparison of replication of NS5A mutants in both Huh7 and Huh7.5 cells over 72 hpe. WT represents the wildtype mSGR-luc-JFH1. P35A, V67A, and P145A are the mutants of domain I which can replicate at lower levels than WT in Huh7 cells; D329 is located at the C terminus of NS5A domain II (Ross-Thriepland et al., 2013). Data from three independent experiments are shown and error bars represent the standard error of the mean. ns: no statistically significant difference from WT.

However, it was important to confirm that this permissiveness mediated by the RIG-I defect in Huh7.5 cells was not a phenomenon that was specific for domain I. To this end, an SGR containing a mutation (D329A) within NS5A domain II (Ross-Thriepland et al., 2013), which was previously reported replicated approximately 5-fold lower than WT, was electroporated into both Huh7 and Huh7.5 cells. As shown in Figure 3.4D, D329A was also able to replicate more efficiently in Huh7.5, demonstrating that this effect was not specific for domain I.

3.2.3 Lethal mutations do not disrupt polyprotein processing.

To investigate whether the defect in replication observed in the remaining mutants resulted from the loss or disruption of a specific function of NS5A, or disruption of polyprotein translation or proteolytic processing, all 12 mutants were cloned into an expression construct in which the NS3-5B coding sequencing of JFH1 were expressed from a human cytomegalovirus (CMV) promoter (pCMV10-NS3-5B), thus allowing replication - independent expression of replicase proteins.

These plasmids were transfected into Huh7.5 cells. After protein quantification, cell lysates were analysed for protein expression by western blot at 48 hours post transfection (hpt), taking HCV NS3 as polyprotein processing control. All 12 mutants expressed levels of NS5A comparable to WT ($p \geq 0.1$) (Figure 3.5). This confirmed that the lethal replication phenotype for these mutants results from loss or disruption of a specific function of NS5A rather than the global effects on NS5A translation and polyprotein cleavage. Nevertheless, the hyperphosphorylated NS5A form for most mutants (except P35A) was detected either at low levels (V67A, G96A, T134A, P145A and 153-158A) or was undetectable. This suggests that some mechanisms to regulate NS5A phosphorylation are affected by these mutations, which needs to be further investigated.

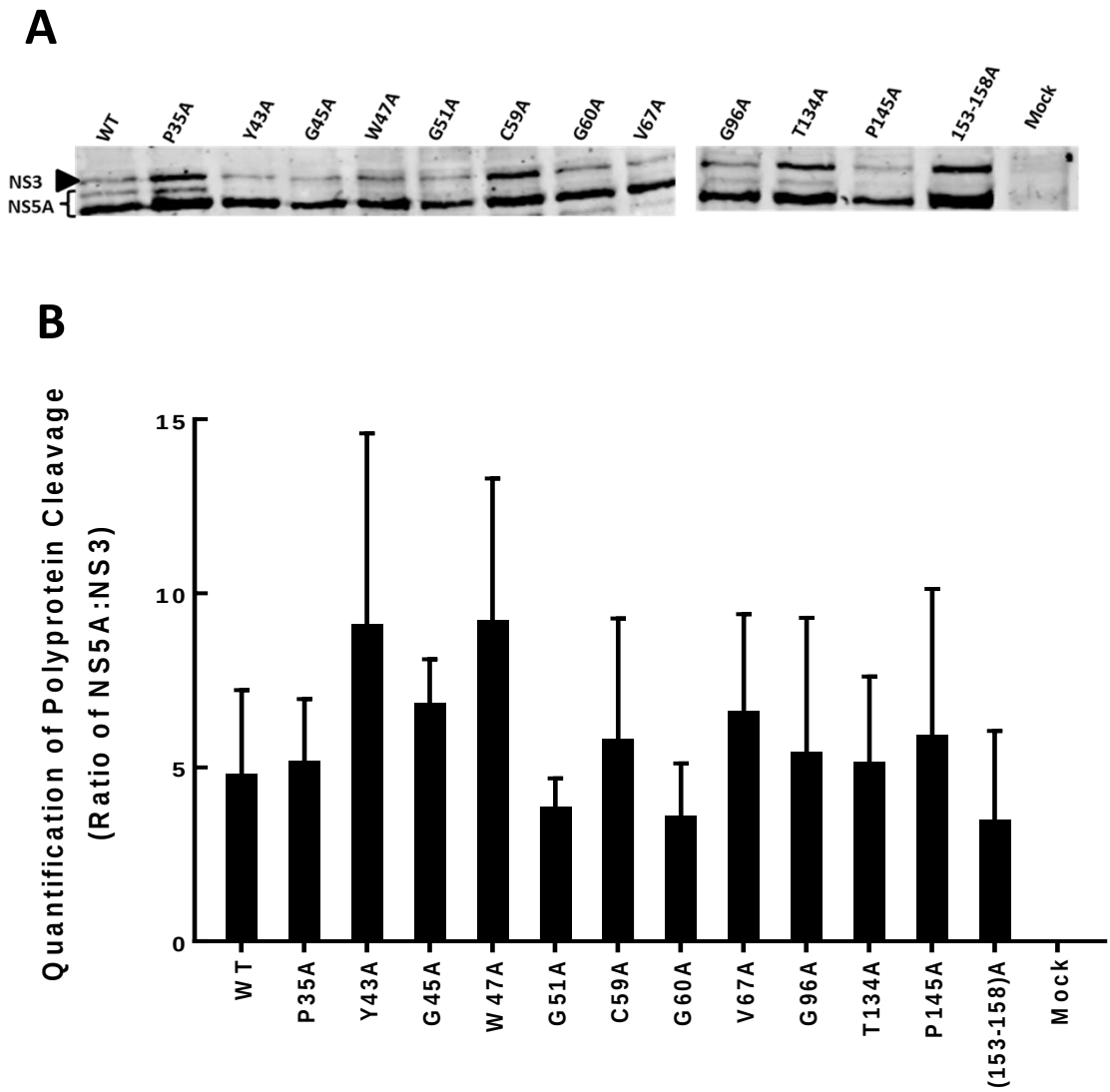

Figure 3.5 Expression of NS5A from pCMV10-NS3-5B expression vector in Huh7.5 cells

A. Huh7.5 cells were transfected with pCMV10-NS3-NS5B expression vector containing the corresponding mutations. At 48hpt, cell lysates were harvested in GLB and analysed by SDS-PAGE and western blot with anti-NS5A (sheep) and anti-NS3 (mouse). **B.** The ratio of NS5A:NS3 was calculated following quantification of western blot signals using a Li-Cor Odyssey Sa infrared imaging system. Data from three independent experiments are shown and error bars represent the standard error of the mean.

3.2.4 Distribution of compartments in replication complex

As all the mutants cannot disrupt cleavage of polyprotein from NS3-NS5B, I wondered whether there is potential redistribution of the replication complexes caused by the mutations. As we know, NS3, the viral protease/helicase, is another key component of genome replication complexes. Therefore, NS5A and NS3 were coimmuno-stained in pCMV10-NS3-NS5B transfected cells with antibodies to both NS5A (sheep α-NS5A) and NS3 (mouse α-NS3) followed by a donkey α-sheep (488 nm) and donkey α-Mouse (594 nm) secondary antibodies. Cells were then stained with DAPI by the addition of Prolonged Gold and imaged. As expected, NS3 can colocalize with NS5A in most cases, both distributing throughout the cytoplasm (Figure 3.6), which suggested that NS5A could interact with NS3 or other NS proteins involving in replication complex. However, in G45A, G51A and (153-158) A mutants transfected cells, NS3 showed significantly reduced co-localisation with NS5A. NS3 exhibited a restricted perinuclear distribution, whereas NS5A spread around cytoplasm. In this case, we can suspect that NS5A with G45A, G51A and (153-158) A mutations impaired the interaction with NS3 and cannot drift the functional replication complex to function as normal. As for the mechanism underlying this interaction, it is still unknown.

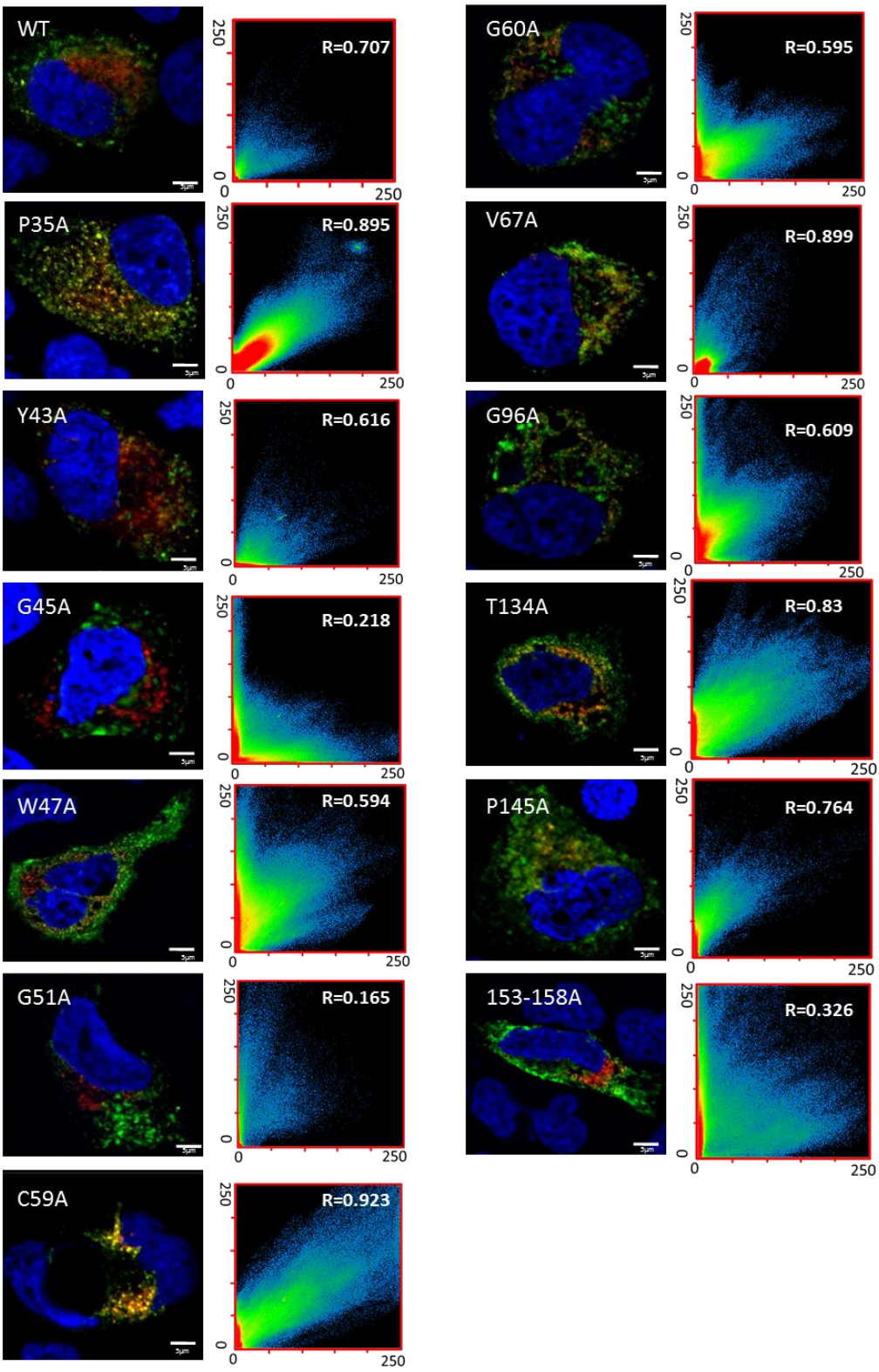

Figure 3.6 Co-localisation of NS5A of domain I mutants with NS3.

Huh7.5 cells were transfected with either pCMV10-NS3-NS5B wildtype or NS5A mutants and seed onto coverslips. At 48h post transfection, cells were fixed and immunostained for NS5A (green) and NS3 (red), nucleus labelled with DAPI (blue). Scale bar, 5 µm. The scatter plots on the right show the co-localization of NS5A and NS3 of individual microscopy images (x and y axes respectively, pixel intensity) and the correlation value (R) is shown for each image.

3.2.5 Trans-complementation

Several research groups have previously demonstrated that some NS5A mutants can be rescued by providing wildtype NS5A in trans in the context of a NS3-NS5B replication competent (WT) or incompetent (GND) replicon (Appel et al., 2005a, Herod et al., 2014, Fridell et al., 2013).

To analyse whether HCV NS5A could be complemented in trans, transient trans-complementation was performed to examine whether the replicative capacity for the mSGR-luc-JFH1 NS5A mutants could be rescued upon co-transfection with a helper RNA, SGR-Neo-JFH1 (WT or GND), relying on supplying functional counterparts of proteins in *trans* that are expressed from separate transcripts to rescue defective NS3-5B replicase units. The helper replicon can translate functional NS5A but does not express firefly luciferase activity. On the other hand, the rescued SGR-Luc-JFH1 (P35A, V67A, P145A or GND) showed reduced luciferase activity because of the defective NS5A. When co-electroporated with helper and rescued replicon RNAs, if the trans-complementation occurs, defective NS5A within the rescued replicon might be exchanged with functional NS5A from the helper replicon (SGR-Neo-JFH1), luciferase activity of the rescued replicon would be increased, which suggested that the function of NS5A could be provided by the helper replicon in *trans* (Appel et al., 2005a). In my experiment, the RNAs were used at a ratio of 5:1; helper: rescue genome (Figure 3.7A and B). The SGR-luc-JFH1 (P341A/P342A/P343A) (SGR-luc-JFH1(PPP)) NS5A , which has been shown to be trans-complemented to some extent (Hughes, 2010), was used as a positive control. As shown in Figure 3.7B, none of mutants of domain I were complemented either by SGR-Neo-JFH1(WT) or GND, while SGR-luc-JFH1(PPP) could be partially trans-complemented by SGR-Neo-JFH1(GND) compared with the GND replication level without helper replicon, but not by SGR-Neo-JFH1(WT) (Figure 3.7B), which is consistent with previously reported results operated by previous colleagues (Hughes, 2010). More recently, an improved system has been developed, in which an intragenomic HCV replicons that carry two ORFs, each driven by separate IRES elements, allowing that the complementing viral proteins are provided in *trans* from distinct translation units but encoded in *cis* from the same RNA molecule (Gomes et al., 2015). Previously SGR-luc-JFH1(PPP) was shown to be trans-complemented (Hughes, 2010) and used as positive control, but it was not significantly rescued in trans in my system, this assay thus needs to be further confirmed with the intragenomic HCV replicons developed by Gomes.

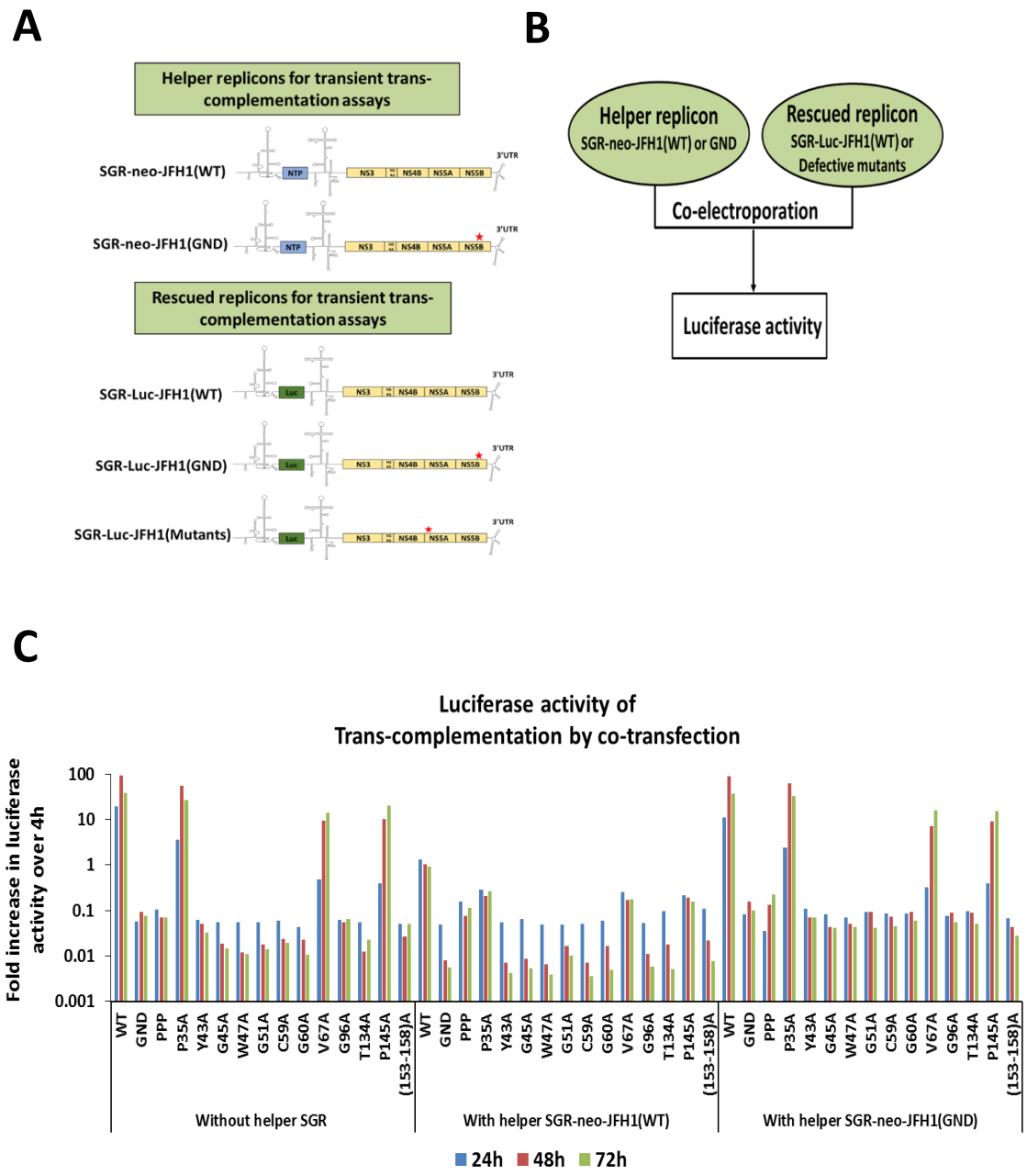

Figure 3.7 Trans-complementation of mSGR-luc-JFH1 mutants.

A. Helper and rescued replicon RNAs used for transient trans-complementation assays were listed. SGR-neo-JFH1 (WT) or SGR-neo-JFH1 (GND) was taken as helper replicon, respectively. SGR-Luc-JFH1(WT), GND (negative control), SGR-Luc-JFH1 NS5A defective mutant (P35A, V67A and P145A) or SGR-Luc-JFH1 (P341A/P342A/P343A) (positive control) (Hughes, 2010) was used as rescued replicon to check whether they can be rescued by helper replicon. **B.** Schematic drawing of the experimental approach used to analyse trans-complementation. The helper genome was either a SGR-Neo-JFH1(WT) or (GND) and co-electroporated in a ratio of 5:1 with the rescue genome SGR-Luc-JFH1(WT), GND, SGR-Luc-JFH1 NS5A defective mutant (P35A, V67A and P145A) or SGR-Luc-JFH1 (P341A/P342A/P343A), respectively. **C.** Trans-complementation assay results. Luciferase activity was measured at 4, 24, 48 and 72 hpe and was normalized to 4 hpe to determine trans-complementation of NS5A domain I mutants.

3.3 Discussion

Compared with domain II and domain III, NS5A domain I is highly structured and the most highly conserved throughout all HCV isolates. It is also well conserved in related viruses such as GBV-B and the new hepaciviruses that have recently been identified in a variety of species. Therefore, this conserved domain must have common functions in the virus life cycle among these 7 genotypes of HCV isolates and related hepaciviruses. To investigate these functions, 12 conserved and surface exposed residues were selected for mutagenic analysis.

Using a subgenomic replicon (SGR) system, 9 conserved residues were identified within this region that were necessary for viral genome replication, as substitution of these amino acids to alanine eliminated genome replication in SGRs. A further three mutations resulted in a significant inhibition of replication, implying that, although these residues are not absolutely essential, they do contribute to genome replication. In next chapter, these three mutations will be cloned into the full-length infectious JFH1 virus molecular clone to examine whether they influence virus assembly and release.

In comparison to the replication results in Huh7.5 cells with those from Huh7 cells, 9 replication-deficient mutants identified from Huh7 cells could not replicate in Huh7.5 cells as well, whereas the SGRs which could replicate in Huh7 cells (WT, P35A, V67A and P145A) all had 10-100 fold of increased replication activity. Especially for V67A and P145A, replication was significantly increased in Huh7.5 cells albeit still lower than WT. One known reason is that the Huh7.5 cell line is RIG-I defective. RIG-I is a pathogen receptor that can bind HCV RNA and then activate IRF3 signalling pathway. Therefore, RIG-I defective cell line-Huh7.5, exhibit a highly permissiveness to HCV replication by inactivation of IRF3 innate immune pathway, allowing both NS5A domain I mutants and domain III mutant (D329A) to replicate with high efficiency. Of note, V67A and P145A showed a more significant increased replication than P35A and D329A in Huh7.5, which suggested that residues V67 and P145 might be involved in a certain innate immune pathway in Huh7.5 cells. Once mutated, V67A and P145A abrogated the activation of these pathways. Hence, why the dramatic increase in replication was observed in V67A and P145A electroporated Huh7.5 cells needs to be further investigated.

For the mutations that did not replicate in neither Huh7 nor Huh7.5 cells, lack of replication could be likely due to two reasons. One is that the mutation disrupts polyprotein translation or proteolytic processing. The other is the loss or disruption of a specific function of NS5A. My data showed that the lethal replication phenotype of these mutations was a direct result of a

loss of NS5A function and was not due to global effects on NS5A structure or inhibition of polyprotein processing. However, co-localisation result showed that G45A, G51A and (153-158) A of 8 non-replicating mutants, disrupted the interaction between NS5A and NS3, which means that they cannot form into functional replication complexes. As for the other non-replicating mutants, the reason why they cannot replicate still needs to be further investigated.

What kind of specific NS5A function are these residues involved in? As described above, NS5A is an important element in the HCV replication complex (RC). It was reported that NS5A is a RNA-binding phosphoprotein, and all three domains can bind the genomic (positive-strand) 3'UTR, which is the initiation site for negative-strand RNA synthesis (Foster et al., 2010). The dimeric structures of NS5A domain I could provide us some clues (Figure 3.2). First of all, domain I has been crystallized in different forms (Lambert et al., 2014, Love et al., 2009, Tellinghuisen et al., 2005). The structure of the NS5A domain I monomer found in each crystallographic form is highly conserved but presents a unique symmetrical dimer interface. These forms are hypothesized to assemble into a polymer network by alternating crystallographic interfaces (Lambert et al., 2014, Love et al., 2009). Two main dimeric structural conformations of NS5A domain I are "closed" (3FQM) (Love et al., 2009)and "open" (1ZH1) (Tellinghuisen et al., 2005), respectively. The open dimer can provide an attractive RNA-binding groove facing away from the membrane, where it could interact with RNA. Modelling suggests the groove is of sufficient dimensions to bind to either single- or double-stranded RNA, which may be dominant in RNA replication (Huang et al., 2004, Tellinghuisen et al., 2008b). In the closed conformation with more residues in the interfaces, a proximal residue, E148 (conserved in both JFH1 and Con1), forms an intramolecular contact via hydrogen bond with R112 on the other monomer. It did not show the pocket for RNA binding and might be inefficient in RNA binding and replication and involved in other functions of HCV life cycle. A hypothesis has been put forward that the closed conformation can be switched into open conformation by changing the dimer interfaces (Ross-Thriepland and Harris, 2014b). For example, it was suspected that S146 phosphorylation could disrupt the interaction between R112 and E148, thereby promoting a switch from the closed to the open conformation. P35 is located in the P29-P35 loop interactions, via which NS5A monomers propagate into NS5A helical hexamer (Sun et al., 2015). Moreover, for P145, it is close to S146 mentioned above and the mutation of this position may be involved in the change of the dimeric conformation. In summary, P35A and P145A may affect the dimeric conformation disturbing the binding to RNA and further affect RNA replication. The position of V67 is exposed on the surface of both dimer structures, which is of high possibility to interact with both host and viral proteins involving in RNA replication

(Figure 3.2). RNA binding assays and analysis of dimerization will be performed in order to provide more detailed molecular information about the interaction in Chapter 5.

Apart from RNA binding activity, when NS5A is involved in the replication complex it can interact with various cellular factors and viral proteins, which is required for HCV replication (Paul et al., 2014). In the replication complex, the phosphorylation of NS5B RdRp was activated by NS5A, at least in vitro. This activation might be mediated by the RNA-binding ability of NS5A or by direct interaction with NS5B (Quezada and Kane, 2013, Shirota et al., 2002). Recent research demonstrated that NS4B and NS5A are two critical replication complex components. Additionally, domain I of NS5A was sufficient to mediate its interaction with NS4B, and then affect viral genome replication (David et al., 2015). The conserved residues on the surface of NS5A domain I are much more available to interact with other proteins. Whether the mutations could disrupt the interaction between NS5A and other viral proteins will be investigated using proteomic analysis in Chapter 6.

In trans-complementation assays, expression of a polyprotein encompassing NS3 to NS5A was sufficient to rescue replication of an NS5A replicon mutant, whereas NS5A expressed on its own did not support trans-complementation, which suggest that the other nonstructural proteins, NS3, NS4A, and NS4B, affect folding of NS5A in a highly ordered complex to produce a functional NS5A protein. With only properly folded NS5A, RNA replication could be able to rescue in trans, but mutations affecting the overall folding could not be rescued (Appel et al., 2005a). From the result of transfection of pCMV10-NS3-NS5A, most of these mutants only could be detected in the basal phosphorylation state, while the expression of hyperphosphorylated NS5A was dramatically reduced or undetectable, indicating a more profound effect on the conformation of the protein (Koch and Bartenschlager, 1999). Together with the trans-complementation result, none of these mutations could be complemented. The reason maybe that mutations in this domain affecting the phosphorylation may therefore result in an NS5A that is non-productively associated with other components of the RC, making trans-complementation very difficult. However, the mechanism of phosphorylation of NS5A domain I is complicated and differential phosphorylation could regulate the various roles of the protein, which remain unclear and need to be investigated with joint efforts.

Chapter 4: NS5A domain I is required for virus assembly

4.1 Introduction

Following RNA replication, nascent viral genomes need to be transported from the sites of RNA replication to distinct, as yet poorly characterised, sites of virus assembly. Here infectious virus particles are generated, bringing together the structural proteins and the viral genome to be packaged in a temporally and spatially organized manner (Gastaminza et al., 2008, Lindenbach and Rice, 2013). An increasing body of evidence points to a role of NS5A in coordinating this process, possibly by transporting the genome RNA to assembly sites and delivering it to the core protein for encapsidation. A further level of complexity arises from the fact that, compared to other enveloped positive-strand viruses, a key feature of infectious HCV particles is that they exhibit unusually low buoyant densities, while particles with higher buoyant densities are less infectious (Lindenbach et al., 2005, Lindenbach, 2013, Wakita et al., 2005). Indeed highly purified HCV particles are rich in lipids and cholesterol resembling very-low density lipoproteins (VLDL) (Merz et al., 2011, Miyanari et al., 2007). This property requires that cellular lipid droplets (LDs), lipid storage organelles surrounded by a phospholipid monolayer, are involved in HCV assembly.

Of the virus structural proteins, core trafficking to LDs is functionally tied to specific lipid metabolism events and serves to sequester the core protein until it is needed for virus assembly, as mutations that prevent trafficking of the core protein to LDs strongly inhibit virus assembly (Boulant et al., 2007, Miyanari et al., 2007, Shavinskaya et al., 2007). High-resolution immunofluorescence microscopy clearly showed that core was completely colocalized with ADRP, residing on the surface of LDs, thus indicating that core also directly associates with the surface of LDs. More importantly, NS5A signal mainly localized around the core positive area, resulting in a doughnut-shaped signal with a diameter slightly larger than that of core. The LD-proximal NS5A signal partially overlapped with the core signal. This concentric staining pattern was also observed with the other NS proteins, indicating that NS proteins associate with core on the surface of LDs (Miyanari et al., 2007) (Figure 4.1). The core-NS5A co-localization may suggest an interaction of the replicase complex with the core protein to deliver the RNA genome and to initiate nucleocapsid formation (Shavinskaya et al., 2007). There is a model of HCV production put forward that core mainly localizes on the monolayer membrane that surrounds the LD, core recruits NS proteins, as well as replication complexes, to the LD-associated membrane and NS proteins around the LD can then participate in infectious virus production (Miyanari et al., 2007).

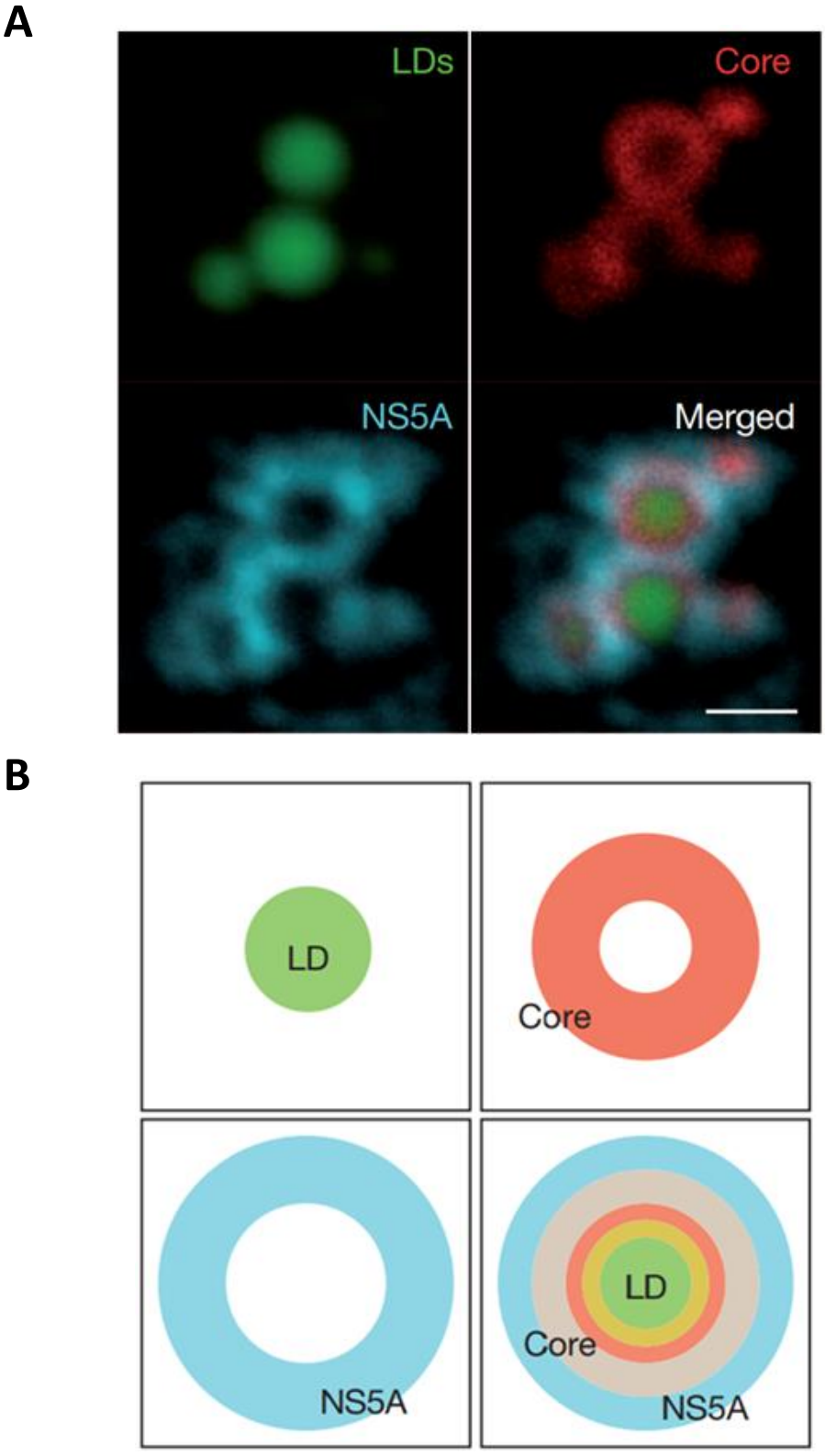

Figure 4.1. Spatial distribution of core and NS5A relative to the LD.

A. The localizations of core and NS5A around the lipid droplets (LDs) in JFH1 replicon-bearing cells were analysed using immunofluorescence microscopy. Scale bars, 1 μm. **B.** Typical images of the localization of LDs, core, NS5A and merged images are shown with the relative scale of each image. Picture is adapted from (Miyanari et al., 2007).

Of three domains of NS5A in HCV life cycle, it is well documented that the RNA binding domain I is essential for RNA replication (Huang et al., 2005); most of domain II is dispensable for the viral replication cycle in cell culture, whereas domain III is required for HCV assembly (Tellinghuisen and Foss, 2008, Appel et al., 2008, Masaki et al., 2008, Tellinghuisen et al., 2008b). Domain III appears to be phosphorylated by casein kinase II at a C-terminal serine residue and this modification might regulate interaction with the core protein and thus virion formation (Tellinghuisen and Foss, 2008, Masaki et al., 2008). Most function of NS5A in virus assembly have been mapped to domain III, as mutations close to the C-terminus of domain III disrupt the ability of NS5A to interact with core, abrogate infectious particle formation and lead to an enhanced accumulation of core on the surface of LDs (Appel et al., 2008).

In addition to interacting with other viral proteins, a number of cellular NS5A-interacting partners have been implicated in LD function/targeting and virus assembly. These include Apolipoprotein E (ApoE), diacylglycerol acyltransferase-1 (DGAT-1), Annexin A2 and Rab18 (Backes et al., 2010, Benga et al., 2010, Camus et al., 2013, Herker et al., 2010, Salloum et al., 2013). NS5A interacts with ApoE, an apolipoprotein (Apo) that is required for virus assembly. Two alanine mutants in domain I of NS5A - JFH1AAA99 or JFH1AAA102 failed to interact with ApoE and impaired recruitment of the other non-structural proteins to the surface of LDs. ApoE-NS5A binding is thus assumed to have a crucial function in the production of infectious particles, and the determinants of this interaction are located on domain I of NS5A (Cun et al., 2010, Benga et al., 2010). Annexin A2, a cellular membrane sorting protein, can enhance virus assembly by being recruited by NS5A domain III (Backes et al., 2010). Of note, both DGAT-1 and Rab18 have been reported to recruit NS5A on to LDs and are proposed to play roles in transporting NS5A and genome RNA between replication sites and LDs/assembly sites (Camus et al., 2013, Salloum et al., 2013). DGAT1 as a host factor for HCV infection has been reported to catalyse core and NS5A proteins trafficking from ER membrane to LDs and enhance interactions of NS5A with core protein but via different determinants of DGAT1 and different processes (Camus et al., 2013, Herker et al., 2010). Rab18 showed a direct association with NS5A promoting the interaction between HCV membranous webs and LDs and might enhance virion assembly by bringing sites of replication in close physical proximity to sites of virion assembly, either on the LD surface or on membranes apposed to the LD. Therefore, HCV particles assemble by budding into ER. An important early step in this process is the interaction between cLD-associated core and NS5A proteins, which might serve to shift RNA out of replication or translation and into virus assembly (Appel et al., 2008, Lindenbach and Rice, 2013, Masaki et al., 2008, Miyanari et al., 2007).

Although virus encapsidation could occur at the LD, it is noteworthy that LD surface is not bound with a conventional phospholipid bilayer ER membrane but delimited by a phospholipid monolayer (Fujimoto and Parton, 2011), therefore the virions cannot obtain their lipid envelope from them. Assembly of an infectious enveloped HCV virion particle must ultimately require that core and virion RNA are transported from LDs (Paul et al., 2014) to a membranous compartment, possibly involving the ESCRT (endosomal sorting complex required for transport) and/or endosomal pathways for viral budding (Ariumi et al., 2011, Corless et al., 2010, Tamai et al., 2012).

4.2 Results

4.2.1 The role of domain I in virus production.

To determine whether the attenuation of genome replication for P35A, V67A and P145A in Huh7 cells was also observed in the context of infectious virus, these mutations were sub-cloned into the full-length mJFH1 infectious clone (Hughes et al., 2009b). Following electroporation of full-length virus transcripts into Huh7 cells virus genome replication activity was determined by quantification of the number of NS5A positive cells using the IncuCyte ZOOM at 48 hpe as previously described (Stewart et al., 2015)(Figure 4.2A). As expected, replication of P35A, V67A and P145A in the context of infectious virus was consistent with the observations in SGRs (Figure 4.2B and 3.3). P35A exhibited a modest reduction, which was not significant, whereas V67A and P145A showed a ~100-fold reduction in replication, indistinguishable from the GND negative control. Consistent with this replication phenotype, neither V67A nor P145A produced any infectious virus particles, either within the cells (intracellular virus), or released into the supernatant (extracellular virus) (Figure 4.2C).

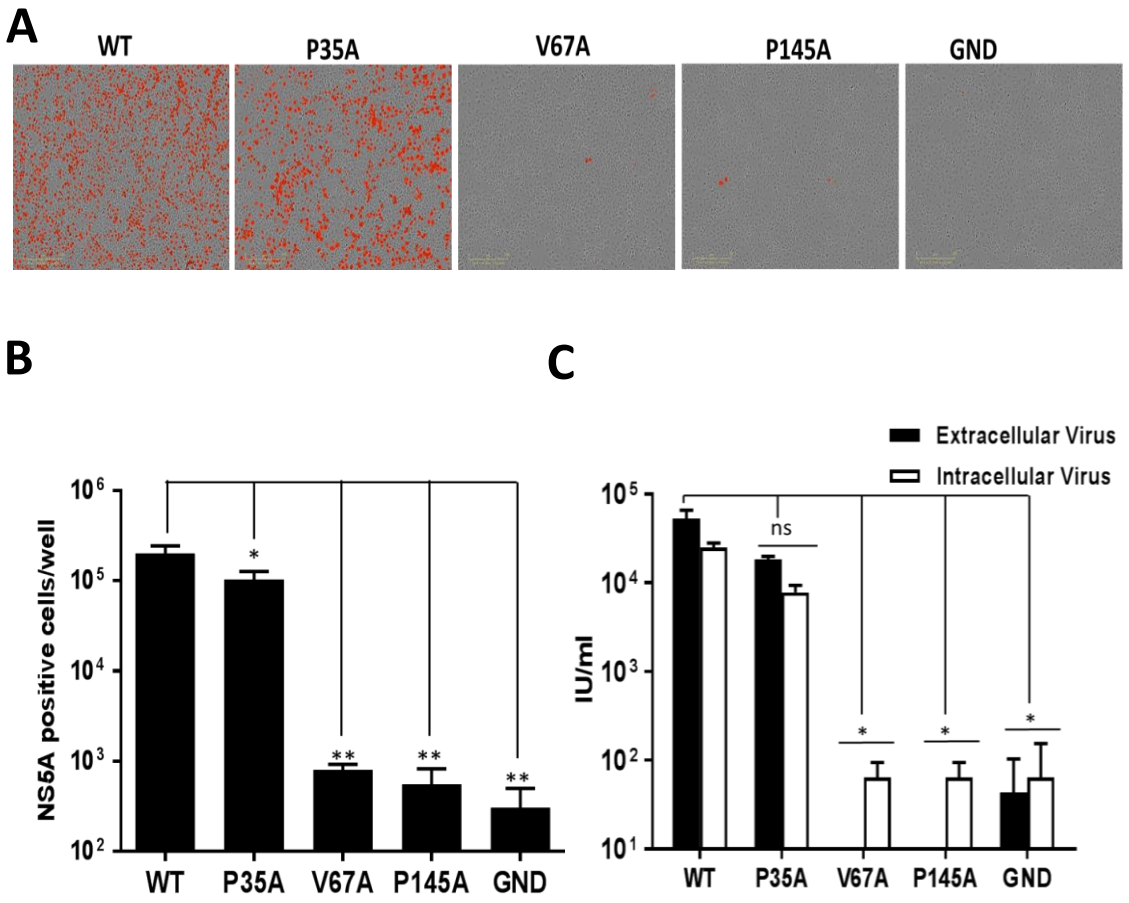

Figure 4.2. Mutations in NS5A domain I disrupt the production of infectious virus in Huh7 cells.

A. In vitro transcripts of mJFH1 containing the indicated mutations were electroporated into Huh7 cells. Cells were fixed at 48 hpe, immunostained with anti-NS5A antibody and visualised by using the IncuCyte ZOOM. **B.** Virus genome replication and protein expression was assayed by quantification of NS5A positive cells from IncuCyte ZOOM. **C**. Intracellular and extracellular infectious virus was titrated at 72 hpe. IU indicates infectious unit of virus. ns indicates not statistically significant, * and ** indicate significant ($P<0.05$) and very significant ($P<0.01$) differences from the results for titre (IU/ml) of mJFH1 WT virus, respectively. For B-C, data from three independent experiments are shown and error bars represent the standard error of the mean.

A different picture emerged when these mutant virus RNAs were electroporated into Huh7.5 cells. As shown in Figure 4.3A (upper panel) and B, replication of P35A was indistinguishable from WT, whereas both V67A and P145A showed only a modest defect. This result was confirmed by western blot analysis for NS5A and core expression (Figure 4.3C). However, despite the restoration of genome replication to WT levels, V67A and P145A were unable to produce any infectious virus (Figure 4.3A lower panels and D). This phenotype mirrored that of the additional control used in this experiment, ΔE1-E2 (a deletion within the envelope glycoprotein coding region previously shown to be unable to assemble infectious virus) (Appel et al., 2008, Hughes et al., 2009b).

I conclude from these data that the two residues V67 and P145 are partially required for genome replication, as mutations of these residues resulted in a reduction of replication that could be rescued by the Huh7.5 RIG-I defect. In contrast these two residues are absolutely required for the assembly of infectious HCV particles. This result was surprising, as it is widely accepted that domain I of NS5A is exclusively involved in genome replication. The one exception to this is the report 10 years ago showing that alanine scanning mutagenesis of residues 99-101 or 102-104 had no effect on genome replication, but blocked release of infectious virus from Huh7.5 cells (Miyanari et al., 2007), although whether these mutants affected assembly of intracellular infectious virus was not determined. It was reasoned that the ability of V67A and P145A to replicate to near WT levels in Huh7.5 cells offered the opportunity to assess the role of domain I in virus assembly, without any confounding replication defect that would make interpretation of the data difficult.

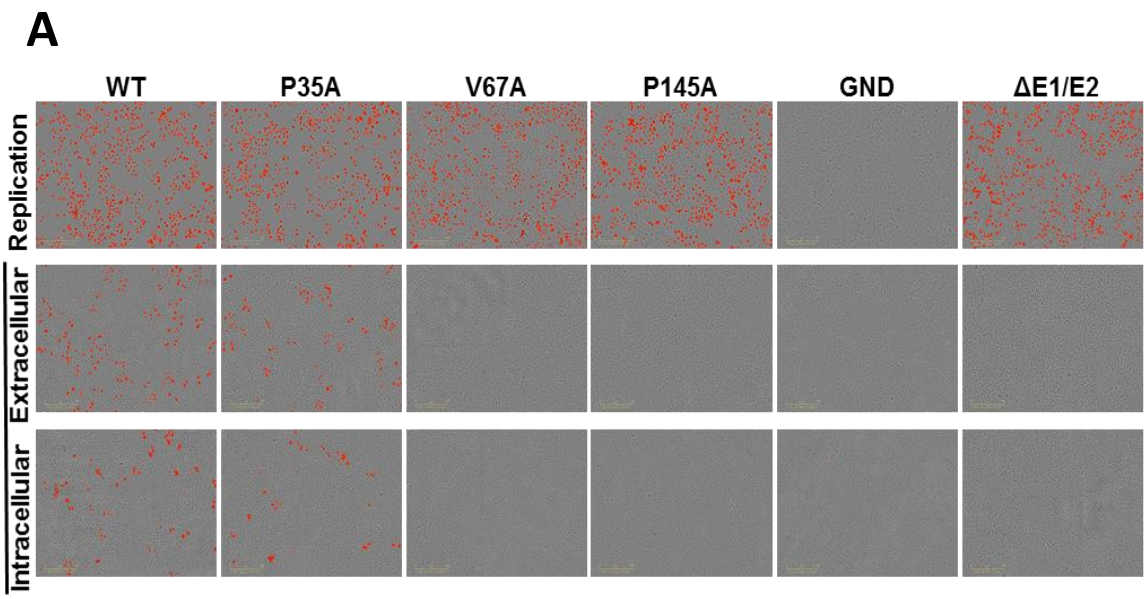
A
WT
P35A
V67A
P145A
GND
ΔE1/E2
Replication
Extracellular
Intracellular

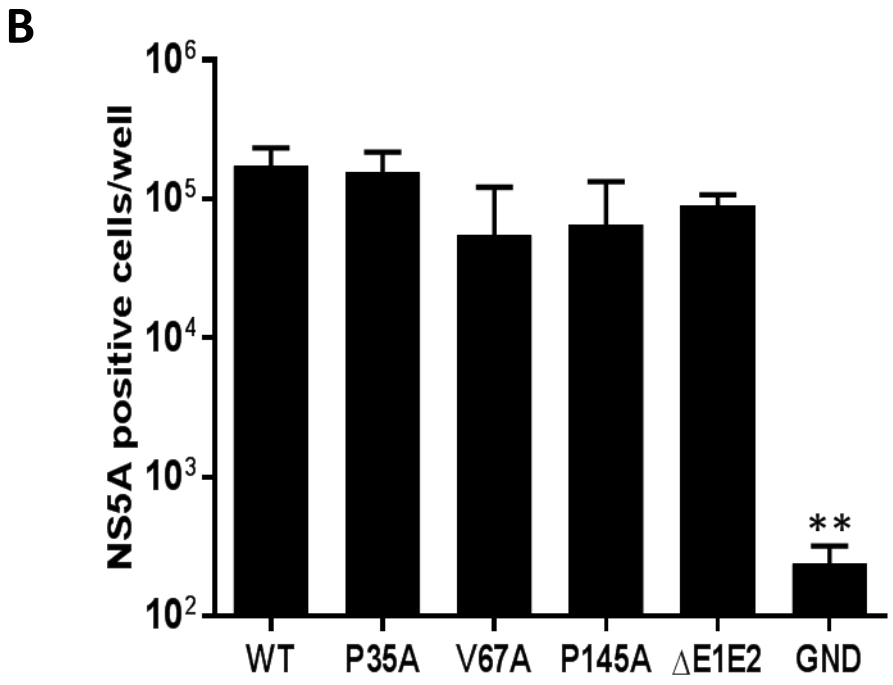
B
NS5A positive cells/well
10^6
10^5
10^4
10^3
10^2
**
WT
P35A
V67A
P145A
ΔE1E2
GND

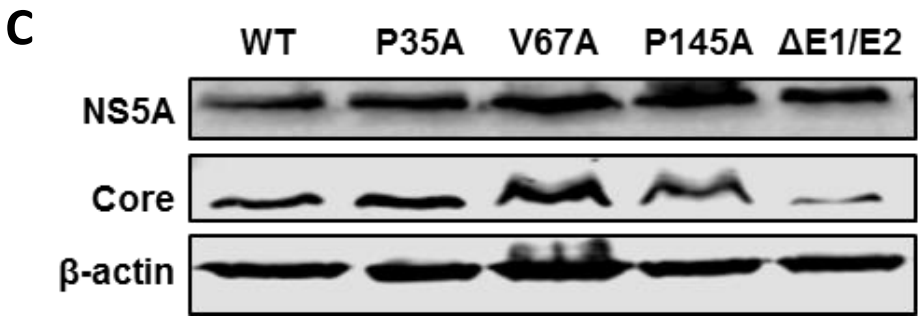
C
WT
P35A
V67A
P145A
ΔE1/E2
NS5A
Core
β-actin

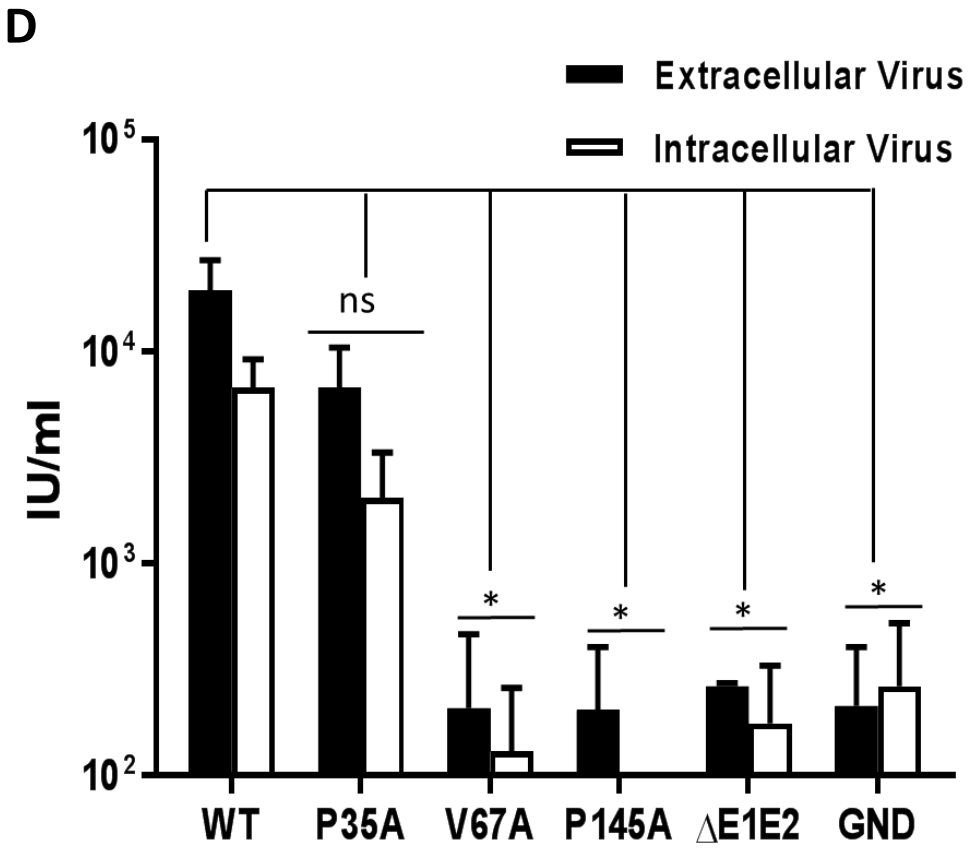

Figure 4.3. Mutations in NS5A domain I disrupt the production of infectious virus in Huh7.5 cells.

A. In vitro transcripts of mJFH1 containing the indicated mutations were electroporated into Huh7.5 cells. Virus genome replication and infection images obtained from Incucyte ZOOM. **B.** Virus genome replication and protein expression was assayed by quantification of NS5A positive cells 48 hpe for Huh7.5 cells by using the Incucyte ZOOM. **C.** Huh7.5 cell lysates at 72 hpe were analysed by western blot with anti-NS5A, anti-core and anti-β-actin antibodies. **D.** Intracellular and extracellular infectious virus was titrated at 72 hpe. IU indicates infectious unit of virus. ns indicates not statistically significant and * and ** indicate significant ($P<0.05$) and very significant ($P<0.01$) differences from the results for titre (IU/ml) of mJFH1 WT virus. For B and D, data from three independent experiments are shown and error bars represent the standard error of the mean.

However, before analysing the phenotype of V67A and P145A in more detail, I confirmed that the phenotypes of these mutants were not due to the acquisition of an additional compensatory mutation during the cloning process. To do this, I generated revertant viruses in which the WT NS5A coding sequence was sub-cloned back into the V67A and P145A virus backbones. As shown in Figure 4.4, following electroporation of revertant RNA into Huh7.5 cells, both genome replication (Figure 4.4A) and production of both intracellular and extracellular virus (Figure 4.4B) was restored to WT levels.

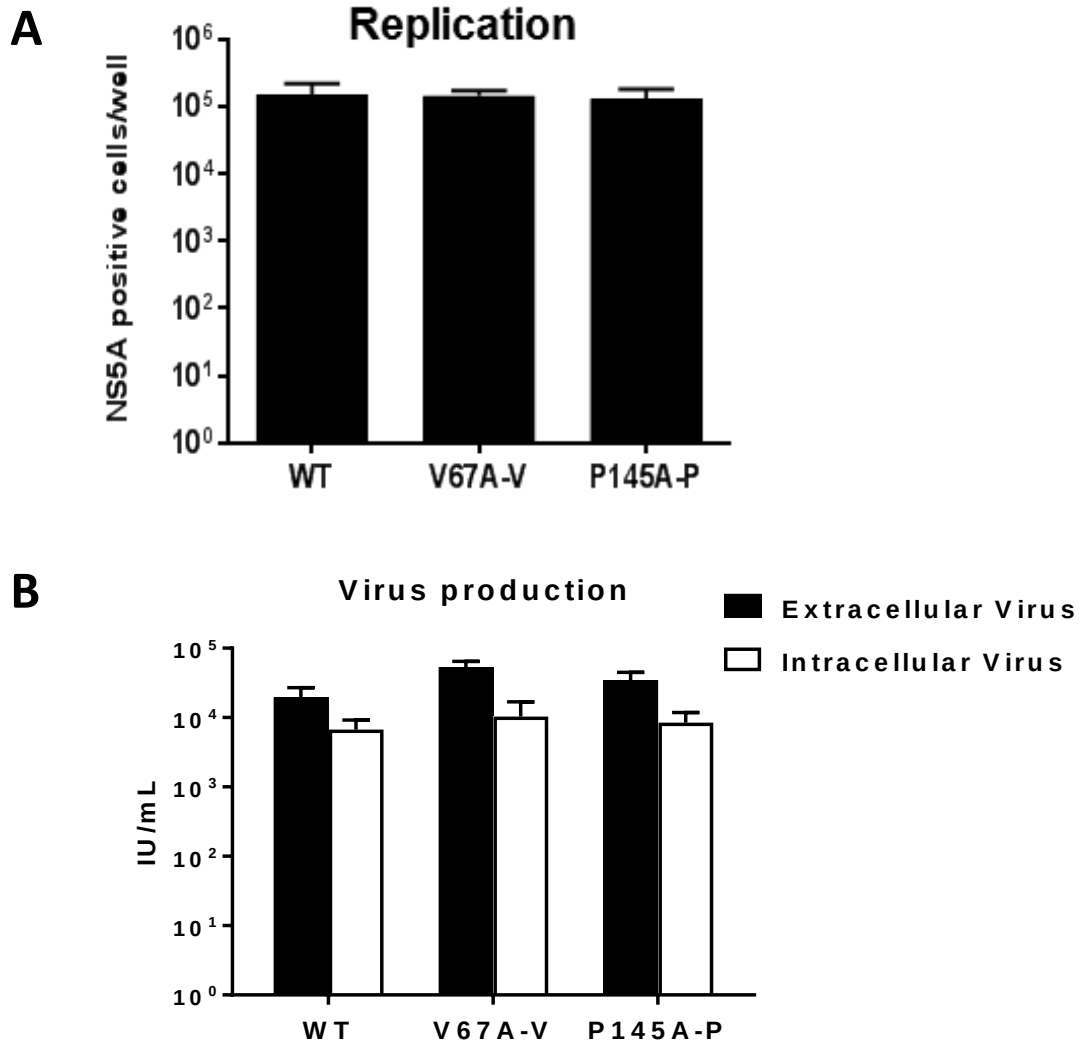

Figure 4.4. Phenotypes of V67A and P145A are not derived from acquisition of an additional compensatory mutation during the cloning process.

A. Revertants were generated by cloning a WT NS5A fragment back into the mJFH1 V67A or P145A mutant plasmids. Huh7.5 cells were electroporated with in vitro transcripts of the resulting V67 or P145 revertants. Virus genome replication and protein expression was assayed by quantification of NS5A positive cells 48 hpe by using the Incucyte ZOOM. **B.** Intracellular and extracellular infectious virus was titrated at 72 hpe. Data from three independent experiments are shown and error bars represent the standard error of the mean.

4.2.2 The role of domain I in the assembly of infectious virus

It was considered that the failure of V67A and P145A to produce infectious virus was either due to a gross assembly defect such that no virus particles were generated, or that virus particles were assembled but were non-infectious. Such non-infectious particles might be empty, lacking the genome, or could exhibit some other more subtle defect such as a failure to associate with lipids. To test this hypothesis, culture medium from Huh7.5 cells electroporated with JFH1 WT, P35A, V67A and P145A RNA was concentrated and fractionated by iodixanol density-gradient centrifugation. As controls, cells were electroporated with GND and ΔE1/E2 RNAs. Each fraction was analysed by quantitative RT-PCR (Figure 4.5A) to determine the presence of genomic RNA, and infectivity was measured using the IncuCyte ZOOM as described (Figure 4.5B). As expected WT JFH1 showed a broad peak of infectivity at a low density (1.064 g/ml) that coincided with a genomic RNA peak, a second larger RNA peak at a higher density (1.1005 g/ml) was less infectious, consistent with previous reports (Merz et al., 2011, Miyanari et al., 2007). P35A also showed two coincident peaks of infectivity and RNA, although the majority of the viral RNA was associated with the higher density fraction which exhibited less infectivity. In contrast, no genomic RNA or infectivity could be detected for either V67A or P145A, these two mutants were indistinguishable from the two negative controls (GND and ΔE1/E2). Gradient fractions were concentrated by methanol precipitation prior to analysis for the presence of core by western blot. This analysis (Figure 4.5C) revealed a complete lack of any core protein in fractions from either V67A or P145A, again in common with the negative controls. In contrast both WT and P35A exhibited core protein correlating with the peaks of infectivity and virus RNA. It was concluded that both V67A and P145A mutations block the assembly of infectious virus particles at an early stage.

A

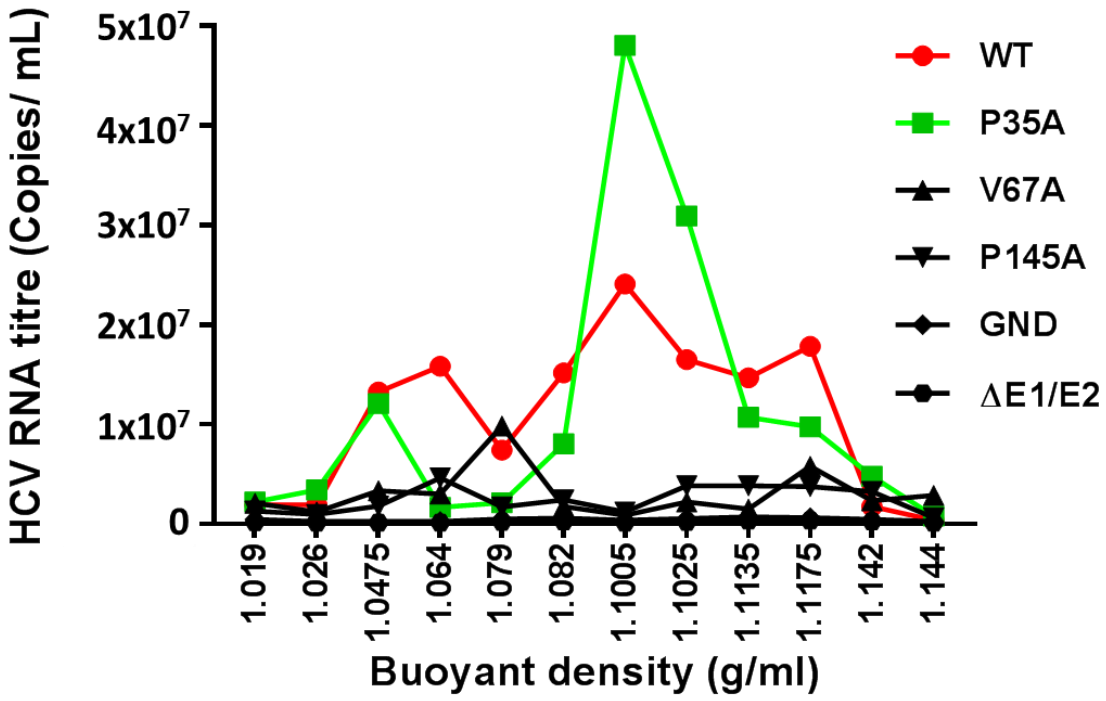
HCV RNA titre (Copies/ mL)
5x10^7
4x10^7
3x10^7
2x10^7
1x10^7
0
1.019
1.026
1.0475
1.064
1.079
1.082
1.1005
1.1025
1.1135
1.1175
1.142
1.144
Buoyant density (g/ml)
WT
P35A
V67A
P145A
GND
ΔE1/E2

B

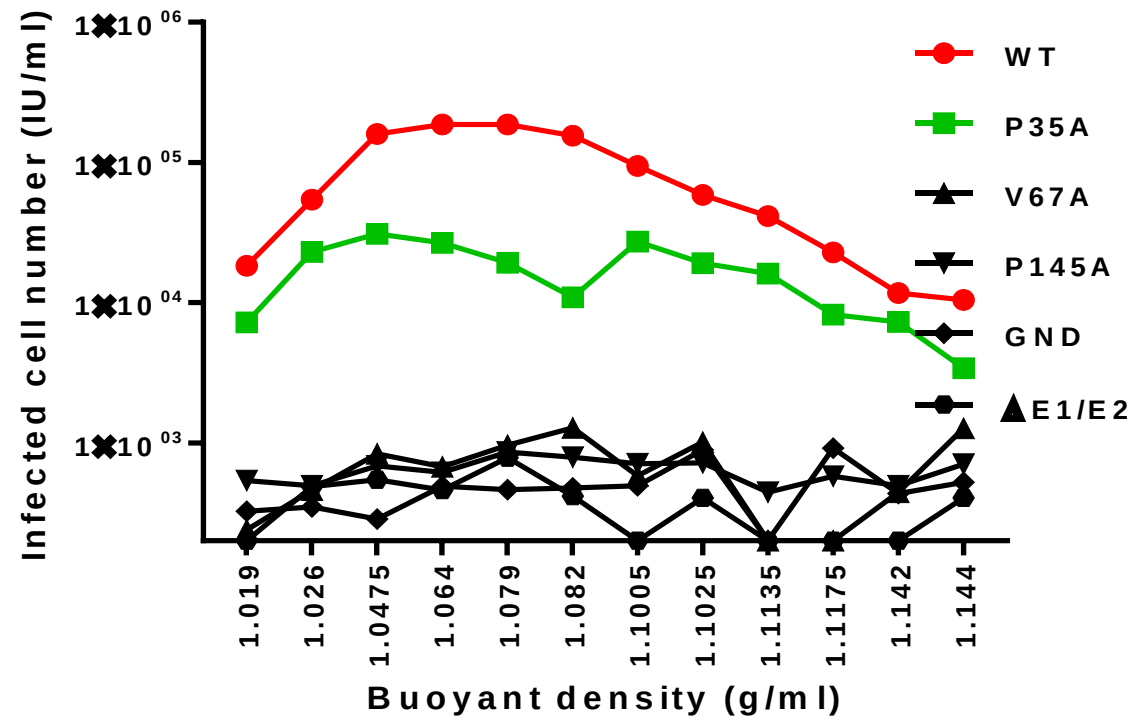
Infected cell number (IU/ml)
1✖10 06
1✖10 05
1✖10 04
1✖10 03
1.019
1.026
1.0475
1.064
1.079
1.082
1.1005
1.1025
1.1135
1.1175
1.142
1.144
Buoyant density (g/ml)
WT
P35A
V67A
P145A
GND
E1/E2

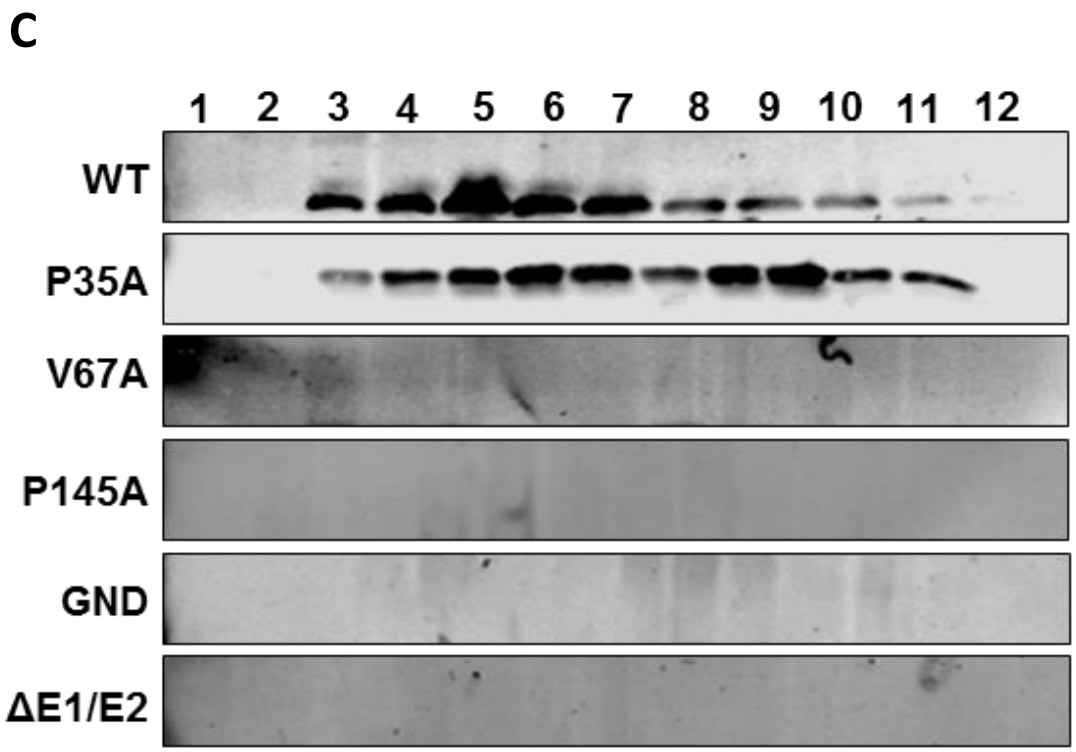

Figure 4.5. Density gradient analysis of mutant viruses.

Huh7.5 cells were electroporated with in vitro transcripts of the indicated virus mutants. Concentrated culture medium was fractionated using 10-40% iodixanol density-gradient centrifugation. For each fraction, HCV RNA (**A**) and infectivity (**B**) were plotted against the buoyant density (n=3), and core protein in each fraction was detected by western blot (**C**). Lanes 1 to 12 in (C) indicated the fractions collected from top to bottom with the buoyant density indicated in (A) and (B). The result of a representative of three independent experiments is shown.

4.2.3 A role for NS5A domain I in the redistribution of LD during infection

To shed light on the phenotype of the V67A and P145A mutations, we applied an imaging approach, using high-resolution confocal microscopy (Airyscan) to assess the distribution of both viral and cellular factors during infection. In this regard, lipid droplets (LD) are important organelles for the assembly of infectious HCV particles, although their precise role remains to be elucidated (Miyanari et al., 2007). Both core and NS5A have been shown to localise with LDs and infection with HCV results in dramatic changes to the distribution and size of LDs. This is demonstrated in Figure 4.6: Huh7.5 cells were electroporated with WT JFH1 RNA and analysed by Airyscan confocal microscopy for the distribution of LD, core and NS5A at various time-points up to 72 hpe (Figure 4.6A). The number (Figure 4.6B), and total area of LDs (Figure 4.6C), together with their distance from the nuclear membrane (Figure 4.6D), were determined. During the first 12 h the number of LDs declined slightly, but then increased at 24 h, followed by a further dramatic decline by 48/72 h. Importantly however, the total area of LDs within the cytoplasm (a measure of the amount of lipids stored in LDs) increased significantly at 48/72 h, indicative of an increase in the size of LDs. There were more subtle changes to the distribution of LDs: at early times (12/24 h) - they scattered throughout the cytoplasm, whereas later the distribution was more restricted to the perinuclear area (48 h) and exhibited a clustering (72 h). As previously documented, both core and NS5A were associated with LDs at later time points. Core can be seen to completely coat the surface of LDs whereas NS5A is restricted to punctate areas on the surface. The same pattern of changes in cells infected with JFH1 was observed (Figure 4.7).

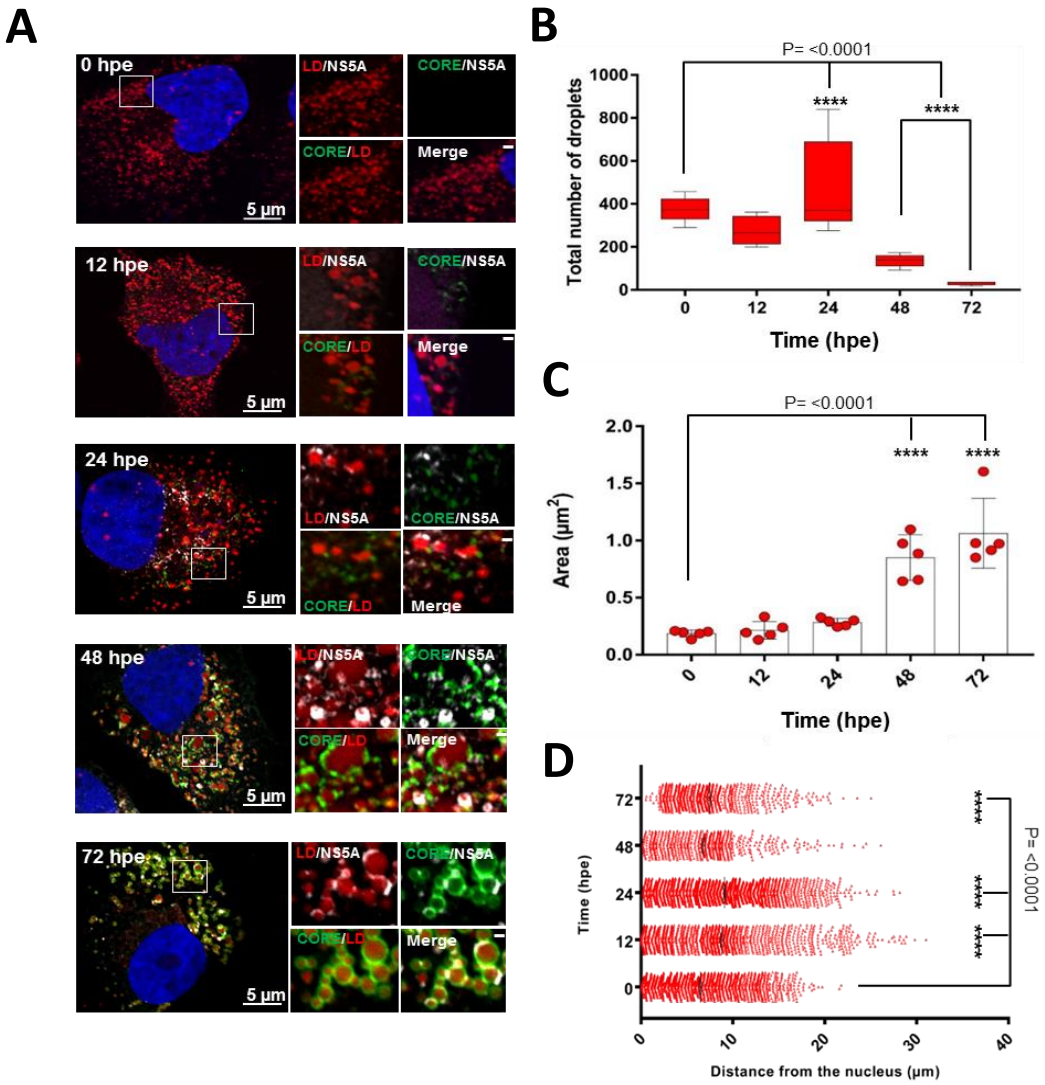

Figure 4.6. Time-course immunofluorescence analysis of LDs, NS5A and core in WT transfected cells.

A. Huh7.5 cells were electroporated with an in vitro transcript of mJFH1 WT. At the indicated hpe cells were fixed and stained with anti-NS5A and core antibodies, BODIPY 558/568-C12, and DAPI. **B-D.** Spatial data for LDs were determined from 10 cells for each time point using Fiji. These data were used to determine the number of LDs per cell (B), the average size of LDs (C) and the distance of each LD from nucleus at different time points (D). **C.** To determine the total area of LD, the grayscale rendered 16-bit tagged image file format (TIFF) images were subjected to threshold-based analysis of LD areas for 10 randomly selected cells for each sample. Two-dimensional (2D) masks of the labelled regions were constructed and were used for computing the 2D area of LDs. Two-dimensional areas (μm^2) of the LDs were also measured using the Analyze Particles function in Fiji. **D.** The distance of the centroid of each LD to the edge of the cell's nucleus, visualised using DAPI stain, was looked up using a Euclidean distance map computed with the Distance Transform module of Fiji and exported as a list of distance 2D measurements via the Analyze Particle function. Two-dimensional measurements in this experiment was used as a proxy for the 3D distance from the LD to the nucleus. **** indicates significant difference (P<0.0001) from the results for LDs in untransfected cells. The scale bars are 5µm and 0.5 µm, respectively. This work was performed by Niluka Goonawardane.

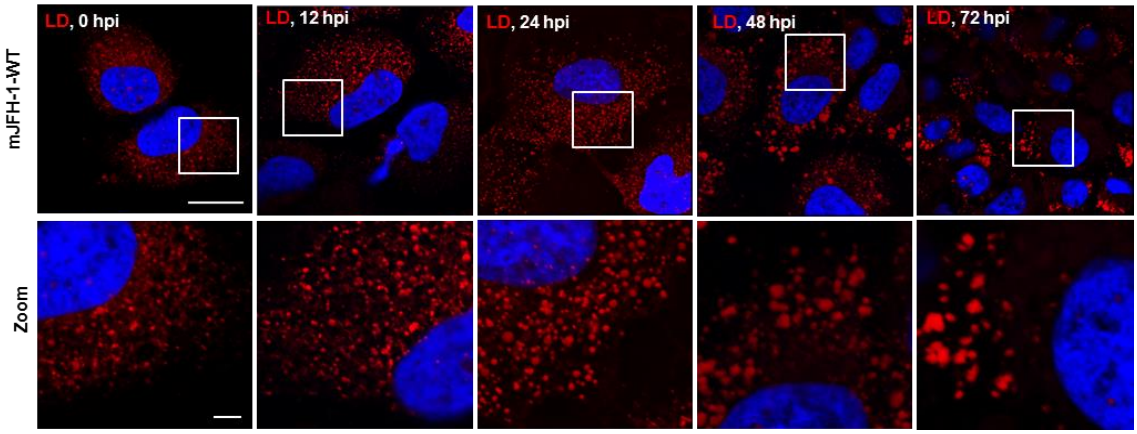

Figure 4.7 Time-course immunofluorescence analysis of LDs in JFH1 WT virus infected cells.

Huh7.5 cells were infected with JFH1 virus at MOI =0.5. At the indicated hpe cells were fixed and stained with anti-NS5A, BODIPY 558/568-C12, and DAPI. Image showed here is LD in red and DAPI in blue of NS5A positive cells. NS5A staining channel is not showed to highlight the phenotype of LD. The scale bars are 5µm and 0.5 µm, respectively. This work was performed by Niluka Goonawardane.

The distribution of LDs was then examined, core and NS5A at 72 hpe in Huh7.5 cells electroporated with RNA for the three domain I mutants, P35A, V67A and P145A (Figure 4.8). Airyscan imaging of these cells revealed some striking differences: P35A was largely indistinguishable from WT but V67A and P145A exhibited distinct phenotypes. The most notable difference was that for V67A and P145A the size of the LDs was dramatically reduced compared to WT and P35A (Figure 4.8). Quantification confirmed this visual conclusion (Figure 4.9), in WT and P35A transfected cells, the majority of LDs had an area of between 0.2-0.6 μm^2, whereas for V67A and P145A the majority were below 0.2 μm^2. Compared to the phenotype of LDs in the untransfected Huh7.5 mock cells, V67A and P145A followed the similar pattern that such size of LDs did not get enlarged. Hence, it can be deduced that V67A and P145A might fail to produce infectious virus that abrogate to activate the LDs biogenesis, following the phenotype of LDs within virus uninfected cells.

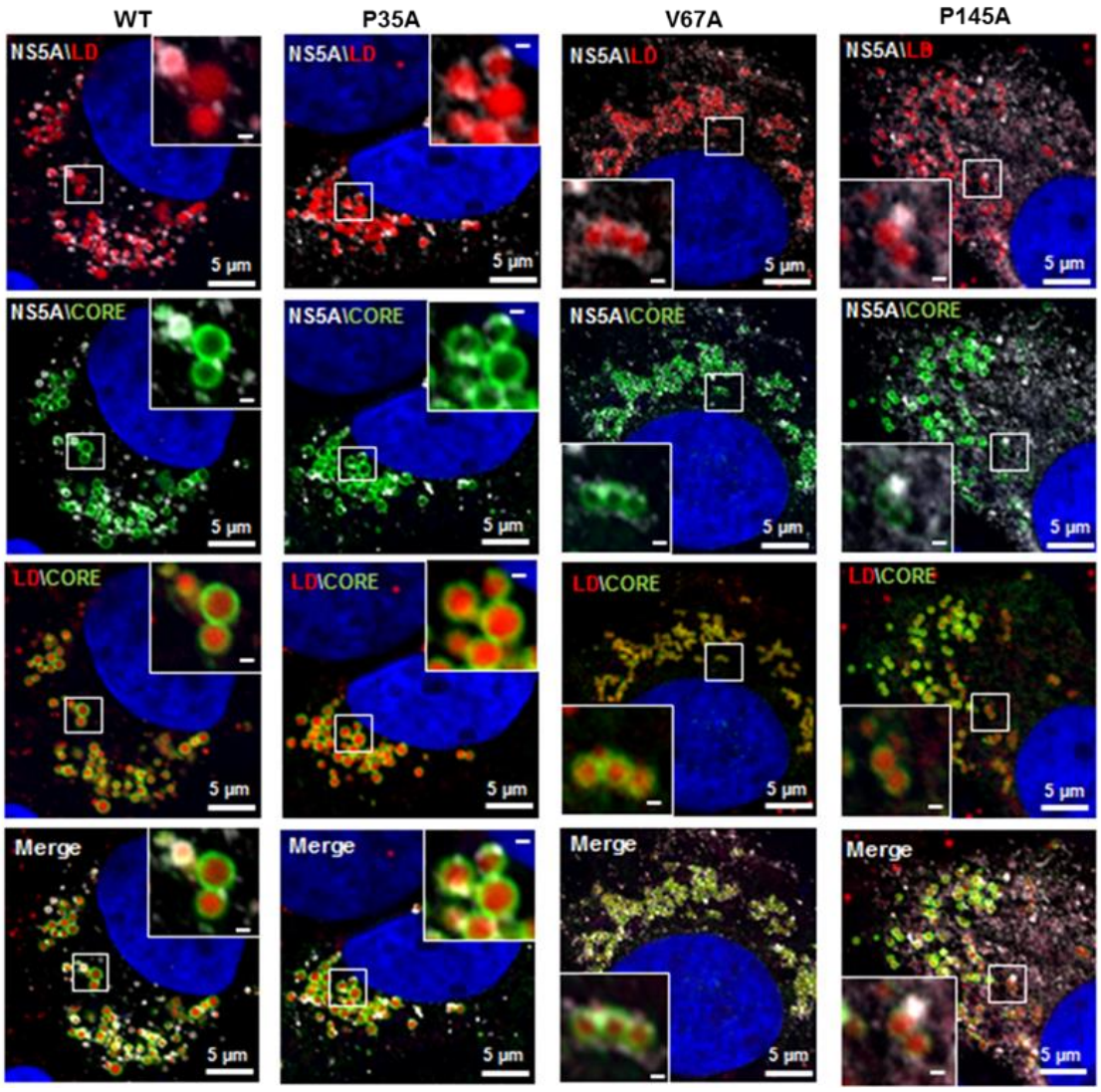

Figure 4.8 Subcellular distribution of core and NS5A relative to the LDs in infected cells is disrupted by domain I mutations V67A and P145A.

Spatial distribution of core and NS5A relative to the LD in Huh7.5 cells electroporated with in vitro transcripts of either wild-type mJFH1, or NS5A mutants P35A, V67A and P145A. Cells were seeded onto coverslips and incubated for 72 hpe prior to fixation and immunostaining for core (rabbit, 1:500), NS5A (sheep, 1:2000) and LD (BODIPY 558/568-C12, 1:1000), and imaging by confocal microscopy. The scale bars are 5µm and 0.5 µm, respectively. This work was performed by Niluka Goonawardane.

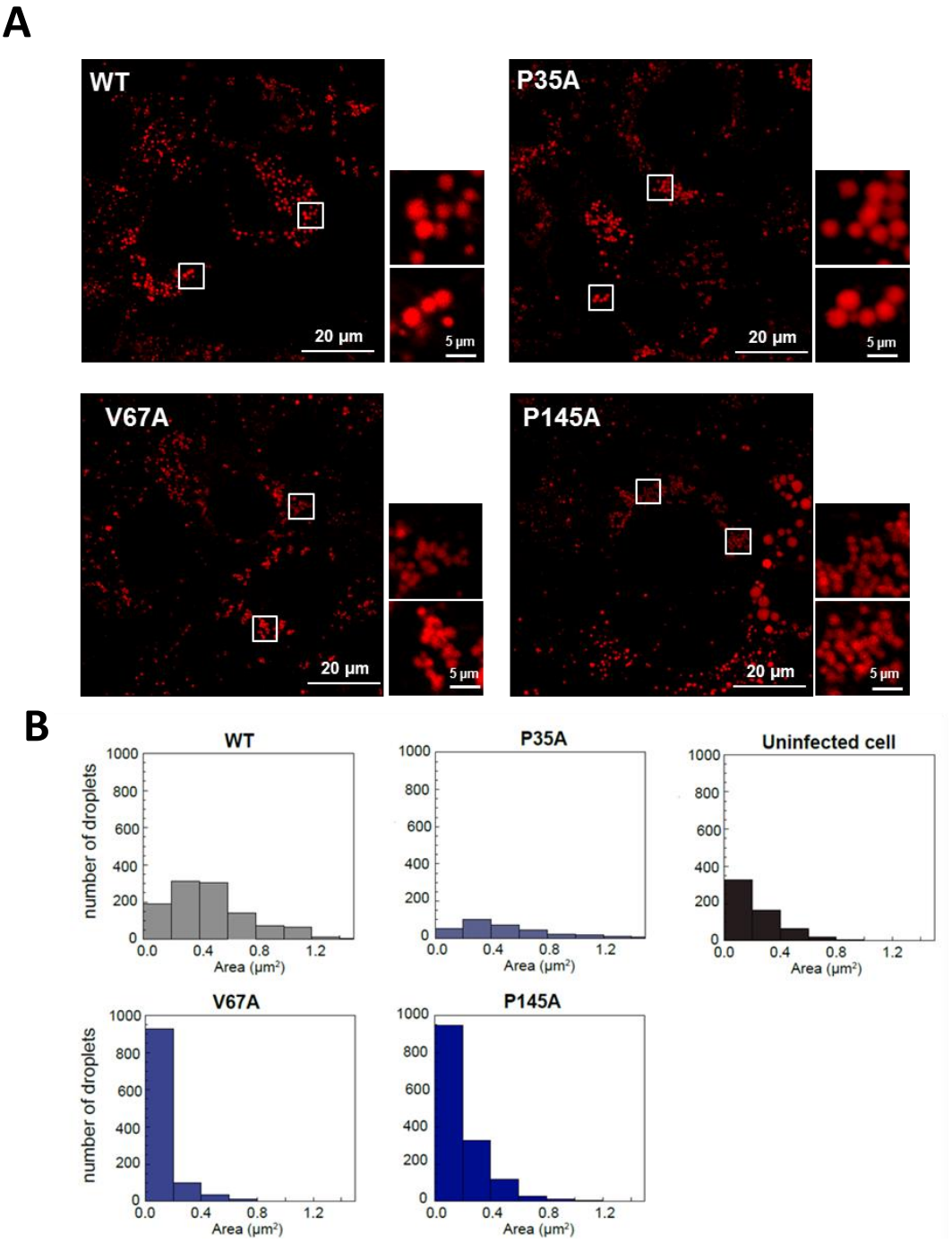

Figure 4.9 V67A and P145A mutations disrupt the HCV-mediated increase in LD size.

A. LDs in Huh7.5 cells electroporated with the indicated JFH1 constructs were visualized by staining with BODIPY 558/568-C12. **B.** To determine the total area of LD, the grayscale rendered 16-bit tagged image file format (TIFF) images were subjected to threshold-based analysis of LD areas for 10 randomly selected cells for each variant. 2D masks of the labelled regions were constructed and were used for computing the 2D area of LDs. The size of individual LD was determined and plotted as a histogram. The area (μm^2) is taken as an indication of the three-dimensional volume of the LD. For comparison similar data was determined from the uninfected Huh7.5 cells. This work was performed by Niluka Goonawardane.

In addition, there were some other differences between WT/P35A and V67A/P145A: in particular the amount of NS5A localised at the surface of lipid droplets appears to be much less for the latter two mutants. This was confirmed by quantitative analysis (Figure 4.10A), the percentage of NS5A fluorescence that co-localised with LD was significantly reduced. However, the reciprocal analysis (percentage of LD that co-localised with NS5A) showed no differences. This suggested that the proportion of LDs that were associated with NS5A was no different to WT. However, compared to WT, the majority of NS5A did not associate with LDs. Quantitative analysis of the NS5A: core co-localisation revealed a similar trend whereby the percentage of NS5A co-localised with core was significantly less for V67A and P145A (Figure 4.10B). In contrast, although the percentage of core that co-localised with LD was significantly reduced for V67A and P145A, the reduction was much less dramatic (Figure 4.10C). Lastly, it was observed that there were differences in the distribution of LDs: for both V67A and P145A the LDs were significantly closer to the nucleus, albeit not as close as in either GND-electroporated or mock control cells (Figure 4.10D).

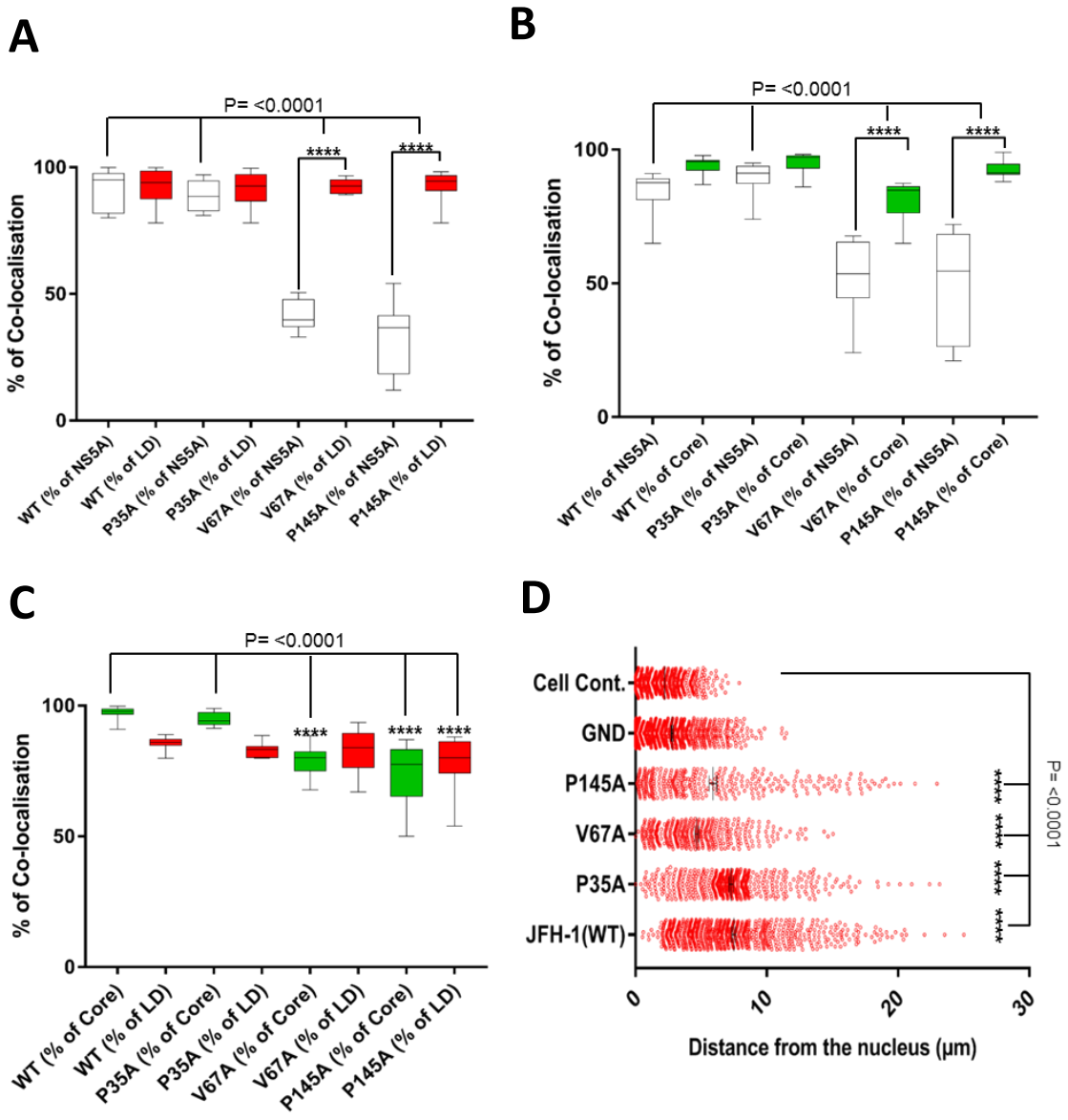

Figure 4.10 V67A and P145A disrupt the co-localization between NS5A and core or LDs.

A. Quantification of the percentages of NS5A colocalized with LD (white blocks), or LD colocalized with NS5A (red blocks). **B.** Quantification of the percentages of NS5A colocalized with core (white blocks), or core colocalized with NS5A (green blocks). **C.** Quantification of the percentages of core colocalized with LD (green blocks), or LD colocalized with core (red blocks). **D.** Spatial data for the distance of LDs from the nuclear envelope were determined from 10 cells for each construct using Fiji. **** indicates significant difference (P<0.0001) from the results for WT. This work was performed by Niluka Goonawardane.

4.2.4 A role for NS5A domain I in formation of lipid droplets during infection

To further check the formation of lipid droplets (LDs), this imaging analysis was complemented by investigating the composition of LDs. LDs were purified from electroporated cells by density gradient centrifugation and analysed by western blot for NS5A and core, using antibody to the LD-associated adipose differentiation-related protein (ADRP, also known as adipophilin or perilipin 2) (Boulant et al., 2008, Miyanari et al., 2007) as a marker for LDs. The integrity of the LDs and lack of contamination with other cellular components was demonstrated by the absence of GAPDH (Wang et al., 2015).

As shown in Figure 4.11, ADRP was exclusively present in the LD fraction (not in the cytosolic or membrane fractions) and western blot for GAPDH confirmed the absence of cytosol and other membranes in the LD fraction. GAPDH can only be detected in fractions of cytosol and cytoplasmic membranes and showed in reduced level compared with that in total cytoplasm because of the dilution by LD purification buffers (see 2.5.9). Both NS5A and core were also detected in the LD fractions, however the relative distribution and amounts of these two viral proteins differed between the mutants and WT (Figure 4.11 and 4.12). Both V67A and P145A showed significantly less NS5A in the LD fraction (Figure 4.11 and 4.12A), consistent with the fluorescence data (Figure 4.8 and 10A). In contrast the amount of core in the LD fraction of V67A and P145A was increased (Figure 4.11 and 4.12B). These data are consistent with a scenario whereby NS5A transports nascent genomes to LDs where it is transferred to the core protein for subsequent movement to assembly sites.

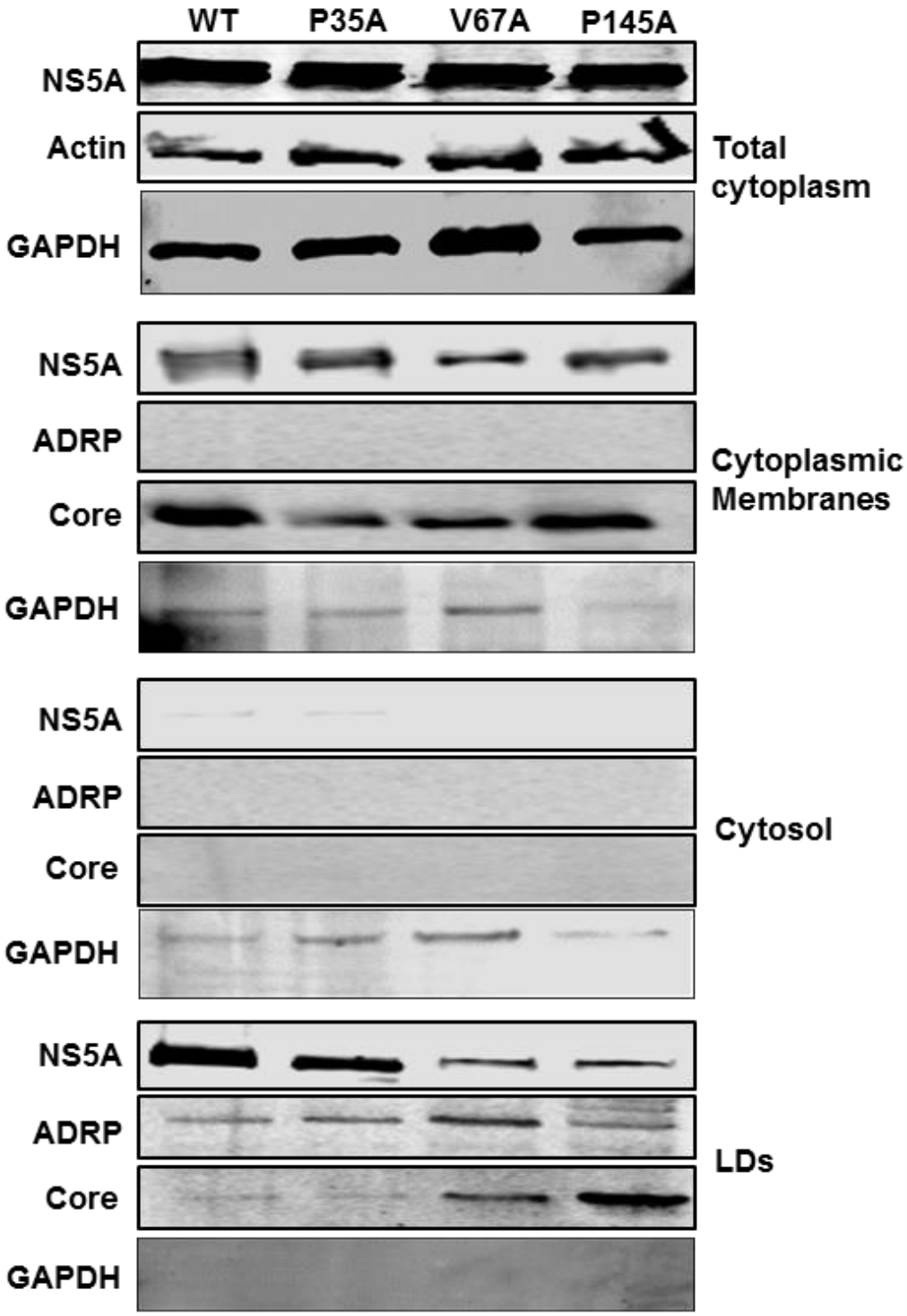

Figure 4.11 V67A and P145A disrupt the recruitment of NS5A and core to LDs.

Huh7.5 cells were electroporated with in vitro transcript of mJFH1 WT and mJFH1 mutants. Cells were harvest for LD purification 72 hpe. Western blot analysis of NS5A and core proteins and the LD marker protein ADRP and GAPDH in purified LD fractions compared with whole cytoplasm, cytoplasmic membrane and cytosolic fractions.

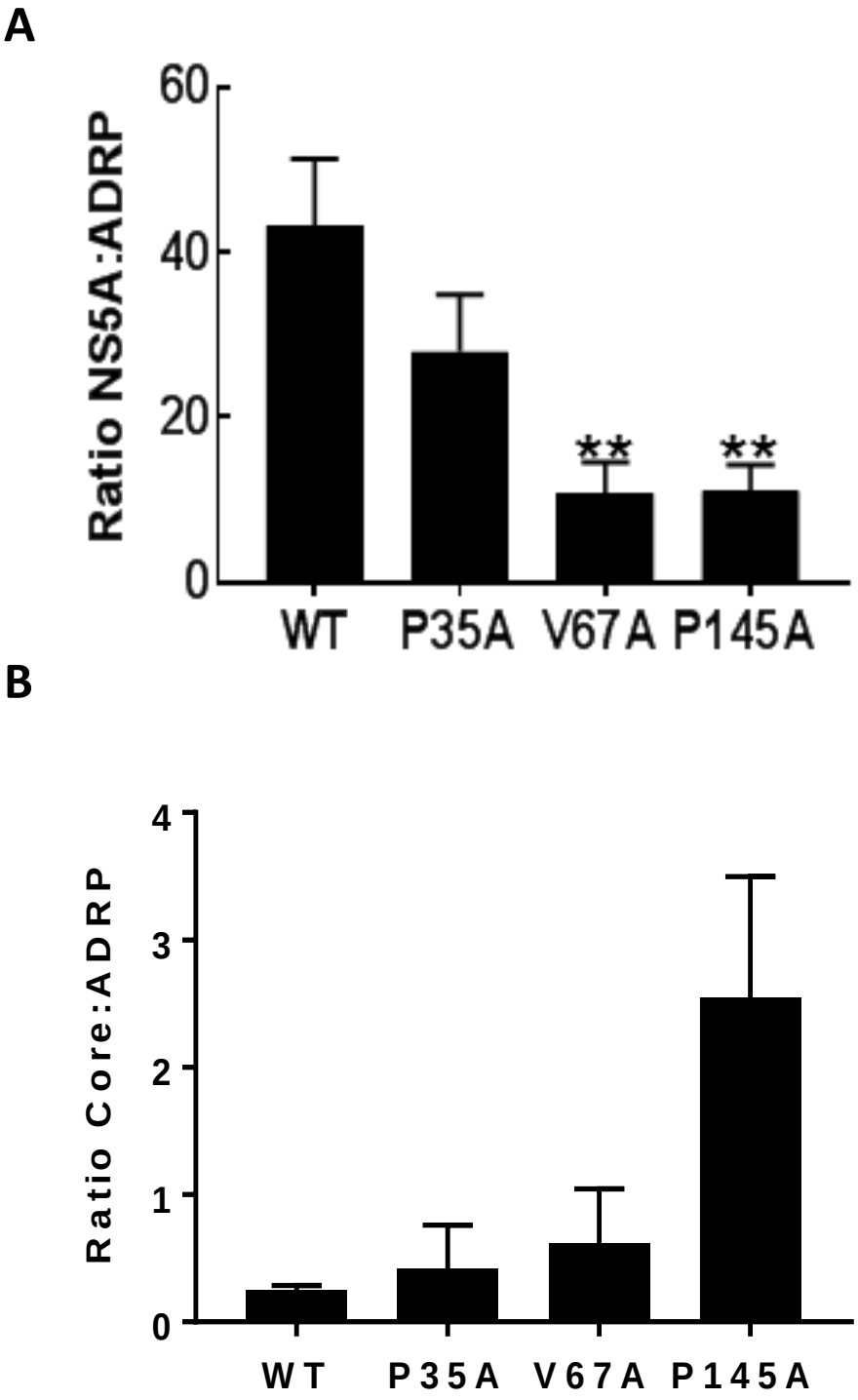

Figure 4.12 Quantification of the abundance of NS5A and core in LDs.

A-B The abundance of NS5A (B) and core (C) in the LD fractions was quantified and normalised to the LD fraction ADRP value acquired by western blot using a Li-Cor Odyssey Sa, enabling highly accurate quantification. Error bars represent the standard error of the mean of three independent experiments. ** indicates significant difference (P<0.01) from WT.

4.2.5 Recruitment of viral RNA into LD and viral particles

As shown above, recruitment of NS5A was prohibited into LDs, which will lead to the disruption of recruitment of NS5A into intact viral particle and finally failure of virus assembly. As the RNA binding protein, NS5A serves as the vector to transport RNA from RC into viral particles. Given that the RNA binding protein-NS5A cannot interact with LD and core protein, I wondered whether RNA can still be recruited into LDs or viral particles.

To confirm this, I used qRT-PCR to quantify the amount of viral RNA in the LD fractions. This analysis revealed that for both V67A and P145A there was a significant reduction in genomic RNA associated with LDs (Figure 4.13A). In addition, core immunoprecipitates revealed significant reductions in the amount of genomic RNA bound to core for V67A and P145A (Figure 4.13B). Moreover, the amount of genomic RNA bound to NS5A in the context of each mutation will be discussed in Chapter 5. These analyses were consistent with a scenario whereby NS5A transports nascent genomes to LDs where it is transferred to the core protein for subsequent movement to assembly sites.

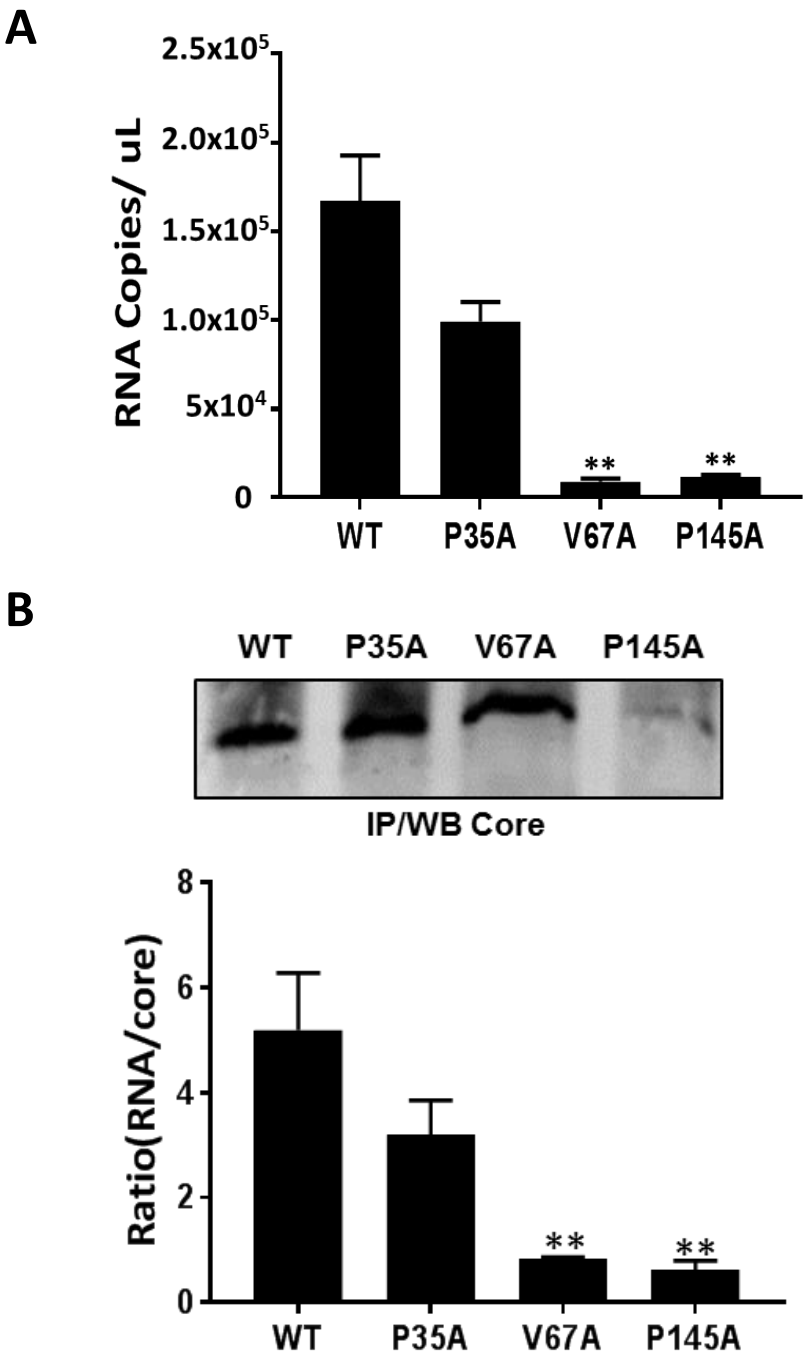

Figure 4.13 RNA levels in LDs and bound to viral core protein were decreased for V67A and P145A mutant transfected cells.

A. Post purification of LDs from each JFH1 transfected cells, the amount of viral RNA in LD fractions was determined by qRT-PCR. **B.** Cells were lysed at 72 hpe and core was immunoprecipitated from cell lysates. After enough washing, the beads were subjected to analysis by western blot and RNA extraction. qRT-PCR were performed to quantify the level of positive genome RNA bound with viral protein-core. The binding capacity of core is shown in the ratio of RNA copies to NS5A (n=2). Error bars represent the standard error of the mean of two independent experiments. ** indicates significant difference ($P<0.01$) from WT.

4.3 Discussion

4.3.1 Domain I of NS5A is involved in HCV assembly

In chapter 3, I analysed 12 residues that are both conserved and surface exposed in domain I by site directed mutagenesis within JFH1 subgenomic replicons. Most of them were absolutely required for genome replication. However, three residues (P35A, V67A and P145A) were identified in NS5A domain I for which alanine substitution had a modest effect on genome replication, keeping partial replication phenotype, while replication of them even reached to almost wild type level in Huh7.5 cells, a permissive cell line.

In this chapter, P35A, V67A and P145A were introduced into JFH1 full-length virus backbone to check whether they are involved in virus production pathways. Firstly, these mutants together with JFH1 wildtype and negative control GND were electroporated into Huh7 cells. Virus replication was first analysed by IncuCyte Zoom method (Stewart et al., 2015), this result is consistent with the observation in SGRs (Section 3.2.2). Then both intracellular and extracellular viruses were harvested and titrated in naïve Huh7 cells. Compared with WT and GND, P35A could be detected by both intra and extracellular viruses but with about 10-fold reduction, which can make sense because of the inhibition of replication level. However, V67A and P145A mutants failed to produce intracellular infectious virus. This result might stem from the extremely low replication, so that the virus level is hard to be detected, or due to the failure to produce virus. To exclude the former possibility, permissive cell line, Huh7.5 were utilised to perform virus transfection and titration. Replication of V67A and P145A virus was increased to WT level as expected. Based on this level, virus harvested was then titrated on naïve Huh7.5 cells and no virus was detected as well, which confirmed that V67A and P145A impaired production of virus. Previously, domain I has been assumed only to function during genome replication, and to our knowledge this is the first detailed analysis of a role for domain I in virus assembly, which is an important and new finding since JFH1AAA99 were reported to be involved in HCV release (Miyanari et al., 2007).

I reasoned that mutants of V67A and P145A could either assemble into virus non-infectious particles or they could prevent the formation of intact viral particles. To test these two options, 100-fold concentrated virus culture medium (extracellular virus) were subjected to analyses of viral protein (core), RNA and virus infectivity. All these results consistently exhibited that there are no viral particles released. Thus, these phenotypes were attributed to assembly defect to the mutations of V67A and P145A.

4.3.2 Domain I of NS5A is required for the recruitment of NS5A to lipid droplets

As for the HCV assembly pathway, it is well accepted that lipid droplets are the important organelles that provide the place for virus assembly (Miyanari et al., 2007). In this pathway, core protein is initially transferred onto the surface of LDs where it can recruit NS proteins including NS5A and viral genomes from replication complexes (Bartenschlager et al., 2011, Miyanari et al., 2007). Utilizing this model, I checked the co-localization of N5SA, core and LD using high-resolution microscopy, Airyscan (Korobchevskaya et al., 2017, Huff, 2016, Huff, 2015).

Firstly, taking JFH1 HCV wildtype as example, the biological changes of LDs in Huh7.5 cells were analysed after either post transfection or infection with HCV. With virus infection, the size of lipid droplets get enlarged while the number of them decrease and the distribution was more restricted to the perinuclear area typically after 24 hours post transfection or infection. Especially at 72 hpe, the size of LDs is significantly bigger than that in non-transfected cells, which suggested that some reactions related to HCV happen in LDs. As described previously, LD is the place for virus assembly (Miyanari et al., 2007, Filipe and McLauchlan, 2015). Thus, there is tight relationship between LD biogenesis and virus production. This evidence prompted us to further investigate the phenotype of LDs in V67A and P145A transfected cells together with the distribution of core and NS5A proteins, which are associated with LDs. As expected, LDs in V67A and P145A transfected cells are reduced in both their size and the number compared to wild type. P35A, which can produce infectious viruses, exhibited indistinguishable LDs from wild type. More importantly, it was also found that the co-localization between NS5A and LDs or core protein is significantly disrupted for V67A and P145A. Based on the HCV assembly pathway in which core associated LDs will recruit NS5A to participate in viral assembly, the disruption of co-localization of NS5A with LDs or core suggested that recruitment of NS5A to LDs might be inhibited.

To support this hypothesis, I set up a biochemical analysis of purified LDs from each JFH1 mutant transfected cell using ultracentrifugation. Compared with the expression level of NS5A in whole cell lysates, nuclei or membrane fractions, both V67A and P145A showed a dramatic reduction of NS5A in LDs. This result is consistent with what was initially hypothesised that recruitment of NS5A to LDs is more likely to be impaired. As supporting evidence, recruitment of RNA to both LDs and viral particles (core protein) was also disrupted in V67A and P145A transfected cells, which confirmed that NS5A domain I with V67A and P145A mutations impaired virus assembly by abrogating recruitment of both NS5A and genomic RNA to viral

assembly sites-LDs. For the relationship between LDs and core, one apparent discrepancy in my data relates to the co-localisation of core with LDs. Specifically, the imaging data (Figures 4.8 and 4.10) showed a modest reduction in core: LD co-localisation for V67A and P145A, whereas these mutants showed higher levels of core co-purified with LDs (Figure 4.11 and 4.12). Two factors may help to explain this discrepancy: firstly, it is possible that in the case of V67A and P145A, core associates more strongly with LDs, possibly because it has not been displaced by NS5A. Secondly, V67A and P145A infected cells exhibit larger numbers of smaller LDs, thus the available LD surface area for interaction with core is also likely to be larger, allowing more core to associate.

These observations imply that domain I of NS5A plays multiple roles in virus assembly. It is required for the association of NS5A with LD as well as the increase in LD size and altered distribution (movement away from the nuclear membrane) that is also seen during HCV infection. In addition, it was noticed that the phenotype of LDs of V67A and P145A is more like that of WT at the earliest transfection time point (24 hpe). Hence it was suspected that V67A and P145A are trapped in the early virus process such as replication and cannot transferred from replication complex and proceed into next virus assembly sites-LDs, which can explain why the phenotype of LDs for V67A and P145A at 72hpe is more like that of WT at 24 hpe and why there are no virus particles produced for V67A and P145A. Furthermore, viral RNA is inhibited to shifting into LDs and viral particle as well. As expected, NS5A is the RNA binding protein that can transfer RNA from replication sites into assembly sites. Significantly, reduced RNA levels associated in both LDs and viral particles in mutants (V167A and P145A) may indicate that NS5A together with genome RNA was inhibited from interacting with LDs and failed into viral assembly. However, what is the exact mechanism of NS5A domain I involved in virus assembly pathway? More research needs be done to answer this question.

Chapter 5: Biochemical analysis of domain I

5.1 Introduction

As mentioned previously, domain I of NS5A is the most highly structured of the three domains. The domain I monomer can be divided into two subdomains: the N-terminal subdomain IA and the C-terminal subdomain IB (Figure 5.1). Subdomain IA consists of an N-terminal extended loop lying adjacent to a three-stranded anti-parallel β-sheet (strands B1–B3), with α-helix H2 (designated H2 to allow numbering of the N-terminal membrane-anchoring helix as H1) at the C terminus of the third β-strand. These elements comprise the structural scaffold for a four-cysteine zinc-atom-coordination site (Cys 39, Cys 57, Cys 59 and Cys 80) at one end of the β-sheet (Tellinghuisen et al., 2005). Subdomain IB consists of a four-strand anti-parallel β-sheet (B4–B7) and a small, two-strand anti-parallel β-sheet (B8 and B9) near the C terminus, surrounded by extensive random coil structure. Additionally, the presence of a disulphide bond near the C terminus of domain I connecting the sidechains of the conserved Cys 142 and Cys 190 is important for the structure of domain I.

The other unique feature of domain I is that it exhibits dimeric structures. Although the exact function of dimerization has not yet been determined, four different dimeric structures of Domain I were solved by three independent research groups (Tellinghuisen et al., 2005, Love et al., 2009, Lambert et al., 2014). All the dimers were formed with the same monomers, but they interact with each other with different interfaces and orientations. There is evidence showing that different dimers might be assigned with different functions mainly by transformation between open and closed conformations of domain I (Tellinghuisen et al., 2005, Love et al., 2009, Lambert et al., 2014, Sun et al., 2015, Ross-Thriepland and Harris, 2014b).

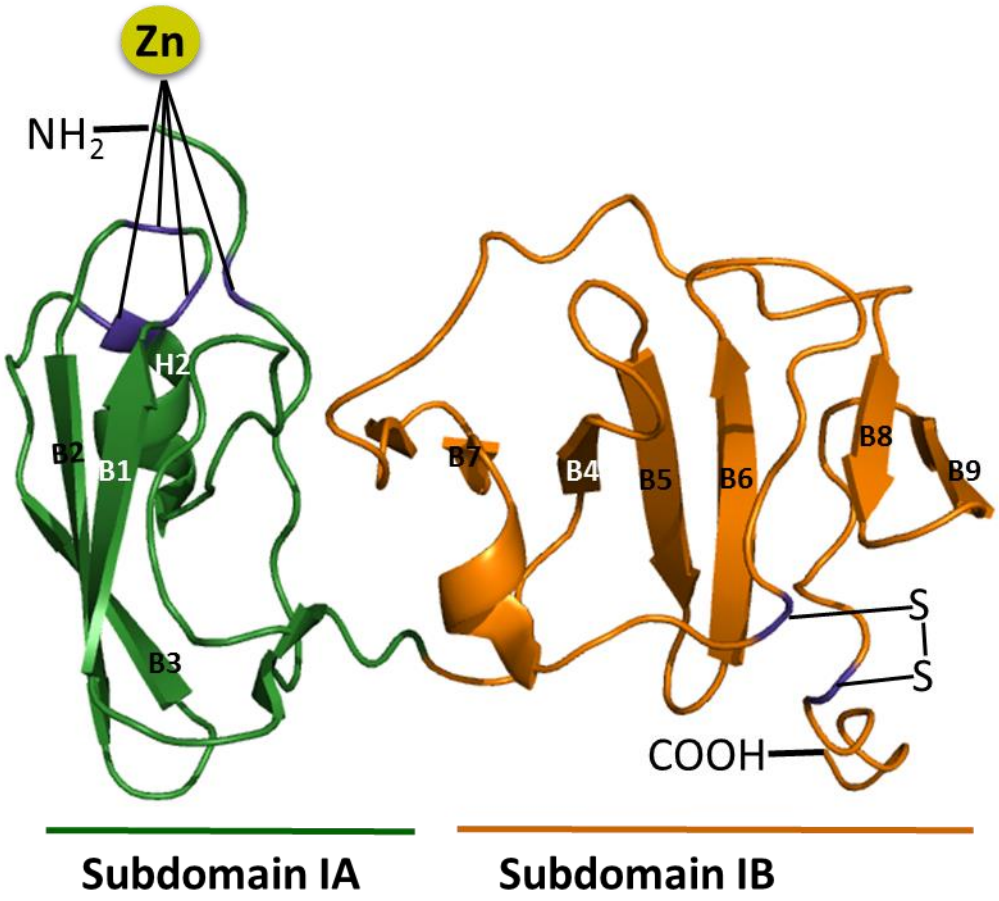

Figure 5.1 An overview of the detailed NS5A domain I structures.

Ribbon diagram of the structure of domain I. The polypeptide chain is coloured from the N terminus (green) to C terminus (orange). β-sheets (B1-B3) and H2 of Subdomain IA are in green. β-sheets of Subdomain IB (B4-B9) are in orange. Cys 39, Cys 57, Cys 59 and Cys 80 are shown in red in Subdomain IA and the coordinated zinc atom is shown in yellow. The C-terminal disulphide bond is labelled.

Of the four structures of domain I dimers, there are two dimeric forms from genotype 1b. One is NS5A (36-198) reported by Tellinghuisen in 2005 (Figure 5.2A) (Tellinghuisen et al., 2005). The crystal asymmetric unit (PDB accession code: 1ZH1) is composed of two identical domain I monomers in a dimeric conformation that forms a large, positively charged groove. This architecture reveals conserved external surfaces that might interact with other proteins, as well as a highly basic channel that might be involved in RNA binding (Lindenbach and Rice, 2005). When this structure was computationally modelled with the N-terminal amphipathic helix on a phospholipid membrane, it was predicted that NS5A would be anchored to the membrane such that the putative RNA binding groove was projected outwards in a manner

that could facilitate the binding of RNA, illustrated in (Tellinghuisen et al., 2005). Atomic absorption spectroscopy confirmed that domain I bound a single atom of zinc, whilst mutations in the tetracysteine motif abolished this interaction and abrogated genome replication in the SGR system. Zinc binding therefore appears to be essential for HCV RNA replication (Tellinghuisen et al., 2004).

The second model of domain I of NS5A (33-202) also from genotype 1b was described in 2009 by Love et al (PDB accession code: 3FQM) (Figure 5.2B) (Love et al., 2009). The association of the monomers within the dimer of NS5A (33-202) is significantly different from that in the previous structure of NS5A (36-198) (Tellinghuisen et al., 2005). In NS5A (33-202), the long axes of the monomers are nearly parallel, with numerous interactions along the entire side of each monomer. The two N termini are found on the same end of the dimer (Figure 5.2B), implying a co-localisation of the two amphipathic N-terminal helices, and this is a feature shared with the previous structure (1ZH1). The polypeptide fold within each monomer of the dimer of NS5A (33-202) is very similar to that reported previously for NS5A (36-198); the zinc-binding site displays the same coordination geometry as observed earlier. Interestingly the disulphide bond present in the Tellinghuisen et al. structure, between Cys142 and Cys190, was not present in this structure although the thiol groups remained in close proximity. The monomer-monomer interface of NS5A (33-202) features an extensive buried surface area involving the most-highly conserved face of each monomer. The two alternative structural forms of domain I now available may be indicative of the multiple roles emerging for NS5A in viral RNA replication and viral particle assembly.

Subsequently another structural study, using a genotype 1a NS5A domain I, revealed two new dimeric forms of this domain (PDB accession code: 4CL1) (Figure 5.2C and D). One of them displays a similar interface to that previously reported in the Love's model) (Love et al., 2009), but the orientation of one of the monomer is reversed creating a head-to-tail conformation, rather than head-to-head (Figure 5.2C) (Lambert et al., 2014). The other form shows an approximately twofold symmetry axis, composed of the monomers aligned in a head-to-head conformation (Figure 5.2D). The physical and chemical properties and the dimensions of the cleft between the head-to-head dimer match well with that of the daclatasvir (DCV) molecule, a new direct acting antiviral (DAA). The new dimer models observed in the genotype 1a NS5A structure not only extends our knowledge of interactional surfaces that could play a role in the action of symmetrical NS5A inhibitors, but supports the notion that NS5A dimers play a critical physiological role in the viral life cycle.

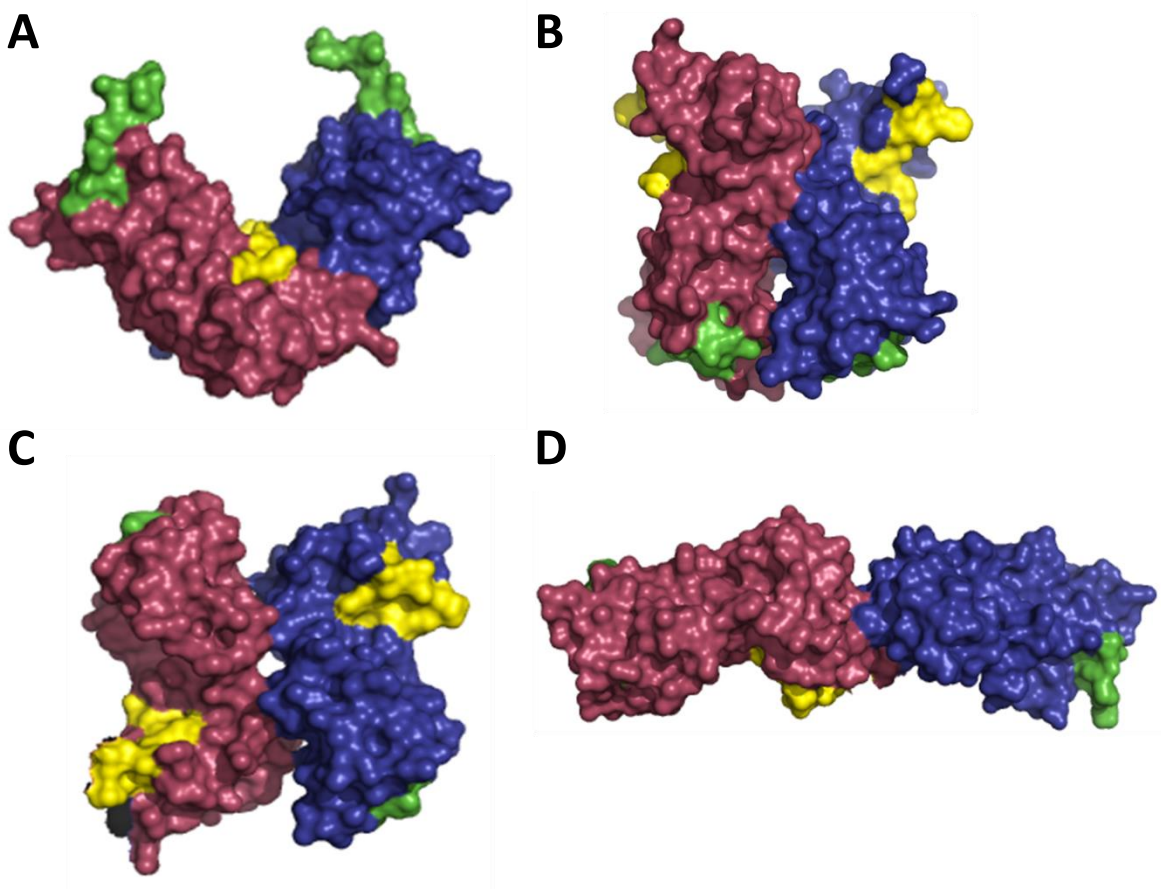

Figure 5.2 Summary of dimeric conformations of NS5A domain I from genotype 1b and 1a (1ZH1, 3FQM and 4CL1).

Monomers are shown in red and blue. A and B are genotype 1b dimers, C and D are genotype 1a dimers. **A.** The first crystal structure from Tellinghuisen et al is NS5A (36-198) (Tellinghuisen et al., 2005). **B.** The second genotype 1b dimer NS5A (33-202) is juxtaposed in parallel from Love et al (Love et al., 2009). **C.** Two monomers from genotype 1a NS5A domain I crystal structure share the same interface as the Love et al. dimer shown in B but with the monomers in an antiparallel arrangement (Lambert et al., 2014). **D.** Monomers form an N-terminal, head-to-head dimer fashion (Lambert et al., 2014). N-terminus of each dimer is in yellow and C-terminus is in green.

These observations are consistent with the notion that the structure of the NS5A domain I monomer in each crystallographic form is highly conserved, but the different crystal asymmetric units present unique symmetrical dimer interfaces. These forms are hypothesized to assemble into a polymer network by alternating crystallographic interfaces (Love et al., 2009, Lambert et al., 2014, Sun et al., 2015). However, to date there is no biochemical evidence for NS5A dimerization in infected cells. Indirect evidence provided by Lim et al demonstrated that NS5A dimerization, RNA binding and HCV replication are correlated (Lim et al., 2012). HCV RNA replication was greatly impacted when any of the cysteines (Cys-39, Cys-57, Cys59, and Cys-80) in the domain I is mutated, and these cysteine mutants of domain I failed to dimerize in *vitro* (Lim et al., 2012). Hence, it is likely that the best or even a unique way to definitely demonstrate that NS5A dimerization is vital for HCV replication would be to identify specific inhibitors of NS5A dimerization and to test them for their capacities to block viral replication (Lim et al., 2012). Following that, other indirect evidence comes from the observations that daclatasvir (DCV) is symmetrical and can dock across the dimer interface of domain I between and under the 28-35 loops to disrupt the natural packing of the NS5A N termini (Tellinghuisen et al., 2005, Sun et al., 2015). DCV resistance mutations, which are typically smaller amino acids (L31V, Y93H) (Fridell et al., 2010), partially compensate for the DCV-induced disturbance and are able to restore HCV replication function in the presence of bound inhibitors. However, synergistic binding of the NS5A inhibitor analogue (Syn-395) can potentiate the effect of DCV to introduce a conformational change that resensitizes the resistant NS5A towards inhibition (Sun et al., 2015). In addition, investigation of NS5A phosphorylation also put forward that S146 phosphorylation of NS5A might affect the NS5A conformation at the point of dimerization or be involved in switching between open conformation and closed conformation (Ross-Thriepland and Harris, 2014b). Although the relationship between dimerization and phosphorylation needs to be further investigated, all these findings provide indirect evidence of a dimeric structure for domain I. Up to date, all the research about dimerization and RNA binding ability of NS5A domain I are focused on in *vitro* analysis. It lacks direct evidence about how domain I behaves in cell culture to support this hypothesis.

In the previous chapter, I presented data demonstrating that domain I plays roles in HCV assembly by affecting the recruitment of NS5A to the assembly site-Lipid Droplets. In order to investigate the molecular mechanism of the recruitment, I performed biochemical analysis focused on dimeric notion and RNA binding of domain I. Moreover, these results in *vitro* were applied to cell cultures to demonstrate further. In addition, effects of these mutations in protein- protein interactions of NS5A were investigated in Chapter 6. Utilizing this information,

this chapter will present the dimerization and RNA binding activity of V67A and P145A using in *vitro* purified domain I proteins and try to verify them in HCV infected cell cultures.

5.2 Results

5.2.1 Purification of NS5A domain I

5.2.1.1 Cloning of NS5A domain I ORF into pET28a-SUMO expression vector

Domain I ORFs spanning from 35 to 215 amino acids were amplified from JFH1 virus constructs and cloned into pET28a-SUMO vector. These recombinant constructs will be referred to pET28a-SUMO-Domain I and result in the expression of the His-SUMO tagged NS5A domain I fusion protein (His-SUMO-Domain I). Following cleavage of the His-SUMO tag with SUMO protease, two non-native residues (Gly-Ser) remained at the N-terminus of domain I. A schematic representation of pET28a-SUMO-NS5A-Domain I is shown in (Figure 5.3).

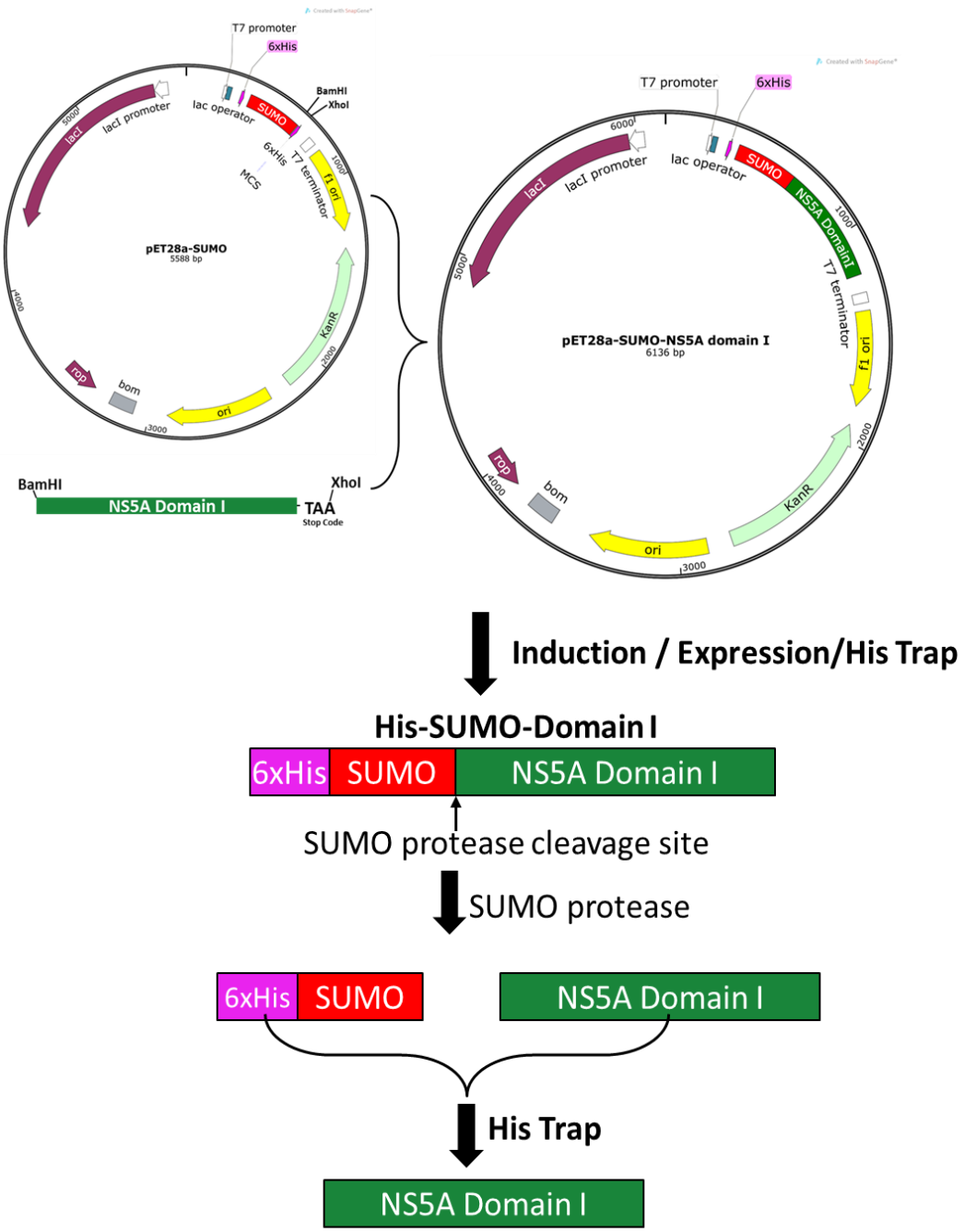

Figure 5.3 Strategy for construction and purification of NS5A domain I.

NS5A domain I fragments flanked with *BamH*I and *Xho*I were amplified from JFH1 virus constructs and cloned into pET28a-SUMO vector, which express His-SUMO tagged domain I under the induction of IPTG in BL21 PLysS competent E.*coli*. Fusion protein His-SUMO-Domain I will be purified using His trap column followed cleavage with SUMO protease. Post second round of His Trap column, native NS5A domain I was harvested.

5.2.1.2 Optimization of expression of HCV NS5A domain I

His-SUMO-Domain I was expressed in BL21 plysS cells by IPTG induction at 18°C for 6 hours at different concentrations. Cells were harvested by centrifugation and resuspended in lysis buffer. Post sonication, cell lysates were clarified by centrifugation at 18,000 rpm for 1h at 4°C. Both supernatants and pellets were subjected to SDS-PAGE analysis. This result showed that His-SUMO-Domain I was well expressed in the soluble fractions after the induction with 0.1 mM IPTG, although there was a large amount of insoluble His-SUMO-Domain I (Figure 5.4). The predicted molecular weight of His-SUMO-Domain I is 34 kDa.

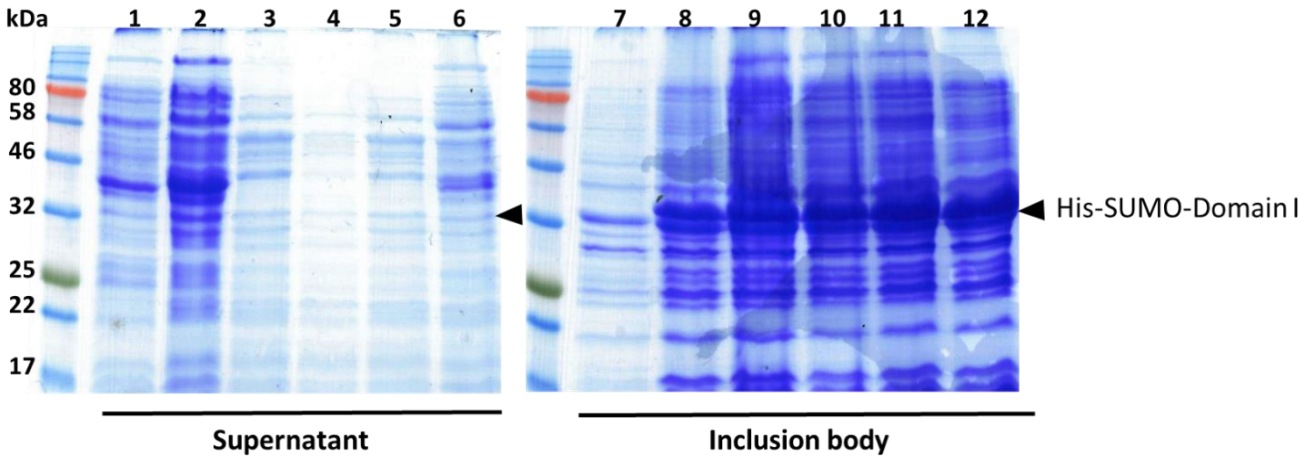

Figure 5.4 Optimization of conditions for expression of His-SUMO-Domain I.

IPTG with different concentrations (0.1mM, 0.2mM, 0.3mM, 0.4mM, 0.5mM) were used for induction of the expression of His-SUMO-Domain I (34 KDa) at 18°C for 6 h. Bacterial cell lysates were harvested by centrifugation and lysed in lysis buffer for sonication. Both supernatant and inclusion body pellet after centrifugation were analysed by SDS-PAGE and Coomassie Brilliant Blue staining. Lane 1: Un-induced supernatant, Lane 2-6: Supernatants after induction with 0.1mM, 0.2mM, 0.3mM, 0.4mM, 0.5mM IPTG; Lane 7: Un-induced inclusion body pellet, Lane 2-6: Inclusion body pellet after induction with 0.1mM, 0.2mM, 0.3mM, 0.4mM, 0.5mM IPTG.

5.2.1.3 Purification of NS5A domain I

Following expression of His-SUMO-Domain I, HisTrap™ HP was used to purify His-SUMO-Domain I from supernatant of bacterial cell lysates. HisTrap™ HP is a prepacked, ready-to-use column for the preparative purification of His-tagged recombinant proteins by immobilized metal affinity chromatography (IMAC). HisTrap™ HP was firstly pre-equilibrated with wash buffer and then loaded with clarified and filtered supernatants of bacterial cell lysates allowing His-SUMO-Domain I binding to Ni+ resin and let the unbound proteins go through from the

column. After 3 washes with wash buffer (each 5x the column volume), bound His-SUMO-Domain I in column was eluted using elution buffer (Figure 5.5).

Eluted fractions of His-SUMO-Domain I were dialysed in dialysis buffer (20mM Tris, pH8.2, 150mM NaCl, 10% glycerol) together with His tagged SUMO protease to cleave His-SUMO tag at 4°C overnight. For further purification of NS5A domain I to separate the fully cleaved domain I from fusion protein His-SUMO-Domain I, His-SUMO and SUMO protease (His tagged), these mixtures were centrifuged to remove the precipitates and clarified supernatants were loaded onto a pre-equilibrated HisTrap™ HP for second round of purification by collecting flowthrough and wash fractions containing native domain I protein (Figure 5.5). Fractions containing cleaved domain I were concentrated using Amicon® Ultra Centrifugal filters (10,000 NMWL). All of these processes resulted in the purification of a ~ 21-kDa protein (the correct predicted molecular weight for NS5A domain I) when visualised by SDS-PAGE and Coomassie staining (Figure 5.5).

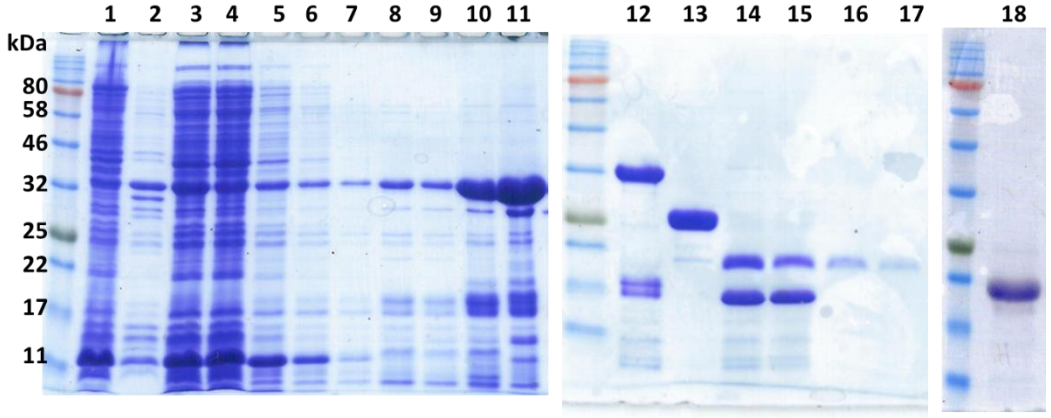

Figure 5.5 Expression of His-SUMO-Domain I and removal of the His-SUMO tag.

Purification of SUMO protease cleavage of His-SUMO-Domain I resulted in the release of soluble NS5A domain I with an apparent molecular weight (MW) of 21kDa. SDS-PAGE showed the purification of His-SUMO-Domain I by HisTrap™ HP affinity chromatography and cleavage of His-SUMO-Domain I with SUMO protease to release NS5A domain I. Lane 1 : Input of induced supernatant; Lane 2: Flowthrough; Lane 3-9: Wash fractions with 20 mM imidazole; Lane 10-11: Eluted fractions with 250 mM imidazole; Lane 12: pooled fractions of eluted before SUMO protease cleavage; Lane 13: SUMO protease; Lane 14-15: Cleavage with SUMO protease; Lane 16: Floughthrow containing cleaved domain I; Lane 17: Wash fraction containing cleaved domain I; Lane 18: Pooled and concentrated domain I from Lane 16 and 17.

5.2.1.4 Characterization of domain I by mass spectrometry

Purified domain I protein was analysed using mass spectrometry to confirm its identity. Domain I exhibited 100% coverage of the known domain I sequence (Figure 5.6), confirming that NS5A domain I was expressed correctly and could be used for further analysis.

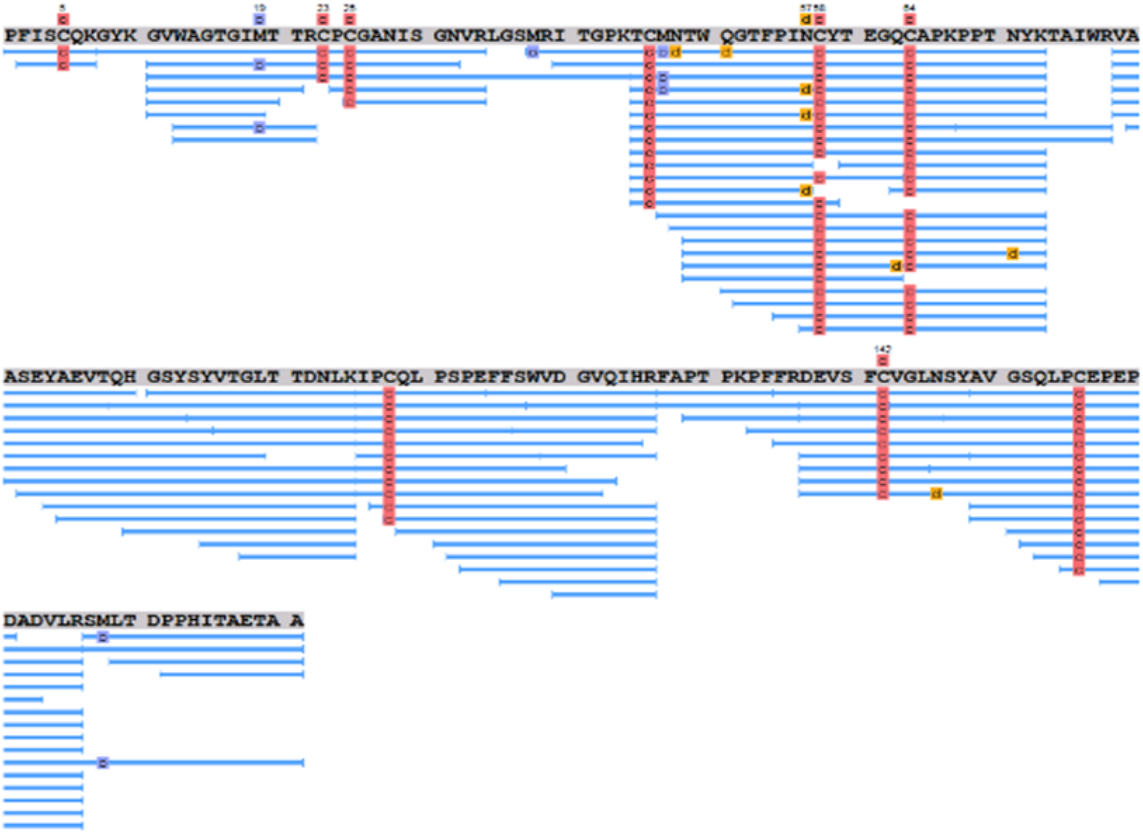

Figure 5.6 Identification of protein ID.

Protein peptides digested by trypsin were analysed by mass spectrometry and then compared with the known expressed protein sequence and protein database. The sequence at the top is the translated domain I amino acid sequence. A series of peptides below in blue are the digested domain I fragments for mass spectrometry.

5.2.1.5 Size exclusion chromatography

After removal of the His-SUMO tag and SUMO protease, further purification of NS5A domain I was aimed to remove protein contaminants and to analyse the oligomeric status of domain I. To achieve this, size exclusion chromatography (SEC) was carried out. The principle of SEC is based on the size of the protein that larger proteins and multimers are eluted first as they cannot enter the pores in the beads and pass straight through the column; smaller proteins

are eluted afterwards as they interact with the pores in the beads and take longer time to pass through the column.

The size exclusion column was equilibrated in gel filtration buffer overnight and then domain I protein was concentrated to 5ml and injected into Kata column. The column was run at a flow rate of 2ml/min, fractions were collected from around 90ml until a full column volume of buffer (~320ml) had eluted (Figure 5.7A). Three peaks of protein were observed and the fractions from each peak were analysed by SDS-PAGE (Figure 5.7B). The result demonstrated that all the fractions from three peaks (1-3) contained domain I protein. For Peak 3, it should be monomeric domain I (~20 kDa), which is expected and can be used for further analysis. However, peak 1 and 2 also exhibited in domain I, which suggested domain I can form into different oligomers. As NS5A domain I is dimeric *in vitro* as reported previously (Tellinghuisen et al., 2005, Love et al., 2009, Lambert et al., 2014) , it could be speculated that fractions of peak 2 might be dimers of domain I. Whereas, peak 1 that was eluted first is more likely to represent the aggregation of domain I, as domain I protein is not stable in the solution and precipitates at room temperature.

The limitation of SDS-PAGE is its denaturation of proteins prior to electrophoresis so that protein binding interactions and oligomeric protein generally cannot be determined on proteins isolated by SDS-PAGE. To further determine the nature of forms of domain I protein, pooled fractions from peaks 1 to 3 were analysed by native gel, which can assay native protein properties. Surprisingly, all of the peaks contained three different forms of Domain I after native gel electrophoresis (Figure 5.7C). This result suggested that domain I of NS5A co-exists in three different forms - precipitates (Figure 5.7C-III), dimers (Figure 5.7C-II) and monomers (Figure 5.7C-I), consistent with the observations in SEC analysis. For proteins from Peak 1, it contained precipitates, dimer and monomer of domain I as well two non-specific proteins eluted; proteins from Peak 2 were also separated in three forms including precipitates, dimer and monomers but dimer was predominant; Whereas, Peak 3 which was predicted as monomer showed in common with Peaks 1 and 2 comprising more dimeric forms than monomeric domain I.

To summarize, dimer of domain I is predicted to be the predominant and natural status of NS5A domain I in *vitro* as monomeric domain I tends to dimerize and the proportion of dimer in Peak 3 is significantly more than other two forms (Figure 5.7C). This suspicion was confirmed by SEC-MALLS in next section (Figure 5.8). Nevertheless, how it behaves in *vivo,* still remains unclear.

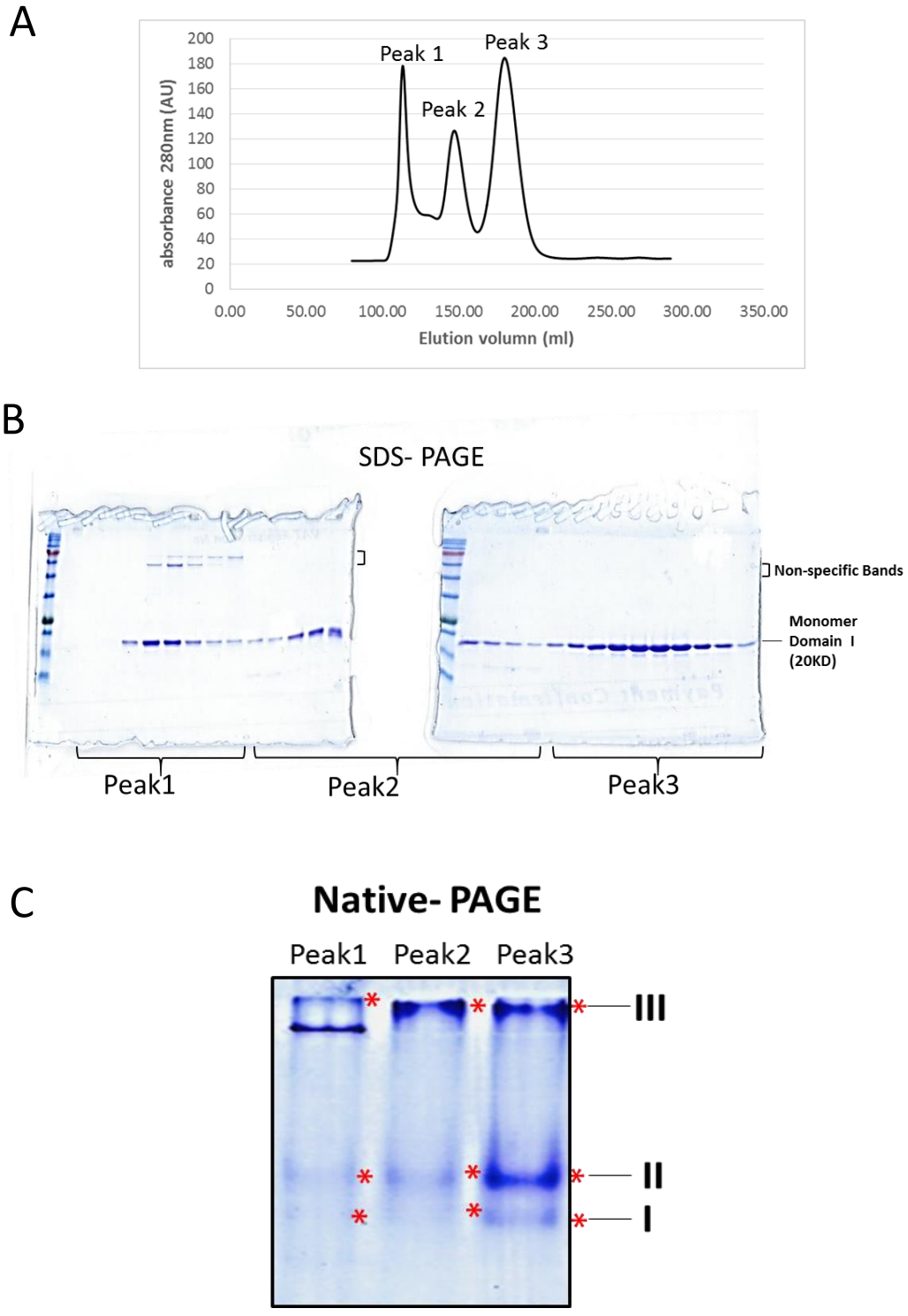

Figure 5.7 Size exclusion chromatography of the cleaved domain I

A. The absorbance peaks at 280nm (A_{280}) indicated protein eluted mainly in 3 peaks: protein of Peak 1 eluted at 114mL, which might be oligomer of domain I; protein of Peak 2 eluted at 150 mL; protein of Peak 3 eluted at 180mL. **B.** SDS-PAGE analysis of fractions from SEC with each peak labelled. NS5A domain I, 20kDa, appeared in all fractions analysed. Fractions from Peak 3 (about 170-190ml at elution volume) were polled together and analysed by SEC-MALLS (**see Figure 5.8**) **C.** Native gel analysis of protein from each labelled SEC peak. Asterisks in red indicated three forms of domain I protein in common in three peaks. I is the monomeric domain I, II is dimeric and III might be the aggregated domain I.

5.2.1.6 Analysis of domain I by SEC-MALLS

When light passes through a medium such as a solvent, even a transparent one, interaction with the molecules leads to scattering of the axis of the light beam. This may be observed by a sensitive detector and its intensity measured at different angles to the beam. If a solute of different refractive index is present this will lead to excess scattering dependent on the concentration of solute but also on its molar mass and for large particles, on the scattering angle. In a suitably calibrated system, this may be used to determine the molar mass of the solute. Based on this principle, the combination of Size Exclusion Chromatography with Multi-Angle Laser Light Scattering analysis (SEC-MALLS) - is a technique for determining molar mass in solution, overcoming the limitations of column calibration.

Protein pooled from Peak 3 fractions in the last step was analysed by SEC-MALLS to confirm the exact molecular weight of different domain I forms. As suspected, LS (light scattering) peak at Peak 1 at the void volume (5min) showed that this is likely to represent aggregates of domain I. LS (light scattering), UV (ultraviolet) and dRI (differential refractive index) peaks overlapped at about 11.5min means that protein in this form is of good quality and solubility (Figure 5.8). Combining these factors, molecular weight of this form of domain I was determined approximately at 44kDa ±11.522%, suggesting that this is a dimer of domain I. Whereas, protein under SEC-MALLS is the fraction from Peak 3 in SEC (5.2.1.5) which was previously predicted as monomer. Intriguingly, SEC-MALLS did not detect the signal of protein around 20 kDa. It might be due to the low proportion of monomeric domain I (Figure 5.7 C-I), or the monomer has dimerized into dimeric domain I.

Combining these observations in section 5.2.1.5 and 5.2.1.6 together with previous research of NS5A domain I, I speculate that dimer is the natural unit of domain I in *vitro* as monomer of domain I is not stable in nature and tend to dimerize, whereas it needs to be further investigated whether NS5A is dimeric in its life cycle (replication complex formation, RNA replication, budding, viral assembly, etc.).

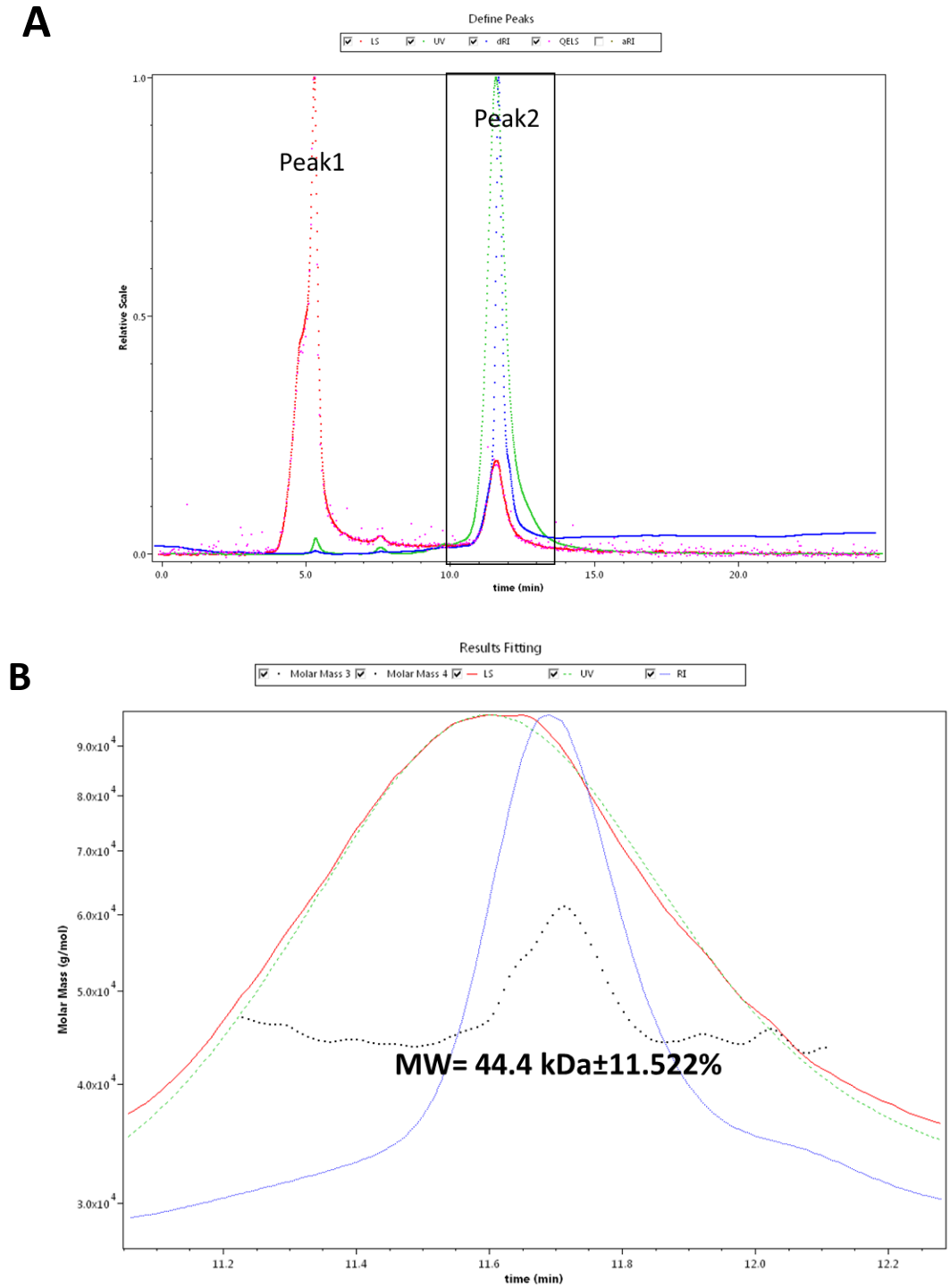

Figure 5.8 SEC-MALLS analysis of purified domain I to determine the molecular weight.

A. SEC-MALLS chromatogram of SEC peak 3 (Figure 5.7) purified NS5A domain I. LS peak 1 observed at the void volume (5 min) indicated the degree of aggregation of protein; LS, UV and dRI peaks at 11.5 min is the main formation of domain I, which can be used to calculate the correct molecular weight of domain I showed in **B**. Alignment of the LS, UV and dRI peaks, and a correct molecular weight (MW) was calculated (MW=MW= 44.4 kDa±11.522%). LS: Light scattering; UV: Ultraviolet; dRI: Differential refractive index; QELS: Quasi elastic light scattering; aRI: absolute refractive index.

5.2.2 Purification of domain I of mutants

5.2.2.1 Expression and purification of mutated domain I

NS5A domain I ORF spanning from 35 to 215aa with corresponding single mutation (P35A, V67A and P145A) was amplified from JFH1 mutants (see 4.2.1) and cloned into pET28a-SUMO vector to generate pET28a-SUMO-Domain I expression plasmids. Following the same expression and purification protocol of wildtype, domain I of P35A, V67A and P145A were purified and analysed by SDS-PAGE (Figure 5.9A) and western blot using NS5A polyclonal antibody (Figure 5.9B).

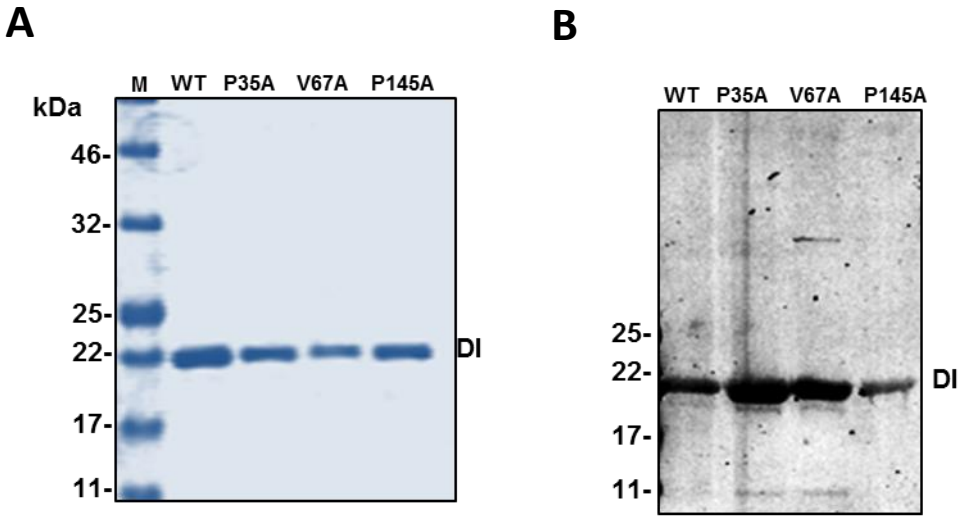

Figure 5.9 Expression of WT and domain I mutants

Purification of domain I (35-215) with corresponding mutations analysed by SDS-PAGE (A) western blot (B) using an anti-His antibody. All domain I proteins are of the correct size (~20kDa).

5.2.2.2 Purification of His tagged domain I and GST tagged domain I

SEC-MALLS result above suggested that domain I of NS5A is a dimeric protein, GST pull down assay was conducted to visualize whether domain I mutants could dimerize. To set up GST pull down assay, GST tagged domain I and His tagged domain I needed to be constructed and purified. Domain I ORFs flanked with *BamH*I and *Xho*I spanning from 35aa to 249aa were amplified from mJFH1 virus constructs. After digestion with *BamH*I and *Xho*I, domain I fragments were ligated into either His-SUMO vector or pGEX-6p-2 vector to generate recombinant constructs that can express His-SUMO-Domain I and GST-Domain I.

Expression of His-SUMO tagged and GST-tagged domain I proteins were performed in the BL21 (PlysS) strain of E. *coli* after induction with 0.1mM isopropyl -D-thiogalactopyranoside (IPTG). They were purified following the protocol described in section 2.7.5. Purified His-SUMO-Domain I (His-SUMO-DI) and GST-Domain I (GST-DI) with their corresponding mutations were analysed by western blot using anti-His and anti-GST monoclonal antibodies (Figure 5.10).

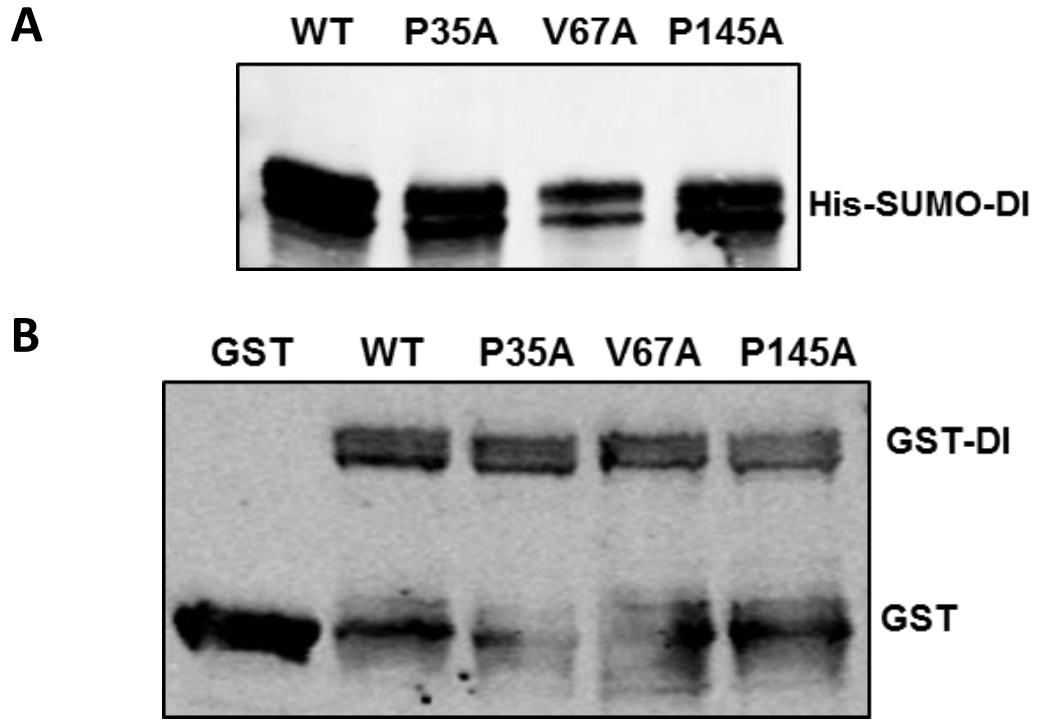

Figure 5.10 Expression of WT and domain I mutants for GST pull down assay

A. Purification of His-SUMO-Domain I (35-249) analysed by western blot using an anti-His antibody. **B.** Purification of GST control protein and GST-Domain I (35-249) analysed by western blot using an anti-GST antibody.

5.2.3 Characterization of dimerization of domain I

5.2.3.1 GST pull down assay

NS5A has also been reported to dimerize, both in the published crystal structures and in biochemical analyses (Lim et al., 2012). Examination of the different dimer structures revealed that P35 was located at the dimer interface of the 'open' conformation (Lambert et al., 2014, Love et al., 2009, Tellinghuisen et al., 2005). P145 was located at the interface of the 'closed' conformation (Lambert et al., 2014, Love et al., 2009, Tellinghuisen et al., 2005, Ross-Thriepland and Harris, 2014b). In contrast, V67 was distal to the dimer interfaces in both

conformations (Figure 5.11). Note that these mutants were initially selected to be on the surface of the domain I monomer (see section 3.2.1).

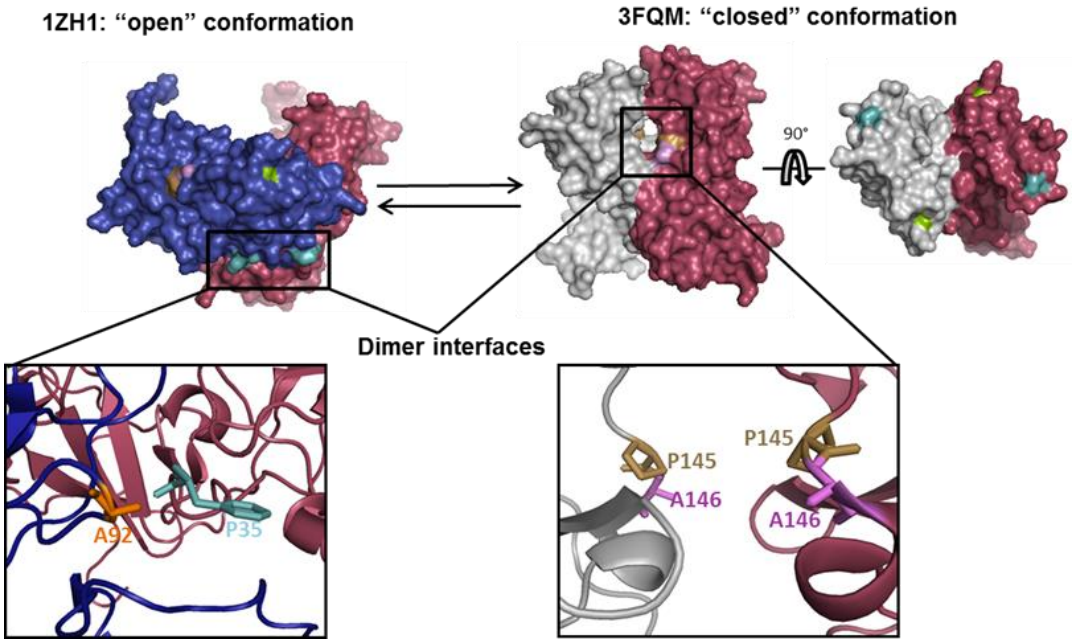

Figure 5.11 Summary of the position and potential role of domain I mutants.

The two different dimeric conformations of NS5A domain I are shown, "open" (1ZH1) (left, blue/red) (Tellinghuisen et al., 2005) and "closed" (3FQM) (right, grey/red) (Love et al., 2009). P35 highlighted in aquamarine is located in the P29-P35 interaction loop of NS5A dimers in the open conformation; V67 in green is exposed on the surface of both dimer structures; P145 in burlywood is at the interaction surface of the closed dimer. It is likely that P35 can interact with A92 (orange) from the other monomer that is involved in dimerization of the open conformation. P145 and A146 in the closed dimer face each other across the interaction surface and could possibly exert an effect on dimer interactions.

To test the effects of the three mutations on dimerization, I conducted GST pull down assays using GST-tagged domain I as bait to precipitate His-tagged domain I. We observed that GST-domain I (WT), but not GST alone, precipitated His-Domain I (WT) which means that domain I can dimerize (Figure 5.12A). Firstly, His-tagged domain I (WT) was incubated with GST-Domain I mutant, separately. Both GST-Domain I-P35A and V67A could precipitate His-tagged domain I (WT), while GST-Domain I (P145A) failed (Figure 5.12).

Next was to investigate whether these three mutants could dimerize without presence of wildtype domain I. Similar level of His-Domain I proteins was used as input. Then GST pull down assays described above were conducted using GST or mutated GST-Domain I as baits and corresponding mutated His-Domain I NS5A as preys. Compared with WT, GST-Domain I (P35A)

was also able to precipitate His-Domain I (P35A) with a modest but non-significant reduction in binding. In contrast, both V67A and P145A mutant GST-Domain I proteins were significantly inhibited to precipitate the cognate His-Domain I proteins (Figure 5.13A and B), indicating that these two residues are required for dimerization of domain I and implicating a role for NS5A dimerization in virus assembly. The faint band of His-Domain I in P145A lane (Figure 5.13A) might be due to the inadequate wash of the glutathione beads in this trial, as His-Domain I of P145A could not be detected in the repeated trials.

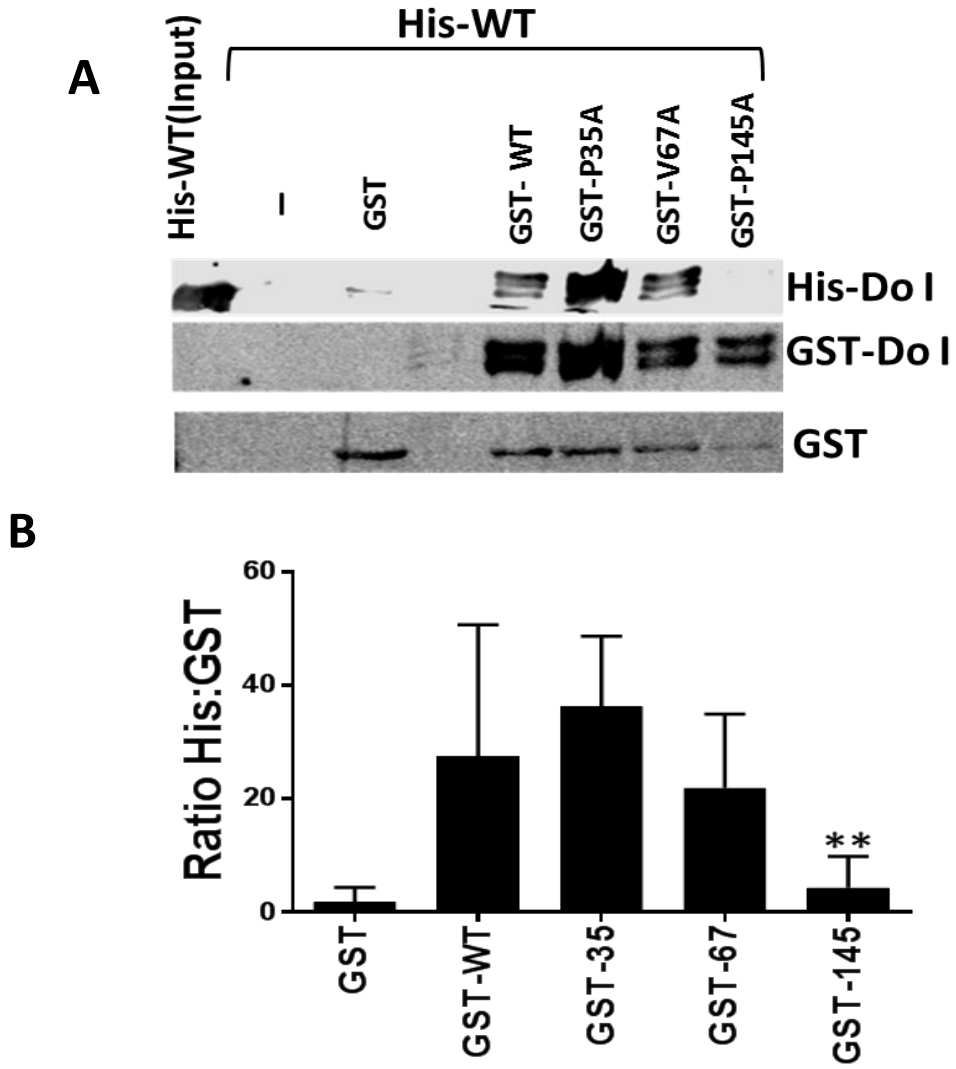

Figure 5.12 Domain I of P145A fails to dimerize with WT domain I.

A. His-tagged domain I (WT) was used as prey in pull down assays with GST or GST-Domain I with corresponding mutations as baits. Precipitated proteins were analysed by western blot using anti-His and anti-GST antibodies. **B.** The His:GST ratio was calculated following quantification of western blot signals using a Li-Cor Odyssey Sa infrared imaging system and represented graphically as a measure of the dimerization activity. ** indicates significant difference ($P<0.01$) from WT.

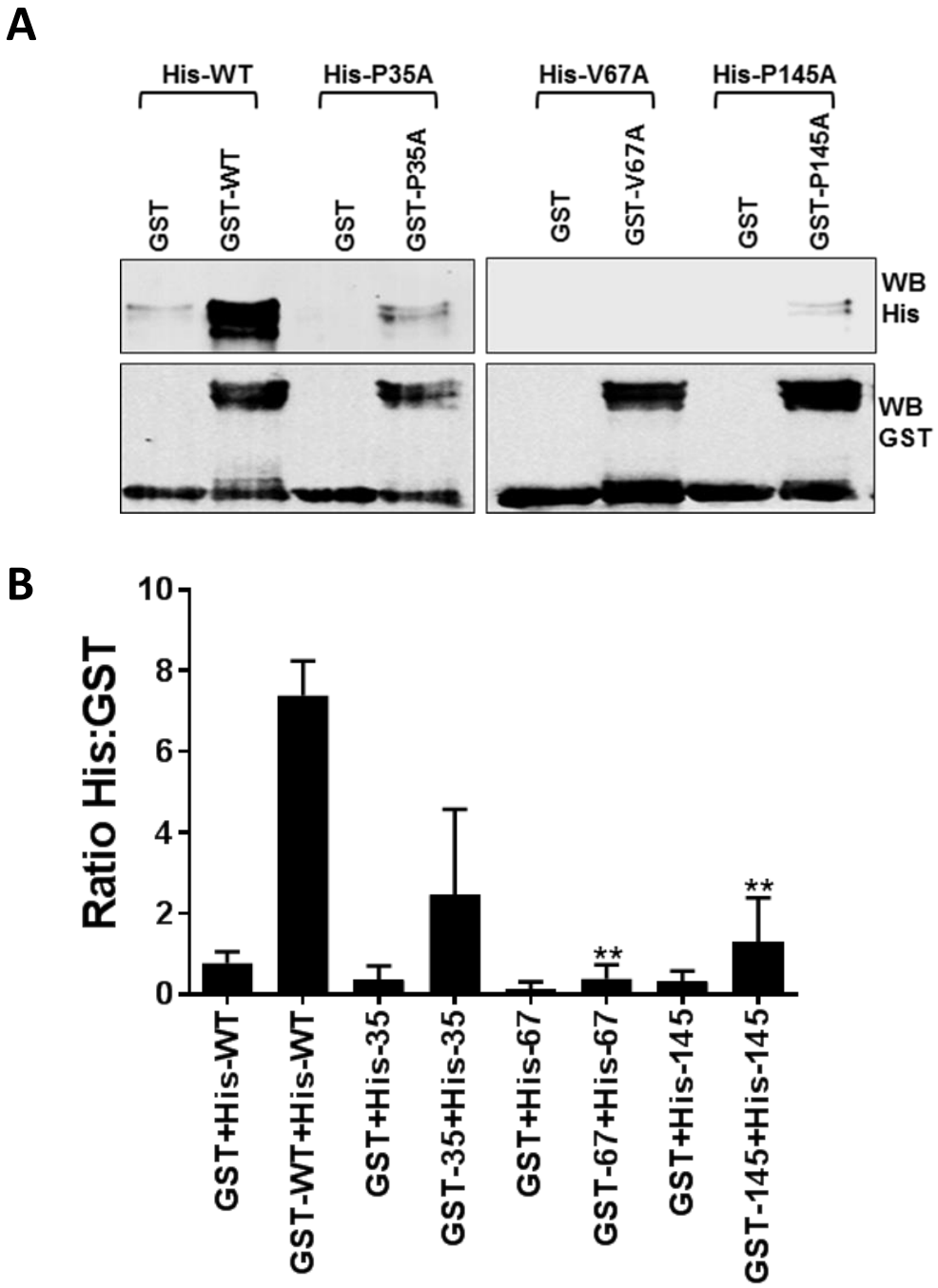

Figure 5.13 Residues at positions V67 and P145 of domain I are involved in NS5A dimerization.

A. His-tagged domain I proteins with mutations was used as prey in pull down assays incubated with corresponding GST-Domain I proteins. Precipitated proteins were also analysed by western blot using anti-His and anti-GST antibodies. **B.** Quantification of His to GST signals using a Li-Cor Odyssey Sa infrared imaging system and represented graphically as a measure of the dimerization activity. These data were representative of three independent experiments using different batches of purified domain I proteins. ** indicates significant difference ($P<0.01$) from WT.

5.2.3.2 Identification of dimerization by SEC-MALLS

The combination of both GST-pull down assay and SEC-MALLS (Figure 5.8 and 5.12) revealed that WT NSSA domain I was able to dimerize in *vitro*. However, the GST pull down assay revealed a defect in dimerization for V67A and P145A (Figure 5.13). To support the pull down assay result, purified domain I of P145A was analysed by SEC-MALLS in parallel with WT (Figure 5.8 in Section 5.2.1.6). As shown in Figure 5.14, P145A exhibited a very different profile to WT. Even the accurate molecular weight could not be determined, the main peak of domain I (P145A) at 16 min eluted later than WT (at 11.5 min) for 4 minutes, which means that the size of P145A domain I is much smaller than WT. Therefore, it was concluded that the predominant form of P145A was a monomer, which is consistent with the GST pull down assay in section 5.2.3.1 (Figure 5.13).

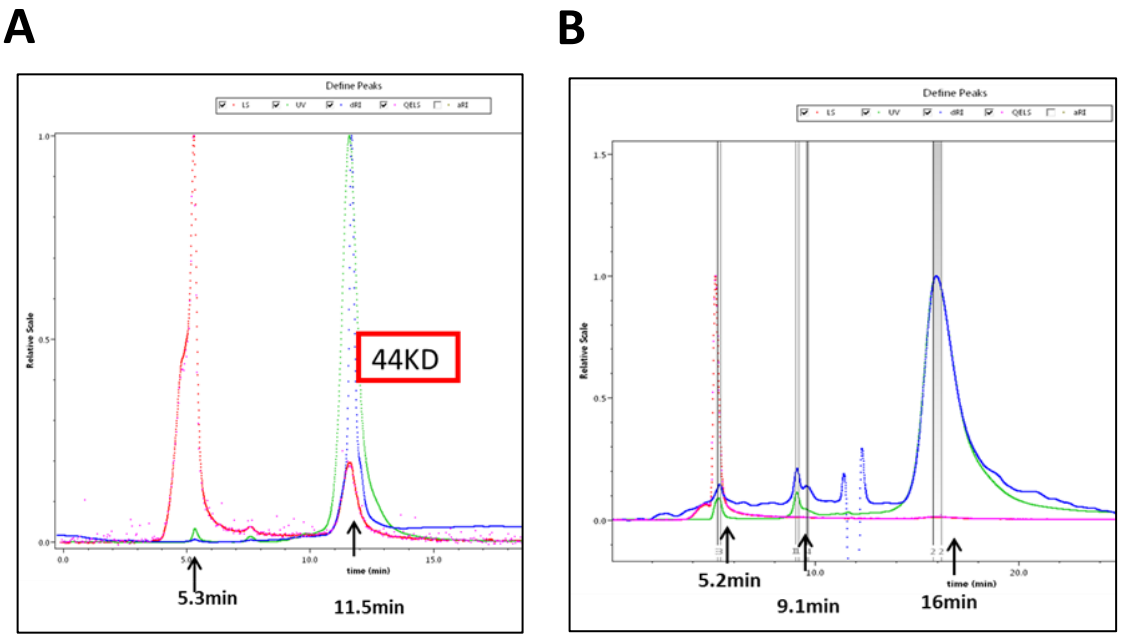

Figure 5.14 SEC-MALLS verifies that P145A disrupts dimerization of domain I.

SEC-MALLS chromatogram of purified domain I (35-215) (WT) (**A**) and domain I (35-215) (P145A) (**B**). **A.** LS peak at the void volume (5 min) indicated the level of aggregation, the multiple LS, UV and dRI peaks at 11.5 min with 44kDa exhibited the main form of domain I (WT) –Dimer (see details in Figure 5.8A). **B.** Domain I (P145A) aggregated and the peak came out at 5min as well, main UV and dRI peaks exhibited at 16min, later than WT domain I.

5.2.4 Dimerization of domain I in cell cultures

To the best of our knowledge, despite the fact that X-ray crystallography data showed that NS5A domain I was a dimer in *vitro* as early as 2005 (Tellinghuisen et al., 2005, Love et al., 2009, Lambert et al., 2014), in 12 years of research since then no-one has been able to demonstrate that NS5A dimerizes in intact cells. Dimerization has only been convincingly shown using purified proteins in *vitro* (Lim et al., 2012).

I did attempt to identify dimerization in cultured cells using a variety of approaches. Firstly, Huh7.5 cells stably harbouring the SGR-Neo-JFH1 (Figure 5.15, Lane 2) or SGR-Neo-JFH1 (NS5A- OST) (Figure 5.15, Lane 3) replicons that can stably express NS5A, were electroporated with mSGR-Luc-JFH1(GFP). The other is the transient electroporation assay, in which both mSGR-Luc-JFH1 (GFP) and pCMV10-NS3-NS5B (Figure 5.15, Lane 4) or mSGR-Luc-JFH1 RNA (Figure 5.15, Lane 5 and 6) were co-electroporated or co-transfected (Figure 5.15, Lane 7) into Huh7.5 cells. If dimerization of NS5A occurs in *vivo*, GFP-NS5A expressed from mSGR-Luc-JFH1 (GFP) replicon and untagged NS5A from pCMV10-NS3-NS5B or mSGR-Luc-JFH1 replicon would dimerize with each other in the replicons cultured cells. In this case, cell lysates of each sample harvested 72 hpe or 48 hpt were subjected to GFP pull down assay following the GFP-Trap® (ChromoTek) protocol so that GFP tagged NS5A (GFP-NS5A) together with its interacting partners can be precipitated and detected with α -NS5A antibody (Sheep). The result of input panel suggested that both electroporation and transfection of mSGR-Luc-JFH1 (GFP), mSGR-Luc-JFH1 and pCMV10-NS3-NS5B were successful as both GFP-NS5A and untagged NS5A were detected by western blot (Figure 5.15 upper panel). However, post GFP-Trap, only GFP-NS5A can be detected from the precipitates, so it cannot be concluded that NS5A dimerises in vivo.

The explanation of this result might be that a minor proportion of cells were successfully transfected with both constructs for dimerization. If it cannot be guaranteed that NS5A are expressed in the same cell, it is impossible for them to interact with its dimerizing partner-monomer NS5A with the other tag. This is also the major limitation of the research into NS5A dimerization in cells, which is urgent for construction of platform to investigate mechanism of dimerization.

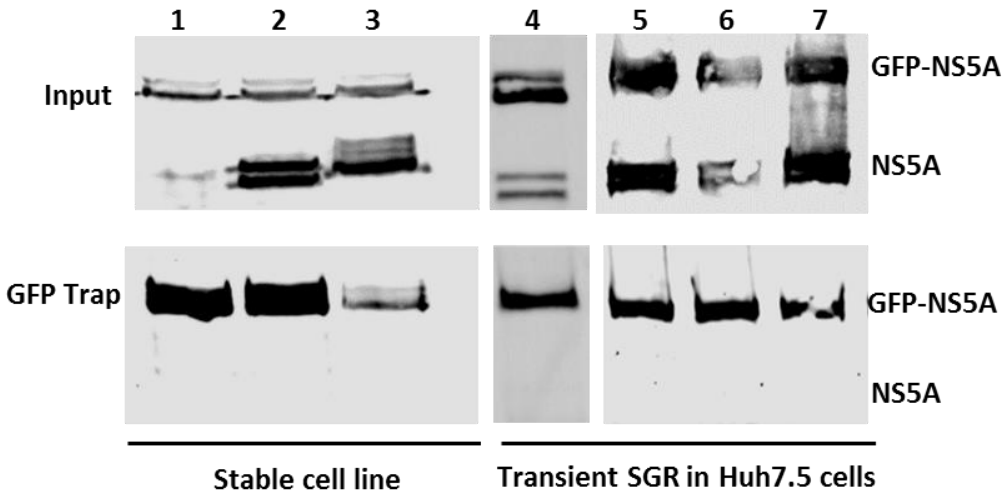

Figure 5.15 Lack of NS5A dimerization in intact cells.

A modified version of mSGR-Luc-JFH1 containing a GFP tag near the C-terminus of domain III of NS5A (termed mSGR-Luc-JFH1(GFP)) was a kind gift from John McLauchlan (Jones et al., 2007b). In vitro transcribed mSGR-Luc-JFH1(GFP) RNA was electroporated into Huh7.5 cells (lane 1), or Huh7.5 cells stably harbouring the SGR-Neo-JFH1 (Kelly et al., 2017) (lane 2) or SGR-Neo-JFH1(NS5A- OST) (Goonawardane et al., 2017) (lane 3), or co-electroporated with either pCMV10-NS3-NS5B plasmid (lane 4) or mSGR-Luc-JFH1 RNA (lanes 5. 6) into Huh7.5 cells. Alternatively, DNA constructs of both pCMV10-NS3-NS5B (GFP) (GFP tagged NS5A) and pCMV10-NS3-NS5B were co-transfected into Huh7.5 cells (lane 7). Cells were harvested into GLB at 72 hpe or 48 hpt and subjected to GFP pull down assay following the GFP-Trap® (ChromoTek) protocol. After GFP-Trap, protein bound on beads (lower panel) together with input samples (upper panel) were analysed by western blot using anti-NS5A antibody.

5.2.5 V67A and P145A increased binding affinity to HCV 3'UTR

Implicit in the above scenario is the specific interaction of NS5A with genomic RNA. In this context, domain I has been shown by us, and others (Foster et al., 2010, Huang et al., 2005, Hwang et al., 2010), to bind specifically to the HCV 3'UTR. RNA binding activity was supported by the "open" dimeric structure, as it provides an attractive groove for RNA-binding. The protein 'arms' extending out past this groove are more acidic, and might serve to prevent RNA from exiting the groove (Tellinghuisen et al., 2005). Hence, dimerization and RNA binding of domain I is potentially linked.

I therefore asked whether the three mutations affected this binding capacity. To address this, I expressed domain I WT and mutants as a His-SUMO fusion protein in *E.coli*. The fusion proteins were purified and cleaved to release the untagged domain I (Figure 5.9). The RNA binding capacity of the WT and mutant domain I proteins was determined by RNA filter binding assay utilizing ^{32}P-labelled HCV 3'UTR RNA (Figure 5.16). Intriguingly, it was found that V67A and P145A showed strong binding affinity to HCV 3'UTR RNA, exhibiting a 10-20 fold increase in Kd value compared to WT or P35A, despite with the similar Rmax values (Table 5.1). For WT and P35A the Kd values were 246.3 ± 77.19 nM and 245.7 ± 70.09 nM respectively. However for V67A and P145A, the values were 12.89 ± 6.25 nM and 22.35 ± 9.58 nM respectively (Table 5.1).

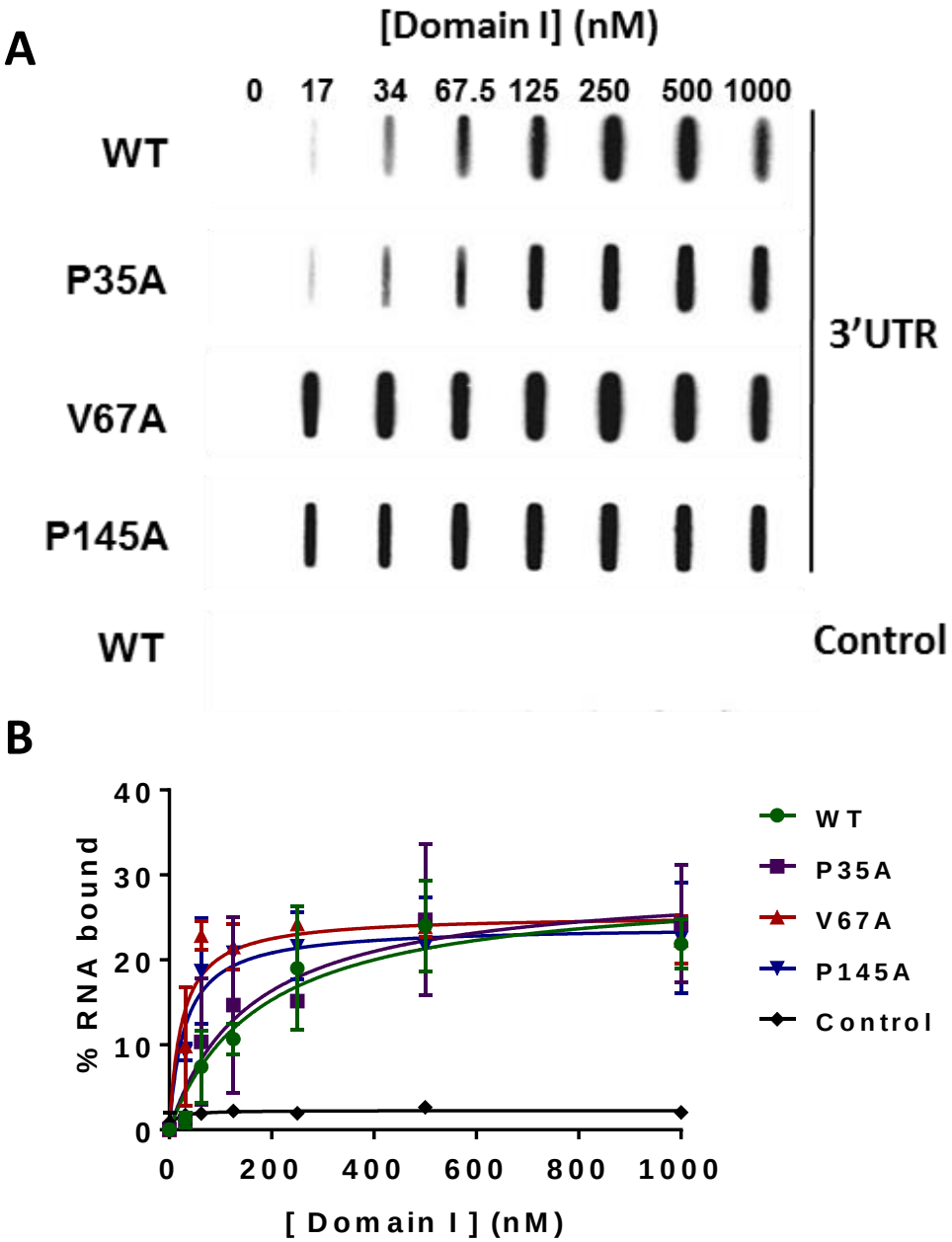

Figure 5.16 Residues at positions V67 and P145 of domain I are involved in NS5A RNA binding.

A. Filter binding analysis of the interaction between NS5A domain I and the HCV 3'UTR RNA. The indicated proteins were incubated with ^{32}P -radiolabelled RNA (1nM), either HCV 3'UTR (upper panels) or control FMDV 3D aptamer (lower panel) (Foster et al., 2010), before application to a slot blot apparatus, filtering through nitrocellulose and Hybond-N membranes. Representative slot blot analysis of RNA-protein complexes captured on nitrocellulose membrane in a filter binding assay was visualized by phosphorimaging. From left to right, the slots contained 0, 17, 34, 67.5, 125, 250, 500, and 1000 nM domain I protein. **B**. % RNA bound is shown graphically, quantified by phosphoimaging analysis. The data were fitted to a hyperbolic equation. These data were representative of three independent experiments using different batches of purified domain I protein.

	Kd,nM (mean ±SE)	Rmax, % (mean ±SE)
WT	246.3 ±77.19	26.84 ±3.225
P35A	245.7±70.09	25.67 ± 2.841
V67A	12.89±6.253	23.13 ± 1.378
P145A	22.35±9.582	19.72 ±1.416

Table 5.1 Binding of 3'UTR to NS5A domain I proteins is evaluated by filter binding assay.

Rmax is the maximal percentage of RNA competent for binding, and Kd is the apparent dissociation constant. These data were from three independent experiments.

To validate this in *vitro* data, NS5A was immunoprecipitated using α-NS5A antibody (sheep) from Huh7.5 cells electroporated with either JFH-1 WT or the three mutants and the amount of viral RNA in the immunoprecipitates was assessed by qRT-PCR. Consistent with the in *vitro* RNA filter binding assay data, both V67A and P145A bound more viral RNA compared to WT and P35A (Figure 5.17). In contrast, a similar analysis of Core immunoprecipitates revealed significant reductions in the amount of genomic RNA bound to Core or LDs for V67A and P145A (Figure 4. 13). Therefore, NS5A of V67A and P145A in virus transfected cells exhibited higher affinity to genomic RNA; as a result, less RNA was delivered from NS5A to viral nucleocapsid protein-Core for virus assembly.

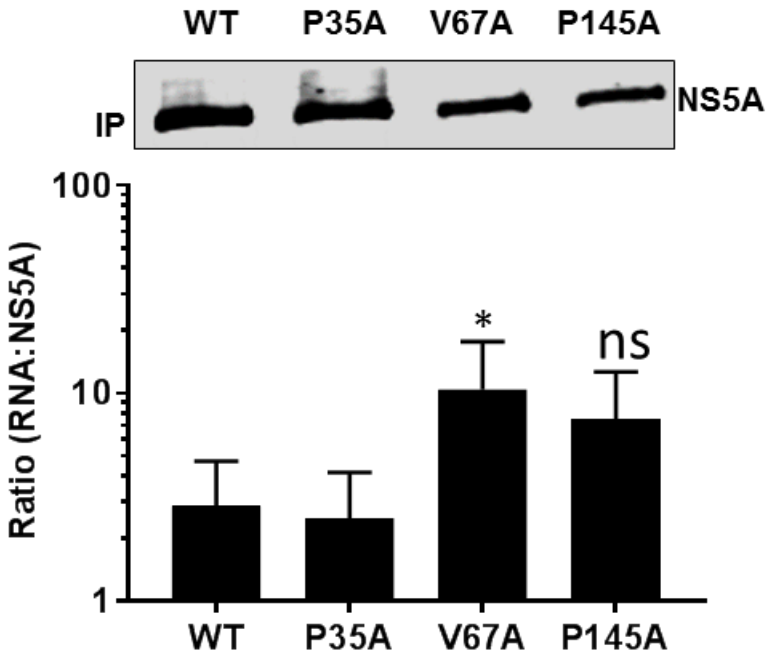

Figure 5.17 V67A and P145A binds more genomic RNA in cells transfected with mutant virus.

Huh7.5 cells were electroporated with in vitro transcripts of mJFH1 WT or the indicated mutants. Cells were lysed at 72 hpe and NS5A was immunoprecipitated from cell lysates. After washing the beads were subjected to analysis by western blot and RNA extraction. qRT-PCR were performed to quantify the level of (+) genome RNA bound to NS5A. The graph on the right shows the ratio of RNA copies to NS5A (n=2). *indicates significant difference ($P<0.05$) from WT, and ns indicates that there is no significant difference from WT.

5.2.6 DAA sensitivity

As P35, V67 and P145 were located on the exposed surface of domain I, it was considered that these non-lethal mutants might be further involved in sensitivity to NS5A targeting DAAs, such as Daclatasvir (DCV). To quantify changes in DCV sensitivity for P35A, V67A and P145A and to interrogate the drug-protein interaction surface, wild type and mutants SGR replicons were electroporated into Huh7.5 cells and then were treated with 10 fold serial concentrations of Daclatasvir (from 10^{-4} pM to 10^{7}pM) at 4 hpe. After 48-hour treatment of DCV, cells were collected and the replication of each mutant was measured. The fitness curve and EC_{50} of each mutant were calculated by Prism7 (Figure 5.18). Here EC_{50} result showed us that all the mutants shared the similar sensitivity to DCV compared with WT.

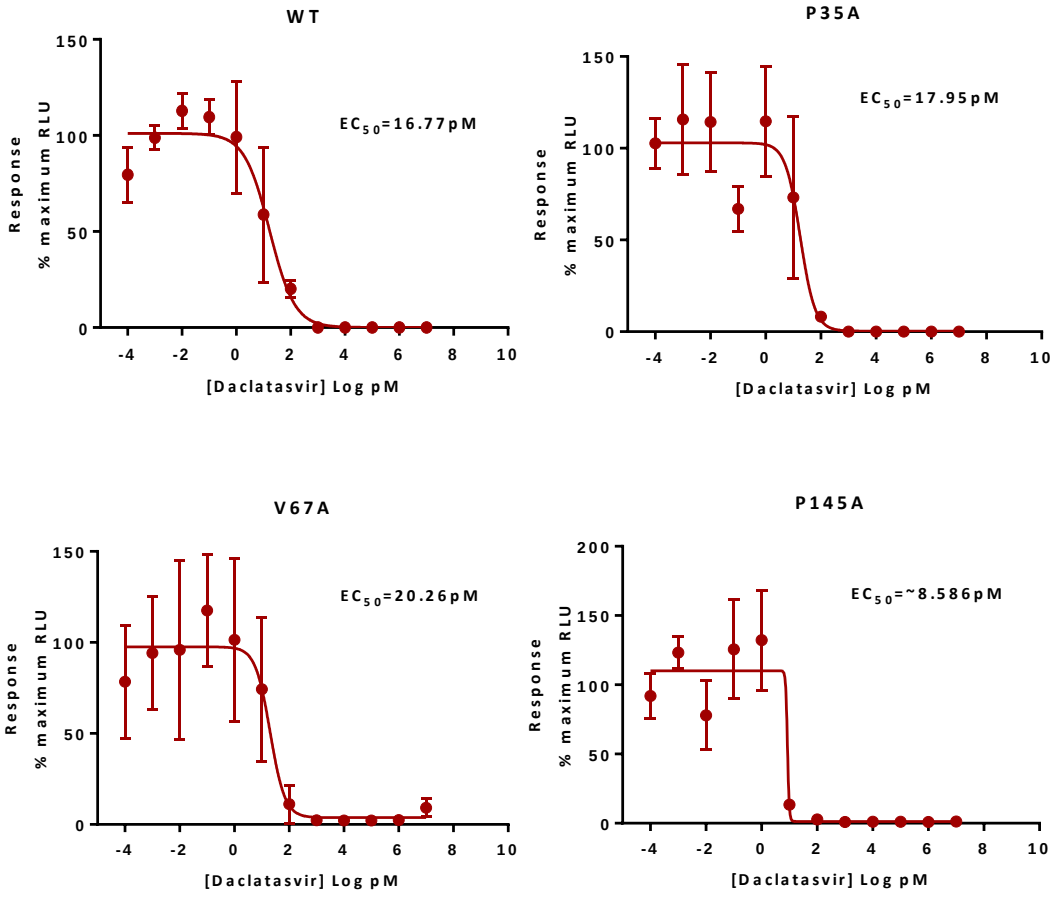

Figure 5.18 Sensitivity of domain I mutants to DCV treatment is not altered.

Huh7.5 cells were electroporated with the denoted mSGR-Luc-JFH1 WT and NS5A domain I mutants. Cells were treated with serial 10-fold dilutions of daclatasvir in 0.2% DMSO solutions 4 hpe. After treatment for 72 hrs, cells were harvested in PLB and then luciferase activity was determined. EC_{50} curves and EC_{50} of each replicon were calculated using Graphpad Prism7.

5.3 Discussion

5.3.1 Dimerization of domain I might be related to the virus assembly pathway

In this study, it was determined via SEC and SEC-MALLS that WT NS5A domain I can exist as a dimer *in vitro*. Consistently, SEC-MALLS analysis of the NS5A domain I (33-202) by Ascher also showed that domain I assembles almost exclusively as dimers in solution (Ascher et al., 2014). Considering the specificity of mutations in its structures, it is possible to suggest that dimerization of domain I might be affected by the mutants. To test this, I performed GST pull down assay by using GST tagged domain I as bait to prey His tagged domain I, and if His tagged domain I could be detected, this means that domain I can be dimerized. In two parallel GST pull down assay with His-Domain I (WT) or mutated His-Domain I (WT) as preys, P35A showed WT level of dimerization despite modest inhibition with His-P35A, which is expected as it is indistinguishable in both RNA replication and virus production. Additionally, V67A showed different phenotypes when incubated with His-Domain I (WT) and His-Domain I (V67A), and P145A cannot dimerize with or without His-Domain I (WT) (Table 5.2). For such differences, we should look back to the position of these three residues, both P35A and P145A are located at the interfaces of dimers but with different interaction faces.

For P35, it is on the head of domain monomer and dimerizes into 1ZH1 form by interaction with another non-P35 residue - A92 in the other monomer (Figure 5.11). When incubated with His-WT, A92 in GST-P35A could interact with P35 in His-WT domain I normally (Figure 5.12), but A92 showed modest reduction in interaction with A35 (P to A) from His-P35A (Figure 5.13). However, P145 residues from both monomers of the dimer face each other and both participate in the interface, which suggested that both P145 residues would be essential for interaction of monomers. Although His-WT was used as prey, P145 in His-WT and A145 in GST-P145A still can interact with each other, hence dimerization could not be compensated. That is why P145A still cannot dimerize in presence of wildtype domain I while P35A can dimerize. Whereas in terms of V67A, it is surface exposed on the head in all four domain I dimeric conformations and not involved in dimer interactions. The mechanism of how V67A takes part in dimerization needs to be further demonstrated and to be supported by the characterization in cell cultures. Additionally, the model of domain I for structural analysis and hypothesis is informed by the dimeric domain I structures from genotype 1 because the structure of domain I from JFH1 (genotype 2a) has not yet been determined. Despite that the phenotypes of NS5A mutants cannot directly be extrapolated to other genotypes, it is worthwhile to take them as the targets within other HCV genotype like genotype 3 for further research in the future.

	GST-WT	GST-P35A	GST-V67A	GST-P145A
His-WT	++			
His-P35A	++	+		
His-V67A	++		–	
His-P145A	–			–

Table 5.2 Summary of GST pull down assay.

'GST- 'represents GST tagged domain I, the bait of GST pull down; 'His-' represents His tagged domain I, the prey of GST pull down. '++' and '+' indicate the positive binding between GST tagged domain I and His tagged domain I, but '+' showed modest reduction in dimerization. '– ' means they could not dimerize.

Growing evidence suggested that dimerization of NS5A is related to RNA binding and replication (Tellinghuisen et al., 2004, Tellinghuisen et al., 2005, Lim et al., 2012), however it is interesting to speculate about the role of dimerization in virus assembly. Intriguingly, it was reported that a small-molecule inhibitor of NS5A relocalizes NS5A from the ER to LDs in cells expressing a genotype 1b replicon (Targett-Adams et al., 2011), suggesting that the interaction between NS5A and LDs may also be regulated by NS5A conformation. In Targett-Adams research, they suggested that binding of the inhibitor to NS5A serves to lock, or alter, the conformation of the protein, rendering NS5A incapable of replication complex (RC) incorporation, resulting in the redistribution to LD surface. This hypothesis suggested that the conformation of domain I is important in the incorporation of NS5A into RC and assembly sites. Nevertheless, replication of V67A and P145A retained at a high level with a modest reduction compared with WT but cannot produce virus. Therefore, I propose that disruption of dimerization for V67A and P145A does not affect the formation of RC (Figure 5.19A). Furthermore, I propose that the monomeric NS5A cannot be recruited to core associated LDs as the monomeric domain I is not able to fit the interface between core proteins, in comparison with well-structured dimeric NS5A (Figure 5.19B and C).

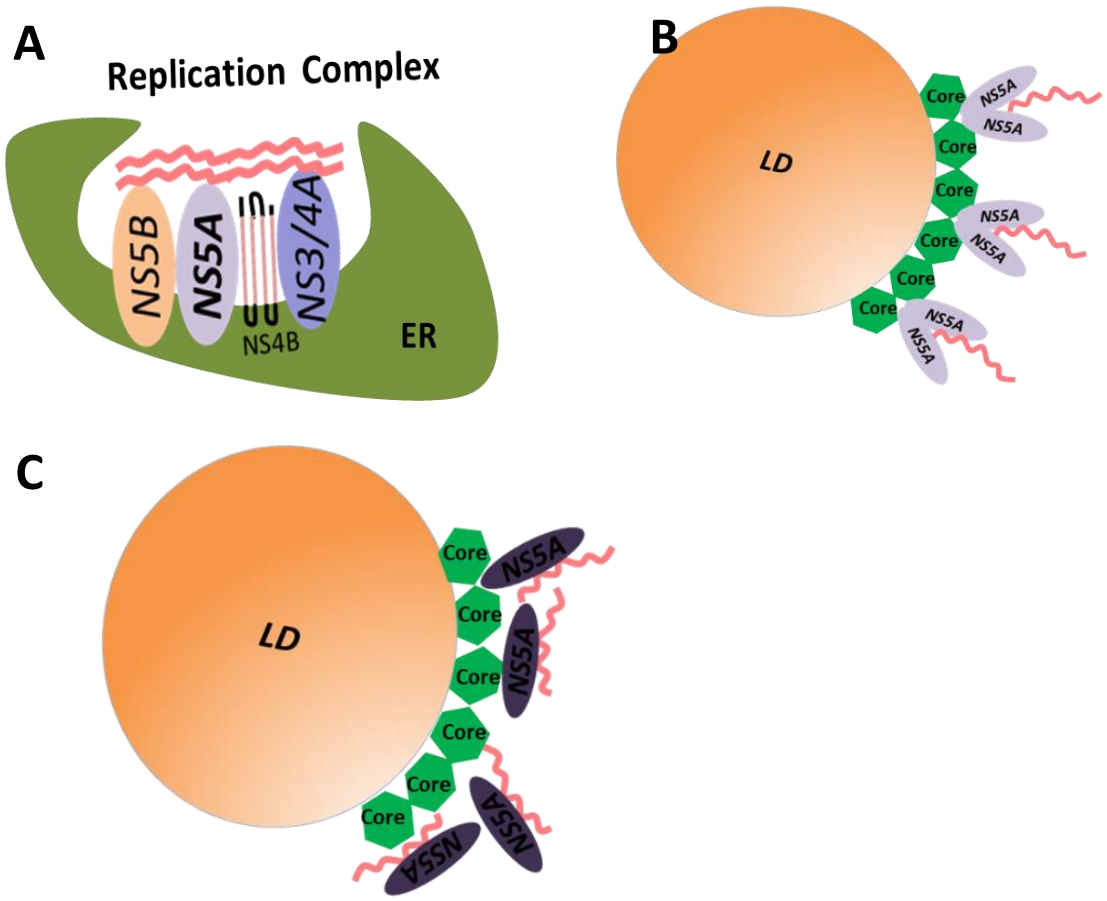

Figure 5.19 Model of NS5A in replication complex and assembly sites.

A. Formation of replicases including NS3 to NS5B of HCV together with genomic RNA in preformed RCs. **B.** Dimeric NS5A was recruited to core positive LDs –viral assembly sites. Well-structured dimer can interact with core protein and fit into the interfaces between core proteins. **C.** Monomeric NS5A randomly goes into LDs sites but cannot interact with core proteins.

5.3.2 RNA binding of domain I is key for NS5A shuttling from replication complex to virus assembly sites

As mentioned, there is a correlation between dimerization and RNA binding (Lim et al., 2012). V67A and P145A abrogating dimerization of NS5A are expected to further affect RNA binding activity, as NS5A has been demonstrated to bind the initiation site of negative-strand RNA synthesis, namely, the HCV genomic (positive-strand) 3' UTR (Foster et al., 2010). To address this, the binding affinity for HCV positive-strand 3' UTR RNA of domain I of either P35A, V67A and P145A or WT were assayed.

Unlike the abrogation of RNA binding seen in previous research for the NS5A mutants that did not dimerize (Lim et al., 2012), V67A and P145A exhibited an increased binding affinity to HCV 3'UTR. To some extent, this can make sense because V67A and P145A retained the ability to replicate which indicates that they should retain RNA binding activity. For the increased RNA affinity, it might be that the monomeric domain I without dimer interfaces has more surface exposed, which can allow more regions of domain I with affinity for RNA to bind more RNA. In other words, monomeric NS5A is much more flexible to interact with 3'UTR. To validate this in *vitro* data, NS5A was immunoprecipitated from Huh7.5 cells electroporated with either JFH1 WT or the three mutants and the amount of viral RNA in the immunoprecipitates was assessed by qRT-PCR. Consistent with the in vitro RNA filter binding assay data, both V67A and P145A bound more viral RNA compared to WT and P35A (Figure 5.17). In contrast, a similar analysis of core immunoprecipitates revealed significant reductions in the amount of genomic RNA bound to core or LDs for V67A and P145A (Figure 4.13).

Taken collectively, these data suggest that NS5A binds specifically to the nascent genomic RNA but that during the assembly process this must be released to core. By increasing the affinity of NS5A for the 3'UTR RNA, these mutations are preventing this transfer. These observations lead us to conclude a model in which domain I of NS5A binds to the 3'UTR of nascent genomes and transports them from sites of replication to LD. Here, analogous to the handing on of a baton in a relay race, the RNA is transferred to core and then subsequently transported to assembly sites. The latter remain to be unambiguously defined but may be endosomal membrane compartments (Mankouri et al., 2016, Lai et al., 2010). The enhanced binding of V67A or P145A to the 3'UTR RNA may prevent the release of RNA for transfer to core. The LD distribution in cells infected with V67A or P145A at 72 hpe resembles that in wildtype at 12/24 hpe (Figure 4.7), suggesting that these mutations might block the transition from genome replication to virus assembly. Furthermore, the loss of dimerization by these two mutants implies that, in contrast to the accepted model of an open NS5A dimer revealing a basic RNA-binding groove, monomeric NS5A is able to bind RNA. It tempts me to speculate that monomeric NS5A might transport nascent RNA to LDs, then dimerizes and releases the RNA to core.

For the assembly of HCV particles, it is well accepted that lipid droplets are the important organelles. Firstly following synthesis on the ER, the core protein homodimerizes and is trafficked to cytosolic lipid droplets (LDs). After then, NS5A bound with genomic RNA will be recruited to core positive areas via interaction between NS5A and core protein (Figure 5.20)

(Lindenbach and Rice, 2013, Miyanari et al., 2007). Previously it was believed that determinants of NS5A for virus assembly are in its C-terminal unfolded domain (Appel et al., 2008, Kim et al., 2011, Tellinghuisen et al., 2008a). Nevertheless, here it is pointed out that the N-terminal domain of NS5A -domain I - is also involved in viral assembly, which might be related to its dimeric structures and RNA binding activity for the first time.

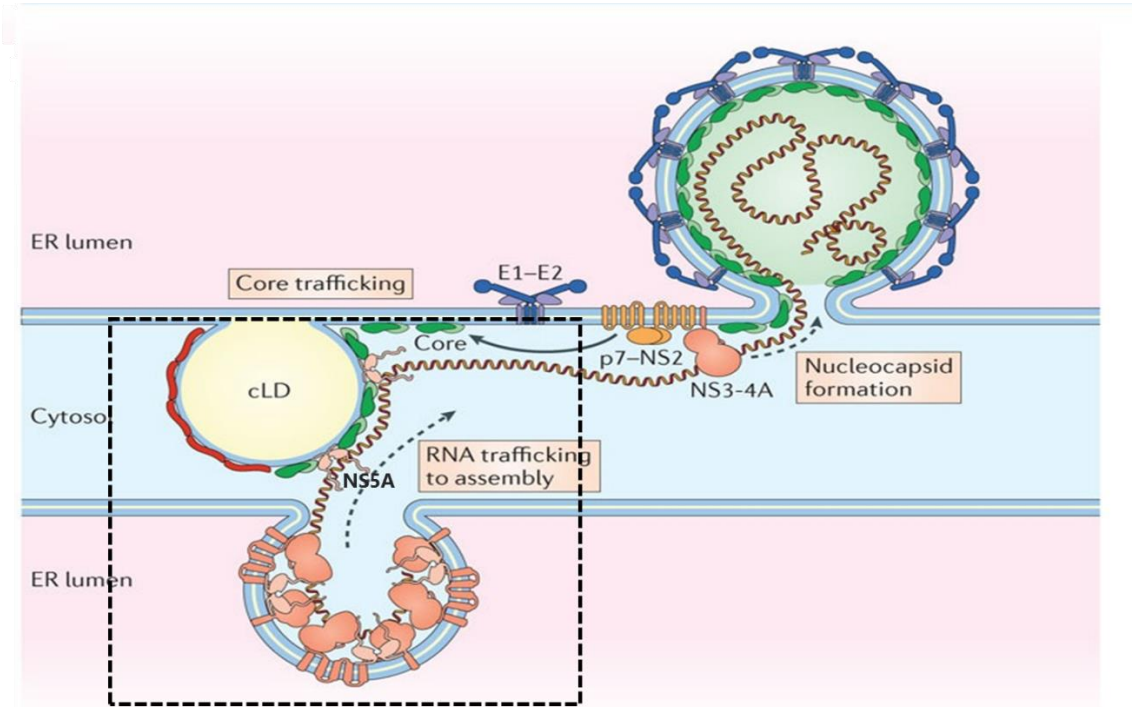

Figure 5.20 Model of NS5A in HCV assembly pathway.

Post trafficking of core dimers to cytosolic lipid droplets (cLDs). NS5A and viral RNA is shifted out of replication and translation, and towards virus assembly. The interaction of p7–NS2 (Jirasko et al., 2010, Popescu et al., 2011, Jones et al., 2007a, Gentzsch et al., 2013) with NS3‑4A (Phan et al., 2011, Ma et al., 2008) recruits viral core protein to the site of virus assembly (Lindenbach and Rice, 2013). Picture is adapted from (Lindenbach and Rice, 2013).

5.3.3 Involvement of domain I in daclatasvir induced inhibition of HCV assembly

Although it is known that daclatasvir (DCV) specifically targets NS5A, particularly its domain I, the mechanism of DCV's action is unclear. Initially chemical genetics strategy has identified that action of inhibition of DCV is the suppression of virus replication via the inhibition of the formation of double-membrane vesicles (DMVs) (Gao et al., 2010, Berger et al., 2014). Following that, a novel insight into its mechanism was proposed that DCV could rapidly inhibit intracellular assembly of HCV virions by blocking transfer of the viral genome to assembly sites (McGivern et al., 2014, Boson et al., 2017). From the perspective of DCV, the block of virus

assembly is correlational with domain I dimeric structures and RNA binding. DCV has been reported to target domain I, as judged by the location of DCV-resistance mutations (e.g. L31M and Y93H). Firstly, the structure of DCV is symmetrical and has the greatest chemical complementarity when docked across the dimer interface of domain I between and under the 28-35 loops to change the conformation of dimer and disrupt the natural packing of the NS5A N termini (Sun et al., 2015). Secondly, the binding of DCV to NS5A domain I inhibits RNA binding of NS5A domain I (Ascher et al., 2014). In combination of these observations, the mechanism of NS5A inhibitors in interrupting HCV assembly pathways can be shared with why V67A and P145A abrogate virus assembly.

In this point, I suspect that binding of DCV of NS5A and mutations of NS5A domain I exhibit the same effect on function of NS5A-blocking assembly of virions. Hence, it is necessary to confirm the sensitivity of V67A and P145A to DCV to check whether V67 or P145 is also involved in the binding of DCV to NS5A so that mutation of these residues result in the defect of HCV assembly. If residues V67 and P145 is involved in the action of DCV to HCV, mutation of them might enable V67A and P145A resistant with DCV. Previous modelling viral kinetics of the therapeutic response to DCV revealed a dual mode of action involving both suppression of viral RNA synthesis (RNA replication) and inhibition of viral assembly (Guedj et al., 2013). Measurement of HCV genome replication post treatment with DCV showed that V67A and P145A exhibited wild type level of DCV sensitivity, which suggested that V67A and P145A did not affect DCV's inhibition of RNA replication. It is hard to confirm whether V67A and P145A are further involved in the effect of DCV on virus assembly as V67A and P145A have already been shown to be deficient in virus assembly.

Chapter 6: Proteomic analysis of NS5A binding partners

6.1 Introduction

It is well accepted that the roles of NS5A in the virus life cycle are dependent on the interaction with other viral and cellular proteins. Firstly, the precise role of NS5A in genome replication remains obscure, despite NS5A mediating binding to viral RNA, other NS proteins and interactions with various cellular factors, including vesicle-associated membrane protein-associated proteins A and B (VAP-A, VAP-B), cyclophilin A (CypA) and phosphatidylinositol-4-kinase IIIα (PI4KIIIα), which are required for HCV replication (Evans et al., 2004, Gao et al., 2004, Goonawardane et al., 2017, Ngure et al., 2016, Berger et al., 2009, Hamamoto et al., 2005). Secondly, Apolipoprotein E (ApoE), diacylglycerol acyltransferase-1 (DGAT-1), Annexin A2, cell-death-inducing DFFA-like effector B (CIDEB) and Rab18 in host cells can interact with NS5A to promote assembly of HCV particles. Of the proteins that NS5A interacts with, most involve NS5A domain III or unclear (Section 1.3.3). To further identify protein-protein interactions, I will firstly check the known NS5A-cellular protein interactions through Strep-tagged NS5A pull down assay or proximity ligation assay (PLA).

The introduction of the isotope-coded affinity tag (ICAT) was one of the milestones to isotopic chemical labelling for relative quantification of peptides/proteins with mass spectrometry (MS). Tandem Mass Tagging (TMT) is a quantitative proteomic approach, which allows the comparison of protein levels in up to 10 different samples in a single experiment. With this approach, it is possible to identify and quantitate thousands of proteins in a single experiment. Samples for TMT analysis are labelled, fractionated and analysed by Nano-LC MS. Protein quantitation is based on the median values of multiple peptides identified from the same protein, resulting in highly accurate protein quantitation between samples. Measuring protein changes between mutants with significantly different phenotypes and wildtype is one of the important tasks of proteomics.

To understand the molecular mechanism underpinning the phenotype of the mutants of domain I, it can be explained by the roles of domain I in regulating interactions between NS5A and cellular proteins. To address this, affinity purification of One-Strep-tagged NS5A was used in conjunction with TMT quantitative proteomics analysis to compare the interactome of wild type and mutants of domain I after pull down assays from virus transfected cells by nano-LC mass spectrometry and quantitative proteomic analysis. The abundance ratio of the peptide for each samples were taken as the parameters for comparing with untagged WT and Strep-tagged WT as negative and positive controls. After quantification, proteins reduced in abundance by between 2- and 100-fold were further investigated in the protein network.

6.2 Results

6.2.1 Purification of One-strep tagged (OST) NS5A from virus transfected cells

NS5A is known to be involved in numerous interactions with host proteins and pathways. As I have revealed that mutations (V67A and P145A) in domain I of NS5A disrupted virus assembly and caused disruption of dimerization of domain I. These changes of phenotypes are likely involved with changes of certain interaction of proteins. To address this gap in our understanding, I took advantage of the fact that domain III of NS5A is able to tolerate in-frame insertions with no effect on the functions of protein in virus RNA replication or assembly. Specifically, JFH1 full-length virus construct -mJFH1 (NS5A-OST) was utilized, in which NS5A C-terminal was tagged with the One-Strep affinity tag (OST). Insertion of this short tag was shown not to affect virus replication (Figure 6.1A) and to provide a highly efficient purification strategy (Amako et al., 2009, Ross-Thriepland and Harris, 2014b).

Purification of OST-NS5A was performed using strep tag resins (Strep-Tactin® Sepharose®) from cytoplasmic lysates harvested at 72 hpe. Purification of OST-NS5A from JFH1-OST (WT) cell lysates was initially followed the Strep tag purification protocol (IBA Lifesciences) and improved for other virus samples (Figure 6.1B). After enough washes, protein bound resins were analysed by western blot using anti-NS5A antibody (Figure 6.1C) and stored at -80 °C for further analysis.

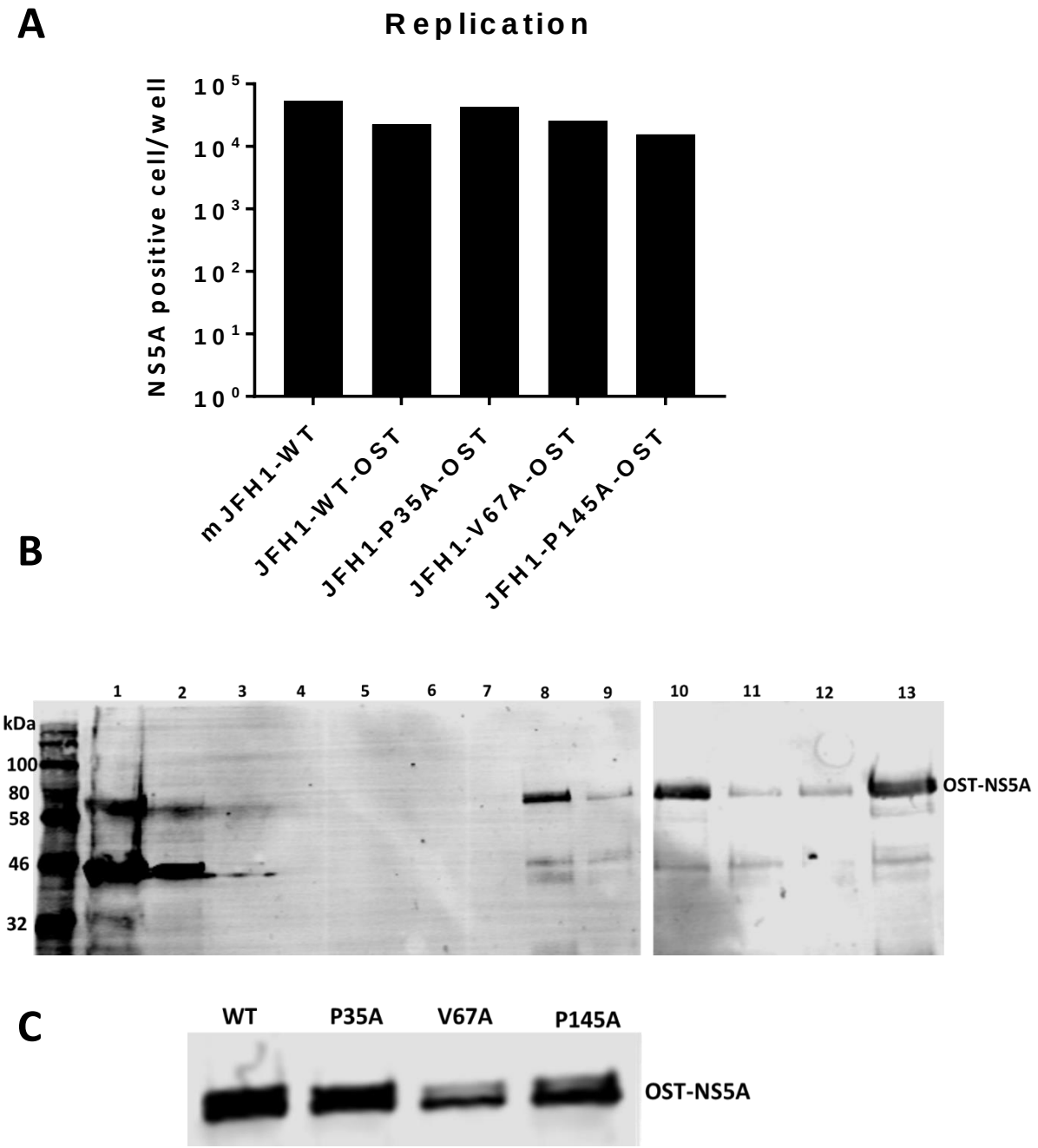

Figure 6.1 Purification of Strep Tagged NS5A (OST-NS5A).

A. Both untagged JFH1 (WT) and OST tagged viruses with corresponding mutations were electroporated into Huh7.5 cells and fixed 48 hpe for IncuCyte ZOOM. Replication of OST tagged JFH1 viruses were determined by counting NS5A positive cells**. B.** 72 hpe, supernatants of JFH1-OST (WT) cell lysates were harvested in GLB and incubated with Strep tag purification resins, washed 5 times using wash buffer and then eluted by wash buffer supplemented with 2.5 mM desthiobiotin. Fractions collected from each step were analysed by western blot using anti-NS5A antibody**.** Lane 1: Input of cell lysates; Lane 2: flow through after incubation with Strep tag purification resins; Lane 3-7: Wash fractions of resins; Lane 8-12: Elution fractions from resins; Lane 13: Resins after wash and before elution. **C.** Strep tag resins after purification of each OST-JFH1 virus were analysed by western blot.

6.2.2 V67 and P145 are not involved in interaction between NS5A and DGAT1, Rab18 and ApoE

In regards to virus assembly and NS5A protein, Diacylglycerol acyltransferase-1 (DGAT1) is one of the targets worthy of investigation. During virus assembly, it was shown that the trafficking of NS5A to LDs depends on catalytical activity of DGAT1 (Camus et al., 2013) . DGAT1 could form a complex with NS5A and core and facilitates the interaction between both viral proteins. Our previous results exhibited that NS5A of V67A and P145A failed to interact with core protein and be recruited to LDs. Then I analysed the pooled NS5A protein complexes bound to Strep tag beads by western blot using both anti-NS5A and anti-DGAT1 antibodies to check whether NS5A of V67A and P145A could co-precipitate with DGAT1. Compared to untagged WT and tagged WT, all the mutants (P35A, V67A and P145A) still kept interaction with DGAT1 (Figure 6.2A, upper panel), whereas P35A exhibited a lower interaction level.

The other target is Rab18, which is also known to associate with LDs and promote physical interaction between LDs and ER membranes through a direct association between NS5A and the active, GTP-bound form of Rab18. Rab-18 promoted interaction between HCV membranous webs and LDs might enhance virion assembly by bringing sites of replication in close physical proximity to sites of virion assembly. In this case, here we also verified that it is not this pathway that V67A and P145A disrupted as both mutants showed WT level of interaction with Rab18 by check the NS5A co-precipitates (Figure 6.2A, lower panel).

Very-low-density lipoprotein (VLDL) pathway has been shown to play a role in the assembly and maturation of infectious virus particles (Huang et al., 2007a, Gastaminza et al., 2008). Apolipoprotein B (ApoB), Apolipoprotein E (ApoE) and microsomal triglyceride transfer protein are required for the assembly of VLDV assembly (Huang et al., 2007a, Jiang and Luo, 2009). In this pathway, apoE can be recruitment by NS5A for the assembly and release of infectious viral particles. It was previously reported that mutants of NS5A domain I at 99-101 and 102-104 disrupted the ApoE-NS5A interaction and showed a defect in viral assembly (Benga et al., 2010a). Hence, PLA assay was conducted to check whether V67A and P145A of domain I failed to interact with ApoE. Here we can clearly notice that domain I mutants (P35A, V67A and P145A) and mJFH1 (WT) are indistinguishable in the level of interaction between ApoE and NS5A (Figure 6.2B).

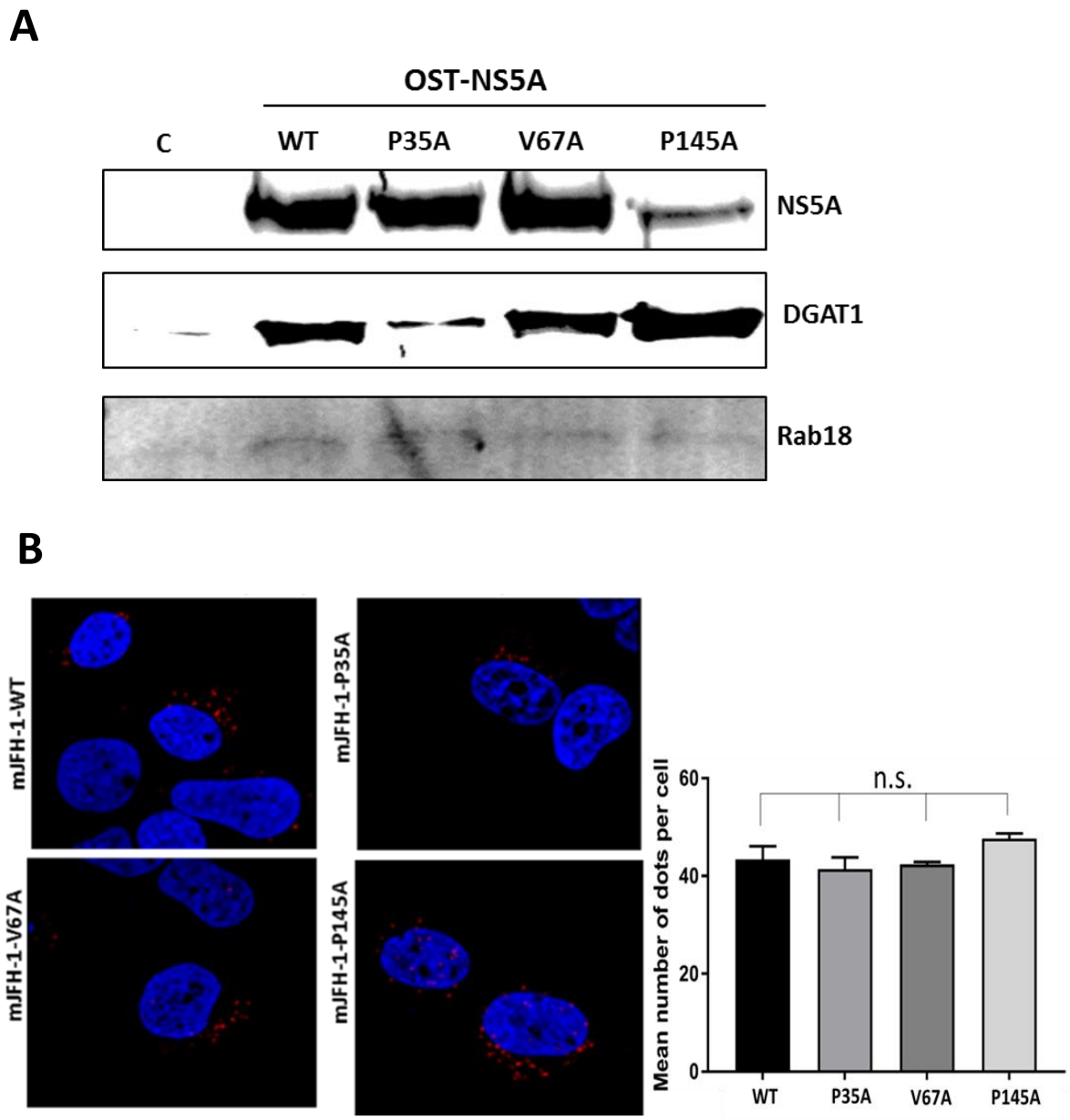

Figure 6.2 V67A and P145A exhibited WT level of interaction with DGAT1, Rab18 and ApoE.

A. JFH1-OST RNA constructs were electroporated into Huh7.5s. Cell lysates were harvested 72 hpe and Strep tagged HCV NS5A from Huh7.5 cells was purified by using Strep tag pull down assay. Co-precipitated DGAT1 or Rab18 with NS5A were detected by western blot with respective antibodies**.** C is the JFH1 negative control without OST. **B.** Interaction of NS5A and ApoE in Huh7.5 cells studies with proximity ligation assay (PLA). Post electroporation of mJFH1 transcripts of either mutants or WT, cells were seeded onto coverslips and incubated for 72h prior to fixation, immunostaining for NS5A (mouse monoclonal antibody) and endogenous ApoE (Rabbit polyclonal antibody), followed by PLA probes minus and plus, ligation and rolling-circle amplification (RCA). The hybridization probes were labelled with Alexa 555 (red), and the nuclei were counterstained with DAPI (blue). Scale bar represents 20µm. For each experiment, the PLA signals (counts per well) of each sample were counted using Imaris, from a minimum of 20 cells.

After pull down from each mutant virus transfected cells using Strep-Tactin® resin, strep tagged NS5A (OST-NS5A) bound with the Strep-Tactin® resin was then send for tandem mass tagged (TMT) mass spectrometry (TMT-MS) (University of Bristol) to analyse NS5A interacting partners. And the untagged JFH1-WT incubated resin was taken as the negative control. Here the TMT-MS result was consistent with what we observed above (Table 6.1), NS5A from either WT or mutants retained the interaction with DGAT1, Rab18 and ApoE. Intriguingly, P35A showed a reduction in the interaction with DGAT1, Rab18 and ApoE compared with V67A and P145A.

Description	Abundance Ratio			
	OST-WT:WT	OST-P35A:OST-WT	OST-V67A:OST-WT	OST-P145A:OST-WT
DGAT1	2.70	0.52	1.26	1.81
ApoE	3.05	0.53	1.02	1.99
Rab18	3.07	0.53	1.24	2.67

Table 6.1 Characterization of interacting partners (DGAT1, ApoE and Rab18) of NS5A from tandem mass tagged (TMT) mass spectrometry (TMT-MS) (University of Bristol).

Abundance ratio is the ratio of protein abundance between Strep tagged JFH1-WT (OST-WT) pull down to the untagged JFH1-1 (WT) beads control, or the ratio of abundance of Strep tagged JFH1 mutants (OST-P35A, OST-V67A and OST-P145A) to JFH1-WT (OST-WT). An abundance ratio of OST-WT: WT ≥1.5 were considered to have been specifically pulled down by NS5A.

6.2.3 Potential mechanism of NS5A domain I involved

To identify cellular candidates that are potentially involved in the P35A, V67A and P145A phenotypes, bound fractions following affinity purification from cytoplasmic lysates of Strep-tagged wildtype (OST-WT), P35A (OST-P35A), and V67A (OST-V67A) and P145A (OST-P145A) NS5A together with untagged wildtype were analysed by mass spectrometry. A great number of known NS5A interacting proteins were identified by this approach. These proteins had at least two high confidence peptide matches per protein ($p < 0.05$). After a series of comparisons of abundance of interacting partners between WT and mutants or negative control (Untagged JFH1) (Figure 6.3), interaction networks that NS5A domain I mutant is involved in was determined.

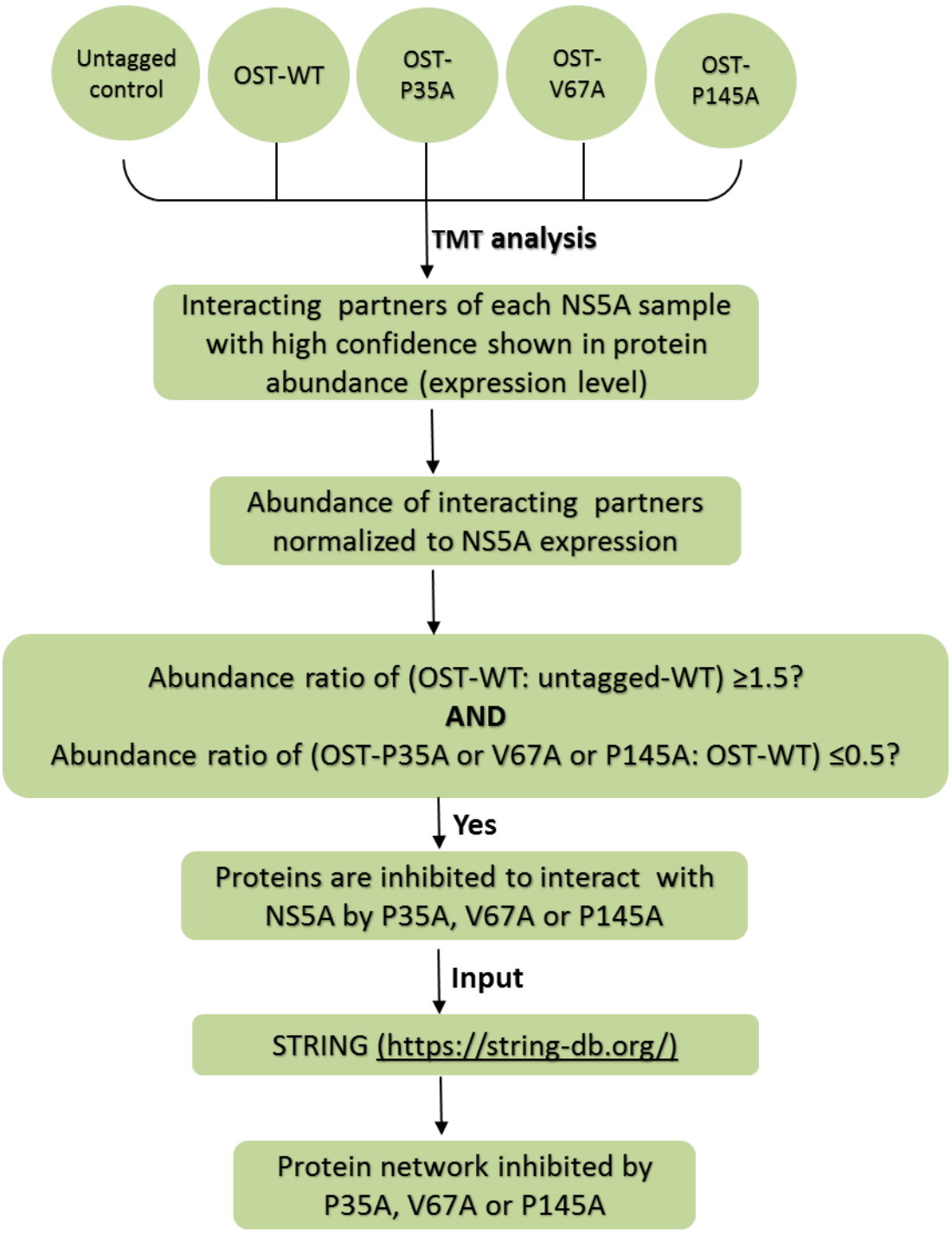

Figure 6.3 Flow chart of comparative analysis of NS5A-interacting proteins involved by domain I mutants (P35A, V67A and P145A).

6.2.3.1 NS5A-interacting proteins potentially abrogated by P35A

As described in the previous chapters, P35A is partially involved in RNA replication (Figure 3.2), and showed modest reduction in virus production compared with wildtype (Figure 4.2, 4.3A and 4.5), which was most likely due to the reduction in RNA replication.

After proteomic analysis and comparison of the protein expression levels between wildtype and P35A, two big groups of host proteins were identified. The first one is the GTPase associated proteins including Rab GTPase family (Rab1b, Rab8b and Rab34), Ras-related proteins (Rap1A, Rap1B and RalA), Rho family of GTPases (Rac1), and GTP-binding protein (GTPBP4), which are all involved in the GTPase activating and downstream signalling pathways (Bourne et al., 1990). GTPase acts as a molecular switch whose 'on' and 'off' states are triggered by binding and hydrolysis of GTP, playing important roles in signal transduction, protein translation, cell division and transport of vesicles (Scheffzek and Ahmadian, 2005, Hippenstiel et al., 2002).

The other group of proteins inhibited by P35A are mostly apolipoproteins (ApoA1, ApoC1, ApoC3 and ApoE) and DGAT1, which both participate in lipid metabolism (Figure 6.4 and Table 6.1), which were supported by the immunochemistry analyses in the OST-NS5A pull down and PLA assays for interaction between NS5A and DGAT1 and ApoE (Figure 6.2). According to the density gradient analysis of P35A virus (Figure 4.5), the fraction with higher density (≥1.1005) contains more virus particles but with less infectivity. As previously reported that JFH1AAA99 of NS5A domain I could only release non-infectious viral particles because of the abrogation of interaction of ApoE (Miyanari et al., 2007). Combination of this result, the decreased level of both ApoE and DGAT1 indicated that synthesis of LDs is critical for producing infectious viruses, whereas production of non-infectious viruses seems to follow a different pathway. Both P35A and JFH1AAA99 are likely to be at the determinant region of interaction between NS5A domain I and ApoE (Benga et al., 2010, Shavinskaya et al., 2007).

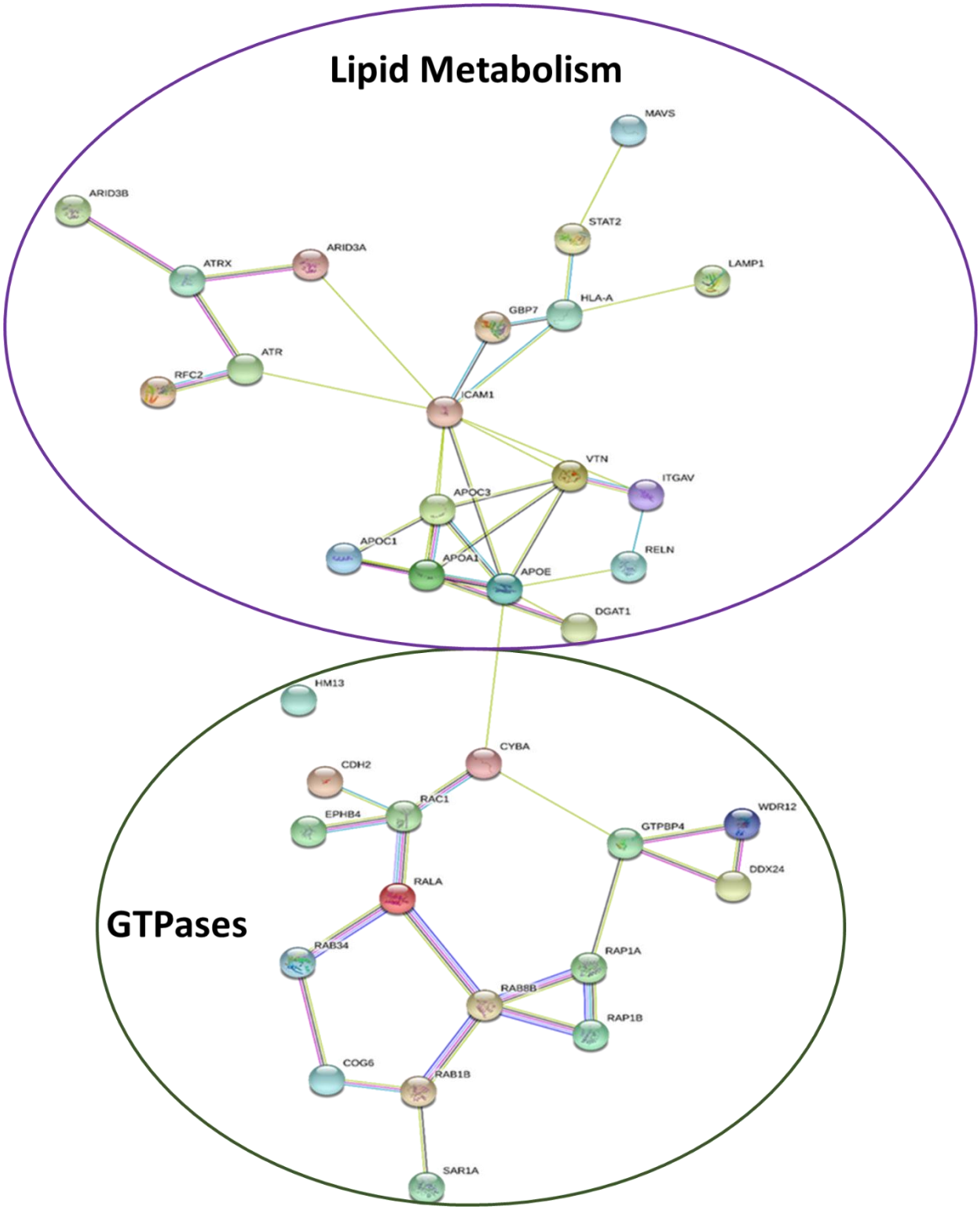

Figure 6.4 NS5A interacting protein network inhibited by P35A.

Network illustration of the interactions analysed via STRING (https://string-db.org/) by input the proteins showed more than 2 -fold reduction in abundance ratio between P35A and WT. Two main groups of host proteins were identified as Lipid Metabolism and GTPases.

6.2.3.2 NS5A-interacting proteins potentially abrogated by V67A

Post proteomic analysis of V67A, a large number of 40S ribosomal subunit were identified at lower interaction level including RPS 3, 5,10, 19, and 24, together with one 28S ribosomal protein MRPS12 and eukaryotic translation initiation factor 2 subunit 3 (eIF2S3) (Figure 6.5), which are known to be tightly bound by the HCV IRES to facilitate initiation of translation of HCV polyproteins (Lytle et al., 2002, Fukushi et al., 2001, Otto and Puglisi, 2004). Additionally, a Tyrosyl-tRNA synthetase (YARS) and Histidyl-tRNA synthetase (HARS) catalyse the aminoacylation of transfer RNA (tRNA) by their cognate amino acid and plays an important role in RNA translation.

Nucleosome assembly protein 1-like proteins 1 and 4 (NAP1L1 and NAP1L4) identified at the downstream of the ribosomal protein pathway (Figure 6.5), are thought to act as histone chaperones, shuttling both nuclear core and linker histones from their site of synthesis in the cytoplasm to the nucleus (Rodriguez et al., 1997).

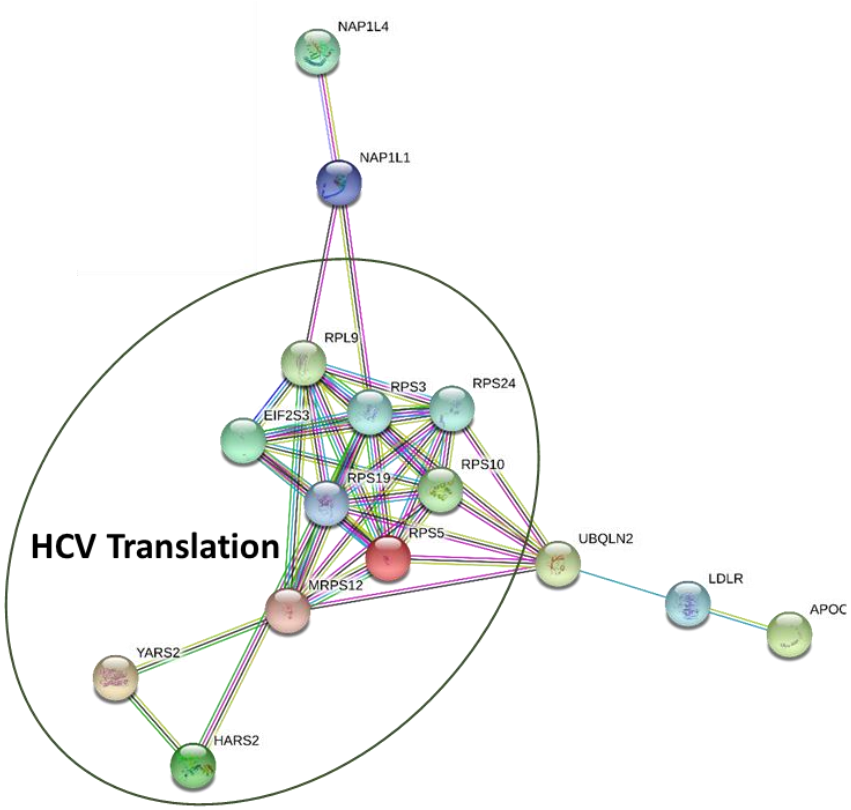

Figure 6.5 NS5A interacting protein network inhibited by V67A.

Network illustration of the interactions analysed via STRING (https://string-db.org/) by input the proteins showed more than 2 -fold reduction in abundance ratio between V67A and WT. A big group of host proteins related to HCV translation were identified. NAP1L1 and NAP1L4 are nucleosome assembly protein 1-like proteins 1 and 4.

6.2.3.3 NS5A-interacting proteins potentially abrogated by P145A

Similar with V67A, P145A exhibited an series of reductions in interaction with ribosomal proteins (RPS 20, RPL 18, RPL 38, MRPL 4, MRPS 7, MRPS 27 and MRPS34) (Figure 6.6), whose functions are unknown in HCV life cycle.

Sec61B belonging to Sec61 complex is the central component of the protein translocation apparatus of the endoplasmic reticulum (ER) membrane, trafficking proteins from ER to the nucleus and gene expression (Liao and Carpenter, 2007, Knight and High, 1998). SSR4, also called translocon-associated protein subunit delta (TRAPD), is another protein for translocation, which has ever been identified by proteomics analysis of crude replication complexes (MacPherson et al., 2011). The translocon is involved in protein translocation across the ER membrane and is formed by the association of the Sec61p complex, the translocation associated membrane protein (TRAM) and the translocon-associated protein (TRAP) complexes (Losfeld et al., 2014). Hence, direct or indirect Interaction between NS5A with Sec61B or SSR4 may regulate the genome replication and translation of viral proteins by association with the HCV replication complex (Figure 6.6).

Sterol O-acyltransferase 1 (SOAT1), also called acyl-CoA: cholesterol acyltransferase 1 (ACAT1), is the enzyme responsible for cholesterol esterification, which also identified in the disrupted interaction network of P145A (Figure 6.6). As important organelles for HCV assembly, LDs core is primarily composed of triglycerides (TAGs), cholesterol esters (CEs), together with diacylglycerides (DAGs) (Fujimoto and Parton, 2011). Based on the phenotype of P145A in disruption of LDs formation (Figure 4.8 and 4.9), the impaired interaction between NS5A and SOAT1 is an interesting candidate to define the phenotype of this mutant in viral assembly.

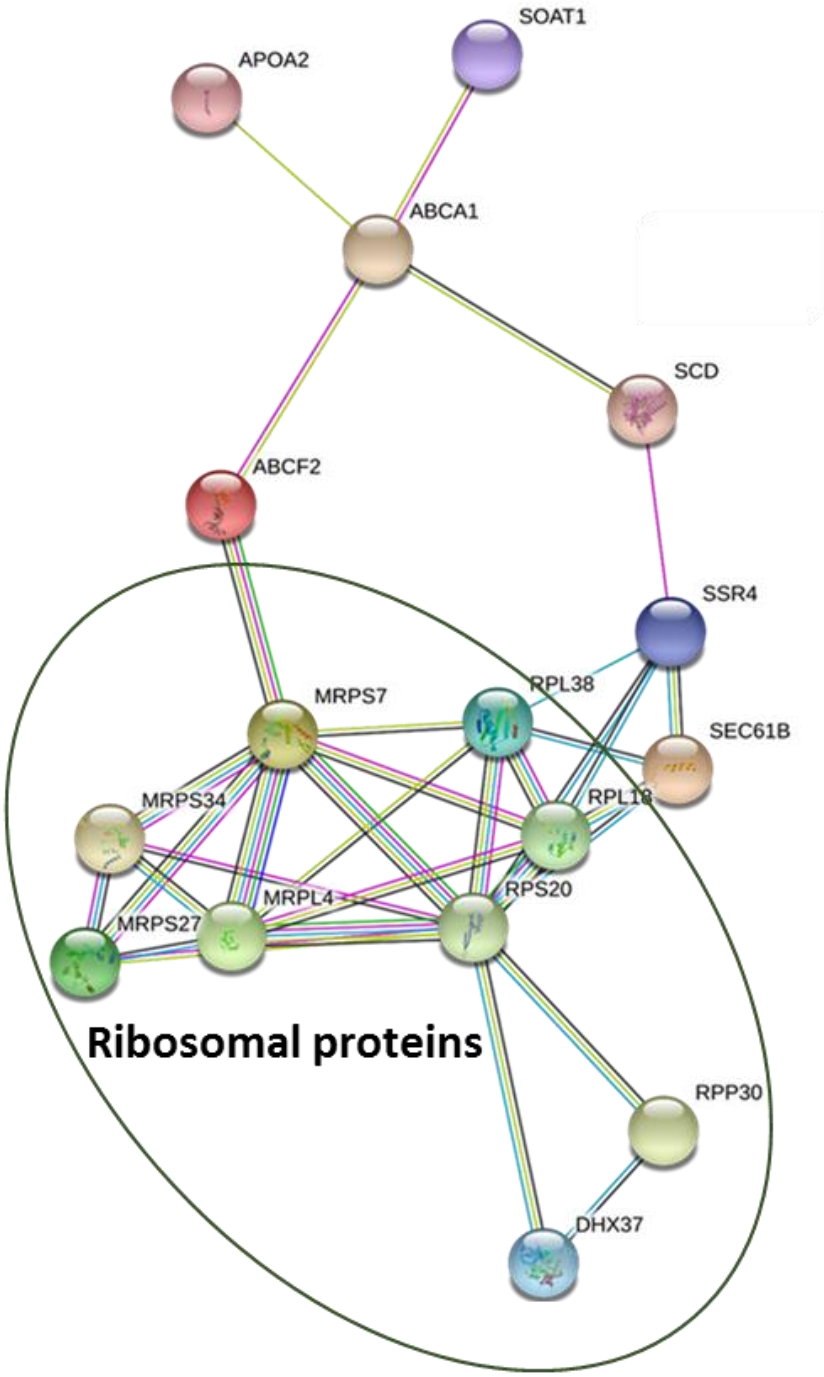

Figure 6.6 NS5A interacting protein network inhibited by P145A.

Network illustration of the interactions analysed via STRING (https://string-db.org/) by input the proteins showed more than 2 -fold reduction in abundance ratio between P145A and WT. A major group of host proteins mainly including ribosomal proteins was identified. SOAT1: Sterol O-acyltransferase 1.

6.3 Discussion

6.3.1 Characterization of interaction of NS5A and known host proteins in virus assembly and lipid metabolism pathways

It is well known that a common condition in HCV-infected individuals is steatosis, characterized by an accumulation of LDs. The mechanisms underlying development of steatosis include direct effects of the virus on lipid metabolism. LDs play a central role in generation of infectious virions as the target of viral proteins (Filipe and McLauchlan, 2015). It has been demonstrated that mutations in domain I impaired the interaction between NS5A and core- associated LDs resulting in size reduction of LDs. In addition, the disrupted mechanisms of virus assembly were defined to the lipid metabolism pathways. Whether the increase in LD size is a direct consequence of recruitment of NS5A, or indirectly driven by NS5A-mediated effects on lipid metabolism, remains unclear. Nevertheless, both the recruitment of NS5A to LDs and the biogenesis of LDs should depend on protein - protein interactions to achieve virus assembly.

Considering the recruitment of NS5A to LDs and lipid metabolism, DGAT-1 could be the foremost target as both core and NS5A were previously shown to be trafficked to LDs by DGAT1, functioning as a molecular bridge between the two proteins to ensure that they are targeted to the same LD (Herker et al., 2010, Camus et al., 2013). Moreover, synthesis of triglycerides stored in LDs also require DGAT enzymes (Herker et al., 2010). The second factor identified with a role in LD targeting of NS5A is Ras-related protein 18 (Rab18), which can promote the physical association of NS5A and other components of the viral replicase machinery with LDs (Salloum et al., 2013). HCV particle production is tightly linked to apolipoproteins E (ApoE), ApoA1, ApoC1, and ApoB (Bartenschlager et al., 2011). ApoE exhibited an interaction with NS5A and viral envelope glycoprotein to facilitate assembly of viral particles. Following that, mature HCV particles containing ApoB, ApoE and eventually other apolipoproteins are then transported along the VLDL secretory pathway (Olofsson et al., 2009). However, the phenotype of V67A or P145A cannot be explained by a lack of binding to these proteins, both DGAT-1 and (to a lesser extent) Rab18 precipitated with both WT and the three mutant NS5As, difference in interaction with ApoE also was not detected for both V67A and P145A. To extend this analysis, a proteomic approach was used to determine the interactome of the three mutant NS5As in comparison to WT.

6.3.2 Proteomic analysis of NS5A interacting partners

Utilising Strep-tagged NS5A based pull down assay and Tandem Mass Tagging quantitative proteomic, thousands of host proteins in various cellular pathways have been identified. To characterize the mechanism of NS5A mutants affected in RNA replication or even virus assembly, peptide binding abundance of the mutated NS5A that was dramatically decreased was filtered into the protein network.

P35 that are assumed only involved in RNA replication seems participate in more pathways. It is noteworthy that P35A slightly impairs the interaction with ApoE and DGAT1, which can explain the reduction in infectious particles release by P35A. In general, most released HCV virus particles are infectious with low density via the LD assembly pathway requiring ApoE and DGAT1 (Miyanari et al., 2007). Compared to WT, a large proportion of P35A particles purified in the higher density fraction with low infectivity might assemble into viral particles via another pathway other than LD associated virus assembly. Beyond that, it was revealed that P35A was also involved in Rab protein signalling via cascade activation of a series of GTPase-activating proteins. The Rab family is part of the Ras superfamily of small GTPases. Rab GTPases recruit specific sets of effector proteins onto membranes via bound to GTP (Stenmark and Olkkonen, 2001). It has been reported that Rab1 regulates ER-Golgi traffic and several Rabs including Rab8 modulate biosynthetic traffic from the trans-Golgi network (TGN) to the plasma membrane (Hutagalung and Novick, 2011). In HCV life cycle, Rab1 GTPase activity can be activated through interaction between TBC1D20 and Rab1. Furthermore, the Rab1 GTPase-activating protein-TBC1D20 interacts with HCV NS5A, which is a prerequisite for LD homeostasis as well as for maintenance of viral replication complexes (Nevo-Yassaf et al., 2012, Sklan et al., 2007a). Combined with the function of other GTPases, it suggests that the impairment of replication for P35A might be due to the inhibition of GTPase activity.

My study showed that both V67A and P145A inhibited the translation of proteins through abrogation of interaction with a series of ribosome proteins. There is only one study describing that HCV NS5A protein downregulates HCV IRES-dependent translation, whereas the molecular basis of the inhibitory effect of NS5A on HCV IRES has not been elucidated (Kalliampakou et al., 2005). It is still unclear what is the relationship between weak interaction with these translation factor and defects in RNA replication or viral assembly for V67A and P145.

The suppressed RNA replication of V67A might involve the nucleosome assembly pathway. NAP1L1 has been shown to interact with HCV core and NS5A (Germain et al., 2014, Pichlmair et al., 2012) as well as Kaposi's sarcoma herpesvirus (KSHV) LANA and HIV-1 Tat (De Marco et al., 2010, Gupta et al., 2016). Although its roles in the nucleus associated with chromatin structure and gene expression are well defined, NAP1L1 and NAP1L4 are predominantly located in the cytoplasm, where its function(s) remains to be elucidated. Recently, Goonawardane *et al* reported that NAP1L1 could regulate genome replication of HCV via interaction with hyperphosphorylated NS5A (Goonawardane et al., 2017). Here domain I of NS5A is also likely to be involved in RNA replication through interaction with NAP1L1 or NAP1L4, which remains to be elucidated.

Of note, the interruption of the interaction between NS5A and acyl-CoA: cholesterol acyltransferase 1 (ACAT1 or SOAT1) can explain why the LDs in P145A transfected cells were smaller. Acyl-CoA: cholesterol acyltransferase is the important component in the synthesis of LDs through catalysing cholesterol into cholesterol esters. Although how LDs contribute to virion production has not been clearly elucidated, I showed evidence for the participation of LDs in HCV assembly. SiRNAs or inhibitors that target host factors involved in LD biogenesis including DGAT1, ApoE, ApoB and ACAT can effectively inhibit infectious HCV production (Barter and Rye, 2016, Hu et al., 2017, Liefhebber et al., 2014). Hence, the impairment of the interaction with ACAT1 disrupted the functional LDs metabolism furthermore P145A failed to assemble into viral particles, whereas remains to be demonstrated.

To summarize, my data provides a comprehensive identification of the HCV NS5A proteome, and insight into the change in proteome between HCV wildtype and domain I mutants, which will serve as useful resources. These identified NS5A interacting partners disrupted by domain I mutations, such as ApoE and SOAT1, are of important value to be investigated in future research.

Chapter 7: Conclusion and future perspectives

NS5A as an important target of direct acting antivirals (DAAs) plays essential roles throughout the HCV lifecycle, which demands for extensive research in order to find more effective DAAs targeting vital sites or regions in NS5A. In this context, domain I of NS5A is both dimeric and highly conserved, providing more possibilities than the unstructured domains II and III.

Previous efforts to investigate functions of NS5A in the HCV lifecycle have been focused on domain II and III together with phosphorylation of NS5A. Although much work has demonstrated that both domain II and III are required for both RNA replication and virus production, very little research about such functions of domain I has yet been defined. As domain I might present in a dimeric structure with RNA binding sites and with more conserved amino acids, this study attempts to reveal domain I by both functional and structural analyses. To investigate these functions, 12 residues of domain I conserved among all HCV genotypes and surface exposed were chosen for a mutagenic analysis. Taking advantage of sub-genomic replicons (SGR) and JFH1 full-length virus systems, this study identified nine of these residues in NS5A domain I for which alanine substitution absolutely disrupted HCV genome replication via modulation of the replication complex, whereas three residues (P35A, V67A and P145A) had a modest effect on genome replication, but significant defects in the production of infectious virus particles.

The data of non-replicating mutants presented here shows the lethal replication phenotype is a direct result of a loss of NS5A function rather than the disruption of polyprotein processing. The observation that co-localisation between NS5A and NS3 in mutants (G45A, G51A and (153-158)A) transfected cells is significantly disrupted points towards the important role of domain I in the formation of replication complex via interaction with other non-structural proteins, which is consistent with existing data about the important role of NS5A in the replication complex (Paul et al., 2014). The trans-complementation result demonstrates that all these negative mutants cannot be *trans*-complemented by helper RNA, which suggest that deficient NS5A within replication complex could not be replaced by functional NS5A from helper genome. These data are interesting as other trans-complementation studies have shown that both 1b and JFH-1 NS5A mutant replicons can be trans-complemented by an autonomously replicating stable cell line (Appel et al., 2005a, Tong and Malcolm, 2006). NS5A is predicted to be easily trans-complemented as it is only tethered to intracellular membranes via an amphipathic helix (Brass et al., 2002) and can therefore easily be replaced by a functional NS5A protein. Although the interpretation of these trans-complementation results in this study

remains inconclusive, I suspect it might be attributed to the unique structure and location of domain I in the replication factory.

In particular, my attention was focussed on V67A and P145A in this study. Both V67A and P145A mutants were shown to fail to produce intracellular infectious virus and consequently failed to release any virus particles, as judged by the lack of virus RNA or core protein in cell culture supernatants. In addition, this was not due to a lack of genome replication or core protein within the cells, as levels of both were similar to WT. Taken collectively, V67A and P145A were confirmed to completely abrogate virus assembly. Previously, domain I has been assumed only to function during genome replication, and to my knowledge, this is the first detailed analysis of a role for domain I in virus assembly. Moreover, high-resolution confocal microscopy clearly showed that in cells infected with V67A or P145A mutant viruses there were defects in LD production. Compared to WT, LD were smaller, closer to the nucleus and disruption of co-localisation of NS5A and LD or core tempt me to speculate that NS5A recruitment to LDs was impaired. Lastly, these two mutants enhanced binding of domain I to the HCV 3'UTR RNA and inhibited dimerization *in vitro*.

Firstly, combination of these observations suggest that the dimeric and conserved domain I impart NS5A with multiple roles in virus assembly. Both the association of NS5A with LD and the increase in LD size and altered distribution are essential for the virus assembly during HCV infection. Taken together with the in *vitro* data, these support a model in which domain I of NS5A binds to the 3'UTR of nascent genomes and transports them from sites of replication to LD. Here, analogous to the handing on of a baton in a relay race, the RNA is transferred to core and then subsequently transported to assembly sites. The enhanced binding of V67A or P145A to the 3'UTR RNA may prevent the release of RNA for transfer to core post replication in the replicase factory. Additionally and importantly, the LD distribution in cells infected with V67A or P145A at 72 hpe resembles that in wildtype at 12/24 hpe, suggesting that these mutations might block the transition from genome replication to virus assembly. Furthermore, the loss of dimerization by these two mutants implies that, in contrast to the accepted model of an open NS5A dimer revealing a basic RNA-binding groove, monomeric NS5A is able to bind RNA. However, we cannot rule out the possibility that in the intact protein, domains II and III influence both dimerization and RNA binding by domain I. In this regard, it is noted that the attempts to detect NS5A dimerization within intact cells have so far been unsuccessful, despite testing a variety of experimental protocols. Despite this, it is tempting to speculate that

monomeric NS5A might transport nascent RNA to LDs, then dimerizes and releases the RNA to core.

Data in my study are consistent with previous studies into the role of NS5A during virus assembly, which support a model whereby NS5A orchestrates the processes of genome replication, and virus assembly. However, these studies have exclusively focused on the role of domain III (Appel et al., 2008, Pietschmann et al., 2009), and it has been widely accepted that the determinants of virus assembly within NS5A lie entirely within domain III. For example, a serine near the C-terminus of domain III is implicated in the interaction between NS5A and core, and it has been proposed that phosphorylation of this residue by casein kinase II is required for virus assembly (Tellinghuisen et al., 2008a). More recently, mutations of a basic cluster at the N-terminus of domain III resulted in modest impairment of core-RNA and NS5A-RNA interactions and virus particle envelopment, leading to a 100-fold reduction in released virus titres (Zayas et al., 2016). Data from my study extend these observations, providing evidence that domain I also makes a major contribution to virus assembly.

Other implications of this study concern the modifications to LD morphology that occur during HCV infection. Post transfection or infection of HCV, increases in LD size and total volume most likely reflect the coalescence of smaller LDs into larger structures. Our data indicate that domain I of NS5A plays a role in this process, as V67A and P145A do not exhibit this increase. NS5A is recruited to LDs, in most cases to discrete punctate locations on the surface, in contrast to the complete coating of LDs with core. Whether the increase in LD size is a direct consequence of recruitment of NS5A, or indirectly driven by NS5A-mediated effects on lipid metabolism, remains unclear. In this context, NS5A has previously been shown to interact with a number of LD-associated proteins, including DGAT-1 (Camus et al., 2013), Rab18 (Salloum et al., 2013) and ApoE (Benga et al., 2010). However, the phenotype of V67A or P145A cannot be explained by a lack of binding to these proteins as both DGAT-1 and Rab18 can be precipitated NS5A and ApoE exhibit WT level of interaction with NS5A in V67A and P145A transfected cells. Using a proteomic approach to determine the interactome of the three mutant NS5As in comparison to WT, it has been extended and confirmed that V67A and P145A are not involved in the either DGAT, Rab18 or ApoE related LDs biogenesis.

In contrast to V67A and P145A, P35A exhibited a moderate virus assembly phenotype with only a small (less than 10-fold) reduction in virus titre. Nevertheless, some important observations can be made: firstly, in the density gradient analysis the peak of infectivity for P35A resolved at a lower buoyant density than WT (1.0475 g/ml compared with 1.064 g/ml).

In contrast, the second peak of infectivity with higher buoyant density for P35A was associated with more genome RNA and core than WT. These data imply subtle differences in the association of virus particles with VLDL or other lipids. Intriguingly, the proteomic analysis provides us with the evidence why more virus particles from P35A exhibited higher buoyant density but lower infectivity. P35A inhibits the VLDL assembly pathway associated with ApoE, DGAT1 and Rab18, whereas production of non-infectious viruses seems to follow a different pathway. This phenomenon was also observed by the other domain I mutant JFH1AAA99 (Miyanari et al., 2007). In all other analyses (LD size and distribution, NS5A recruitment to LD, dimerization and 3'UTR binding), P35A was not statistically significantly different from WT. In fact, purification of JFH1 WT particles also exhibits two main density peaks, but the majority of particles are of low density and high infectivity (Figure 4.5), which suggests the VLDL assembly pathway predominates in the production of WT JFH1 virus. These observations tempt me to put forward that assembly of HCV take place in different pathways, while LDs associated VLDL pathway is responsible for the infectious HCV particles.

Lastly, it is important to consider our results in the context of the class of potent DAAs that are defined as NS5A inhibitors, exemplified by daclatasvir (DCV). Although initially developed as inhibitors of genome replication (Gao et al., 2010), it has become clear that DCV also has an independent effect on virus assembly. Treatment of infected cells with DCV resulted in a rapid (2 h) block to virus assembly, preceding the inhibition of genome replication which was only apparent at later time points (24 h) (McGivern et al., 2014). More recently, it has been shown that DCV treatment prevented the transfer of genomic RNA to assembly sites (Boson et al., 2017). DCV has been reported to target domain I, as judged by the location of DCV-resistance mutations (e.g. L31M and Y93H). With similar phenotypes of domain I mutants (V67A and P145A) and DCV treatment in virus assembly, it is important to note that none of the three mutations analysed in this study exhibited any effect on the activity of DCV measured against HCV genome replication, which suggests that V67 and P145 are not the sites for DCV binding. However, our observation that domain I is directly implicated in virus assembly does provide a rationale for the rapid effect of DCV on this process, and may therefore help to explain the extraordinary potency of DCV and related compounds.

In pursuit of a greater insight into how NS5A domain I regulate HCV assembly pathway, this study also set out to establish the NS5A-host protein interaction network using quantitative proteomic analysis. A number of partners involved in RNA translation and VLDL assembly pathway has been identified, which provides the supporting evidence for the phenotypes of

domain I mutants. Impairment of interaction with LD-associated proteins (DGAT1, Rab18 and ApoE) confirm that P35A produces more less infectious HCV particles via a non- VLDL assembly pathway and not just due to the reduction of RNA replication. A novel host protein - SOAT1 identified by P145A indicates a direction to investigate the role of domain I in virus assembly. This quantitative proteomic analysis serves as a versatile platform both to verify the currently known NS5A-interacting partners involved by NS5A domain I and to discriminate potential different pathways inhibited by domain I mutants. More importantly, more efforts need to be invested to corroborate it.

A novel role of domain I of HCV NS5A protein in HCV assembly has been identified in this study and characterized to be related to lipid droplets of host cell and intrinsic activities of domain I including dimeric structures and RNA binding. In one word, NS5A is more likely to modulate processes from RNA replication to viral assembly. Nevertheless, there are a number of key unanswered questions. We need a clearer picture of how nucleocapsids are assembled, how NS5A protein contributes to this process and the relationship of virus particle assembly to lipid droplets during viral assembly. What are the clear roles that domain I participate in? Are there other NS5A domain I interacting host proteins involved in virus assembly pathway? Ultimately, to answer these questions, there is yet much work to be done.

Chapter 8: References

AFDHAL, N., ZEUZEM, S., KWO, P., CHOJKIER, M., GITLIN, N., PUOTI, M., ROMERO-GOMEZ, M., ZARSKI, J. P., AGARWAL, K., BUGGISCH, P., FOSTER, G. R., BRAU, N., BUTI, M., JACOBSON, I. M., SUBRAMANIAN, G. M., DING, X., MO, H., YANG, J. C., PANG, P. S., SYMONDS, W. T., MCHUTCHISON, J. G., MUIR, A. J., MANGIA, A., MARCELLIN, P. & INVESTIGATORS, I. O. N. 2014. Ledipasvir and sofosbuvir for untreated HCV genotype 1 infection. *N Engl J Med,* 370**,** 1889-98.

AGNELLO, V., ABEL, G., ELFAHAL, M., KNIGHT, G. B. & ZHANG, Q. X. 1999. Hepatitis C virus and other flaviviridae viruses enter cells via low density lipoprotein receptor. *Proc Natl Acad Sci U S A,* 96**,** 12766-71.

AGO, H., ADACHI, T., YOSHIDA, A., YAMAMOTO, M., HABUKA, N., YATSUNAMI, K. & MIYANO, M. 1999. Crystal structure of the RNA-dependent RNA polymerase of hepatitis C virus. *Structure,* 7**,** 1417-26.

AIZAKI, H., MORIKAWA, K., FUKASAWA, M., HARA, H., INOUE, Y., TANI, H., SAITO, K., NISHIJIMA, M., HANADA, K., MATSUURA, Y., LAI, M. M., MIYAMURA, T., WAKITA, T. & SUZUKI, T. 2008. Critical role of virion-associated cholesterol and sphingolipid in hepatitis C virus infection. *J Virol,* 82**,** 5715-24.

ALTAN-BONNET, N. & BALLA, T. 2012. Phosphatidylinositol 4-kinases: hostages harnessed to build panviral replication platforms. *Trends Biochem Sci,* 37**,** 293-302.

ALTER, M. J. 2007. Epidemiology of hepatitis C virus infection. *World J Gastroenterol,* 13**,** 2436-41.

ALTER, M. J., KRUSZON-MORAN, D., NAINAN, O. V., MCQUILLAN, G. M., GAO, F., MOYER, L. A., KASLOW, R. A. & MARGOLIS, H. S. 1999. The prevalence of hepatitis C virus infection in the United States, 1988 through 1994. *N Engl J Med,* 341**,** 556-62.

AMAKO, Y., IGLOI, Z., MANKOURI, J., KAZLAUSKAS, A., SAKSELA, K., DALLAS, M., PEERS, C. & HARRIS, M. 2013. Hepatitis C virus NS5A inhibits mixed lineage kinase 3 to block apoptosis. *J Biol Chem,* 288**,** 24753-63.

AMAKO, Y., SARKESHIK, A., HOTTA, H., YATES, J., 3RD & SIDDIQUI, A. 2009. Role of oxysterol binding protein in hepatitis C virus infection. *J Virol,* 83**,** 9237-46.

ANDRE, P., KOMURIAN-PRADEL, F., DEFORGES, S., PERRET, M., BERLAND, J. L., SODOYER, M., POL, S., BRECHOT, C., PARANHOS-BACCALA, G. & LOTTEAU, V. 2002. Characterization of low- and very-low-density hepatitis C virus RNA-containing particles. *J Virol,* 76**,** 6919-28.

ANGGAKUSUMA, ROMERO-BREY, I., BERGER, C., COLPITTS, C. C., BOLDANOVA, T., ENGELMANN, M., TODT, D., PERIN, P. M., BEHRENDT, P., VONDRAN, F. W., XU, S., GOFFINET, C., SCHANG, L. M., HEIM, M. H., BARTENSCHLAGER, R., PIETSCHMANN, T. & STEINMANN, E. 2015. Interferon-inducible cholesterol-25-hydroxylase restricts hepatitis C virus replication through blockage of membranous web formation. *Hepatology,* 62**,** 702-14.

APPEL, N., HERIAN, U. & BARTENSCHLAGER, R. 2005a. Efficient rescue of hepatitis C virus RNA replication by trans-complementation with nonstructural protein 5A. *J Virol,* 79**,** 896-909.

APPEL, N., PIETSCHMANN, T. & BARTENSCHLAGER, R. 2005b. Mutational analysis of hepatitis C virus nonstructural protein 5A: potential role of differential phosphorylation in RNA replication and identification of a genetically flexible domain. *J Virol,* 79**,** 3187-94.

APPEL, N., ZAYAS, M., MILLER, S., KRIJNSE-LOCKER, J., SCHALLER, T., FRIEBE, P., KALLIS, S., ENGEL, U. & BARTENSCHLAGER, R. 2008. Essential role of domain III of nonstructural protein 5A for hepatitis C virus infectious particle assembly. *PLoS Pathog,* 4**,** e1000035.

APPLEBY, T. C., ANDERSON, R., FEDOROVA, O., PYLE, A. M., WANG, R., LIU, X., BRENDZA, K. M. & SOMOZA, J. R. 2011. Visualizing ATP-dependent RNA translocation by the NS3 helicase from HCV. *J Mol Biol,* 405**,** 1139-53.

APPLEBY, T. C., PERRY, J. K., MURAKAMI, E., BARAUSKAS, O., FENG, J., CHO, A., FOX, D., 3RD, WETMORE, D. R., MCGRATH, M. E., RAY, A. S., SOFIA, M. J., SWAMINATHAN, S. & EDWARDS, T. E. 2015. Viral replication. Structural basis for RNA replication by the hepatitis C virus polymerase. *Science,* 347**,** 771-5.

ARIUMI, Y., KUROKI, M., MAKI, M., IKEDA, M., DANSAKO, H., WAKITA, T. & KATO, N. 2011. The ESCRT System Is Required for Hepatitis C Virus Production. *Plos One,* 6.

ARUMUGASWAMI, V., REMENYI, R., KANAGAVEL, V., SUE, E. Y., NGOC HO, T., LIU, C., FONTANES, V., DASGUPTA, A. & SUN, R. 2008. High-resolution functional profiling of hepatitis C virus genome. *PLoS Pathog,* 4**,** e1000182.

ASCHER, D. B., WIELENS, J., NERO, T. L., DOUGHTY, L., MORTON, C. J. & PARKER, M. W. 2014. Potent hepatitis C inhibitors bind directly to NS5A and reduce its affinity for RNA. *Sci Rep,* 4**,** 4765.

BACKES, P., QUINKERT, D., REISS, S., BINDER, M., ZAYAS, M., RESCHER, U., GERKE, V., BARTENSCHLAGER, R. & LOHMANN, V. 2010. Role of Annexin A2 in the Production of Infectious Hepatitis C Virus Particles. *Journal of Virology,* 84**,** 5775-5789.

BANKWITZ, D., STEINMANN, E., BITZEGEIO, J., CIESEK, S., FRIESLAND, M., HERRMANN, E., ZEISEL, M. B., BAUMERT, T. F., KECK, Z. Y., FOUNG, S. K., PECHEUR, E. I. & PIETSCHMANN, T. 2010. Hepatitis C virus hypervariable region 1 modulates receptor interactions, conceals the CD81 binding site, and protects conserved neutralizing epitopes. *J Virol,* 84**,** 5751-63.

BAROUCH-BENTOV, R., NEVEU, G., XIAO, F., BEER, M., BEKERMAN, E., SCHOR, S., CAMPBELL, J., BOONYARATANAKORNKIT, J., LINDENBACH, B., LU, A., JACOB, Y. & EINAV, S. 2016. Hepatitis C Virus Proteins Interact with the Endosomal Sorting Complex Required for Transport (ESCRT) Machinery via Ubiquitination To Facilitate Viral Envelopment. *MBio,* 7.

BARTENSCHLAGER, R., AHLBORN-LAAKE, L., MOUS, J. & JACOBSEN, H. 1994. Kinetic and structural analyses of hepatitis C virus polyprotein processing. *J Virol,* 68**,** 5045-55.

BARTENSCHLAGER, R., LOHMANN, V., WILKINSON, T. & KOCH, J. O. 1995. Complex formation between the NS3 serine-type proteinase of the hepatitis C virus and NS4A and its importance for polyprotein maturation. *J Virol,* 69**,** 7519-28.

BARTENSCHLAGER, R., PENIN, F., LOHMANN, V. & ANDRE, P. 2011. Assembly of infectious hepatitis C virus particles. *Trends Microbiol,* 19**,** 95-103.

BARTENSCHLAGER, R. & SPARACIO, S. 2007. Hepatitis C virus molecular clones and their replication capacity in vivo and in cell culture. *Virus Res,* 127**,** 195-207.

BARTER, P. J. & RYE, K. A. 2016. New Era of Lipid-Lowering Drugs. *Pharmacol Rev,* 68**,** 458-75.

BASSETT, S. E., BRASKY, K. M. & LANFORD, R. E. 1998. Analysis of hepatitis C virus-inoculated chimpanzees reveals unexpected clinical profiles. *J Virol,* 72**,** 2589-99.

BELEMA, M. & MEANWELL, N. A. 2014. Discovery of daclatasvir, a pan-genotypic hepatitis C virus NS5A replication complex inhibitor with potent clinical effect. *J Med Chem,* 57**,** 5057-71.

BENGA, W. J., KRIEGER, S. E., DIMITROVA, M., ZEISEL, M. B., PARNOT, M., LUPBERGER, J., HILDT, E., LUO, G., MCLAUCHLAN, J., BAUMERT, T. F. & SCHUSTER, C. 2010. Apolipoprotein E interacts with hepatitis C virus nonstructural protein 5A and determines assembly of infectious particles. *Hepatology,* 51**,** 43-53.

BERAN, R. K., LINDENBACH, B. D. & PYLE, A. M. 2009. The NS4A protein of hepatitis C virus promotes RNA-coupled ATP hydrolysis by the NS3 helicase. *J Virol,* 83**,** 3268-75.

BERGER, C., ROMERO-BREY, I., RADUJKOVIC, D., TERREUX, R., ZAYAS, M., PAUL, D., HARAK, C., HOPPE, S., GAO, M., PENIN, F., LOHMANN, V. & BARTENSCHLAGER, R. 2014. Daclatasvir-like inhibitors of NS5A block early biogenesis of hepatitis C virus-induced membranous replication factories, independent of RNA replication. *Gastroenterology,* 147**,** 1094-105 e25.

BERGER, K. L., COOPER, J. D., HEATON, N. S., YOON, R., OAKLAND, T. E., JORDAN, T. X., MATEU, G., GRAKOUI, A. & RANDALL, G. 2009. Roles for endocytic trafficking and phosphatidylinositol 4-kinase III alpha in hepatitis C virus replication. *Proc Natl Acad Sci U S A,* 106**,** 7577-82.

BERTAUX, C. & DRAGIC, T. 2006. Different domains of CD81 mediate distinct stages of hepatitis C virus pseudoparticle entry. *J Virol,* 80**,** 4940-8.

BIANCO, A., REGHELLIN, V., DONNICI, L., FENU, S., ALVAREZ, R., BARUFFA, C., PERI, F., PAGANI, M., ABRIGNANI, S., NEDDERMANN, P. & DE FRANCESCO, R. 2012. Metabolism of phosphatidylinositol 4-kinase IIIalpha-dependent PI4P Is subverted by HCV and is targeted by a 4-anilino quinazoline with antiviral activity. *PLoS Pathog,* 8**,** e1002576.

BINDER, M., SULAIMANOV, N., CLAUSZNITZER, D., SCHULZE, M., HUBER, C. M., LENZ, S. M., SCHLODER, J. P., TRIPPLER, M., BARTENSCHLAGER, R., LOHMANN, V. & KADERALI, L. 2013. Replication vesicles are load- and choke-points in the hepatitis C virus lifecycle. *PLoS Pathog,* 9**,** e1003561.

BISSIG, K. D., WIELAND, S. F., TRAN, P., ISOGAWA, M., LE, T. T., CHISARI, F. V. & VERMA, I. M. 2010. Human liver chimeric mice provide a model for hepatitis B and C virus infection and treatment. *J Clin Invest,* 120**,** 924-30.

BLACKARD, J. T., KEMMER, N. & SHERMAN, K. E. 2006. Extrahepatic replication of HCV: insights into clinical manifestations and biological consequences. *Hepatology,* 44**,** 15-22.

BLIGHT, K. J., MCKEATING, J. A. & RICE, C. M. 2002. Highly permissive cell lines for subgenomic and genomic hepatitis C virus RNA replication. *J Virol,* 76**,** 13001-14.

BLIGHT, K. J. & RICE, C. M. 1997. Secondary structure determination of the conserved 98-base sequence at the 3' terminus of hepatitis C virus genome RNA. *J Virol,* 71**,** 7345-52.

BOONSTRA, A., VAN DER LAAN, L. J., VANWOLLEGHEM, T. & JANSSEN, H. L. 2009. Experimental models for hepatitis C viral infection. *Hepatology,* 50**,** 1646-55.

BOSON, B., DENOLLY, S., TURLURE, F., CHAMOT, C., DREUX, M. & COSSET, F. L. 2017. Daclatasvir Prevents Hepatitis C Virus Infectivity by Blocking Transfer of the Viral Genome to Assembly Sites. *Gastroenterology,* 152**,** 895-+.

BOSON, B., GRANIO, O., BARTENSCHLAGER, R. & COSSET, F. L. 2011. A concerted action of hepatitis C virus p7 and nonstructural protein 2 regulates core localization at the endoplasmic reticulum and virus assembly. *PLoS Pathog,* 7**,** e1002144.

BOULANT, S., DOUGLAS, M. W., MOODY, L., BUDKOWSKA, A., TARGETT-ADAMS, P. & MCLAUCHLAN, J. 2008. Hepatitis C virus core protein induces lipid droplet redistribution in a microtubule- and dynein-dependent manner. *Traffic,* 9**,** 1268-82.

BOULANT, S., MONTSERRET, R., HOPE, R. G., RATINIER, M., TARGETT-ADAMS, P., LAVERGNE, J. P., PENIN, F. & MCLAUCHLAN, J. 2006. Structural determinants that target the hepatitis C virus core protein to lipid droplets. *J Biol Chem,* 281**,** 22236-47.

BOULANT, S., TARGETT-ADAMS, P. & MCLAUCHLAN, J. 2007. Disrupting the association of hepatitis C virus core protein with lipid droplets correlates with a loss in production of infectious virus. *Journal of General Virology,* 88**,** 2204-2213.

BOURNE, H. R., SANDERS, D. A. & MCCORMICK, F. 1990. The GTPase superfamily: a conserved switch for diverse cell functions. *Nature,* 348**,** 125-32.

BRADLEY, D. W., MAYNARD, J. E., POPPER, H., COOK, E. H., EBERT, J. W., MCCAUSTLAND, K. A., SCHABLE, C. A. & FIELDS, H. A. 1983. Posttransfusion non-A, non-B hepatitis: physicochemical properties of two distinct agents. *J Infect Dis,* 148**,** 254-65.

BRADLEY, D. W., MCCAUSTLAND, K. A., COOK, E. H., SCHABLE, C. A., EBERT, J. W. & MAYNARD, J. E. 1985. Posttransfusion non-A, non-B hepatitis in chimpanzees. Physicochemical evidence that the tubule-forming agent is a small, enveloped virus. *Gastroenterology,* 88**,** 773-9.

BRASS, V., BIECK, E., MONTSERRET, R., WOLK, B., HELLINGS, J. A., BLUM, H. E., PENIN, F. & MORADPOUR, D. 2002. An amino-terminal amphipathic alpha-helix mediates membrane association of the hepatitis C virus nonstructural protein 5A. *J Biol Chem,* 277**,** 8130-9.

BRASS, V., PAL, Z., SAPAY, N., DELEAGE, G., BLUM, H. E., PENIN, F. & MORADPOUR, D. 2007. Conserved determinants for membrane association of nonstructural protein 5A from hepatitis C virus and related viruses. *J Virol,* 81**,** 2745-57.

BRAZZOLI, M., BIANCHI, A., FILIPPINI, S., WEINER, A., ZHU, Q., PIZZA, M. & CROTTA, S. 2008. CD81 is a central regulator of cellular events required for hepatitis C virus infection of human hepatocytes. *J Virol,* 82**,** 8316-29.

BRESSANELLI, S., TOMEI, L., ROUSSEL, A., INCITTI, I., VITALE, R. L., MATHIEU, M., DE FRANCESCO, R. & REY, F. A. 1999. Crystal structure of the RNA-dependent RNA polymerase of hepatitis C virus. *Proc Natl Acad Sci U S A,* 96**,** 13034-9.

BUKH, J. 2004. A critical role for the chimpanzee model in the study of hepatitis C. *Hepatology,* 39**,** 1469-75.

BUKH, J., PIETSCHMANN, T., LOHMANN, V., KRIEGER, N., FAULK, K., ENGLE, R. E., GOVINDARAJAN, S., SHAPIRO, M., ST CLAIRE, M. & BARTENSCHLAGER, R. 2002. Mutations that permit efficient replication of hepatitis C virus RNA in

Huh-7 cells prevent productive replication in chimpanzees. *Proc Natl Acad Sci U S A,* 99**,** 14416-21.

BURBELO, P. D., DUBOVI, E. J., SIMMONDS, P., MEDINA, J. L., HENRIQUEZ, J. A., MISHRA, N., WAGNER, J., TOKARZ, R., CULLEN, J. M., IADAROLA, M. J., RICE, C. M., LIPKIN, W. I. & KAPOOR, A. 2012. Serology-enabled discovery of genetically diverse hepaciviruses in a new host. *J Virol,* 86**,** 6171-8.

BURCKSTUMMER, T., KRIEGS, M., LUPBERGER, J., PAULI, E. K., SCHMITTEL, S. & HILDT, E. 2006. Raf-1 kinase associates with Hepatitis C virus NS5A and regulates viral replication. *FEBS Lett,* 580**,** 575-80.

CALVARUSO, V., PETTA, S. & CRAXI, A. 2018. Is global elimination of HCV realistic? *Liver Int,* 38 Suppl 1**,** 40-46.

CAMUS, G., HERKER, E., MODI, A. A., HAAS, J. T., RAMAGE, H. R., FARESE, R. V., JR. & OTT, M. 2013. Diacylglycerol acyltransferase-1 localizes hepatitis C virus NS5A protein to lipid droplets and enhances NS5A interaction with the viral capsid core. *J Biol Chem,* 288**,** 9915-23.

CATANESE, M. T., URYU, K., KOPP, M., EDWARDS, T. J., ANDRUS, L., RICE, W. J., SILVESTRY, M., KUHN, R. J. & RICE, C. M. 2013. Ultrastructural analysis of hepatitis C virus particles. *Proc Natl Acad Sci U S A,* 110**,** 9505-10.

CEVIK, R. E., CESAREC, M., DA SILVA FILIPE, A., LICASTRO, D., MCLAUCHLAN, J. & MARCELLO, A. 2017. Hepatitis C Virus NS5A Targets Nucleosome Assembly Protein NAP1L1 To Control the Innate Cellular Response. *J Virol,* 91.

CHAN, D. P., SUN, H. Y., WONG, H. T., LEE, S. S. & HUNG, C. C. 2016. Sexually acquired hepatitis C virus infection: a review. *Int J Infect Dis,* 49**,** 47-58.

CHATTERJI, U., BOBARDT, M., SELVARAJAH, S., YANG, F., TANG, H., SAKAMOTO, N., VUAGNIAUX, G., PARKINSON, T. & GALLAY, P. 2009. The isomerase active site of cyclophilin A is critical for hepatitis C virus replication. *J Biol Chem,* 284**,** 16998-7005.

CHEN, S. L. & MORGAN, T. R. 2006. The natural history of hepatitis C virus (HCV) infection. *Int J Med Sci,* 3**,** 47-52.

CHEN, Y., WANG, S., YI, Z., TIAN, H., ALIYARI, R., LI, Y., CHEN, G., LIU, P., ZHONG, J., CHEN, X., DU, P., SU, L., QIN, F. X., DENG, H. & CHENG, G. 2014. Interferon-inducible cholesterol-25-hydroxylase inhibits hepatitis C virus replication via distinct mechanisms. *Sci Rep,* 4**,** 7242.

CHEN, Y. C., SU, W. C., HUANG, J. Y., CHAO, T. C., JENG, K. S., MACHIDA, K. & LAI, M. M. 2010a. Polo-like kinase 1 is involved in hepatitis C virus replication by hyperphosphorylating NS5A. *J Virol,* 84**,** 7983-93.

CHEN, Y. J., CHEN, Y. H., CHOW, L. P., TSAI, Y. H., CHEN, P. H., HUANG, C. Y., CHEN, W. T. & HWANG, L. H. 2010b. Heat shock protein 72 is associated with the hepatitis C virus replicase complex and enhances viral RNA replication. *J Biol Chem,* 285**,** 28183-90.

CHOO, Q. L., KUO, G., WEINER, A. J., OVERBY, L. R., BRADLEY, D. W. & HOUGHTON, M. 1989. Isolation of a cDNA clone derived from a blood-borne non-A, non-B viral hepatitis genome. *Science,* 244**,** 359-62.

COELMONT, L., HANOULLE, X., CHATTERJI, U., BERGER, C., SNOECK, J., BOBARDT, M., LIM, P., VLIEGEN, I., PAESHUYSE, J., VUAGNIAUX, G., VANDAMME, A. M., BARTENSCHLAGER, R., GALLAY, P., LIPPENS, G. & NEYTS, J. 2010. DEB025

(Alisporivir) inhibits hepatitis C virus replication by preventing a cyclophilin A induced cis-trans isomerisation in domain II of NS5A. *PLoS One,* 5**,** e13687.

COLLER, K. E., BERGER, K. L., HEATON, N. S., COOPER, J. D., YOON, R. & RANDALL, G. 2009. RNA interference and single particle tracking analysis of hepatitis C virus endocytosis. *PLoS Pathog,* 5**,** e1000702.

COLLER, K. E., HEATON, N. S., BERGER, K. L., COOPER, J. D., SAUNDERS, J. L. & RANDALL, G. 2012. Molecular determinants and dynamics of hepatitis C virus secretion. *PLoS Pathog,* 8**,** e1002466.

CORDEK, D. G., CROOM-PEREZ, T. J., HWANG, J., HARGITTAI, M. R., SUBBA-REDDY, C. V., HAN, Q., LODEIRO, M. F., NING, G., MCCRORY, T. S., ARNOLD, J. J., KOC, H., LINDENBACH, B. D., SHOWALTER, S. A. & CAMERON, C. E. 2014. Expanding the proteome of an RNA virus by phosphorylation of an intrinsically disordered viral protein. *J Biol Chem,* 289**,** 24397-416.

CORLESS, L., CRUMP, C. M., GRIFFIN, S. D. & HARRIS, M. 2010. Vps4 and the ESCRT-III complex are required for the release of infectious hepatitis C virus particles. *J Gen Virol,* 91**,** 362-72.

COUNIHAN, N. A., RAWLINSON, S. M. & LINDENBACH, B. D. 2011. Trafficking of hepatitis C virus core protein during virus particle assembly. *PLoS Pathog,* 7**,** e1002302.

CUN, W., JIANG, J. Y. & LUO, G. X. 2010. The C-Terminal alpha-Helix Domain of Apolipoprotein E Is Required for Interaction with Nonstructural Protein 5A and Assembly of Hepatitis C Virus. *Journal of Virology,* 84**,** 11532-11541.

DAO THI, V. L., GRANIER, C., ZEISEL, M. B., GUERIN, M., MANCIP, J., GRANIO, O., PENIN, F., LAVILLETTE, D., BARTENSCHLAGER, R., BAUMERT, T. F., COSSET, F. L. & DREUX, M. 2012. Characterization of hepatitis C virus particle subpopulations reveals multiple usage of the scavenger receptor BI for entry steps. *J Biol Chem,* 287**,** 31242-57.

DAVID, N., YAFFE, Y., HAGOEL, L., ELAZAR, M., GLENN, J. S., HIRSCHBERG, K. & SKLAN, E. H. 2015. The interaction between the hepatitis C proteins NS4B and NS5A is involved in viral replication. *Virology,* 475**,** 139-49.

DE CHASSEY, B., NAVRATIL, V., TAFFOREAU, L., HIET, M. S., AUBLIN-GEX, A., AGAUGUE, S., MEIFFREN, G., PRADEZYNSKI, F., FARIA, B. F., CHANTIER, T., LE BRETON, M., PELLET, J., DAVOUST, N., MANGEOT, P. E., CHABOUD, A., PENIN, F., JACOB, Y., VIDALAIN, P. O., VIDAL, M., ANDRE, P., RABOURDIN-COMBE, C. & LOTTEAU, V. 2008. Hepatitis C virus infection protein network. *Mol Syst Biol,* 4**,** 230.

DE MARCO, A., DANS, P. D., KNEZEVICH, A., MAIURI, P., PANTANO, S. & MARCELLO, A. 2010. Subcellular localization of the interaction between the human immunodeficiency virus transactivator Tat and the nucleosome assembly protein 1. *Amino Acids,* 38**,** 1583-93.

DIAMOND, D. L., SYDER, A. J., JACOBS, J. M., SORENSEN, C. M., WALTERS, K. A., PROLL, S. C., MCDERMOTT, J. E., GRITSENKO, M. A., ZHANG, Q., ZHAO, R., METZ, T. O., CAMP, D. G., 2ND, WATERS, K. M., SMITH, R. D., RICE, C. M. & KATZE, M. G. 2010. Temporal proteome and lipidome profiles reveal hepatitis C virus-associated reprogramming of hepatocellular metabolism and bioenergetics. *PLoS Pathog,* 6**,** e1000719.

DIAO, J., PANTUA, H., NGU, H., KOMUVES, L., DIEHL, L., SCHAEFER, G. & KAPADIA, S. B. 2012. Hepatitis C virus induces epidermal growth factor receptor activation via CD81 binding for viral internalization and entry. *J Virol,* 86**,** 10935-49.

DIAZ, O., DELERS, F., MAYNARD, M., DEMIGNOT, S., ZOULIM, F., CHAMBAZ, J., TREPO, C., LOTTEAU, V. & ANDRE, P. 2006. Preferential association of Hepatitis C virus with apolipoprotein B48-containing lipoproteins. *J Gen Virol,* 87**,** 2983-91.

DIMITROVA, M., IMBERT, I., KIENY, M. P. & SCHUSTER, C. 2003. Protein-protein interactions between hepatitis C virus nonstructural proteins. *J Virol,* 77**,** 5401-14.

DONAHUE, J. G., MUNOZ, A., NESS, P. M., BROWN, D. E., JR., YAWN, D. H., MCALLISTER, H. A., JR., REITZ, B. A. & NELSON, K. E. 1992. The declining risk of post-transfusion hepatitis C virus infection. *N Engl J Med,* 327**,** 369-73.

DORNER, M., HORWITZ, J. A., ROBBINS, J. B., BARRY, W. T., FENG, Q., MU, K., JONES, C. T., SCHOGGINS, J. W., CATANESE, M. T., BURTON, D. R., LAW, M., RICE, C. M. & PLOSS, A. 2011. A genetically humanized mouse model for hepatitis C virus infection. *Nature,* 474**,** 208-11.

DOUAM, F. & PLOSS, A. 2015. Proteomic approaches to analyzing hepatitis C virus biology. *Proteomics,* 15**,** 2051-65.

DUBUISSON, J., PENIN, F. & MORADPOUR, D. 2002. Interaction of hepatitis C virus proteins with host cell membranes and lipids. *Trends Cell Biol,* 12**,** 517-23.

DUVET, S., COCQUEREL, L., PILLEZ, A., CACAN, R., VERBERT, A., MORADPOUR, D., WYCHOWSKI, C. & DUBUISSON, J. 1998. Hepatitis C virus glycoprotein complex localization in the endoplasmic reticulum involves a determinant for retention and not retrieval. *J Biol Chem,* 273**,** 32088-95.

EGGER, D., WOLK, B., GOSERT, R., BIANCHI, L., BLUM, H. E., MORADPOUR, D. & BIENZ, K. 2002. Expression of hepatitis C virus proteins induces distinct membrane alterations including a candidate viral replication complex. *J Virol,* 76**,** 5974-84.

EL OMARI, K., IOURIN, O., KADLEC, J., SUTTON, G., HARLOS, K., GRIMES, J. M. & STUART, D. I. 2014. Unexpected structure for the N-terminal domain of hepatitis C virus envelope glycoprotein E1. *Nat Commun,* 5**,** 4874.

ELAZAR, M., CHEONG, K. H., LIU, P., GREENBERG, H. B., RICE, C. M. & GLENN, J. S. 2003. Amphipathic helix-dependent localization of NS5A mediates hepatitis C virus RNA replication. *J Virol,* 77**,** 6055-61.

EVANS, M. J., RICE, C. M. & GOFF, S. P. 2004. Phosphorylation of hepatitis C virus nonstructural protein 5A modulates its protein interactions and viral RNA replication. *Proc Natl Acad Sci U S A,* 101**,** 13038-43.

EVANS, M. J., VON HAHN, T., TSCHERNE, D. M., SYDER, A. J., PANIS, M., WOLK, B., HATZIIOANNOU, T., MCKEATING, J. A., BIENIASZ, P. D. & RICE, C. M. 2007. Claudin-1 is a hepatitis C virus co-receptor required for a late step in entry. *Nature,* 446**,** 801-5.

FARQUHAR, M. J., HARRIS, H. J., DISKAR, M., JONES, S., MEE, C. J., NIELSEN, S. U., BRIMACOMBE, C. L., MOLINA, S., TOMS, G. L., MAUREL, P., HOWL, J., HERBERG, F. W., VAN IJZENDOORN, S. C., BALFE, P. & MCKEATING, J. A. 2008. Protein kinase A-dependent step(s) in hepatitis C virus entry and infectivity. *J Virol,* 82**,** 8797-811.

FARQUHAR, M. J., HU, K., HARRIS, H. J., DAVIS, C., BRIMACOMBE, C. L., FLETCHER, S. J., BAUMERT, T. F., RAPPOPORT, J. Z., BALFE, P. & MCKEATING, J. A. 2012. Hepatitis C virus induces CD81 and claudin-1 endocytosis. *J Virol,* 86**,** 4305-16.

FELD, J. J. 2014. Interferon-free strategies with a nucleoside/nucleotide analogue. *Semin Liver Dis,* 34**,** 37-46.

FELMLEE, D. J., SHERIDAN, D. A., BRIDGE, S. H., NIELSEN, S. U., MILNE, R. W., PACKARD, C. J., CASLAKE, M. J., MCLAUCHLAN, J., TOMS, G. L., NEELY, R. D. & BASSENDINE, M. F. 2010. Intravascular transfer contributes to postprandial increase in numbers of very-low-density hepatitis C virus particles. *Gastroenterology,* 139**,** 1774-83, 1783 e1-6.

FERRARI, E., HE, Z., PALERMO, R. E. & HUANG, H. C. 2008. Hepatitis C virus NS5B polymerase exhibits distinct nucleotide requirements for initiation and elongation. *J Biol Chem,* 283**,** 33893-901.

FERRARIS, P., BLANCHARD, E. & ROINGEARD, P. 2010. Ultrastructural and biochemical analyses of hepatitis C virus-associated host cell membranes. *J Gen Virol,* 91**,** 2230-7.

FEUERSTEIN, S., SOLYOM, Z., ALADAG, A., FAVIER, A., SCHWARTEN, M., HOFFMANN, S., WILLBOLD, D. & BRUTSCHER, B. 2012. Transient structure and SH3 interaction sites in an intrinsically disordered fragment of the hepatitis C virus protein NS5A. *J Mol Biol,* 420**,** 310-23.

FILIPE, A. & MCLAUCHLAN, J. 2015. Hepatitis C virus and lipid droplets: finding a niche. *Trends in Molecular Medicine,* 21**,** 34-42.

FISCHER, J., BOHM, S., SCHOLZ, M., MULLER, T., WITT, H., GEORGE, J., SARRAZIN, C., SUSSER, S., SCHOTT, E., SUPPIAH, V., BOOTH, D. R., STEWART, G. J., VAN BOMMEL, F., BRODZINSKI, A., FULOP, B., MIGAUD, P. & BERG, T. 2012. Combined effects of different interleukin-28B gene variants on the outcome of dual combination therapy in chronic hepatitis C virus type 1 infection. *Hepatology,* 55**,** 1700-10.

FOSTER, T. L., BELYAEVA, T., STONEHOUSE, N. J., PEARSON, A. R. & HARRIS, M. 2010. All three domains of the hepatitis C virus nonstructural NS5A protein contribute to RNA binding. *J Virol,* 84**,** 9267-77.

FOSTER, T. L., GALLAY, P., STONEHOUSE, N. J. & HARRIS, M. 2011. Cyclophilin A interacts with domain II of hepatitis C virus NS5A and stimulates RNA binding in an isomerase-dependent manner. *J Virol,* 85**,** 7460-4.

FOY, E., LI, K., WANG, C., SUMPTER, R., JR., IKEDA, M., LEMON, S. M. & GALE, M., JR. 2003. Regulation of interferon regulatory factor-3 by the hepatitis C virus serine protease. *Science,* 300**,** 1145-8.

FRIDELL, R. A., QIU, D., WANG, C., VALERA, L. & GAO, M. 2010. Resistance analysis of the hepatitis C virus NS5A inhibitor BMS-790052 in an in vitro replicon system. *Antimicrob Agents Chemother,* 54**,** 3641-50.

FRIDELL, R. A., VALERA, L., QIU, D., KIRK, M. J., WANG, C. & GAO, M. 2013. Intragenic complementation of hepatitis C virus NS5A RNA replication-defective alleles. *J Virol,* 87**,** 2320-9.

FROMENTIN, R., MAJEAU, N., LALIBERTE GAGNE, M. E., BOIVIN, A., DUVIGNAUD, J. B. & LECLERC, D. 2007. A method for in vitro assembly of hepatitis C virus core protein and for screening of inhibitors. *Anal Biochem,* 366**,** 37-45.

FUJIMOTO, T. & PARTON, R. G. 2011. Not just fat: the structure and function of the lipid droplet. *Cold Spring Harb Perspect Biol,* 3.

FUKASAWA, M., NAGASE, S., SHIRASAGO, Y., IIDA, M., YAMASHITA, M., ENDO, K., YAGI, K., SUZUKI, T., WAKITA, T., HANADA, K., KUNIYASU, H. & KONDOH, M. 2015. Monoclonal antibodies against extracellular domains of claudin-1 block hepatitis C virus infection in a mouse model. *J Virol,* 89**,** 4866-79.

FUKUSHI, S., OKADA, M., STAHL, J., KAGEYAMA, T., HOSHINO, F. B. & KATAYAMA, K. 2001. Ribosomal protein S5 interacts with the internal ribosomal entry site of hepatitis C virus. *J Biol Chem,* 276**,** 20824-6.

GAO, L., AIZAKI, H., HE, J. W. & LAI, M. M. 2004. Interactions between viral nonstructural proteins and host protein hVAP-33 mediate the formation of hepatitis C virus RNA replication complex on lipid raft. *J Virol,* 78**,** 3480-8.

GAO, M., NETTLES, R. E., BELEMA, M., SNYDER, L. B., NGUYEN, V. N., FRIDELL, R. A., SERRANO-WU, M. H., LANGLEY, D. R., SUN, J. H., O'BOYLE, D. R., 2ND, LEMM, J. A., WANG, C., KNIPE, J. O., CHIEN, C., COLONNO, R. J., GRASELA, D. M., MEANWELL, N. A. & HAMANN, L. G. 2010. Chemical genetics strategy identifies an HCV NS5A inhibitor with a potent clinical effect. *Nature,* 465**,** 96-100.

GASTAMINZA, P., CHENG, G., WIELAND, S., ZHONG, J., LIAO, W. & CHISARI, F. V. 2008. Cellular determinants of hepatitis C virus assembly, maturation, degradation, and secretion. *J Virol,* 82**,** 2120-9.

GASTAMINZA, P., DRYDEN, K. A., BOYD, B., WOOD, M. R., LAW, M., YEAGER, M. & CHISARI, F. V. 2010. Ultrastructural and biophysical characterization of hepatitis C virus particles produced in cell culture. *J Virol,* 84**,** 10999-1009.

GASTAMINZA, P., KAPADIA, S. B. & CHISARI, F. V. 2006. Differential biophysical properties of infectious intracellular and secreted hepatitis C virus particles. *J Virol,* 80**,** 11074-81.

GENTILE, I., BUONOMO, A. R. & BORGIA, G. 2014. Dasabuvir: A Non-Nucleoside Inhibitor of NS5B for the Treatment of Hepatitis C Virus Infection. *Rev Recent Clin Trials,* 9**,** 115-23.

GENTZSCH, J., BROHM, C., STEINMANN, E., FRIESLAND, M., MENZEL, N., VIEYRES, G., PERIN, P. M., FRENTZEN, A., KADERALI, L. & PIETSCHMANN, T. 2013. hepatitis c Virus p7 is critical for capsid assembly and envelopment. *PLoS Pathog,* 9**,** e1003355.

GERMAIN, M. A., CHATEL-CHAIX, L., GAGNE, B., BONNEIL, E., THIBAULT, P., PRADEZYNSKI, F., DE CHASSEY, B., MEYNIEL-SCHICKLIN, L., LOTTEAU, V., BARIL, M. & LAMARRE, D. 2014. Elucidating novel hepatitis C virus-host interactions using combined mass spectrometry and functional genomics approaches. *Mol Cell Proteomics,* 13**,** 184-203.

GERMI, R., CRANCE, J. M., GARIN, D., GUIMET, J., LORTAT-JACOB, H., RUIGROK, R. W., ZARSKI, J. P. & DROUET, E. 2002. Cellular glycosaminoglycans and low density lipoprotein receptor are involved in hepatitis C virus adsorption. *J Med Virol,* 68**,** 206-15.

GOFFARD, A., CALLENS, N., BARTOSCH, B., WYCHOWSKI, C., COSSET, F. L., MONTPELLIER, C. & DUBUISSON, J. 2005. Role of N-linked glycans in the functions of hepatitis C virus envelope glycoproteins. *J Virol,* 79**,** 8400-9.

GOKHALE, N. S., VAZQUEZ, C. & HORNER, S. M. 2014. Hepatitis C Virus. Strategies to Evade Antiviral Responses. *Future Virol,* 9**,** 1061-1075.

GOMES, R. G., ISKEN, O., TAUTZ, N., MCLAUCHLAN, J. & MCCORMICK, C. J. 2015. Polyprotein-Driven Formation of Two Interdependent Sets of Complexes Supporting Hepatitis C Virus Genome Replication. *J Virol,* 90**,** 2868-83.

GOONAWARDANE, N., GEBHARDT, A., BARTLETT, C., PICHLMAIR, A. & HARRIS, M. 2017. Phosphorylation of Serine 225 in Hepatitis C Virus NS5A Regulates Protein-Protein Interactions. *J Virol,* 91.

GOSERT, R., EGGER, D., LOHMANN, V., BARTENSCHLAGER, R., BLUM, H. E., BIENZ, K. & MORADPOUR, D. 2003. Identification of the hepatitis C virus RNA replication complex in Huh-7 cells harboring subgenomic replicons. *J Virol,* 77**,** 5487-92.

GOUTTENOIRE, J., PENIN, F. & MORADPOUR, D. 2010a. Hepatitis C virus nonstructural protein 4B: a journey into unexplored territory. *Rev Med Virol,* 20**,** 117-29.

GOUTTENOIRE, J., ROINGEARD, P., PENIN, F. & MORADPOUR, D. 2010b. Amphipathic alpha-helix AH2 is a major determinant for the oligomerization of hepatitis C virus nonstructural protein 4B. *J Virol,* 84**,** 12529-37.

GRAKOUI, A., MCCOURT, D. W., WYCHOWSKI, C., FEINSTONE, S. M. & RICE, C. M. 1993. A second hepatitis C virus-encoded proteinase. *Proc Natl Acad Sci U S A,* 90**,** 10583-7.

GRIFFIN, S. D., BEALES, L. P., CLARKE, D. S., WORSFOLD, O., EVANS, S. D., JAEGER, J., HARRIS, M. P. & ROWLANDS, D. J. 2003. The p7 protein of hepatitis C virus forms an ion channel that is blocked by the antiviral drug, Amantadine. *FEBS Lett,* 535**,** 34-8.

GRISE, H., FRAUSTO, S., LOGAN, T. & TANG, H. 2012. A conserved tandem cyclophilin-binding site in hepatitis C virus nonstructural protein 5A regulates Alisporivir susceptibility. *J Virol,* 86**,** 4811-22.

GROSS, D. A. & SILVER, D. L. 2014. Cytosolic lipid droplets: from mechanisms of fat storage to disease. *Crit Rev Biochem Mol Biol,* 49**,** 304-26.

GU, M. & RICE, C. M. 2010. Three conformational snapshots of the hepatitis C virus NS3 helicase reveal a ratchet translocation mechanism. *Proc Natl Acad Sci U S A,* 107**,** 521-8.

GUEDJ, J., DAHARI, H., RONG, L., SANSONE, N. D., NETTLES, R. E., COTLER, S. J., LAYDEN, T. J., UPRICHARD, S. L. & PERELSON, A. S. 2013. Modeling shows that the NS5A inhibitor daclatasvir has two modes of action and yields a shorter estimate of the hepatitis C virus half-life. *Proc Natl Acad Sci U S A,* 110**,** 3991-6.

GUO, M., PEI, R., YANG, Q., CAO, H., WANG, Y., WU, C., CHEN, J., ZHOU, Y., HU, X., LU, M. & CHEN, X. 2015. Phosphatidylserine-specific phospholipase A1 involved in hepatitis C virus assembly through NS2 complex formation. *J Virol,* 89**,** 2367-77.

GUPTA, N., THAKKER, S. & VERMA, S. C. 2016. KSHV encoded LANA recruits Nucleosome Assembly Protein NAP1L1 for regulating viral DNA replication and transcription. *Sci Rep,* 6**,** 32633.

HADZIYANNIS, S. J., SETTE, H., JR., MORGAN, T. R., BALAN, V., DIAGO, M., MARCELLIN, P., RAMADORI, G., BODENHEIMER, H., JR., BERNSTEIN, D., RIZZETTO, M., ZEUZEM, S., POCKROS, P. J., LIN, A., ACKRILL, A. M. & GROUP, P. I. S. 2004. Peginterferon-alpha2a and ribavirin combination therapy in chronic hepatitis

C: a randomized study of treatment duration and ribavirin dose. *Ann Intern Med,* 140**,** 346-55.

HAMAMOTO, I., NISHIMURA, Y., OKAMOTO, T., AIZAKI, H., LIU, M., MORI, Y., ABE, T., SUZUKI, T., LAI, M. M., MIYAMURA, T., MORIISHI, K. & MATSUURA, Y. 2005. Human VAP-B is involved in hepatitis C virus replication through interaction with NS5A and NS5B. *J Virol,* 79**,** 13473-82.

HAN, Q., MANNA, D., BELTON, K., COLE, R. & KONAN, K. V. 2013. Modulation of hepatitis C virus genome encapsidation by nonstructural protein 4B. *J Virol,* 87**,** 7409-22.

HANOULLE, X., BADILLO, A., WIERUSZESKI, J. M., VERDEGEM, D., LANDRIEU, I., BARTENSCHLAGER, R., PENIN, F. & LIPPENS, G. 2009a. Hepatitis C virus NS5A protein is a substrate for the peptidyl-prolyl cis/trans isomerase activity of cyclophilins A and B. *J Biol Chem,* 284**,** 13589-601.

HANOULLE, X., VERDEGEM, D., BADILLO, A., WIERUSZESKI, J. M., PENIN, F. & LIPPENS, G. 2009b. Domain 3 of non-structural protein 5A from hepatitis C virus is natively unfolded. *Biochem Biophys Res Commun,* 381**,** 634-8.

HARRIS, H. J., DAVIS, C., MULLINS, J. G., HU, K., GOODALL, M., FARQUHAR, M. J., MEE, C. J., MCCAFFREY, K., YOUNG, S., DRUMMER, H., BALFE, P. & MCKEATING, J. A. 2010. Claudin association with CD81 defines hepatitis C virus entry. *J Biol Chem,* 285**,** 21092-102.

HARRUS, D., AHMED-EL-SAYED, N., SIMISTER, P. C., MILLER, S., TRICONNET, M., HAGEDORN, C. H., MAHIAS, K., REY, F. A., ASTIER-GIN, T. & BRESSANELLI, S. 2010. Further insights into the roles of GTP and the C terminus of the hepatitis C virus polymerase in the initiation of RNA synthesis. *J Biol Chem,* 285**,** 32906-18.

HASHEM, Y., DES GEORGES, A., DHOTE, V., LANGLOIS, R., LIAO, H. Y., GRASSUCCI, R. A., PESTOVA, T. V., HELLEN, C. U. & FRANK, J. 2013. Hepatitis-C-virus-like internal ribosome entry sites displace eIF3 to gain access to the 40S subunit. *Nature,* 503**,** 539-43.

HAZUDA, D. J., BURROUGHS, M., HOWE, A. Y., WAHL, J. & VENKATRAMAN, S. 2013. Development of boceprevir: a first-in-class direct antiviral treatment for chronic hepatitis C infection. *Ann N Y Acad Sci,* 1291**,** 69-76.

HE, L. F., ALLING, D., POPKIN, T., SHAPIRO, M., ALTER, H. J. & PURCELL, R. H. 1987. Determining the size of non-A, non-B hepatitis virus by filtration. *J Infect Dis,* 156**,** 636-40.

HERKER, E., HARRIS, C., HERNANDEZ, C., CARPENTIER, A., KAEHLCKE, K., ROSENBERG, A. R., FARESE, R. V., JR. & OTT, M. 2010. Efficient hepatitis C virus particle formation requires diacylglycerol acyltransferase-1. *Nat Med,* 16**,** 1295-8.

HEROD, M. R., SCHREGEL, V., HINDS, C., LIU, M., MCLAUCHLAN, J. & MCCORMICK, C. J. 2014. Genetic complementation of hepatitis C virus nonstructural protein functions associated with replication exhibits requirements that differ from those for virion assembly. *J Virol,* 88**,** 2748-62.

HEZODE, C., REAU, N., SVAROVSKAIA, E. S., DOEHLE, B. P., SHANMUGAM, R., DVORY-SOBOL, H., HEDSKOG, C., MCNALLY, J., OSINUSI, A., BRAINARD, D. M., MILLER, M. D., MO, H., ROBERTS, S. K., O'LEARY, J. G., SHAFRAN, S. D. & ZEUZEM, S. 2017. Resistance Analysis in Patients with Genotype 1-6 HCV Infection Treated with Sofosbuvir/Velpatasvir in the Phase 3 Studies. *J Hepatol*.

HIJIKATA, M., SHIMIZU, Y. K., KATO, H., IWAMOTO, A., SHIH, J. W., ALTER, H. J., PURCELL, R. H. & YOSHIKURA, H. 1993. Equilibrium centrifugation studies of hepatitis C virus: evidence for circulating immune complexes. *J Virol,* 67**,** 1953-8.

HIPPENSTIEL, S., SCHMECK, B., N'GUESSAN, P. D., SEYBOLD, J., KRULL, M., PREISSNER, K., EICHEL-STREIBER, C. V. & SUTTORP, N. 2002. Rho protein inactivation induced apoptosis of cultured human endothelial cells. *Am J Physiol Lung Cell Mol Physiol,* 283**,** L830-8.

HSU, S. C., LO, C. W., PAN, T. C., LEE, K. Y. & YU, M. J. 2017. Serine 235 Is the Primary NS5A Hyperphosphorylation Site Responsible for Hepatitis C Virus Replication. *J Virol,* 91.

HU, L., LI, J., CAI, H., YAO, W., XIAO, J., LI, Y. P., QIU, X., XIA, H. & PENG, T. 2017. Avasimibe: A novel hepatitis C virus inhibitor that targets the assembly of infectious viral particles. *Antiviral Res,* 148**,** 5-14.

HUANG, H., SUN, F., OWEN, D. M., LI, W., CHEN, Y., GALE, M., JR. & YE, J. 2007a. Hepatitis C virus production by human hepatocytes dependent on assembly and secretion of very low-density lipoproteins. *Proc Natl Acad Sci U S A,* 104**,** 5848-53.

HUANG, L., HWANG, J., SHARMA, S. D., HARGITTAI, M. R., CHEN, Y., ARNOLD, J. J., RANEY, K. D. & CAMERON, C. E. 2005. Hepatitis C virus nonstructural protein 5A (NS5A) is an RNA-binding protein. *J Biol Chem,* 280**,** 36417-28.

HUANG, L. Y., SINEVA, E. V., HARGITTA, M. R. S., SHARMA, S. D., SUTHAR, M., RANEY, K. D. & CAMERON, C. E. 2004. Purification and characterization of hepatitis C virus non-structural protein 5A expressed in Escherichia coli. *Protein Expression and Purification,* 37**,** 144-153.

HUANG, Y., STASCHKE, K., DE FRANCESCO, R. & TAN, S. L. 2007b. Phosphorylation of hepatitis C virus NS5A nonstructural protein: a new paradigm for phosphorylation-dependent viral RNA replication? *Virology,* 364**,** 1-9.

HUANG, Z. S., WANG, C. C. & WU, H. N. 2010. HCV NS3 protein helicase domain assists RNA structure conversion. *FEBS Lett,* 584**,** 2356-62.

HUFF, J. 2015. The Airyscan detector from ZEISS: confocal imaging with improved signal-to-noise ratio and super-resolution. *Nature Methods,* 12.

HUFF, J. 2016. The Fast mode for ZEISS LSM 880 with Airyscan: high-speed confocal imaging with super-resolution and improved signal-to-noise ratio. *Nature Methods,* 13**,** I-Ii.

HUGHES, M., GRETTON, S., SHELTON, H., BROWN, D. D., MCCORMICK, C. J., ANGUS, A. G., PATEL, A. H., GRIFFIN, S. & HARRIS, M. 2009a. A conserved proline between domains II and III of hepatitis C virus NS5A influences both RNA replication and virus assembly. *J Virol,* 83**,** 10788-96.

HUGHES, M., GRIFFIN, S. & HARRIS, M. 2009b. Domain III of NS5A contributes to both RNA replication and assembly of hepatitis C virus particles. *J Gen Virol,* 90**,** 1329-34.

HUGHES, M. E. 2010. *Identification of residues in hepatitis C virus NS5A with a critical role in genome replication or particle assembly.* University of Leeds.

HUTAGALUNG, A. H. & NOVICK, P. J. 2011. Role of Rab GTPases in membrane traffic and cell physiology. *Physiol Rev,* 91**,** 119-49.

HWANG, J., HUANG, L., CORDEK, D. G., VAUGHAN, R., REYNOLDS, S. L., KIHARA, G., RANEY, K. D., KAO, C. C. & CAMERON, C. E. 2010. Hepatitis C virus nonstructural protein 5A: biochemical characterization of a novel structural class of RNA-binding proteins. *J Virol,* 84**,** 12480-91.

IGLOI, Z., KAZLAUSKAS, A., SAKSELA, K., MACDONALD, A., MANKOURI, J. & HARRIS, M. 2015. Hepatitis C virus NS5A protein blocks epidermal growth factor receptor degradation via a proline motif- dependent interaction. *J Gen Virol,* 96**,** 2133-44.

INOUE, H., NOJIMA, H. & OKAYAMA, H. 1990. High efficiency transformation of Escherichia coli with plasmids. *Gene,* 96**,** 23-8.

IVANYI-NAGY, R., KANEVSKY, I., GABUS, C., LAVERGNE, J. P., FICHEUX, D., PENIN, F., FOSSE, P. & DARLIX, J. L. 2006. Analysis of hepatitis C virus RNA dimerization and core-RNA interactions. *Nucleic Acids Res,* 34**,** 2618-33.

JAAFAR, Z. A., OGURO, A., NAKAMURA, Y. & KIEFT, J. S. 2016. Translation initiation by the hepatitis C virus IRES requires eIF1A and ribosomal complex remodeling. *Elife,* 5.

JABLONSKI, S. A. & MORROW, C. D. 1995. Mutation of the aspartic acid residues of the GDD sequence motif of poliovirus RNA-dependent RNA polymerase results in enzymes with altered metal ion requirements for activity. *J Virol,* 69**,** 1532-9.

JACOBSEN, K. H. & WIERSMA, S. T. 2010. Hepatitis A virus seroprevalence by age and world region, 1990 and 2005. *Vaccine,* 28**,** 6653-7.

JAMMART, B., MICHELET, M., PECHEUR, E. I., PARENT, R., BARTOSCH, B., ZOULIM, F. & DURANTEL, D. 2013. Very-low-density lipoprotein (VLDL)-producing and hepatitis C virus-replicating HepG2 cells secrete no more lipoviroparticles than VLDL-deficient Huh7.5 cells. *J Virol,* 87**,** 5065-80.

JIA, L., BETTERS, J. L. & YU, L. 2011. Niemann-pick C1-like 1 (NPC1L1) protein in intestinal and hepatic cholesterol transport. *Annu Rev Physiol,* 73**,** 239-59.

JIANG, J. & LUO, G. 2009. Apolipoprotein E but not B is required for the formation of infectious hepatitis C virus particles. *J Virol,* 83**,** 12680-91.

JIRASKO, V., MONTSERRET, R., APPEL, N., JANVIER, A., EUSTACHI, L., BROHM, C., STEINMANN, E., PIETSCHMANN, T., PENIN, F. & BARTENSCHLAGER, R. 2008. Structural and functional characterization of nonstructural protein 2 for its role in hepatitis C virus assembly. *J Biol Chem,* 283**,** 28546-62.

JIRASKO, V., MONTSERRET, R., LEE, J. Y., GOUTTENOIRE, J., MORADPOUR, D., PENIN, F. & BARTENSCHLAGER, R. 2010. Structural and functional studies of nonstructural protein 2 of the hepatitis C virus reveal its key role as organizer of virion assembly. *PLoS Pathog,* 6**,** e1001233.

JONES, C. T., MURRAY, C. L., EASTMAN, D. K., TASSELLO, J. & RICE, C. M. 2007a. Hepatitis C virus p7 and NS2 proteins are essential for production of infectious virus. *J Virol,* 81**,** 8374-83.

JONES, D. M., ATOOM, A. M., ZHANG, X., KOTTILIL, S. & RUSSELL, R. S. 2011. A genetic interaction between the core and NS3 proteins of hepatitis C virus is essential for production of infectious virus. *J Virol,* 85**,** 12351-61.

JONES, D. M., GRETTON, S. N., MCLAUCHLAN, J. & TARGETT-ADAMS, P. 2007b. Mobility analysis of an NS5A-GFP fusion protein in cells actively replicating hepatitis C virus subgenomic RNA. *J Gen Virol,* 88**,** 470-5.

JONES, D. M., PATEL, A. H., TARGETT-ADAMS, P. & MCLAUCHLAN, J. 2009. The hepatitis C virus NS4B protein can trans-complement viral RNA replication and modulates production of infectious virus. *J Virol,* 83**,** 2163-77.

KALLIAMPAKOU, K. I., KALAMVOKI, M. & MAVROMARA, P. 2005. Hepatitis C virus (HCV) NS5A protein downregulates HCV IRES-dependent translation. *J Gen Virol,* 86**,** 1015-25.

KANEKO, T., TANJI, Y., SATOH, S., HIJIKATA, M., ASABE, S., KIMURA, K. & SHIMOTOHNO, K. 1994. Production of two phosphoproteins from the NS5A region of the hepatitis C viral genome. *Biochem Biophys Res Commun,* 205**,** 320-6.

KAPADIA, S. B. & CHISARI, F. V. 2005. Hepatitis C virus RNA replication is regulated by host geranylgeranylation and fatty acids. *Proc Natl Acad Sci U S A,* 102**,** 2561-6.

KAPOOR, A., SIMMONDS, P., GEROLD, G., QAISAR, N., JAIN, K., HENRIQUEZ, J. A., FIRTH, C., HIRSCHBERG, D. L., RICE, C. M., SHIELDS, S. & LIPKIN, W. I. 2011. Characterization of a canine homolog of hepatitis C virus. *Proc Natl Acad Sci U S A,* 108**,** 11608-13.

KAPOOR, A., SIMMONDS, P., SCHEEL, T. K., HJELLE, B., CULLEN, J. M., BURBELO, P. D., CHAUHAN, L. V., DURAISAMY, R., SANCHEZ LEON, M., JAIN, K., VANDEGRIFT, K. J., CALISHER, C. H., RICE, C. M. & LIPKIN, W. I. 2013. Identification of rodent homologs of hepatitis C virus and pegiviruses. *MBio,* 4**,** e00216-13.

KATO, T., DATE, T., MIYAMOTO, M., FURUSAKA, A., TOKUSHIGE, K., MIZOKAMI, M. & WAKITA, T. 2003. Efficient replication of the genotype 2a hepatitis C virus subgenomic replicon. *Gastroenterology,* 125**,** 1808-17.

KATZE, M. G., KWIECISZEWSKI, B., GOODLETT, D. R., BLAKELY, C. M., NEDDERMANN, P., TAN, S. L. & AEBERSOLD, R. 2000. Ser(2194) is a highly conserved major phosphorylation site of the hepatitis C virus nonstructural protein NS5A. *Virology,* 278**,** 501-13.

KAUL, A., WOERZ, I., MEULEMAN, P., LEROUX-ROELS, G. & BARTENSCHLAGER, R. 2007. Cell culture adaptation of hepatitis C virus and in vivo viability of an adapted variant. *J Virol,* 81**,** 13168-79.

KEATING, G. M. 2016. Elbasvir/Grazoprevir: First Global Approval. *Drugs,* 76**,** 617-24.

KELLY, L., BADHAN, A., ROBERTS, G. C., MBISA, J. L. & HARRIS, M. 2017. Manipulation of both virus- and cell-specific factors is required for robust transient replication of a hepatitis C virus genotype 3a sub-genomic replicon. *J Gen Virol*.

KHAN, A. G., MILLER, M. T. & MARCOTRIGIANO, J. 2015. HCV glycoprotein structures: what to expect from the unexpected. *Curr Opin Virol,* 12**,** 53-8.

KHAN, A. G., WHIDBY, J., MILLER, M. T., SCARBOROUGH, H., ZATORSKI, A. V., CYGAN, A., PRICE, A. A., YOST, S. A., BOHANNON, C. D., JACOB, J., GRAKOUI, A. & MARCOTRIGIANO, J. 2014a. Structure of the core ectodomain of the hepatitis C virus envelope glycoprotein 2. *Nature,* 509**,** 381-4.

KHAN, I., KATIKANENI, D. S., HAN, Q., SANCHEZ-FELIPE, L., HANADA, K., AMBROSE, R. L., MACKENZIE, J. M. & KONAN, K. V. 2014b. Modulation of hepatitis C virus genome replication by glycosphingolipids and four-phosphate adaptor protein 2. *J Virol,* 88**,** 12276-95.

KIELIAN, M. 2006. Class II virus membrane fusion proteins. *Virology,* 344**,** 38-47.

KIM, J., LEE, D. & CHOE, J. 1999. Hepatitis C virus NS5A protein is phosphorylated by casein kinase II. *Biochem Biophys Res Commun,* 257**,** 777-81.

KIM, S., WELSCH, C., YI, M. & LEMON, S. M. 2011. Regulation of the production of infectious genotype 1a hepatitis C virus by NS5A domain III. *J Virol,* 85**,** 6645-56.

KNIGHT, B. C. & HIGH, S. 1998. Membrane integration of Sec61alpha: a core component of the endoplasmic reticulum translocation complex. *Biochem J,* 331 (Pt 1)**,** 161-7.

KOCH, J. O. & BARTENSCHLAGER, R. 1999. Modulation of hepatitis C virus NS5A hyperphosphorylation by nonstructural proteins NS3, NS4A, and NS4B. *J Virol,* 73**,** 7138-46.

KOLYKHALOV, A. A., FEINSTONE, S. M. & RICE, C. M. 1996. Identification of a highly conserved sequence element at the 3' terminus of hepatitis C virus genome RNA. *J Virol,* 70**,** 3363-71.

KOLYKHALOV, A. A., MIHALIK, K., FEINSTONE, S. M. & RICE, C. M. 2000. Hepatitis C virus-encoded enzymatic activities and conserved RNA elements in the 3' nontranslated region are essential for virus replication in vivo. *J Virol,* 74**,** 2046-51.

KONO, Y., HAYASHIDA, K., TANAKA, H., ISHIBASHI, H. & HARADA, M. 2003. High-density lipoprotein binding rate differs greatly between genotypes 1b and 2a/2b of hepatitis C virus. *J Med Virol,* 70**,** 42-8.

KOROBCHEVSKAYA, K., LAGERHOLM, B. C., COLIN-YORK, H. & FRITZSCHE, M. 2017. Exploring the Potential of Airyscan Microscopy for Live Cell Imaging. *Photonics,* 4.

KUKOLJ, G., MCGIBBON, G. A., MCKERCHER, G., MARQUIS, M., LEFEBVRE, S., THAUVETTE, L., GAUTHIER, J., GOULET, S., POUPART, M. A. & BEAULIEU, P. L. 2005. Binding site characterization and resistance to a class of non-nucleoside inhibitors of the hepatitis C virus NS5B polymerase. *J Biol Chem,* 280**,** 39260-7.

KWO, P., GANE, E. J., PENG, C. Y., PEARLMAN, B., VIERLING, J. M., SERFATY, L., BUTI, M., SHAFRAN, S., STRYSZAK, P., LIN, L., GRESS, J., BLACK, S., DUTKO, F. J., ROBERTSON, M., WAHL, J., LUPINACCI, L., BARR, E. & HABER, B. 2017. Effectiveness of Elbasvir and Grazoprevir Combination, With or Without Ribavirin, for Treatment-Experienced Patients With Chronic Hepatitis C Infection. *Gastroenterology,* 152**,** 164-175 e4.

KWONG, A. D. 2014. The HCV Revolution Did Not Happen Overnight. *ACS Med Chem Lett,* 5**,** 214-220.

KWONG, A. D., KAUFFMAN, R. S., HURTER, P. & MUELLER, P. 2011. Discovery and development of telaprevir: an NS3-4A protease inhibitor for treating genotype 1 chronic hepatitis C virus. *Nat Biotechnol,* 29**,** 993-1003.

LAHSER, F. C., BYSTOL, K., CURRY, S., MCMONAGLE, P., XIA, E., INGRAVALLO, P., CHASE, R., LIU, R., BLACK, T., HAZUDA, D., HOWE, A. Y. & ASANTE-APPIAH, E. 2016. The Combination of Grazoprevir, a Hepatitis C Virus (HCV) NS3/4A Protease Inhibitor, and Elbasvir, an HCV NS5A Inhibitor, Demonstrates a High Genetic Barrier to Resistance in HCV Genotype 1a Replicons. *Antimicrob Agents Chemother,* 60**,** 2954-64.

LAI, C. K., JENG, K. S., MACHIDA, K. & LAI, M. M. C. 2010. Hepatitis C Virus Egress and Release Depend on Endosomal Trafficking of Core Protein. *Journal of Virology,* 84**,** 11590-11598.

LAMBERT, S. M., LANGLEY, D. R., GARNETT, J. A., ANGELL, R., HEDGETHORNE, K., MEANWELL, N. A. & MATTHEWS, S. J. 2014. The crystal structure of NS5A domain 1 from genotype 1a reveals new clues to the mechanism of action for dimeric HCV inhibitors. *Protein Sci,* 23**,** 723-34.

LAUCK, M., SIBLEY, S. D., LARA, J., PURDY, M. A., KHUDYAKOV, Y., HYEROBA, D., TUMUKUNDE, A., WENY, G., SWITZER, W. M., CHAPMAN, C. A., HUGHES, A. L., FRIEDRICH, T. C., O'CONNOR, D. H. & GOLDBERG, T. L. 2013. A novel hepacivirus with an unusually long and intrinsically disordered NS5A protein in a wild Old World primate. *J Virol,* 87**,** 8971-81.

LAUER, G. M. & WALKER, B. D. 2001. Hepatitis C virus infection. *N Engl J Med,* 345**,** 41-52.

LAWITZ, E., MAKARA, M., AKARCA, U. S., THULUVATH, P. J., PREOTESCU, L. L., VARUNOK, P., MORILLAS, R. M., HALL, C., MOBASHERY, N., REDMAN, R., PILOT-MATIAS, T., VILCHEZ, R. A. & HEZODE, C. 2015. Efficacy and Safety of Ombitasvir, Paritaprevir, and Ritonavir in an Open-Label Study of Patients With Genotype 1b Chronic Hepatitis C Virus Infection With and Without Cirrhosis. *Gastroenterology,* 149**,** 971-80 e1.

LEE, K. Y., CHEN, Y. H., HSU, S. C. & YU, M. J. 2016. Phosphorylation of Serine 235 of the Hepatitis C Virus Non-Structural Protein NS5A by Multiple Kinases. *PLoS One,* 11**,** e0166763.

LEE, N. P. & LUK, J. M. 2010. Hepatic tight junctions: from viral entry to cancer metastasis. *World J Gastroenterol,* 16**,** 289-95.

LEHMANN, M., MEYER, M. F., MONAZAHIAN, M., TILLMANN, H. L., MANNS, M. P. & WEDEMEYER, H. 2004. High rate of spontaneous clearance of acute hepatitis C virus genotype 3 infection. *J Med Virol,* 73**,** 387-91.

LEMAY, K. L., TREADAWAY, J., ANGULO, I. & TELLINGHUISEN, T. L. 2013. A hepatitis C virus NS5A phosphorylation site that regulates RNA replication. *J Virol,* 87**,** 1255-60.

LESBURG, C. A., CABLE, M. B., FERRARI, E., HONG, Z., MANNARINO, A. F. & WEBER, P. C. 1999. Crystal structure of the RNA-dependent RNA polymerase from hepatitis C virus reveals a fully encircled active site. *Nat Struct Biol,* 6**,** 937-43.

LI, K., FOY, E., FERREON, J. C., NAKAMURA, M., FERREON, A. C., IKEDA, M., RAY, S. C., GALE, M., JR. & LEMON, S. M. 2005. Immune evasion by hepatitis C virus NS3/4A protease-mediated cleavage of the Toll-like receptor 3 adaptor protein TRIF. *Proc Natl Acad Sci U S A,* 102**,** 2992-7.

LI, Y. & MODIS, Y. 2014. A novel membrane fusion protein family in Flaviviridae? *Trends Microbiol,* 22**,** 176-82.

LIANG, Y., YE, H., KANG, C. B. & YOON, H. S. 2007. Domain 2 of nonstructural protein 5A (NS5A) of hepatitis C virus is natively unfolded. *Biochemistry,* 46**,** 11550-8.

LIAO, H. J. & CARPENTER, G. 2007. Role of the Sec61 translocon in EGF receptor trafficking to the nucleus and gene expression. *Mol Biol Cell,* 18**,** 1064-72.

LIEFHEBBER, J. M., HAGUE, C. V., ZHANG, Q., WAKELAM, M. J. & MCLAUCHLAN, J. 2014. Modulation of triglyceride and cholesterol ester synthesis impairs assembly of infectious hepatitis C virus. *J Biol Chem,* 289**,** 21276-88.

LIM, P. J., CHATTERJI, U., CORDEK, D., SHARMA, S. D., GARCIA-RIVERA, J. A., CAMERON, C. E., LIN, K., TARGETT-ADAMS, P. & GALLAY, P. A. 2012. Correlation between NS5A dimerization and hepatitis C virus replication. *J Biol Chem,* 287**,** 30861-73.

LIM, Y. S., TRAN, H. T., PARK, S. J., YIM, S. A. & HWANG, S. B. 2011. Peptidyl-prolyl isomerase Pin1 is a cellular factor required for hepatitis C virus propagation. *J Virol,* 85**,** 8777-88.

LIN, C. C., TSAI, P., SUN, H. Y., HSU, M. C., LEE, J. C., WU, I. C., TSAO, C. W., CHANG, T. T. & YOUNG, K. C. 2014. Apolipoprotein J, a glucose-upregulated molecular chaperone, stabilizes core and NS5A to promote infectious hepatitis C virus virion production. *J Hepatol,* 61**,** 984-93.

LINDENBACH, B. D. 2013. Virion Assembly and Release. *Hepatitis C Virus: From Molecular Virology to Antiviral Therapy,* 369**,** 199-218.

LINDENBACH, B. D., EVANS, M. J., SYDER, A. J., WOLK, B., TELLINGHUISEN, T. L., LIU, C. C., MARUYAMA, T., HYNES, R. O., BURTON, D. R., MCKEATING, J. A. & RICE, C. M. 2005. Complete replication of hepatitis C virus in cell culture. *Science,* 309**,** 623-6.

LINDENBACH, B. D., MEULEMAN, P., PLOSS, A., VANWOLLEGHEM, T., SYDER, A. J., MCKEATING, J. A., LANFORD, R. E., FEINSTONE, S. M., MAJOR, M. E., LEROUX-ROELS, G. & RICE, C. M. 2006. Cell culture-grown hepatitis C virus is infectious in vivo and can be recultured in vitro. *Proc Natl Acad Sci U S A,* 103**,** 3805-9.

LINDENBACH, B. D. & RICE, C. M. 2013. The ins and outs of hepatitis C virus entry and assembly. *Nat Rev Microbiol,* 11**,** 688-700.

LOHMANN, V. & BARTENSCHLAGER, R. 2014. On the history of hepatitis C virus cell culture systems. *J Med Chem,* 57**,** 1627-42.

LOHMANN, V., KORNER, F., KOCH, J., HERIAN, U., THEILMANN, L. & BARTENSCHLAGER, R. 1999a. Replication of subgenomic hepatitis C virus RNAs in a hepatoma cell line. *Science,* 285**,** 110-3.

LOHMANN, V., OVERTON, H. & BARTENSCHLAGER, R. 1999b. Selective stimulation of hepatitis C virus and pestivirus NS5B RNA polymerase activity by GTP. *J Biol Chem,* 274**,** 10807-15.

LOSFELD, M. E., NG, B. G., KIRCHER, M., BUCKINGHAM, K. J., TURNER, E. H., EROSHKIN, A., SMITH, J. D., SHENDURE, J., NICKERSON, D. A., BAMSHAD, M. J., UNIVERSITY OF WASHINGTON CENTER FOR MENDELIAN, G. & FREEZE, H. H. 2014. A new congenital disorder of glycosylation caused by a mutation in SSR4, the signal sequence receptor 4 protein of the TRAP complex. *Hum Mol Genet,* 23**,** 1602-5.

LOVE, R. A., BRODSKY, O., HICKEY, M. J., WELLS, P. A. & CRONIN, C. N. 2009. Crystal structure of a novel dimeric form of NS5A domain I protein from hepatitis C virus. *J Virol,* 83**,** 4395-403.

LUNDIN, M., LINDSTROM, H., GRONWALL, C. & PERSSON, M. A. 2006. Dual topology of the processed hepatitis C virus protein NS4B is influenced by the NS5A protein. *J Gen Virol,* 87**,** 3263-72.

LUPBERGER, J., ZEISEL, M. B., XIAO, F., THUMANN, C., FOFANA, I., ZONA, L., DAVIS, C., MEE, C. J., TUREK, M., GORKE, S., ROYER, C., FISCHER, B., ZAHID, M. N., LAVILLETTE, D., FRESQUET, J., COSSET, F. L., ROTHENBERG, S. M., PIETSCHMANN, T., PATEL, A. H., PESSAUX, P., DOFFOEL, M., RAFFELSBERGER,

W., POCH, O., MCKEATING, J. A., BRINO, L. & BAUMERT, T. F. 2011. EGFR and EphA2 are host factors for hepatitis C virus entry and possible targets for antiviral therapy. *Nat Med,* 17**,** 589-95.

LYTLE, J. R., WU, L. & ROBERTSON, H. D. 2002. Domains on the hepatitis C virus internal ribosome entry site for 40s subunit binding. *RNA,* 8**,** 1045-55.

MA, Y., ANANTPADMA, M., TIMPE, J. M., SHANMUGAM, S., SINGH, S. M., LEMON, S. M. & YI, M. 2011. Hepatitis C virus NS2 protein serves as a scaffold for virus assembly by interacting with both structural and nonstructural proteins. *J Virol,* 85**,** 86-97.

MA, Y., YATES, J., LIANG, Y., LEMON, S. M. & YI, M. 2008. NS3 helicase domains involved in infectious intracellular hepatitis C virus particle assembly. *J Virol,* 82**,** 7624-39.

MACDONALD, A., CROWDER, K., STREET, A., MCCORMICK, C. & HARRIS, M. 2004. The hepatitis C virus NS5A protein binds to members of the Src family of tyrosine kinases and regulates kinase activity. *J Gen Virol,* 85**,** 721-9.

MACPHERSON, J. I., SIDDERS, B., WIELAND, S., ZHONG, J., TARGETT-ADAMS, P., LOHMANN, V., BACKES, P., DELPUECH-ADAMS, O., CHISARI, F., LEWIS, M., PARKINSON, T. & ROBERTSON, D. L. 2011. An integrated transcriptomic and meta-analysis of hepatoma cells reveals factors that influence susceptibility to HCV infection. *PLoS One,* 6**,** e25584.

MANKOURI, J., DALLAS, M. L., HUGHES, M. E., GRIFFIN, S. D., MACDONALD, A., PEERS, C. & HARRIS, M. 2009. Suppression of a pro-apoptotic K+ channel as a mechanism for hepatitis C virus persistence. *Proc Natl Acad Sci U S A,* 106**,** 15903-8.

MANKOURI, J., GRIFFIN, S. & HARRIS, M. 2008. The hepatitis C virus non-structural protein NS5A alters the trafficking profile of the epidermal growth factor receptor. *Traffic,* 9**,** 1497-509.

MANKOURI, J., WALTER, C., STEWART, H., BENTHAM, M., PARK, W. S., HEO, W. D., FUKUDA, M., GRIFFIN, S. & HARRIS, M. 2016. Release of Infectious Hepatitis C Virus from Huh7 Cells Occurs via a trans-Golgi Network-to-Endosome Pathway Independent of Very-Low-Density Lipoprotein Secretion. *J Virol,* 90**,** 7159-70.

MANNS, M. P., CORNBERG, M. & WEDEMEYER, H. 2001. Current and future treatment of hepatitis C. *Indian J Gastroenterol,* 20 Suppl 1**,** C47-51.

MANNS, M. P. & VON HAHN, T. 2013. Novel therapies for hepatitis C - one pill fits all? *Nat Rev Drug Discov,* 12**,** 595-610.

MANTRY, P. S. & PATHAK, L. 2016. Dasabuvir (ABT333) for the treatment of chronic HCV genotype I: a new face of cure, an expert review. *Expert Rev Anti Infect Ther,* 14**,** 157-65.

MARINO, Z., VAN BOMMEL, F., FORNS, X. & BERG, T. 2014. New concepts of sofosbuvir-based treatment regimens in patients with hepatitis C. *Gut,* 63**,** 207-15.

MARTIN, D. N. & UPRICHARD, S. L. 2013. Identification of transferrin receptor 1 as a hepatitis C virus entry factor. *Proc Natl Acad Sci U S A,* 110**,** 10777-82.

MASAKI, T., MATSUNAGA, S., TAKAHASHI, H., NAKASHIMA, K., KIMURA, Y., ITO, M., MATSUDA, M., MURAYAMA, A., KATO, T., HIRANO, H., ENDO, Y., LEMON, S. M., WAKITA, T., SAWASAKI, T. & SUZUKI, T. 2014. Involvement of hepatitis C virus

NS5A hyperphosphorylation mediated by casein kinase I-alpha in infectious virus production. *J Virol,* 88**,** 7541-55.

MASAKI, T., SUZUKI, R., MURAKAMI, K., AIZAKI, H., ISHII, K., MURAYAMA, A., DATE, T., MATSUURA, Y., MIYAMURA, T., WAKITA, T. & SUZUKI, T. 2008. Interaction of hepatitis C virus nonstructural protein 5A with core protein is critical for the production of infectious virus particles. *J Virol,* 82**,** 7964-76.

MASUMI, A., AIZAKI, H., SUZUKI, T., DUHADAWAY, J. B., PRENDERGAST, G. C., KOMURO, K. & FUKAZAWA, H. 2005. Reduction of hepatitis C virus NS5A phosphorylation through its interaction with amphiphysin II. *Biochem Biophys Res Commun,* 336**,** 572-8.

MCCORMICK, C. J., MAUCOURANT, S., GRIFFIN, S., ROWLANDS, D. J. & HARRIS, M. 2006. Tagging of NS5A expressed from a functional hepatitis C virus replicon. *J Gen Virol,* 87**,** 635-40.

MCCOWN, M. F., RAJYAGURU, S., KULAR, S., CAMMACK, N. & NAJERA, I. 2009. GT-1a or GT-1b subtype-specific resistance profiles for hepatitis C virus inhibitors telaprevir and HCV-796. *Antimicrob Agents Chemother,* 53**,** 2129-32.

MCGIVERN, D. R., MASAKI, T., WILLIFORD, S., INGRAVALLO, P., FENG, Z., LAHSER, F., ASANTE-APPIAH, E., NEDDERMANN, P., DE FRANCESCO, R., HOWE, A. Y. & LEMON, S. M. 2014. Kinetic analyses reveal potent and early blockade of hepatitis C virus assembly by NS5A inhibitors. *Gastroenterology,* 147**,** 453-62 e7.

MCLAUCHLAN, J. 2000. Properties of the hepatitis C virus core protein: a structural protein that modulates cellular processes. *J Viral Hepat,* 7**,** 2-14.

MCLAUCHLAN, J., LEMBERG, M. K., HOPE, G. & MARTOGLIO, B. 2002. Intramembrane proteolysis promotes trafficking of hepatitis C virus core protein to lipid droplets. *EMBO J,* 21**,** 3980-8.

MCWHIRTER, S. M., FITZGERALD, K. A., ROSAINS, J., ROWE, D. C., GOLENBOCK, D. T. & MANIATIS, T. 2004. IFN-regulatory factor 3-dependent gene expression is defective in Tbk1-deficient mouse embryonic fibroblasts. *Proc Natl Acad Sci U S A,* 101**,** 233-8.

MEEX, S. J., ANDREO, U., SPARKS, J. D. & FISHER, E. A. 2011. Huh-7 or HepG2 cells: which is the better model for studying human apolipoprotein-B100 assembly and secretion? *J Lipid Res,* 52**,** 152-8.

MERCER, D. F., SCHILLER, D. E., ELLIOTT, J. F., DOUGLAS, D. N., HAO, C., RINFRET, A., ADDISON, W. R., FISCHER, K. P., CHURCHILL, T. A., LAKEY, J. R., TYRRELL, D. L. & KNETEMAN, N. M. 2001. Hepatitis C virus replication in mice with chimeric human livers. *Nat Med,* 7**,** 927-33.

MERZ, A., LONG, G., HIET, M. S., BRUGGER, B., CHLANDA, P., ANDRE, P., WIELAND, F., KRIJNSE-LOCKER, J. & BARTENSCHLAGER, R. 2011. Biochemical and morphological properties of hepatitis C virus particles and determination of their lipidome. *J Biol Chem,* 286**,** 3018-32.

MESMIN, B., BIGAY, J., MOSER VON FILSECK, J., LACAS-GERVAIS, S., DRIN, G. & ANTONNY, B. 2013. A four-step cycle driven by PI(4)P hydrolysis directs sterol/PI(4)P exchange by the ER-Golgi tether OSBP. *Cell,* 155**,** 830-43.

MESSINA, J. P., HUMPHREYS, I., FLAXMAN, A., BROWN, A., COOKE, G. S., PYBUS, O. G. & BARNES, E. 2015. Global distribution and prevalence of hepatitis C virus genotypes. *Hepatology,* 61**,** 77-87.

MILLER, S. & KRIJNSE-LOCKER, J. 2008. Modification of intracellular membrane structures for virus replication. *Nat Rev Microbiol,* 6**,** 363-74.

MIYANARI, Y., ATSUZAWA, K., USUDA, N., WATASHI, K., HISHIKI, T., ZAYAS, M., BARTENSCHLAGER, R., WAKITA, T., HIJIKATA, M. & SHIMOTOHNO, K. 2007. The lipid droplet is an important organelle for hepatitis C virus production. *Nat Cell Biol,* 9**,** 1089-97.

MOHD HANAFIAH, K., GROEGER, J., FLAXMAN, A. D. & WIERSMA, S. T. 2013. Global epidemiology of hepatitis C virus infection: new estimates of age-specific antibody to HCV seroprevalence. *Hepatology,* 57**,** 1333-42.

MONAZAHIAN, M., BOHME, I., BONK, S., KOCH, A., SCHOLZ, C., GRETHE, S. & THOMSSEN, R. 1999. Low density lipoprotein receptor as a candidate receptor for hepatitis C virus. *J Med Virol,* 57**,** 223-9.

MONTSERRET, R., SAINT, N., VANBELLE, C., SALVAY, A. G., SIMORRE, J. P., EBEL, C., SAPAY, N., RENISIO, J. G., BOCKMANN, A., STEINMANN, E., PIETSCHMANN, T., DUBUISSON, J., CHIPOT, C. & PENIN, F. 2010. NMR structure and ion channel activity of the p7 protein from hepatitis C virus. *J Biol Chem,* 285**,** 31446-61.

MORADPOUR, D., EVANS, M. J., GOSERT, R., YUAN, Z., BLUM, H. E., GOFF, S. P., LINDENBACH, B. D. & RICE, C. M. 2004. Insertion of green fluorescent protein into nonstructural protein 5A allows direct visualization of functional hepatitis C virus replication complexes. *J Virol,* 78**,** 7400-9.

MORIKAWA, K., LANGE, C. M., GOUTTENOIRE, J., MEYLAN, E., BRASS, V., PENIN, F. & MORADPOUR, D. 2011. Nonstructural protein 3-4A: the Swiss army knife of hepatitis C virus. *J Viral Hepat,* 18**,** 305-15.

MOSLEY, R. T., EDWARDS, T. E., MURAKAMI, E., LAM, A. M., GRICE, R. L., DU, J., SOFIA, M. J., FURMAN, P. A. & OTTO, M. J. 2012. Structure of hepatitis C virus polymerase in complex with primer-template RNA. *J Virol,* 86**,** 6503-11.

NAKABAYASHI, H., TAKETA, K., MIYANO, K., YAMANE, T. & SATO, J. 1982. Growth of human hepatoma cells lines with differentiated functions in chemically defined medium. *Cancer Res,* 42**,** 3858-63.

NEDDERMANN, P., CLEMENTI, A. & DE FRANCESCO, R. 1999. Hyperphosphorylation of the hepatitis C virus NS5A protein requires an active NS3 protease, NS4A, NS4B, and NS5A encoded on the same polyprotein. *J Virol,* 73**,** 9984-91.

NEVEU, G., BAROUCH-BENTOV, R., ZIV-AV, A., GERBER, D., JACOB, Y. & EINAV, S. 2012. Identification and targeting of an interaction between a tyrosine motif within hepatitis C virus core protein and AP2M1 essential for viral assembly. *PLoS Pathog,* 8**,** e1002845.

NEVO-YASSAF, I., YAFFE, Y., ASHER, M., RAVID, O., EIZENBERG, S., HENIS, Y. I., NAHMIAS, Y., HIRSCHBERG, K. & SKLAN, E. H. 2012. Role for TBC1D20 and Rab1 in hepatitis C virus replication via interaction with lipid droplet-bound nonstructural protein 5A. *J Virol,* 86**,** 6491-502.

NGURE, M., ISSUR, M., SHKRIABAI, N., LIU, H. W., COSA, G., KVARATSKHELIA, M. & GOTTE, M. 2016. Interactions of the Disordered Domain II of Hepatitis C Virus NS5A with Cyclophilin A, NS5B, and Viral RNA Show Extensive Overlap. *Acs Infectious Diseases,* 2**,** 839-851.

NUNEZ, M. & SORIANO, V. 2005. Hepatitis C virus (HCV) genotypes and disease progression in HIV/HCV-coinfected patients. *J Infect Dis,* 191**,** 1-3.

OKAMOTO, T., NISHIMURA, Y., ICHIMURA, T., SUZUKI, K., MIYAMURA, T., SUZUKI, T., MORIISHI, K. & MATSUURA, Y. 2006. Hepatitis C virus RNA replication is regulated by FKBP8 and Hsp90. *EMBO J,* 25**,** 5015-25.

OLOFSSON, S. O., BOSTROM, P., ANDERSSON, L., RUTBERG, M., PERMAN, J. & BOREN, J. 2009. Lipid droplets as dynamic organelles connecting storage and efflux of lipids. *Biochimica Et Biophysica Acta-Molecular and Cell Biology of Lipids,* 1791**,** 448-458.

OTT, J. J., STEVENS, G. A., GROEGER, J. & WIERSMA, S. T. 2012. Global epidemiology of hepatitis B virus infection: new estimates of age-specific HBsAg seroprevalence and endemicity. *Vaccine,* 30**,** 2212-9.

OTTO, G. A. & PUGLISI, J. D. 2004. The pathway of HCV IRES-mediated translation initiation. *Cell,* 119**,** 369-80.

PAESHUYSE, J., KAUL, A., DE CLERCQ, E., ROSENWIRTH, B., DUMONT, J. M., SCALFARO, P., BARTENSCHLAGER, R. & NEYTS, J. 2006. The non-immunosuppressive cyclosporin DEBIO-025 is a potent inhibitor of hepatitis C virus replication in vitro. *Hepatology,* 43**,** 761-70.

PALOMARES-JEREZ, M. F., GUILLEN, J. & VILLALAIN, J. 2010. Interaction of the N-terminal segment of HCV protein NS5A with model membranes. *Biochim Biophys Acta,* 1798**,** 1212-24.

PAREDES, A. M. & BLIGHT, K. J. 2008. A genetic interaction between hepatitis C virus NS4B and NS3 is important for RNA replication. *J Virol,* 82**,** 10671-83.

PATEL, E. U., COX, A. L., MEHTA, S. H., BOON, D., MULLIS, C. E., ASTEMBORSKI, J., OSBURN, W. O., QUINN, J., REDD, A. D., KIRK, G. D., THOMAS, D. L., QUINN, T. C. & LAEYENDECKER, O. 2016. Use of Hepatitis C Virus (HCV) Immunoglobulin G Antibody Avidity as a Biomarker to Estimate the Population-Level Incidence of HCV Infection. *J Infect Dis,* 214**,** 344-52.

PAUL, D. & BARTENSCHLAGER, R. 2013. Architecture and biogenesis of plus-strand RNA virus replication factories. *World J Virol,* 2**,** 32-48.

PAUL, D. & BARTENSCHLAGER, R. 2015. Flaviviridae Replication Organelles: Oh, What a Tangled Web We Weave. *Annu Rev Virol,* 2**,** 289-310.

PAUL, D., HOPPE, S., SAHER, G., KRIJNSE-LOCKER, J. & BARTENSCHLAGER, R. 2013. Morphological and biochemical characterization of the membranous hepatitis C virus replication compartment. *J Virol,* 87**,** 10612-27.

PAUL, D., MADAN, V. & BARTENSCHLAGER, R. 2014. Hepatitis C virus RNA replication and assembly: living on the fat of the land. *Cell Host Microbe,* 16**,** 569-79.

PAUL, D., ROMERO-BREY, I., GOUTTENOIRE, J., STOITSOVA, S., KRIJNSE-LOCKER, J., MORADPOUR, D. & BARTENSCHLAGER, R. 2011. NS4B self-interaction through conserved C-terminal elements is required for the establishment of functional hepatitis C virus replication complexes. *J Virol,* 85**,** 6963-76.

PEARLMAN, B. L. & SJOGREN, M. H. 2010. Treatment options for HCV nonresponders and relapse patients. *Gastroenterol Hepatol (N Y),* 6**,** 1-12.

PEARLMAN, B. L. & TRAUB, N. 2011. Sustained virologic response to antiviral therapy for chronic hepatitis C virus infection: a cure and so much more. *Clin Infect Dis,* 52**,** 889-900.

PENIN, F., BRASS, V., APPEL, N., RAMBOARINA, S., MONTSERRET, R., FICHEUX, D., BLUM, H. E., BARTENSCHLAGER, R. & MORADPOUR, D. 2004. Structure and

function of the membrane anchor domain of hepatitis C virus nonstructural protein 5A. *J Biol Chem,* 279**,** 40835-43.

PEREZ-BERNA, A. J., RODRIGUEZ, M. J., CHICHON, F. J., FRIESLAND, M. F., SORRENTINO, A., CARRASCOSA, J. L., PEREIRO, E. & GASTAMINZA, P. 2016. Structural Changes In Cells Imaged by Soft X-ray Cryo-Tomography During Hepatitis C Virus Infection. *ACS Nano,* 10**,** 6597-611.

PHAN, T., BERAN, R. K., PETERS, C., LORENZ, I. C. & LINDENBACH, B. D. 2009. Hepatitis C virus NS2 protein contributes to virus particle assembly via opposing epistatic interactions with the E1-E2 glycoprotein and NS3-NS4A enzyme complexes. *J Virol,* 83**,** 8379-95.

PHAN, T., KOHLWAY, A., DIMBERU, P., PYLE, A. M. & LINDENBACH, B. D. 2011. The acidic domain of hepatitis C virus NS4A contributes to RNA replication and virus particle assembly. *J Virol,* 85**,** 1193-204.

PICHLMAIR, A., KANDASAMY, K., ALVISI, G., MULHERN, O., SACCO, R., HABJAN, M., BINDER, M., STEFANOVIC, A., EBERLE, C. A., GONCALVES, A., BURCKSTUMMER, T., MULLER, A. C., FAUSTER, A., HOLZE, C., LINDSTEN, K., GOODBOURN, S., KOCHS, G., WEBER, F., BARTENSCHLAGER, R., BOWIE, A. G., BENNETT, K. L., COLINGE, J. & SUPERTI-FURGA, G. 2012. Viral immune modulators perturb the human molecular network by common and unique strategies. *Nature,* 487**,** 486-90.

PIETSCHMANN, T., KAUL, A., KOUTSOUDAKIS, G., SHAVINSKAYA, A., KALLIS, S., STEINMANN, E., ABID, K., NEGRO, F., DREUX, M., COSSET, F. L. & BARTENSCHLAGER, R. 2006. Construction and characterization of infectious intragenotypic and intergenotypic hepatitis C virus chimeras. *Proc Natl Acad Sci U S A,* 103**,** 7408-13.

PIETSCHMANN, T., ZAYAS, M., MEULEMAN, P., LONG, G., APPEL, N., KOUTSOUDAKIS, G., KALLIS, S., LEROUX-ROELS, G., LOHMANN, V. & BARTENSCHLAGER, R. 2009. Production of infectious genotype 1b virus particles in cell culture and impairment by replication enhancing mutations. *PLoS Pathog,* 5**,** e1000475.

PLOEN, D., HAFIRASSOU, M. L., HIMMELSBACH, K., SAUTER, D., BINIOSSEK, M. L., WEISS, T. S., BAUMERT, T. F., SCHUSTER, C. & HILDT, E. 2013. TIP47 plays a crucial role in the life cycle of hepatitis C virus. *J Hepatol,* 58**,** 1081-8.

PODEVIN, P., CARPENTIER, A., PENE, V., AOUDJEHANE, L., CARRIERE, M., ZAIDI, S., HERNANDEZ, C., CALLE, V., MERITET, J. F., SCATTON, O., DREUX, M., COSSET, F. L., WAKITA, T., BARTENSCHLAGER, R., DEMIGNOT, S., CONTI, F., ROSENBERG, A. R. & CALMUS, Y. 2010. Production of infectious hepatitis C virus in primary cultures of human adult hepatocytes. *Gastroenterology,* 139**,** 1355-64.

POL, S., COROUGE, M. & VALLET-PICHARD, A. 2016. Daclatasvir-sofosbuvir combination therapy with or without ribavirin for hepatitis C virus infection: from the clinical trials to real life. *Hepat Med,* 8**,** 21-6.

POLARIS OBSERVATORY, H. C. V. C. 2017. Global prevalence and genotype distribution of hepatitis C virus infection in 2015: a modelling study. *Lancet Gastroenterol Hepatol,* 2**,** 161-176.

POLYAK, S. J., KLEIN, K. C., SHOJI, I., MIYAMURA, T. & LINGAPPA, J. R. 2006. Assemble and Interact: Pleiotropic Functions of the HCV Core Protein. *In:* TAN, S. L. (ed.) *Hepatitis C Viruses: Genomes and Molecular Biology.* Norfolk (UK).

POORDAD, F., FELIZARTA, F., ASATRYAN, A., SULKOWSKI, M. S., REINDOLLAR, R. W., LANDIS, C. S., GORDON, S. C., FLAMM, S. L., FRIED, M. W., BERNSTEIN, D. E., LIN, C. W., LIU, R., LOVELL, S. S., NG, T. I., KORT, J. & MENSA, F. J. 2017. Glecaprevir and pibrentasvir for 12 weeks for hepatitis C virus genotype 1 infection and prior direct-acting antiviral treatment. *Hepatology,* 66**,** 389-397.

POPESCU, C. I., CALLENS, N., TRINEL, D., ROINGEARD, P., MORADPOUR, D., DESCAMPS, V., DUVERLIE, G., PENIN, F., HELIOT, L., ROUILLE, Y. & DUBUISSON, J. 2011. NS2 protein of hepatitis C virus interacts with structural and non-structural proteins towards virus assembly. *PLoS Pathog,* 7**,** e1001278.

PREMKUMAR, A., WILSON, L., EWART, G. D. & GAGE, P. W. 2004. Cation-selective ion channels formed by p7 of hepatitis C virus are blocked by hexamethylene amiloride. *FEBS Lett,* 557**,** 99-103.

QI, H. F., OLSON, C. A., WU, N. C., KE, R. A., LOVERDO, C., CHU, V., TRUONG, S., REMENYI, R., CHEN, Z. G., DU, Y. S., SU, S. Y., AL-MAWSAWI, L. Q., WU, T. T., CHEN, S. H., LIN, C. Y., ZHONG, W. D., LLOYD-SMITH, J. O. & SUN, R. 2014. A Quantitative High-Resolution Genetic Profile Rapidly Identifies Sequence Determinants of Hepatitis C Viral Fitness and Drug Sensitivity. *Plos Pathogens,* 10.

QUEZADA, E. M. & KANE, C. M. 2013. The Stimulatory Mechanism of Hepatitis C Virus NS5A Protein on the NS5B Catalyzed Replication Reaction In Vitro. *Open Biochem J,* 7**,** 11-4.

QUINTAVALLE, M., SAMBUCINI, S., SUMMA, V., ORSATTI, L., TALAMO, F., DE FRANCESCO, R. & NEDDERMANN, P. 2007. Hepatitis C virus NS5A is a direct substrate of casein kinase I-alpha, a cellular kinase identified by inhibitor affinity chromatography using specific NS5A hyperphosphorylation inhibitors. *J Biol Chem,* 282**,** 5536-44.

RANJITH-KUMAR, C. T., GUTSHALL, L., SARISKY, R. T. & KAO, C. C. 2003. Multiple interactions within the hepatitis C virus RNA polymerase repress primer-dependent RNA synthesis. *J Mol Biol,* 330**,** 675-85.

RAU, M., BAUR, K. & GEIER, A. 2012. Host genetic variants in the pathogenesis of hepatitis C. *Viruses,* 4**,** 3281-302.

REIN, D. B., STEVENS, G. A., THEAKER, J., WITTENBORN, J. S. & WIERSMA, S. T. 2012. The global burden of hepatitis E virus genotypes 1 and 2 in 2005. *Hepatology,* 55**,** 988-97.

REISS, S., HARAK, C., ROMERO-BREY, I., RADUJKOVIC, D., KLEIN, R., RUGGIERI, A., REBHAN, I., BARTENSCHLAGER, R. & LOHMANN, V. 2013. The lipid kinase phosphatidylinositol-4 kinase III alpha regulates the phosphorylation status of hepatitis C virus NS5A. *PLoS Pathog,* 9**,** e1003359.

REISS, S., REBHAN, I., BACKES, P., ROMERO-BREY, I., ERFLE, H., MATULA, P., KADERALI, L., POENISCH, M., BLANKENBURG, H., HIET, M. S., LONGERICH, T., DIEHL, S., RAMIREZ, F., BALLA, T., ROHR, K., KAUL, A., BUHLER, S., PEPPERKOK, R., LENGAUER, T., ALBRECHT, M., EILS, R., SCHIRMACHER, P., LOHMANN, V. & BARTENSCHLAGER, R. 2011. Recruitment and activation of a lipid kinase by hepatitis C virus NS5A is essential for integrity of the membranous replication compartment. *Cell Host Microbe,* 9**,** 32-45.

REMENYI, R., QI, H., SU, S. Y., CHEN, Z., WU, N. C., ARUMUGASWAMI, V., TRUONG, S., CHU, V., STOKELMAN, T., LO, H. H., OLSON, C. A., WU, T. T., CHEN, S. H., LIN, C.

Y. & SUN, R. 2014. A comprehensive functional map of the hepatitis C virus genome provides a resource for probing viral proteins. *MBio,* 5**,** e01469-14.

REYNOLDS, J. E., KAMINSKI, A., CARROLL, A. R., CLARKE, B. E., ROWLANDS, D. J. & JACKSON, R. J. 1996. Internal initiation of translation of hepatitis C virus RNA: the ribosome entry site is at the authentic initiation codon. *RNA,* 2**,** 867-78.

REYNOLDS, J. E., KAMINSKI, A., KETTINEN, H. J., GRACE, K., CLARKE, B. E., CARROLL, A. R., ROWLANDS, D. J. & JACKSON, R. J. 1995. Unique features of internal initiation of hepatitis C virus RNA translation. *EMBO J,* 14**,** 6010-20.

RIGAT, K. L., LU, H., WANG, Y. K., ARGYROU, A., FANSLAU, C., BENO, B., WANG, Y., MARCINKEVICIENE, J., DING, M., GENTLES, R. G., GAO, M., ABELL, L. M. & ROBERTS, S. B. 2014. Mechanism of inhibition for BMS-791325, a novel non-nucleoside inhibitor of hepatitis C virus NS5B polymerase. *J Biol Chem,* 289**,** 33456-68.

RODRIGUEZ, P., MUNROE, D., PRAWITT, D., CHU, L. L., BRIC, E., KIM, J., REID, L. H., DAVIES, C., NAKAGAMA, H., LOEBBERT, R., WINTERPACHT, A., PETRUZZI, M. J., HIGGINS, M. J., NOWAK, N., EVANS, G., SHOWS, T., WEISSMAN, B. E., ZABEL, B., HOUSMAN, D. E. & PELLETIER, J. 1997. Functional characterization of human nucleosome assembly protein-2 (NAP1L4) suggests a role as a histone chaperone. *Genomics,* 44**,** 253-65.

ROMERO-BREY, I., MERZ, A., CHIRAMEL, A., LEE, J. Y., CHLANDA, P., HASELMAN, U., SANTARELLA-MELLWIG, R., HABERMANN, A., HOPPE, S., KALLIS, S., WALTHER, P., ANTONY, C., KRIJNSE-LOCKER, J. & BARTENSCHLAGER, R. 2012. Three-dimensional architecture and biogenesis of membrane structures associated with hepatitis C virus replication. *PLoS Pathog,* 8**,** e1003056.

ROSENTHAL, E. S. & GRAHAM, C. S. 2016. Price and affordability of direct-acting antiviral regimens for hepatitis C virus in the United States. *Infect Agent Cancer,* 11**,** 24.

ROSS-THRIEPLAND, D., AMAKO, Y. & HARRIS, M. 2013. The C terminus of NS5A domain II is a key determinant of hepatitis C virus genome replication, but is not required for virion assembly and release. *J Gen Virol,* 94**,** 1009-18.

ROSS-THRIEPLAND, D. & HARRIS, M. 2014a. Hepatitis C virus NS5A: enigmatic but still promiscuous 10 years on! *J Gen Virol*.

ROSS-THRIEPLAND, D. & HARRIS, M. 2014b. Insights into the complexity and functionality of hepatitis C virus NS5A phosphorylation. *J Virol,* 88**,** 1421-32.

ROSS-THRIEPLAND, D. & HARRIS, M. 2015. Hepatitis C virus NS5A: enigmatic but still promiscuous 10 years on! *J Gen Virol,* 96**,** 727-38.

SAINZ, B., JR., BARRETTO, N., MARTIN, D. N., HIRAGA, N., IMAMURA, M., HUSSAIN, S., MARSH, K. A., YU, X., CHAYAMA, K., ALREFAI, W. A. & UPRICHARD, S. L. 2012. Identification of the Niemann-Pick C1-like 1 cholesterol absorption receptor as a new hepatitis C virus entry factor. *Nat Med,* 18**,** 281-5.

SALAM, K. A. & AKIMITSU, N. 2013. Hepatitis C virus NS3 inhibitors: current and future perspectives. *Biomed Res Int,* 2013**,** 467869.

SALLOUM, S., WANG, H., FERGUSON, C., PARTON, R. G. & TAI, A. W. 2013. Rab18 binds to hepatitis C virus NS5A and promotes interaction between sites of viral replication and lipid droplets. *PLoS Pathog,* 9**,** e1003513.

SAPAY, N., MONTSERRET, R., CHIPOT, C., BRASS, V., MORADPOUR, D., DELEAGE, G. & PENIN, F. 2006. NMR structure and molecular dynamics of the in-plane

membrane anchor of nonstructural protein 5A from bovine viral diarrhea virus. *Biochemistry,* 45**,** 2221-33.

SARRAZIN, C. & ZEUZEM, S. 2010. Resistance to direct antiviral agents in patients with hepatitis C virus infection. *Gastroenterology,* 138**,** 447-62.

SCARSELLI, E., ANSUINI, H., CERINO, R., ROCCASECCA, R. M., ACALI, S., FILOCAMO, G., TRABONI, C., NICOSIA, A., CORTESE, R. & VITELLI, A. 2002. The human scavenger receptor class B type I is a novel candidate receptor for the hepatitis C virus. *EMBO J,* 21**,** 5017-25.

SCHEFFZEK, K. & AHMADIAN, M. R. 2005. GTPase activating proteins: structural and functional insights 18 years after discovery. *Cell Mol Life Sci,* 62**,** 3014-38.

SCHOGGINS, J. W. & RICE, C. M. 2013. Innate immune responses to hepatitis C virus. *Curr Top Microbiol Immunol,* 369**,** 219-42.

SCHREIBER, G. B., BUSCH, M. P., KLEINMAN, S. H. & KORELITZ, J. J. 1996. The risk of transfusion-transmitted viral infections. The Retrovirus Epidemiology Donor Study. *N Engl J Med,* 334**,** 1685-90.

SCRIMA, N., CAILLET-SAGUY, C., VENTURA, M., HARRUS, D., ASTIER-GIN, T. & BRESSANELLI, S. 2012. Two crucial early steps in RNA synthesis by the hepatitis C virus polymerase involve a dual role of residue 405. *J Virol,* 86**,** 7107-17.

SHARMA, N. R., MATEU, G., DREUX, M., GRAKOUI, A., COSSET, F. L. & MELIKYAN, G. B. 2011. Hepatitis C virus is primed by CD81 protein for low pH-dependent fusion. *J Biol Chem,* 286**,** 30361-76.

SHAVINSKAYA, A., BOULANT, S., PENIN, F., MCLAUCHLAN, J. & BARTENSCHLAGER, R. 2007. The lipid droplet binding domain of hepatitis C virus core protein is a major determinant for efficient virus assembly. *J Biol Chem,* 282**,** 37158-69.

SHIMAKAMI, T., HIJIKATA, M., LUO, H., MA, Y. Y., KANEKO, S., SHIMOTOHNO, K. & MURAKAMI, S. 2004. Effect of interaction between hepatitis C virus NS5A and NS5B on hepatitis C virus RNA replication with the hepatitis C virus replicon. *J Virol,* 78**,** 2738-48.

SHIROTA, Y., LUO, H., QIN, W., KANEKO, S., YAMASHITA, T., KOBAYASHI, K. & MURAKAMI, S. 2002. Hepatitis C virus (HCV) NS5A binds RNA-dependent RNA polymerase (RdRP) NS5B and modulates RNA-dependent RNA polymerase activity. *J Biol Chem,* 277**,** 11149-55.

SIMISTER, P., SCHMITT, M., GEITMANN, M., WICHT, O., DANIELSON, U. H., KLEIN, R., BRESSANELLI, S. & LOHMANN, V. 2009. Structural and functional analysis of hepatitis C virus strain JFH1 polymerase. *J Virol,* 83**,** 11926-39.

SIMMONDS, P. 2004. Genetic diversity and evolution of hepatitis C virus--15 years on. *J Gen Virol,* 85**,** 3173-88.

SIMMONDS, P. 2012. SSE: a nucleotide and amino acid sequence analysis platform. *BMC Res Notes,* 5**,** 50.

SIMMONDS, P. 2013. The origin of hepatitis C virus. *Curr Top Microbiol Immunol,* 369**,** 1-15.

SIMMONDS, P., BECHER, P., BUKH, J., GOULD, E. A., MEYERS, G., MONATH, T., MUERHOFF, S., PLETNEV, A., RICO-HESSE, R., SMITH, D. B., STAPLETON, J. T. & ICTV REPORT, C. 2017. ICTV Virus Taxonomy Profile: Flaviviridae. *J Gen Virol,* 98**,** 2-3.

SIMMONDS, P., BUKH, J., COMBET, C., DELEAGE, G., ENOMOTO, N., FEINSTONE, S., HALFON, P., INCHAUSPE, G., KUIKEN, C., MAERTENS, G., MIZOKAMI, M., MURPHY, D. G., OKAMOTO, H., PAWLOTSKY, J. M., PENIN, F., SABLON, E., SHIN, I. T., STUYVER, L. J., THIEL, H. J., VIAZOV, S., WEINER, A. J. & WIDELL, A. 2005. Consensus proposals for a unified system of nomenclature of hepatitis C virus genotypes. *Hepatology,* 42**,** 962-73.

SKLAN, E. H., SERRANO, R. L., EINAV, S., PFEFFER, S. R., LAMBRIGHT, D. G. & GLENN, J. S. 2007a. TBC1D20 is a Rab1 GTPase-activating protein that mediates hepatitis C virus replication. *J Biol Chem,* 282**,** 36354-61.

SKLAN, E. H., STASCHKE, K., OAKES, T. M., ELAZAR, M., WINTERS, M., AROETI, B., DANIELI, T. & GLENN, J. S. 2007b. A Rab-GAP TBC domain protein binds hepatitis C virus NS5A and mediates viral replication. *J Virol,* 81**,** 11096-105.

SMITH, D. B., BUKH, J., KUIKEN, C., MUERHOFF, A. S., RICE, C. M., STAPLETON, J. T. & SIMMONDS, P. 2014. Expanded classification of hepatitis C virus into 7 genotypes and 67 subtypes: updated criteria and genotype assignment web resource. *Hepatology,* 59**,** 318-27.

SOFIA, M. J., CHANG, W., FURMAN, P. A., MOSLEY, R. T. & ROSS, B. S. 2012. Nucleoside, nucleotide, and non-nucleoside inhibitors of hepatitis C virus NS5B RNA-dependent RNA-polymerase. *J Med Chem,* 55**,** 2481-531.

SONG, Y., FRIEBE, P., TZIMA, E., JUNEMANN, C., BARTENSCHLAGER, R. & NIEPMANN, M. 2006. The hepatitis C virus RNA 3'-untranslated region strongly enhances translation directed by the internal ribosome entry site. *J Virol,* 80**,** 11579-88.

SOURISSEAU, M., MICHTA, M. L., ZONY, C., ISRAELOW, B., HOPCRAFT, S. E., NARBUS, C. M., PARRA MARTIN, A. & EVANS, M. J. 2013. Temporal analysis of hepatitis C virus cell entry with occludin directed blocking antibodies. *PLoS Pathog,* 9**,** e1003244.

SPAHN, C. M., KIEFT, J. S., GRASSUCCI, R. A., PENCZEK, P. A., ZHOU, K., DOUDNA, J. A. & FRANK, J. 2001. Hepatitis C virus IRES RNA-induced changes in the conformation of the 40s ribosomal subunit. *Science,* 291**,** 1959-62.

STANAWAY, J. D., FLAXMAN, A. D., NAGHAVI, M., FITZMAURICE, C., VOS, T., ABUBAKAR, I., ABU-RADDAD, L. J., ASSADI, R., BHALA, N., COWIE, B., FOROUZANFOUR, M. H., GROEGER, J., HANAFIAH, K. M., JACOBSEN, K. H., JAMES, S. L., MACLACHLAN, J., MALEKZADEH, R., MARTIN, N. K., MOKDAD, A. A., MOKDAD, A. H., MURRAY, C. J. L., PLASS, D., RANA, S., REIN, D. B., RICHARDUS, J. H., SANABRIA, J., SAYLAN, M., SHAHRAZ, S., SO, S., VLASSOV, V. V., WEIDERPASS, E., WIERSMA, S. T., YOUNIS, M., YU, C., EL SAYED ZAKI, M. & COOKE, G. S. 2016. The global burden of viral hepatitis from 1990 to 2013: findings from the Global Burden of Disease Study 2013. *Lancet,* 388**,** 1081-1088.

STAPLEFORD, K. A. & LINDENBACH, B. D. 2011. Hepatitis C virus NS2 coordinates virus particle assembly through physical interactions with the E1-E2 glycoprotein and NS3-NS4A enzyme complexes. *J Virol,* 85**,** 1706-17.

STAPLETON, J. T., FOUNG, S., MUERHOFF, A. S., BUKH, J. & SIMMONDS, P. 2011. The GB viruses: a review and proposed classification of GBV-A, GBV-C (HGV), and GBV-D in genus Pegivirus within the family Flaviviridae. *J Gen Virol,* 92**,** 233-46.

STEINMANN, E., PENIN, F., KALLIS, S., PATEL, A. H., BARTENSCHLAGER, R. & PIETSCHMANN, T. 2007. Hepatitis C virus p7 protein is crucial for assembly and release of infectious virions. *PLoS Pathog,* 3**,** e103.

STEINMANN, E. & PIETSCHMANN, T. 2013. Cell culture systems for hepatitis C virus. *Curr Top Microbiol Immunol,* 369**,** 17-48.

STENMARK, H. & OLKKONEN, V. M. 2001. The Rab GTPase family. *Genome Biol,* 2**,** REVIEWS3007.

STEWART, H., BARTLETT, C., ROSS-THRIEPLAND, D., SHAW, J., GRIFFIN, S. & HARRIS, M. 2015. A novel method for the measurement of hepatitis C virus infectious titres using the IncuCyte ZOOM and its application to antiviral screening. *J Virol Methods,* 218**,** 59-65.

SULKOWSKI, M. S., ERON, J. J., WYLES, D., TRINH, R., LALEZARI, J., WANG, C., SLIM, J., BHATTI, L., GATHE, J., RUANE, P. J., ELION, R., BREDEEK, F., BRENNAN, R., BLICK, G., KHATRI, A., GIBBONS, K., HU, Y. B., FREDRICK, L., SCHNELL, G., PILOT-MATIAS, T., TRIPATHI, R., DA SILVA-TILLMANN, B., MCGOVERN, B., CAMPBELL, A. L. & PODSADECKI, T. 2015. Ombitasvir, paritaprevir co-dosed with ritonavir, dasabuvir, and ribavirin for hepatitis C in patients co-infected with HIV-1: a randomized trial. *JAMA,* 313**,** 1223-31.

SUMPTER, R., JR., LOO, Y. M., FOY, E., LI, K., YONEYAMA, M., FUJITA, T., LEMON, S. M. & GALE, M., JR. 2005. Regulating intracellular antiviral defense and permissiveness to hepatitis C virus RNA replication through a cellular RNA helicase, RIG-I. *J Virol,* 79**,** 2689-99.

SUN, J. H., O'BOYLE, D. R., 2ND, FRIDELL, R. A., LANGLEY, D. R., WANG, C., ROBERTS, S. B., NOWER, P., JOHNSON, B. M., MOULIN, F., NOPHSKER, M. J., WANG, Y. K., LIU, M., RIGAT, K., TU, Y., HEWAWASAM, P., KADOW, J., MEANWELL, N. A., COCKETT, M., LEMM, J. A., KRAMER, M., BELEMA, M. & GAO, M. 2015. Resensitizing daclatasvir-resistant hepatitis C variants by allosteric modulation of NS5A. *Nature,* 527**,** 245-8.

SY, T. & JAMAL, M. M. 2006. Epidemiology of hepatitis C virus (HCV) infection. *Int J Med Sci,* 3**,** 41-6.

TAGUWA, S., OKAMOTO, T., ABE, T., MORI, Y., SUZUKI, T., MORIISHI, K. & MATSUURA, Y. 2008. Human butyrate-induced transcript 1 interacts with hepatitis C virus NS5A and regulates viral replication. *J Virol,* 82**,** 2631-41.

TAI, C. L., CHI, W. K., CHEN, D. S. & HWANG, L. H. 1996. The helicase activity associated with hepatitis C virus nonstructural protein 3 (NS3). *J Virol,* 70**,** 8477-84.

TAMAI, K., SHIINA, M., TANAKA, N., NAKANO, T., YAMAMOTO, A., KONDO, Y., KAKAZU, E., INOUE, J., FUKUSHIMA, K., SANO, K., UENO, Y., SHIMOSEGAWA, T. & SUGAMURA, K. 2012. Regulation of hepatitis C virus secretion by the Hrs-dependent exosomal pathway. *Virology,* 422**,** 377-385.

TARGETT-ADAMS, P., GRAHAM, E. J., MIDDLETON, J., PALMER, A., SHAW, S. M., LAVENDER, H., BRAIN, P., TRAN, T. D., JONES, L. H., WAKENHUT, F., STAMMEN, B., PRYDE, D., PICKFORD, C. & WESTBY, M. 2011. Small molecules targeting hepatitis C virus-encoded NS5A cause subcellular redistribution of their target: insights into compound modes of action. *J Virol,* 85**,** 6353-68.

TARGETT-ADAMS, P., HOPE, G., BOULANT, S. & MCLAUCHLAN, J. 2008. Maturation of hepatitis C virus core protein by signal peptide peptidase is required for virus production. *J Biol Chem,* 283**,** 16850-9.

TARGETT-ADAMS, P. & MCLAUCHLAN, J. 2005. Development and characterization of a transient-replication assay for the genotype 2a hepatitis C virus subgenomic replicon. *J Gen Virol,* 86**,** 3075-80.

TEDBURY, P., WELBOURN, S., PAUSE, A., KING, B., GRIFFIN, S. & HARRIS, M. 2011. The subcellular localization of the hepatitis C virus non-structural protein NS2 is regulated by an ion channel-independent function of the p7 protein. *J Gen Virol,* 92**,** 819-30.

TELLINGHUISEN, T. L. & FOSS, K. L. 2008. Regulation of hepatitis C virion production via phosphorylation of the NS5A protein. *Plos Pathogens,* 4.

TELLINGHUISEN, T. L., FOSS, K. L. & TREADAWAY, J. 2008a. Regulation of hepatitis C virion production via phosphorylation of the NS5A protein. *PLoS Pathog,* 4**,** e1000032.

TELLINGHUISEN, T. L., FOSS, K. L., TREADAWAY, J. C. & RICE, C. M. 2008b. Identification of residues required for RNA replication in domains II and III of the hepatitis C virus NS5A protein. *J Virol,* 82**,** 1073-83.

TELLINGHUISEN, T. L., MARCOTRIGIANO, J., GORBALENYA, A. E. & RICE, C. M. 2004. The NS5A protein of hepatitis C virus is a zinc metalloprotein. *J Biol Chem,* 279**,** 48576-87.

TELLINGHUISEN, T. L., MARCOTRIGIANO, J. & RICE, C. M. 2005. Structure of the zinc-binding domain of an essential component of the hepatitis C virus replicase. *Nature,* 435**,** 374-9.

THOMPSON, A. J., MUIR, A. J., SULKOWSKI, M. S., GE, D., FELLAY, J., SHIANNA, K. V., URBAN, T., AFDHAL, N. H., JACOBSON, I. M., ESTEBAN, R., POORDAD, F., LAWITZ, E. J., MCCONE, J., SHIFFMAN, M. L., GALLER, G. W., LEE, W. M., REINDOLLAR, R., KING, J. W., KWO, P. Y., GHALIB, R. H., FREILICH, B., NYBERG, L. M., ZEUZEM, S., POYNARD, T., VOCK, D. M., PIEPER, K. S., PATEL, K., TILLMANN, H. L., NOVIELLO, S., KOURY, K., PEDICONE, L. D., BRASS, C. A., ALBRECHT, J. K., GOLDSTEIN, D. B. & MCHUTCHISON, J. G. 2010. Interleukin-28B polymorphism improves viral kinetics and is the strongest pretreatment predictor of sustained virologic response in genotype 1 hepatitis C virus. *Gastroenterology,* 139**,** 120-9 e18.

THOMSSEN, R., BONK, S., PROPFE, C., HEERMANN, K. H., KOCHEL, H. G. & UY, A. 1992. Association of hepatitis C virus in human sera with beta-lipoprotein. *Med Microbiol Immunol,* 181**,** 293-300.

TONG, X. & MALCOLM, B. A. 2006. Trans-complementation of HCV replication by non-structural protein 5A. *Virus Res,* 115**,** 122-30.

TRIPATHI, L. P., KAMBARA, H., CHEN, Y. A., NISHIMURA, Y., MORIISHI, K., OKAMOTO, T., MORITA, E., ABE, T., MORI, Y., MATSUURA, Y. & MIZUGUCHI, K. 2013. Understanding the biological context of NS5A-host interactions in HCV infection: a network-based approach. *J Proteome Res,* 12**,** 2537-51.

TROTARD, M., LEPERE-DOUARD, C., REGEARD, M., PIQUET-PELLORCE, C., LAVILLETTE, D., COSSET, F. L., GRIPON, P. & LE SEYEC, J. 2009. Kinases required in hepatitis C virus entry and replication highlighted by small interference RNA screening. *FASEB J,* 23**,** 3780-9.

VAN DER POEL, C. L., REESINK, H. W., LELIE, P. N., LEENTVAAR-KUYPERS, A., CHOO, Q. L., KUO, G. & HOUGHTON, M. 1989. Anti-hepatitis C antibodies and non-A, non-B post-transfusion hepatitis in The Netherlands. *Lancet,* 2**,** 297-8.

VARAKLIOTI, A., VASSILAKI, N., GEORGOPOULOU, U. & MAVROMARA, P. 2002. Alternate translation occurs within the core coding region of the hepatitis C viral genome. *J Biol Chem,* 277**,** 17713-21.

VERDEGEM, D., BADILLO, A., WIERUSZESKI, J. M., LANDRIEU, I., LEROY, A., BARTENSCHLAGER, R., PENIN, F., LIPPENS, G. & HANOULLE, X. 2011. Domain 3 of NS5A protein from the hepatitis C virus has intrinsic alpha-helical propensity and is a substrate of cyclophilin A. *J Biol Chem,* 286**,** 20441-54.

VIEYRES, G., BROHM, C., FRIESLAND, M., GENTZSCH, J., WOLK, B., ROINGEARD, P., STEINMANN, E. & PIETSCHMANN, T. 2013. Subcellular localization and function of an epitope-tagged p7 viroporin in hepatitis C virus-producing cells. *J Virol,* 87**,** 1664-78.

VIEYRES, G., DUBUISSON, J. & PIETSCHMANN, T. 2014. Incorporation of hepatitis C virus E1 and E2 glycoproteins: the keystones on a peculiar virion. *Viruses,* 6**,** 1149-87.

VIEYRES, G. & PIETSCHMANN, T. 2013. Entry and replication of recombinant hepatitis C viruses in cell culture. *Methods,* 59**,** 233-48.

VIEYRES, G., THOMAS, X., DESCAMPS, V., DUVERLIE, G., PATEL, A. H. & DUBUISSON, J. 2010. Characterization of the envelope glycoproteins associated with infectious hepatitis C virus. *J Virol,* 84**,** 10159-68.

VOGT, D. A., CAMUS, G., HERKER, E., WEBSTER, B. R., TSOU, C. L., GREENE, W. C., YEN, T. S. & OTT, M. 2013. Lipid droplet-binding protein TIP47 regulates hepatitis C Virus RNA replication through interaction with the viral NS5A protein. *PLoS Pathog,* 9**,** e1003302.

WAKITA, T., PIETSCHMANN, T., KATO, T., DATE, T., MIYAMOTO, M., ZHAO, Z., MURTHY, K., HABERMANN, A., KRAUSSLICH, H. G., MIZOKAMI, M., BARTENSCHLAGER, R. & LIANG, T. J. 2005. Production of infectious hepatitis C virus in tissue culture from a cloned viral genome. *Nat Med,* 11**,** 791-6.

WALEWSKI, J. L., KELLER, T. R., STUMP, D. D. & BRANCH, A. D. 2001. Evidence for a new hepatitis C virus antigen encoded in an overlapping reading frame. *RNA,* 7**,** 710-21.

WANG, H., PERRY, J. W., LAURING, A. S., NEDDERMANN, P., DE FRANCESCO, R. & TAI, A. W. 2014. Oxysterol-binding protein is a phosphatidylinositol 4-kinase effector required for HCV replication membrane integrity and cholesterol trafficking. *Gastroenterology,* 146**,** 1373-85 e1-11.

WANG, H. & TAI, A. W. 2016. Mechanisms of Cellular Membrane Reorganization to Support Hepatitis C Virus Replication. *Viruses,* 8.

WANG, W., WEI, S., LI, L., SU, X., DU, C., LI, F., GENG, B., LIU, P. & XU, G. 2015. Proteomic analysis of murine testes lipid droplets. *Sci Rep,* 5**,** 12070.

WARIS, G., FELMLEE, D. J., NEGRO, F. & SIDDIQUI, A. 2007. Hepatitis C virus induces proteolytic cleavage of sterol regulatory element binding proteins and stimulates their phosphorylation via oxidative stress. *J Virol,* 81**,** 8122-30.

WELBOURN, S., GREEN, R., GAMACHE, I., DANDACHE, S., LOHMANN, V., BARTENSCHLAGER, R., MEEROVITCH, K. & PAUSE, A. 2005. Hepatitis C virus

NS2/3 processing is required for NS3 stability and viral RNA replication. *J Biol Chem,* 280**,** 29604-11.

WESTBROOK, R. H. & DUSHEIKO, G. 2014. Natural history of hepatitis C. *J Hepatol,* 61**,** S58-68.

WIEGAND, J., BUGGISCH, P., BOECHER, W., ZEUZEM, S., GELBMANN, C. M., BERG, T., KAUFFMANN, W., KALLINOWSKI, B., CORNBERG, M., JAECKEL, E., WEDEMEYER, H., MANNS, M. P. & GERMAN, H. E. P. N. E. T. A. H. C. V. S. G. 2006. Early monotherapy with pegylated interferon alpha-2b for acute hepatitis C infection: the HEP-NET acute-HCV-II study. *Hepatology,* 43**,** 250-6.

WOZNIAK, A. L., GRIFFIN, S., ROWLANDS, D., HARRIS, M., YI, M., LEMON, S. M. & WEINMAN, S. A. 2010. Intracellular proton conductance of the hepatitis C virus p7 protein and its contribution to infectious virus production. *PLoS Pathog,* 6**,** e1001087.

XU, G., XIN, X. & ZHENG, C. 2013. GPS2 is required for the association of NS5A with VAP-A and hepatitis C virus replication. *PLoS One,* 8**,** e78195.

YEN, C. L., STONE, S. J., KOLIWAD, S., HARRIS, C. & FARESE, R. V., JR. 2008. Thematic review series: glycerolipids. DGAT enzymes and triacylglycerol biosynthesis. *J Lipid Res,* 49**,** 2283-301.

YOUNIS, B. B., ARSHAD, R., KHURHSID, S., MASOOD, J., NAZIR, F. & TAHIRA, M. 2015. Fulminant hepatic failure (FHF) due to acute hepatitis C. *Pak J Med Sci,* 31**,** 1009-11.

ZAHID, M. N., TUREK, M., XIAO, F., THI, V. L., GUERIN, M., FOFANA, I., BACHELLIER, P., THOMPSON, J., DELANG, L., NEYTS, J., BANKWITZ, D., PIETSCHMANN, T., DREUX, M., COSSET, F. L., GRUNERT, F., BAUMERT, T. F. & ZEISEL, M. B. 2013. The postbinding activity of scavenger receptor class B type I mediates initiation of hepatitis C virus infection and viral dissemination. *Hepatology,* 57**,** 492-504.

ZAYAS, M., LONG, G., MADAN, V. & BARTENSCHLAGER, R. 2016. Coordination of Hepatitis C Virus Assembly by Distinct Regulatory Regions in Nonstructural Protein 5A. *Plos Pathogens,* 12.

ZECH, B., KURTENBACH, A., KRIEGER, N., STRAND, D., BLENCKE, S., MORBITZER, M., SALASSIDIS, K., COTTEN, M., WISSING, J., OBERT, S., BARTENSCHLAGER, R., HERGET, T. & DAUB, H. 2003. Identification and characterization of amphiphysin II as a novel cellular interaction partner of the hepatitis C virus NS5A protein. *J Gen Virol,* 84**,** 555-60.

ZEISEL, M. B., LUPBERGER, J., FOFANA, I. & BAUMERT, T. F. 2013. Host-targeting agents for prevention and treatment of chronic hepatitis C - perspectives and challenges. *J Hepatol,* 58**,** 375-84.

ZHANG, Z., HARRIS, D. & PANDEY, V. N. 2008. The FUSE binding protein is a cellular factor required for efficient replication of hepatitis C virus. *J Virol,* 82**,** 5761-73.

ZHONG, J., GASTAMINZA, P., CHENG, G., KAPADIA, S., KATO, T., BURTON, D. R., WIELAND, S. F., UPRICHARD, S. L., WAKITA, T. & CHISARI, F. V. 2005. Robust hepatitis C virus infection in vitro. *Proc Natl Acad Sci U S A,* 102**,** 9294-9.

Chapter 9: Appendix

Mutants	Backbones
WT	pcDNA3.1 (+), mSGR-Luc-JFH1, pCMV10-NS3-5B, mJFH1, mJFH1(NS5A-OST), pET28a-SUMO-Domain I, pGEX-6p-2-Domain I
GND	mSGR-Luc-JFH1, mJFH1, mJFH1(NS5A-OST)
P35A	pcDNA3.1 (+), mSGR-Luc-JFH1, pCMV10-NS3-5B, mJFH1, mJFH1(NS5A-OST), pET28a-SUMO-Domain I , pGEX-6p-2-Domain I
Y43A	pcDNA3.1 (+), mSGR-Luc-JFH1, pCMV10-NS3-5B
G45A	pcDNA3.1 (+), mSGR-Luc-JFH1, pCMV10-NS3-5B
W47A	pcDNA3.1 (+), mSGR-Luc-JFH1, pCMV10-NS3-5B
G51A	pcDNA3.1 (+), mSGR-Luc-JFH1, pCMV10-NS3-5B
C59A	pcDNA3.1 (+), mSGR-Luc-JFH1, pCMV10-NS3-5B
G60A	pcDNA3.1 (+), mSGR-Luc-JFH1, pCMV10-NS3-5B
V67A	pcDNA3.1 (+), mSGR-Luc-JFH1, pCMV10-NS3-5B, mJFH1, mJFH1(NS5A-OST), pET28a-SUMO-Domain I , pGEX-6p-2-Domain I
G96A	pcDNA3.1 (+), mSGR-Luc-JFH1, pCMV10-NS3-5B
T134A	pcDNA3.1 (+), mSGR-Luc-JFH1, pCMV10-NS3-5B
P145A	pcDNA3.1 (+), mSGR-Luc-JFH1, , pCMV10-NS3-5B, mJFH1, mJFH1(NS5A-OST), pET28a-SUMO-Domain I , pGEX-6p-2-Domain I
153-158A	pcDNA3.1 (+), mSGR-Luc-JFH1, pCMV10-NS3-5B, mJFH1
ΔE1/E2	mJFH1
99AAA	pcDNA3.1 (+), mJFH1
V67A-V	mJFH1
P145A-P	mJFH1
WT	SGR-Neo-JFH1
WT	SGR-Neo-JFH1(NS5A-OST)
WT	mSGR-Luc-JFH1(GFP)

	Construct (Restriction sites)
Plasmid for transcription of 3'UTR	pCDNA3.1-3'UTR (*Hind*III and *Xba*I)
Plasmid for transcription of FMDV 3D aptamer	pCDNA3.1-FMDV 3D aptamer (*Nhe*I/*Xho*I)

Appendix Table 9.1 List of constructs generated and used throughout this study.

Genotype	Isolates	Accession Number
HCV-1a	H77	JX472009
HCV-1a	HCV-RMT	AB520610
HCV-1b	M094AJK	AB010250
HCV-1b	IBJK	AB559564
HCV-1b	1B-2	GQ259488
HCV-1b	NO.2	AB154177
HCV-2a	JCH-6	AB047645
HCV-2a	JFH1	AB047639
HCV-2a	JCH-2	AB047641
HCV-2a	JCH-1	AB047640
HCV-2b	patient NO.44	AB661373
HCV-2b	acute	AB559564
HCV-2b	1-2b	AB600801
HCV-2b	HC10-0804	AB622121
HCV-3a	NR1	AF320804
HCV-3a	SR1	AF320787
HCV-3a	1S_2	AM493508
HCV-3b	Tr	D49374
HCV-3b	SH37	JQ065709
HCV-3h	QC29	JF735121
HCV-4a	L835	DQ418789
HCV-4b	QC264	FJ462435
HCV-5a	SA13	AF064490
HCV-5a	EUH1480	Y13184
HCV-6a	D9	EU246930
HCV-6b	Th580	D84262
HCV-6c	Th846	EF424629
HCV-6h	VN004	D84265
HCV-7a	QC69	EF108306
BHV	PDB-829	KC796074
BHV	PDB-452	KC796090
BHV	PDB-112	KC796077
GBV	GBV-B	AF179612
GHV-1	BWC04	KC551802
GHV-1	BWC05	KC551801
GHV-1	BWC08	KC551800
NPHV	EF369-11	JX948116
RHV	SAR-46-RSA-2008	KC411807
RHV	339	KC815310

Appendix Table 9.2 Isolates used for NS5A domain I sequence alignment.

Sequences of NS5A amino acids from 29 virus isolates from 7 HCV genotypes and 10 related hepaciviruses were selected from NCBI database for alignment analysis of domain I region (Result was shown in Table 3.1). 15 virus isolates underlined were a subset of the viruses used for the conservation analysis of whole NS5A (Results was shown in Figure 3.1B).

Mutants		Quickchange Primer
P35A	Forward	TGCCCGGCCTCGCCTTCATCTCTTGTCAAA
	Reverse	TTTGACAAGAGATGAAGGCGAGGCCGGGCA
Y43A	Forward	TTGTCAAAAGGGGGCCAAGGGTGTGTGGGC
	Reverse	GCCCACACACCCTTGGCCCCCTTTTGACAA
G45A	Forward	GGGGTACAAGGCTGTGTGGGCCGGCACTGG
	Reverse	CCAGTGCCGGCCCACACAGCCTTGTACCCC
W47A	Forward	GGGGTACAAGGGTGTGGCGGCCGGCACTGG
	Reverse	CCAGTGCCGGCCGCCACACCCTTGTACCCC
G51A	Forward	GGGCCGGCACTGCCATCATGACCACGCGCT
	Reverse	AGCGCGTGGTCATGATGGCAGTGCCGGCCC
C59A	Forward	CGCGCTGCCCTGCCGGCGCCAACATCTCTG
	Reverse	CAGAGATGTTGGCGCCGGCAGGGCAGCGCG
G60A	Forward	CGCGCTGCCCTTGCGCCGCCAACATCTCTG
	Reverse	CAGAGATGTTGGCGGCGCAAGGGCAGCGCG
V67A	Forward	AACATCTCTGGCAATGCCCGCCTGGGCTCT
	Reverse	AGAGCCCAGGCGGGCATTGCCAGAGATGTT
G96A	Forward	TTGCTACACGGAGGCCCAGTGCGCGCCGAA
	Reverse	TTCGGCGCGCACTGGGCCTCCGTGTAGCAA
T134A	Forward	CTCCTATGTAACAGGACTGGCCACTGACAATCTGAAAATT
	Reverse	AATTTTCAGATTGTCAGTGGCCAGTCCTGTTACATAGGAG
P145A	Forward	GAAAATTCCTTGCCAACTAGCTTCTCCAGAGTTTTTCTCC
	Reverse	GGAGAAAAACTCTGGAGAAGCTAGTTGGCAAGGAATTTTC
153-158A (Frag1)	Forward	TCCGGATCCTGGCTCCGCGACG
	Reverse	G*GCCGCCG*CA*G*CG*GCCG*CCCAGGAGAAAAACTCTGGAGAAGGTAGTT G
153-158A (Frag2)	Forward	G*C*GG*CCG*C*T*G*CGGCGGC*CCATAGGTTTGCACCCACACCAAAGCCGTTT
	Reverse	GGGAGTTATTAGCGCTCCGGTCCAGGAGTATGACATGGAGC

Appendix Table 9.3 List of oligonucleotide primers used to generate mutations in NS5A domain I.

Forward and Reverse indicate forward primer and reverse primer, respectively.

	Oligonucleotide Sequences
Domain I-Forward	5'-ctgcccGGATCCCCCTTCATCTCTTGTCAAAAGGG-3'
Domain I-Forward (P35A)	5'-ctgcccGGATCCGCCTTCATCTCTTGTCAAAAGGG-3'
Domain I -249-Reverse	5'-cgtgccCTCGAG*TTA*GGTGTTGCTGTGGGTGGTGCAGG-3'
Domain I -215-Reverse	5'-cgtgccCTCGAG*TTA*CGCCGCAGTCTCCGCCGTG-3'

Appendix Table 9.4 List of oligonucleotide primers used for the expression of recombinant domain I proteins.

	Oligonucleotide Sequences
qRT-PCR-Forward	5'-CTC CCG GGG CAC TCG CAA GC-3'
qRT-PCR-Reverse	5'-GCCTAGCCATGGCGTTAGTA-3'
Probe	5' - 6-FAM-GCT AGC ATT TGG GCG TGC CCC CGC AAG A-TAMRA-Sp -3'

Appendix Table 9.5 List of oligonucleotide primers used for the qRT-PCR for the detection of positive HCV genome RNA.

Accession	Description	Abundance Ratio: (OST-WT) / (JFH1-WT)	Abundance Ratio: (OST-35) / (OST-WT)	Abundance Ratio: (OST-67) / (OST-WT)	Abundance Ratio: (OST-145) / (OST-WT)
Q9UHD9	Ubiquilin-2	100	0.006	0.01	0.01
B2RDG0	Proteasome subunit alpha type	100	0.786	1.131	0.823
Q6PJF5	Inactive rhomboid protein 2	100	0.611	1.113	0.01
T1ECW5	Serine/threonine-protein phosphatase 6 regulatory subunit 2	100	0.499	0.961	1.87
A0A0A7C5E9	MHC class I antigen (Fragment)	100	1.943	0.739	0.626
Q9Y3Z3	Deoxynucleoside triphosphate triphosphohydrolas+C3:C7e	100	1.459	1.718	1.564
P51589	Cytochrome P450 2J2	100	0.414	0.706	0.262
C9JMV9	Protein ABHD14A-ACY1	100	0.349	0.614	0.97
A0A0S2Z5U8	Dystrobrevin binding protein 1	100	0.413	3.748	0.01
B4DR52	Histone H2B	100	0.006	0.01	0.01
Q13535	Serine/threonine-protein kinase ATR	100	0.204	0.313	0.365
Q9UGR2	Zinc finger CCCH domain-containing protein 7B	7.785	1.690	0.478	0.159
A0A0S2Z5X6	L(3)mbt-like 2 (Drosophila)	4.319	0.753	0.681	0.291
D7RF68	AGTRAP-BRAF fusion protein	4.291	0.359	0.829	0.641
Q6ZUJ8	Phosphoinositide 3-kinase adapter protein 1	3.992	0.387	0.282	0.22
A8K8N3	Sperm associated antigen 5 (SPAG5),	3.925	0.558	1.162	0.868
tr	HCV_NS5A_TwinStrep	3.583	1.006	0.732	0.269
Q15773	Myeloid leukemia factor 2	3.338	0.644	1.623	1.093
F8W0W8	Serine/threonine-protein phosphatase	3.271	0.706	0.94	0.903
B4DVR4	Vinexin	2.814	0.973	1.064	0.368
Q8IVH2	Forkhead box protein P4	2.783	0.449	0.838	0.722
C9J1B4	Kalirin (Fragment)	2.77	0.632	1.281	0.709
Q5VUA4	Zinc finger protein 318	2.679	0.680	0.749	0.464
B0LPF3	Growth factor receptor-bound protein 2	2.652	0.923	1.356	0.709
P53582	Methionine aminopeptidase 1	2.51	0.669	0.994	0.762
Q9GZP9	Derlin-2	2.494	0.622	0.765	0.522
Q5JWE9	Guanine nucleotide-binding protein G(s) subunit alpha	2.483	0.442	0.857	0.567
J3KN36	Nodal modulator 3	2.464	0.490	0.849	0.529
H7C0G1	Transmembrane protein 245	2.418	0.436	0.879	0.527
P27449	V-type proton ATPase	2.418	0.471	0.874	0.647
B4E171	Tetraspanin	2.396	0.169	0.951	0.255

O94876	Transmembrane and coiled-coil domains protein 1	2.378	0.477	1.04	0.766
Q9H3R5	Centromere protein H	2.356	0.494	1.197	0.752
Q9UPP1	Histone lysine demethylase PHF8	2.319	0.628	1.409	1.053
Q13625	Apoptosis-stimulating of p53 protein 2	2.294	1.053	1.253	1.496
J3QRU1	Tyrosine-protein kinase	2.289	0.785	0.798	0.494
Q8NC42	E3 ubiquitin-protein ligase RNF149	2.288	0.821	1.374	0.361
Q9GZR7	ATP-dependent RNA helicase DDX24	2.281	0.429	0.805	0.483
Q9UKZ1	CCR4-NOT transcription complex subunit 11	2.274	0.545	0.933	0.615
Q7Z434	Mitochondrial antiviral-signaling protein	2.237	0.436	0.622	0.75
P02647	Apolipoprotein A-I	2.228	0.479	0.741	0.486
J3KQ66	Reelin OS	2.19	0.529	0.99	0.779
B4DK31	Acetyl-CoA carboxylase 1	2.182	0.663	1.68	4.442
A0A0A8K8C7	G protein-coupled receptor 49	2.173	0.975	2.35	0.484
A0A024RBB7	Nucleosome assembly protein 1-like 1	2.155	1.213	0.397	0.27
B2R932	CD99 antigen (CD99)	2.15	0.489	0.779	0.618
Q96HP0	Dedicator of cytokinesis protein 6	2.142	0.915	1.291	0.917
Q13344	Fus-like protein (Fragment)	2.139	0.436	0.734	0.374
D9ZGG2	Vitronectin	2.138	0.524	0.869	0.716
P11117	Lysosomal acid phosphatase	2.136	0.607	0.71	0.484
A0A024R9Y7	Melanoma antigen family D, 2	2.099	0.722	0.733	0.577
O60942	mRNA-capping enzyme	2.085	0.682	1.194	0.934
O14929	Histone acetyltransferase type B catalytic	2.053	0.407	0.873	0.56
Q4LE69	PIK4CA variant protein	2.048	0.606	0.445	0.394
Q9NR31	GTP-binding protein SAR1a	2.041	0.461	0.879	0.76
Q96LJ7	Dehydrogenase/reductase SDR family member 1	2.008	0.441	0.812	0.544
Q92925	SWI/SNF-related matrix-associated actin-dependent regulator of chromatin subfamily D member 2	2.007	0.708	0.739	0.753
Q7L5N1	COP9 signalosome complex subunit 6	1.998	0.640	0.947	0.67
P13498	Cytochrome b-245 light chain	1.989	0.505	0.846	0.551
Q9GZT9	Egl nine homolog 1 OS=Homo sapiens GN=EGLN1 PE=1 SV=1	1.984	0.789	1.421	1.447
A8KAQ3	Sortilin 1 (SORT1)	1.984	0.525	0.916	0.691
Q15906	Vacuolar protein sorting-associated protein 72 homolog	1.97	0.569	0.963	0.595
Q96J42	Thioredoxin domain-containing protein 15	1.967	0.445	1.188	1.329
O95551	Tyrosyl-DNA phosphodiesterase 2	1.956	0.353	1.262	1.153

B2R9U2	FK506 binding protein 4	1.956	0.734	1.036	0.848
Q9UEI6	Polio virus related protein 2, alpha isoform (Fragment)	1.937	0.441	0.886	0.529
O43306	Adenylate cyclase type 6	1.93	0.564	0.864	0.517
Q9NUN5	Probable lysosomal cobalamin transporter	1.929	0.494	0.791	0.478
B5MD23	Tetraspanin	1.918	0.387	0.856	0.362
A0A0D9SFM0	E3 ubiquitin-protein ligase SHPRH	1.917	0.611	0.883	0.855
B4DG73	Golgi complex component 6	1.914	0.520	0.991	0.535
V9GYM3	Apolipoprotein A-II	1.907	0.587	0.906	0.566
Q9UNS2	COP9 signalosome complex subunit 3	1.905	0.617	0.971	0.775
K7ER74	Protein APOC4-APOC2	1.905	0.459	0.794	0.52
B4DS05	Nucleosome assembly protein 1-like 4	1.901	1.932	0.368	0.286
Q9BZQ6	ER degradation-enhancing alpha-mannosidase-like protein 3	1.899	0.691	0.897	0.803
Q9H1C4	Protein unc-93 homolog B1	1.895	0.404	1.153	0.808
Q6FGQ5	ASGR1 protein (Fragment)	1.891	0.477	1.04	0.633
P09564	T-cell antigen CD7	1.88	0.524	0.98	0.582
B4DNC0	Ras-related protein Rab-34	1.876	0.428	0.864	0.773
Q9BWJ5	Splicing factor 3B subunit 5	1.875	0.558	0.883	0.679
A0PJW6	Transmembrane protein 223	1.874	0.568	0.863	0.61
B4DPG9	Growth hormone-inducible transmembrane protein	1.863	0.516	0.897	0.664
I6QTG3	Glypican 3 isoform 2	1.857	0.529	0.929	0.82
A0A0B4J1V9	Helicase, lymphoid-specific, isoform CRA_b	1.848	0.486	0.745	0.687
A0A0S2Z3H8	GNAS complex locus isoform 1	1.847	0.504	0.873	0.773
Q96CQ1	Solute carrier family 25 member 36	1.845	0.460	0.731	0.791
A4D1F3	Similar to Six transmembrane epithelial antigen of prostate	1.829	0.521	0.92	0.587
Q8N370	Large neutral amino acids transporter small subunit 4	1.822	0.749	1.299	0.523
Q9BYV1	Alanine--glyoxylate aminotransferase 2, mitochondrial	1.819	0.808	1.466	1.925
Q96EX1	Small integral membrane protein 12	1.819	0.436	0.789	0.472
Q6NVY4	BNIP3 protein	1.815	0.552	1.245	1.07
Q8WUM0	Nuclear pore complex protein Nup133	1.81	0.539	0.807	0.754
A0A0C4DFL7	Lanosterol 14-alpha demethylase	1.795	0.493	0.859	0.6
Q12770	Sterol regulatory element-binding protein cleavage-activating protein	1.795	0.567	1	0.522

Q9NP77	RNA polymerase II subunit A C-terminal domain phosphatase SSU7	1.795	0.188	1.026	1.042
A8QI98	DIS3	1.789	0.516	0.458	0.51
P62877	E3 ubiquitin-protein ligase RBX1	1.787	0.590	0.904	0.518
B4E0K4	Pre-B-cell leukemia transcription factor interacting protein 1	1.786	0.547	0.909	0.83
Q9BRK5	45 kDa calcium-binding protein	1.786	0.524	1.018	1.095
Q8N8V2	Guanylate-binding protein 7	1.78	0.321	0.868	0.467
Q14997	Proteasome activator complex subunit 4	1.777	0.498	0.907	0.746
A6NMH8	Tetraspanin	1.775	0.453	0.803	0.468
Q13501	Sequestosome-1	1.773	0.648	1.236	0.898
P63096	Guanine nucleotide-binding protein G(i) subunit alpha-1	1.767	0.624	0.333	1.415
B7Z5W1	Junctional adhesion molecule A	1.765	0.419	0.902	0.717
B3KNC3	Nucleolar complex protein 2 homolog	1.763	0.477	0.659	0.639
O14894	Transmembrane 4 L6 family member 5	1.757	0.504	0.82	0.524
B2RAL9	Dual specificity protein phosphatase	1.752	0.454	0.931	0.65
A0A024R5F9	UDP-GlcNAc:betaGal beta-1,3-N-acetylglucosaminyltransferase 6,	1.751	0.458	0.909	0.575
P07307	Asialoglycoprotein receptor 2	1.75	0.489	1.007	0.655
Q9BXF3	Cat eye syndrome critical region protein 2	1.745	0.418	0.914	0.73
A8K4H5	Chloride channel protein	1.74	0.489	0.956	0.561
B2R674	Solute carrier family 19, member 3 (SLC19A3)	1.738	0.496	0.921	0.536
P31151	Protein S100-A7	1.734	1.565	2.323	2.449
I1VE18	SEC22 vesicle trafficking protein B	1.73	0.520	0.957	0.657
B4E2A6	Sad1/unc-84-like protein 21	1.728	0.477	1.069	0.739
Q93074	Mediator of RNA polymerase II transcription subunit 12	1.728	0.473	0.855	0.542
B7ZLZ8	FAM73A protein	1.724	0.463	0.956	0.461
M0QZ12	GRAM domain-containing protein 1A	1.723	0.576	0.846	0.652
A0A024R371	ADP-ribosylation-like factor 6 interacting protein 5	1.721	0.438	0.766	0.558
P13056	Nuclear receptor subfamily 2 group C member 1	1.716	0.615	0.969	0.728
H3BMF4	Protein spinster homolog 1	1.709	0.545	0.841	0.579
A0A024QZN7	Chromosome 10 open reading frame 701	1.708	0.481	0.814	0.533
B2R7U4	Heme oxygenase (decycling) 1	1.705	0.613	0.792	0.51
Q9Y333	U6 snRNA-associated Sm-like protein LSm2	1.704	0.863	1.015	0.905

P60602	Reactive oxygen species modulator 1	1.703	0.423	0.851	0.533
A0A024R1S7	SWI/SNF related, matrix associated, actin dependent regulator of chromatin	1.701	0.484	0.9	0.518
Q7Z509	IFNRC OS	1.688	0.441	0.823	0.416
D2JYI1	TGF-beta receptor type-2	1.681	0.588	1.572	0.721
Q9Y519	Transmembrane protein 184B	1.68	0.542	0.925	0.632
Q541P7	EPH receptor B4	1.679	0.428	0.887	0.611
A0A024R466	Integral membrane protein 2C	1.672	0.521	1.167	1.036
Q15800	Methylsterol monooxygenase 1	1.667	0.487	0.936	0.553
Q6ZUY8	Lipase	1.665	0.523	0.883	0.764
Q86T03	Type 1 phosphatidylinositol 4,5-bisphosphate 4-phosphatase	1.664	0.618	0.833	0.736
A0A024R491	Chromosome 2 open reading frame 33	1.663	0.479	0.971	0.564
A0A024RAF0	Bridging integrator 1	1.66	1.154	0.832	0.409
O15162	Phospholipid scramblase 1	1.66	0.509	0.875	0.566
P00167	Cytochrome b5	1.656	0.493	0.956	0.998
Q96SK2	Transmembrane protein 209	1.655	0.453	0.917	0.682
A0A024RB87	RAP1B	1.651	0.452	0.675	0.469
Q8WW52	Protein FAM151A	1.65	0.510	0.818	0.552
Q9H7Z6	Histone acetyltransferase KAT8	1.65	0.525	0.891	0.829
Q9UNS1	Protein timeless homolog	1.648	0.785	0.656	0.367
P02649	Apolipoprotein E	1.647	0.532	0.748	0.534
Q5VV42	Threonylcarbamoyladenosine tRNA methylthiotransferase	1.647	0.566	0.982	0.695
Q8WU67	Phospholipase ABHD3	1.646	0.543	0.861	0.657
Q9NVT9	Armadillo repeat-containing protein 1	1.646	0.545	0.792	0.7
P15907	Beta-galactoside alpha-2,6-sialyltransferase 1	1.645	0.504	0.929	0.635
A4LAA3	Alpha thalassemia/mental retardation syndrome X-linked	1.64	0.463	1.01	0.634
Q9P227	Rho GTPase-activating protein 23	1.639	0.503	0.803	0.532
G1UI16	SCC-112 proteinGN=PDS5A PE=2 SV=1	1.638	0.512	0.771	0.601
O75054	Immunoglobulin superfamily member 3	1.629	0.463	0.889	0.536
Q6BDS2	UHRF1-binding protein 1	1.628	0.230	0.93	0.656
P11234	Ras-related protein Ral-B	1.627	0.474	0.752	0.614
Q9NV79	Protein-L-isoaspartate O-methyltransferase domain-containing protein 2	1.625	0.454	1.031	0.88
Q92621	Nuclear pore complex protein Nup205	1.624	0.465	0.814	0.688
Q8IVW6	AT-rich interactive domain-containing protein 3B	1.624	0.432	0.827	0.617

B2R6P3	Matrix metallopeptidase 14 (membrane-inserted) (MMP14)	1.623	0.516	0.974	0.728
O00469	Procollagen-lysine,2-oxoglutarate 5-dioxygenase 2	1.621	0.491	0.922	1.109
Q92575	UBX domain-containing protein 4	1.619	0.443	0.814	0.51
Q53HE6	HSPC163 protein variant	1.615	0.415	1.069	0.725
P34741	Syndecan-2	1.608	0.484	0.944	0.605
P11233	Ras-related protein Ral-A	1.607	0.441	0.816	0.515
O95864	Fatty acid desaturase 2	1.603	0.496	0.85	0.572
H0YMD1	Low-density lipoprotein receptor	1.602	0.439	0.612	0.511
A0A090N8Q3	Chromosome 7 open reading frame 21	1.602	0.508	0.853	0.648
P15291	Beta-1,4-galactosyltransferase 1	1.601	0.581	0.998	0.922
A0A0S2Z4L3	Protein S isoform 2	1.599	0.569	1.08	1.197
B4DLJ3	to ADP-ribosylation factor 5	1.596	0.501	0.884	0.919
B2RAF3	Placental protein 6 (PL6)	1.593	0.438	0.91	0.578
Q9HBH0	Rho-related GTP-binding protein RhoF	1.593	0.595	0.942	0.975
P36941	Tumor necrosis factor receptor superfamily member 3	1.589	0.579	1.289	0.647
B7ZMF2	Fanconi anemia, complementation group I	1.584	0.561	0.958	0.778
Q99426	Tubulin-folding cofactor B	1.581	0.548	1.337	1.172
Q8TF05	Serine/threonine-protein phosphatase 4 regulatory subunit 1	1.578	0.623	0.797	0.692
P33908	Mannosyl-oligosaccharide 1,2-alpha-mannosidase IA	1.577	0.484	0.93	0.66
A0A024R438	ATG9 autophagy related 9 homolog A	1.575	0.485	0.965	0.627
A0A024RE09	Transmembrane and coiled-coil domains 3	1.573	0.516	0.909	0.487
E9PGC5	Receptor-type tyrosine-protein phosphatase kappa	1.572	0.568	1.08	0.838
O75976	Carboxypeptidase D	1.566	0.523	0.9	0.706
Q6ZNA5	Ferric-chelate reductase 1	1.566	0.498	0.839	0.641
Q9BV40	Vesicle-associated membrane protein 8	1.564	0.513	0.853	0.554
B5BU16	Mitogen-activated protein kinase kinase 6	1.563	0.546	1.127	1.123
Q9Y570	Protein phosphatase methylesterase 1	1.563	1.002	0.961	1.263
Q9BSA9	Endosomal/lysomomal potassium channel TMEM175	1.562	0.414	1.03	0.563
Q4G0I0	Protein CCSMST1	1.561	0.538	0.863	0.633
Q96EU7	C1GALT1-specific chaperone 1	1.561	0.616	0.981	1.126
Q13740	CD166 antigen ALCAM	1.559	0.460	0.912	0.557
B3KWN0	Ankyrin repeat domain-containing protein 52	1.558	0.591	1.147	0.595

D3DSM6	Solute carrier family 19 (Folate transporter)	1.557	0.469	0.846	0.444
Q14318	Peptidyl-prolyl cis-trans isomerase FKBP8	1.556	0.524	0.905	0.707
H7C5E2	B-cell receptor-associated protein 29	1.556	0.573	0.672	0.41
Q9H3Z4	DnaJ homolog subfamily C member 5	1.553	0.467	0.828	0.581
O14521	Succinate dehydrogenase	1.553	0.486	0.908	0.592
Q6FG93	VAMP5	1.552	0.503	0.818	0.494
Q9NRY5	Protein FAM114A2	1.547	0.531	0.937	0.685
B4DEH1	Dolichyl-phosphate mannosyltransferase	1.546	0.489	0.8	0.5
Q2VJ45	HOOK3-RET fusion protein	1.546	0.354	0.94	0.683
A6NHR9	Structural maintenance of chromosomes flexible hinge domain-containing protein 1	1.543	0.527	1.042	1.096
Q9HCE6	Rho guanine nucleotide exchange factor 10-like protein	1.541	0.503	0.853	0.811
Q7Z4F1	Low-density lipoprotein receptor-related protein 10	1.537	0.542	1.376	0.718
P13688	Carcinoembryonic antigen-related cell adhesion molecule 1	1.532	0.529	0.813	0.738
B4DF33	cDNA FLJ57960 OS=Homo sapiens PE=2 SV=1	1.527	0.477	0.829	0.454
Q9NUV7	Serine palmitoyltransferase 3	1.522	0.592	0.962	0.757
Q8NBP0	Tetratricopeptide repeat protein 13	1.522	0.593	0.929	0.584
A0A090N8N0	Importin alpha-2 subunit	1.519	0.442	0.715	0.604
H3BND4	Pyridoxal-dependent decarboxylase domain-containing protein 1	1.518	0.588	0.974	0.865
I3L2B0	Clustered mitochondria protein homolog	1.518	0.592	0.907	0.759
Q9UG56	Phosphatidylserine decarboxylase proenzyme	1.516	0.519	1.008	0.823
A0A024RAP2	3-hydroxy-3-methylglutaryl coenzyme A reductase	1.512	0.506	0.955	0.565
Q8NF37	Lysophosphatidylcholine acyltransferase 1	1.512	0.552	0.775	0.619
Q9H5K3	Protein O-mannose kinase	1.508	0.494	0.815	0.651
Q9H490	Phosphatidylinositol glycan anchor biosynthesis class U protein	1.504	0.487	0.934	0.572
O43681	ATPase ASNA1	1.502	0.594	0.829	0.712
Q4LE58	EIF4G1 variant protein	1.5	0.499	0.874	0.684
Q8N353	TMEM106B protein	1.5	0.506	0.827	0.524
Q96Q42	Alsin	1.499	0.538	0.93	0.638
Q14151	Scaffold attachment factor B2	1.498	0.567	0.931	0.736

B2RCJ6	Bromodomain and WD repeat domain containing 2 (BRWD2),	1.496	0.596	0.915	0.842
O95219	Sorting nexin-4	1.492	0.525	0.93	0.759
P18858	DNA ligase 1	1.492	0.564	0.96	0.61
A0A0A0MRK6	Metaxin 1, isoform CRA_b	1.491	0.466	0.761	0.611
A4D2P0	Ras-related C3 botulinum toxin substrate 1 (Rho family, small GTP binding protein Rac1)	1.491	0.428	0.805	0.713
A8K9X0	Protein YIPF	1.491	0.441	1.021	0.694
B3KMN2	Homo sapiens SCC-112 protein	1.49	0.424	0.654	0.589
Q8N335	Glycerol-3-phosphate dehydrogenase 1-like protein	1.487	0.606	0.895	0.734
A0A087WX97	Bcl-2-like protein 13 SV=1	1.486	0.470	0.84	0.497
P02786	Transferrin receptor protein 1	1.485	0.476	0.914	0.575
A0A087X1Z3	Proteasome activator complex subunit 2	1.485	0.492	0.754	0.685
B5BUD2	Replication factor C 2 isoform 1 (Fragment)	1.481	0.410	0.845	0.717
Q15554	Telomeric repeat-binding factor 2	1.481	0.539	0.783	0.639
A5Y5A3	PC1/MRPS28 fusion protein	1.479	0.566	0.873	0.75
Q9BX93	Group XIIB secretory phospholipase A2-like protein	1.478	0.622	0.818	0.512
Q6NUQ4	Transmembrane protein 214	1.477	0.443	0.814	0.525
D3DVC4	Nestin, isoform CRA_c	1.477	0.501	0.948	0.894
Q92930	Ras-related protein Rab-8B PE=1 SV=2	1.475	0.458	0.736	0.547
Q9HBM0	Vezatin OS	1.475	0.507	0.833	0.57
A0A024R9G2	Ankyrin repeat domain 46	1.475	0.526	1.027	0.507
X5DR09	General transcription factor IIi isoform A	1.47	0.587	0.983	0.948
Q9NV96	Cell cycle control protein 50A	1.47	0.535	1.096	0.634
Q9P0B6	Coiled-coil domain-containing protein 167	1.47	0.548	0.871	0.66
A0A024R061	Synaptobrevin-like 1	1.468	0.514	0.995	0.636
Q96BZ9	TBC1 domain family member 20	1.468	0.608	0.765	0.548
Q07954	Prolow-density lipoprotein receptor-related protein 1	1.467	0.496	1.003	0.763
Q9HC07	Transmembrane protein 165	1.467	0.528	1.075	0.685
Q9UBV7	Beta-1,4-galactosyltransferase 7	1.467	0.579	0.906	0.703
Q7Z7M9	Polypeptide N-acetylgalactosaminyltransferase 5	1.466	0.537	1.086	0.865
R4GN18	Membrane cofactor protein	1.466	0.471	0.892	0.509
Q99943	1-acyl-sn-glycerol-3-phosphate acyltransferase alpha	1.466	0.483	0.923	0.664
A0A087WT44	Heme oxygenase 2	1.465	0.405	0.842	0.609
O00487	26S proteasome non-ATPase regulatory subunit 14	1.464	0.550	0.941	0.785

Q5STZ8	ATP-binding cassette sub-family F member 1 (Fragment)	1.464	0.638	0.906	0.882
Q9H3S7	Tyrosine-protein phosphatase non-receptor type 23	1.464	0.566	1.053	0.883
O14874	[3-methyl-2-oxobutanoate dehydrogenase [lipoamide]] kinase	1.463	0.535	1.427	1.884
B2RDJ6	Probable cytosolic iron-sulfur protein assembly protein CIAO1	1.462	0.542	0.867	0.713
A0A024R324	Ras homolog gene family, member A	1.461	0.553	0.806	0.74
P19075	Tetraspanin-8	1.461	0.509	0.803	0.662
C9JBG5	SID1 transmembrane family member 2	1.46	0.698	0.556	1.604
Q9Y232	Chromodomain Y-like protein	1.46	0.438	0.711	0.786
Q3BDU4	Rhabdomyosarcoma antigen MU-RMS-40.10B	1.458	0.626	0.898	0.629
P27037	Activin receptor type-2A	1.458	0.960	1.944	0.56
A0A0U1RR27	C-myc promoter-binding protein OS	1.457	0.421	0.767	0.584
A0A0S4XQU8	MHC class I antigen	1.456	0.366	0.826	0.566
P51148	Ras-related protein Rab-5C	1.455	0.499	0.87	0.735
Q8IXI1	Mitochondrial Rho GTPase 2	1.455	0.506	0.962	0.847
P30260	Cell division cycle protein 27 homolog	1.453	0.566	0.753	0.544
Q6IAX1	FDFT1 protein	1.451	0.448	0.864	0.552
Q59G70	Mannosyl (Alpha-1,3-)-glycoprotein beta-1,2-N-acetylglucosaminyltransferase variant	1.451	0.453	0.885	0.618
Q96A57	Transmembrane protein 230	1.449	0.486	0.859	0.495
E5KLJ5	Dynamin-like 120 kDa protein, mitochondrial	1.447	0.487	0.811	0.552
A0A024R8U1	Solute carrier family 16 (Monocarboxylic acid transporters)	1.446	0.489	1.011	0.748
A0A024R9E0	Estrogen receptor binding site associated, antigen	1.446	0.437	0.625	0.527
Q9UKV5	E3 ubiquitin-protein ligase AMFR	1.444	0.489	0.73	0.537
H3BNX8	Cytochrome c oxidase subunit 5A, mitochondrial	1.444	0.533	0.852	0.662
P31689	DnaJ homolog subfamily A member 1	1.443	0.654	0.938	0.844
O95159	Zinc finger protein-like 1	1.443	0.534	0.869	0.641
P05362	Intercellular adhesion molecule 1	1.442	0.432	0.759	0.533
A8K3S3	Kinesin-like protein	1.441	0.639	0.996	0.949
P10589	COUP transcription factor 1	1.44	0.521	0.844	1.065
Q14643	Inositol 1,4,5-trisphosphate receptor type 1	1.44	0.559	1.037	0.67

P09132	Signal recognition particle 19 kDa protein	1.439	0.954	1.393	1.375
P57740	Nuclear pore complex protein Nup107	1.438	0.532	1.103	0.597
Q96HR9	Receptor expression-enhancing protein 6	1.436	0.458	0.804	0.712
I3L0M9	Transcription elongation factor B polypeptide 2	1.435	0.612	1.368	1.45
Q96QK1	Vacuolar protein sorting-associated protein 35	1.434	0.678	1.03	0.535
B5MDU6	Lipid droplet-associated hydrolase	1.433	0.529	1.004	0.586
Q12772	Sterol regulatory element-binding protein 2	1.432	0.633	1.056	0.853
Q6IBW4	Condensin-2 complex subunit H2	1.432	0.733	0.984	0.807
A0A0S2Z5J4	Adaptor-related protein complex 3 beta 1 subunit isoform 1	1.431	0.564	0.844	0.578
A0A0A0MRI2	Sorting nexin 6, isoform CRA_b	1.431	0.469	0.844	0.694
B3KM57	CCR4-NOT transcription complex subunit 7	1.429	0.516	0.906	0.611
A0PK00	Transmembrane protein 120B	1.429	0.523	0.816	0.558
Q9Y277	Voltage-dependent anion-selective channel protein 3	1.428	0.551	0.814	0.885
Q8N6C5	Immunoglobulin superfamily member 1	1.428	0.236	0.697	0.337
P78382	CMP-sialic acid transporter	1.427	0.512	0.977	0.67
P14543	Nidogen-1	1.426	0.649	0.72	0.632
Q4KWH8	1-phosphatidylinositol 4,5-bisphosphate phosphodiesterase eta-1	1.425	0.536	0.729	0.5
Q96KA5	Cleft lip and palate transmembrane protein 1-like protein	1.424	0.489	0.872	0.558
Q13563	Polycystin-2	1.423	0.416	0.86	0.597
O14949	Cytochrome b-c1 complex subunit 8	1.421	0.480	0.783	0.731
A8K2G0	Secretory carrier membrane protein 1 (SCAMP1)	1.42	0.461	0.92	0.609
A6NEM2	Host cell factor 1	1.419	0.501	1.069	0.822
B7ZL91	Metalloendopeptidase	1.418	0.586	1.061	0.728
P35613	Basigin	1.417	0.451	0.917	0.692
B3KQL8	Probable dolichyl pyrophosphateGlc1Man9GlcNAc2 alpha-1,3- glucosyltransferase	1.415	0.509	0.869	0.551
Q9NQG1	Protein MANBAL	1.415	0.468	0.873	0.57
A8KAF0	CCR6 chemokine receptor (CMKBR6)	1.412	0.516	0.847	0.447
A0A0B5HR54	Serine/threonine-protein kinase receptor	1.412	0.526	0.988	0.675
Q504R6	RAB13 protein	1.411	0.519	0.887	0.825

Q9NS00	Glycoprotein-N-acetylgalactosamine 3-beta-galactosyltransferase 1	1.41	0.469	0.88	0.624
Q9NR09	Baculoviral IAP repeat-containing protein 6	1.41	0.626	0.966	0.684
B7Z3D4	Myosin-10	1.41	1.050	0.969	0.925
Q92896	Golgi apparatus protein 1	1.407	0.532	0.911	0.793
O60488	Long-chain-fatty-acid--CoA ligase 4	1.406	0.480	0.874	0.634
O60664	Perilipin-3	1.406	0.499	0.829	0.622
Q8NET6	Carbohydrate sulfotransferase 13	1.405	0.562	1.135	0.897
A8K509	Yip1 interacting factor homolog A	1.405	0.501	1.056	0.733
O43678	NADH dehydrogenase [ubiquinone] 1 alpha subcomplex subunit 2	1.405	0.517	1.061	0.956
B7Z881	Ras GTPase-activating-like protein	1.404	0.592	0.874	0.675
Q9NX62	Inositol monophosphatase 3	1.404	0.496	0.869	0.715
Q9Y6D5	Brefeldin A-inhibited guanine nucleotide-exchange protein 2	1.404	0.566	0.927	0.574
P14625	Endoplasmin	1.402	0.504	0.796	0.52
A0A024R9K7	Chromosome 15 open reading frame 24	1.402	0.471	0.815	0.521
Q6WKZ4	Rab11 family-interacting protein 1	1.402	0.423	0.906	0.834
A0A024R201	Proteasome (Prosome, macropain) 26S subunit, non-ATPase, 13, isoform CRA_a	1.401	0.579	0.874	0.69
P68431	Histone H3.1	1.401	0.606	0.853	0.695

Appendix Table 9.6 Host proteins identified by proteomic analysis.

Host proteins listed here are Strep-tagged NS5A samples from wildtype, P35A, V67A and P145A with more than 1.4- fold enrichment compared with untagged JFH1 wildtype beads. Abundance ratio (OST-WT /JFH1-WT) is the ratio protein abundance for the wildtype OST-N5SA (OST-WT) pull down to the untagged JFH1 wildtype negative control. Abundance ratio (OST-P35A, V67A or P145A /OST-WT) is the ratio protein abundance for the mutated OST-N5SA pull down to the wildtype OST-NS5A positive control.

	RNA Replication	Polyprotein Processing	NS3-NS5A Colocalization	Virus Assembly	Dimerization	RNA binding	Protein interactions
P35A	**WT**	WT	WT	**Impaired**	WT	WT	**ApoE/DGAT1**
C39A	Lethal	WT	WT	n/a	n/a	n/a	n/a
Y43A	Lethal	WT	WT	n/a	n/a	n/a	n/a
G45A	Lethal	WT	**Impaired**	n/a	n/a	n/a	n/a
W47A	Lethal	WT	WT	n/a	n/a	n/a	n/a
G51A	Lethal	WT	**Impaired**	n/a	n/a	n/a	n/a
C57A	Lethal	WT	WT	n/a	n/a	n/a	n/a
C59A	Lethal	WT	WT	n/a	n/a	n/a	n/a
G60A	Lethal	WT	WT	n/a	n/a	n/a	n/a
V67A	**Impaired**	WT	WT	**Lethal**	**Lethal**	**Increased**	**WT**
C80A	Lethal	WT	WT	n/a	n/a	n/a	n/a
P89A	Lethal	WT	WT	n/a	n/a	n/a	n/a
I90A	Lethal	WT	WT	n/a	n/a	n/a	n/a
N91A	Lethal	WT	WT	n/a	n/a	n/a	n/a
G96A	Lethal	WT	WT	n/a	n/a	n/a	n/a
P100A	Lethal	WT	WT	n/a	n/a	n/a	n/a
G132A	Lethal	WT	WT	n/a	n/a	n/a	n/a
T134A	Lethal	WT	WT	n/a	n/a	n/a	n/a
P145A	**Impaired**	WT	WT	**Lethal**	**Lethal**	**Increased**	**WT**
V153A	Lethal	WT	**Impaired**	n/a	n/a	n/a	n/a
D154A							
G155A							
V156A							
L158A							

Appendix Table 9.7 Summary of phenotypes of domain I mutants in HCV (JFH1) lifecycle.